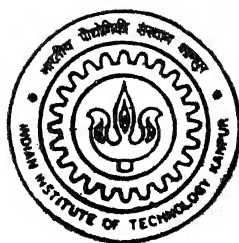


# **A NOVEL PLACEMENT STRATEGY FOR FACTS DEVICES IN MULTIMACHINE POWER SYSTEMS**

By  
**NIKHLESH KUMAR SHARMA**



TH  
12000/P  
h23n

**DEPARTMENT OF ELECTRICAL ENGINEERING  
INDIAN INSTITUTE OF TECHNOLOGY, KANPUR  
JULY, 2000**

**A NOVEL PLACEMENT STRATEGY FOR FACTS  
DEVICES IN MULTIMACHINE POWER SYSTEMS**

0.5461

by

**NIKHLESH KUMAR SHARMA**

**DEPARTMENT OF ELECTRICAL ENGINEERING  
INDIAN INSTITUTE OF TECHNOLOGY**

**July, 2000**



7 JUL 2005/EE

पुस्तकालय काशीनाथ मेहता पुस्तकालय  
भारतीय प्रौद्योगिकी संस्थान कानपुर  
अवधि क्र० A...134207

TH  
EEI2000/P  
Sh23m



## CERTIFICATE

This is to certify that the work contained in the thesis entitled “ **A Novel Placement Strategy for FACTS Devices in Multimachine Power Systems**” by Nikhlesh Kumar Sharma has been carried out under our supervision and this work has not been submitted elsewhere for a degree.

A handwritten signature in dark ink, appearing to read "Arindam Ghosh".

Arindam Ghosh

A handwritten signature in dark ink, appearing to read "Rajiv K. Varma".

Rajiv K. Varma

Department of Electrical Engineering  
Indian Institute of Technology  
Kanpur, India

Dedicated to  
my parents

## ACKNOWLEDGEMENTS

*I consider myself extremely fortunate for having got the opportunity to work and learn under the supervision of my supervisors Prof. Arindam Ghosh and Prof. Rajiv K. Varma. No words are adequate to express my gratefulness to both my supervisors for their constant encouragement, active participation and moral support during this dissertation work.*

*I am extremely grateful to Prof. S. S. Prabhu and Prof. Avinash Joshi for their motivation and support at crucial stages of this work.*

*I am thankful to Prof. S. C. Srivastava, Prof. Sachchidanand, Prof. Ravindra Arora, Prof. G. K. Dubey and Prof. Govind Sharma for their advice and encouragement through out the course of this work.*

*I take this opportunity to thank Jayram Sir, Mahapatra ji, Mr. R. K. Singh, Mr. G. N. Pillai, Mr. M. K. Mishra, Mr. R. K. Tripathi, Mr. Manoranjan Sinha, Mr. R. P. Gupta, Mr. P. V. K. Raddy, Mr. S. K. Patidar and Mr. Rohit Sinha for their company and lively discussion on various topics.*

*I am thankful to Dr. Biswarup Das and Mantu for their constant support and moral help at every stage of this work.*

*The support and cooperation received from Vinay, Anju Bhabhi and Ayushi is unforgettable. I sincerely thank them.*

I am indebted to my parents-in-law for their immense affection, constant encouragement and support at different stages of this work.

I am extremely grateful to my principal, Prof. Pande B. B. Lal, for giving me an opportunity to do this dissertation work.

I thank my daughters Sheenu and Mona for keeping my spirit alive all the time.

And finally, I owe the completion of this work to my wife Ranjna for her mental support, constant inspiration and forbearance through out this project.

Nikhlesh Kumar Sharma

**Thesis Title:** A NOVEL PLACEMENT STRATEGY FOR FACTS DEVICES IN MULTIMACHINE POWER SYSTEMS

**Name:** Nikhlesh Kumar Sharma

**Roll Number:** 9610472

**Thesis Supervisors:** Prof. Arindam Ghosh & Prof. Rajiv K. Varma

**Degree for which submitted:** Ph. D.

## **SYNOPSIS**

A power system is a complex network comprising numerous generators, transmission lines, transformers and variety of loads. Because of the economic as well as environmental problems associated with adding new transmission lines to keep pace with the growing loads and generation, the major task facing utility industry today is the efficient utilization of the existing transmission systems. One of the approaches adopted for efficient utilization involves the use of power electronics technology.

With the growing demand of electrical power, the existing transmission lines get increasingly overloaded. This increased loading of transmission lines has led to various problems associated with stability and maintenance of appropriate voltage levels across the system. A reliable solution of these problems can be achieved with the help of Flexible Alternating Current Transmission System (FACTS) devices, which may be connected in series, shunt or in a combination of series and shunt. FACTS devices include a host of fast, reliable solid state controllers [1]. However, these devices are effective only when they are placed at appropriately determined locations.

There may further be situations where more than one FACTS device is employed in the system for voltage stabilization and stability enhancement etc. Their collaborative interaction can play an important role in improving power transfer capability of the network and the overall power system stability.

In this thesis an attempt has been made to evolve a simple strategy for placement of FACTS devices in a multimachine environment after a careful study of several existing techniques. A general purpose interactive MATLAB program has been developed for small signal analysis of multimachine system. Modeling of SVC, TCSC, STATCOM and SSSC is done and the system stability analyzed using these FACTS devices. Finally, an attempt has also been made to examine the interactions between shunt and series FACTS devices (namely, SVC and TCSC) and their impact on the system stability utilizing the proposed placement strategy.

To obtain optimum system performance, the location of any FACTS device in an interconnected power system must be determined carefully. Four broad categories of techniques have been so far proposed for determining best suited locations. These are

- (1) Jacobian based sensitivity methodologies [2]
- (2) Non-Jacobian based techniques [3, 4]
- (3) Eigenanalysis based methods [5]
- (4) Optimization and Artificial Intelligence based techniques [6]

Placement techniques (3) and (4) are complex and computationally time intensive but are claimed to be more accurate. Techniques (1) and (2) are comparatively simple and are shown to be reasonably accurate even though they do not consider system dynamics as in (3) and system nonlinearities as in (4). Between (1) and (2), the non-Jacobian based techniques are simpler and less time consuming. It is understood that a Jacobian is always utilized to do the load flow studies. In Jacobian based methods the load flow Jacobian elements are utilized for calculating the indices for placement of FACTS devices. However non-Jacobian methods utilize only the load flow results and not the Jacobian elements. The main objective of this thesis is to evolve an efficient non-Jacobian placement strategy, which is less time consuming, yet accurate.

Once the location of a FACTS device is chosen, its performance can be evaluated. A study of the implication of adding various FACTS devices in multimachine environment requires not only an appropriate mathematical model of the system, but also of the FACTS devices as well. Commercial packages such as PEALS (Program for Eigenvalue Analysis of Large Systems), EPRI-ETMSP (Electric Power Research

Institute's Extended Transient/Midterm Stability Program), EPRI-LTSP (EPRI's Long Term Stability Program), PSS/E (PTI's Power System Simulator for Engineers) exist for the analysis of a power system. These are however fairly expensive and due to their specialized nature are not readily available in educational institutions. Furthermore, there is a need for a versatile small signal stability program, which offers the flexibility of modeling different FACTS devices both individually as well as in their different combinations. For this purpose a comprehensive general MATLAB program is developed on the same lines as given in [7]. This methodology has been extended in this thesis to incorporate various FACTS devices and their controls to varying levels of complexity. This multimachine dynamic model can be used to study both small signal stability and voltage stability of an electric power system. The developed MATLAB program is utilized to examine the applicability of the proposed placement strategy through eigenvalue and step response studies.

Modern power systems are heading towards a deregulated environment of operation and control. This will probably require simultaneous installation of different FACTS devices in the system. A need therefore arises to examine possible control interaction amongst these devices. It is noted that each FACTS device will be equipped with higher order controls also to extract the maximum benefit in terms of damping augmentation, stability enhancement, etc. This requires complex in-depth investigations of the control interactions. However an insight into the control interaction, may it be collaborative or adverse, amongst the different devices can still be obtained utilizing basic PI controls installed on these FACTS devices. Detailed investigations are performed in this thesis to look at the interactions between an SVC and a TCSC.

In summary the objectives and scope of the thesis are

1. To develop a non-Jacobian based methodology for placement of FACTS devices.
2. To develop a general versatile MATLAB software package for multimachine environment, which can incorporate various FACTS devices for small signal stability analysis.
3. To examine the placement methodology for FACTS devices with the software package developed.



4. To study the impact of the coordinated control of FACTS devices on system performance.

Research work has been carried out in pursuit of the above objectives and, from the results obtained, the major contributions of the thesis are

- (1) A novel non-Jacobian placement strategy termed as Extended Voltage Phasors Approach (EVPA) is proposed for identification of critical line segment from voltage stability consideration in the power systems. The results of EVPA are compared and validated by Line Flow Indices (LFI) [3] approach as well as voltage profile graphs of the system at base case loading and maximum loading conditions. The EVPA is applied to four systems, viz a 6-bus, a 9-bus, a 39-bus and a 68-bus system at different loading conditions. The EVPA approach also indicates whether the problem at these critical line segments is either due to active power or due to reactive power loading of the system. In EVPA there is no need to compute four indices for each line as is done in LFI approach. Therefore EVPA is computationally more efficient. The EVPA is also applied to 68-bus system at base case loading condition considering various contingencies in the system. It is found that in most cases, the critical link obtained in healthy system study continues to remain critical, but in few special cases some other line becomes more critical.
- (2) A general purpose versatile program for small signal and voltage stability analysis of multimachine power system has been developed using MATLAB 5.3. The developed program uses two axis representation of synchronous machines with both rotating and static type of exciter [7]. The methodology of multimachine modeling is based on power balance form. The results of the developed MATLAB program are compared with published result [7] and it has been found that both match closely.
- (3) Mathematical modeling of various key FACTS devices viz SVC, TCSC, STATCOM and SSSC has been done using power balance form. Different types of controllers employing proportional-integral control and state feedback with integral control have been used with the FACTS devices. All the models developed are modular and can be easily incorporated in developed program.

- (4) It is proposed that the impact of coordinated control of FACTS devices at different loading conditions can be studied using a heuristic root loci technique incorporating modal damping analysis and step response studies. In this technique the set of “desirable” controller parameter is chosen which provide a high degree of modal damping of the sensitive modes, simultaneously, and then “best” set of controller parameters are obtained using step response studies. Extensive studies are done to gain an insight into
- The relative influence of SVC and TCSC on the damping of critical interarea modes.
  - The relative effect of system loading on the “best” settings of SVC and TCSC controller parameters.
  - The impact of nominal series compensation provided by TCSC on the TCSC controller parameters.

## **OUTLINE OF THE THESIS**

Chapter 1 introduces the objective of the thesis and outlines briefly the work done in the thesis. A brief review of FACTS device modeling, placement techniques and their coordinated control is also presented.

In Chapter 2, the multimachine model on the same lines as given in [7] is developed using MATLAB 5.3. The developed MATLAB software package for multimachine system is interactive and general in nature. The results obtained through the developed package are compared with the published result [7] for 9-bus WSCC system. It has been found that both the results match very closely.

In Chapter 3, various FACTS device models such as SVC, TCSC, STATCOM and SSSC are developed. The models are incorporated in the developed MATLAB program in modular fashion. Multiple FACTS device incorporation in multimachine environment is also shown in Chapter 3.

Chapter 4 deals with the proposed placement strategy of FACTS device in multimachine system. A novel technique called EVPA (Extended Voltage Phasors Approach) is proposed. The performance of EVPA is evaluated for four systems (6-bus,

9-bus, 39-bus and 68-bus system) at various loading conditions. The results thus obtained for various systems at different loading conditions are compared with established Line Flow Index Method [3]. The performance of EVPA is also evaluated for various system contingencies. Placement strategy for multiple devices using EVPA is also discussed in Chapter 4.

In Chapter 5, a small signal analysis of above mentioned four systems is done using EVPA technique at various loading conditions. The developed MATLAB program is used for small signal stability analysis. The results of the small signal stability are validated through step response investigations and voltage profile studies.

Chapter 6 deals with the determination of best parameters of FACTS controllers and the study of coordinated control of FACTS devices. The coordinated control of SVC and TCSC are studied for the 9-bus system at various loading conditions. This interaction is also examined with varying levels of series compensation. Root loci method together with modal damping analysis have been used to determine the controller parameters and visualize the impact of coordinated control of FACTS devices. Further refinement of FACTS controller parameters is done using step response studies.

The thesis concludes in Chapter 7, which outlines major contributions and also suggests scope of future work in this area.

## REFERENCES

- [1] N. G. Hingorani and Laszlo Gyugyi, "Understanding FACTS," *IEEE Press*, 1999.
- [2] B. Gao, G. K. Morison and P. Kundur, "Voltage Stability Evaluation using Modal Analysis," *IEEE Trans. on Power Systems*, Vol. 7, No. 4, pp. 1529-1542, November 1992.
- [3] A. Mohamed and G. B. Jasmon, "Determining the Weak Segment of a Power System with Voltage Stability Considerations," *Electric Machines and Power Systems*, Vol. 24, pp. 555-568, 1996.
- [4] F. Gubina and B. Strmcnik, "Voltage Collapse Proximity Index Determination using Voltage Phasors Approach," *IEEE Trans. on Power Systems*, Vol. 10, No. 2, pp 788-792, May 1995.

- [5] Ning Yang, Qinghua Liu and James D. McCalley, " TCSC Controller Design for Damping Interarea Oscillations," *IEEE Trans. on Power Systems*, Vol. 13, No. 4, pp. 1304-1310, November 1998.
- [6] C. S. Chang and J. S. Huang, " Optimal SVC Placement for Voltage Stability Reinforcement," *Electric Power Systems Research*, Vol. 42, pp. 165-172, 1997.
- [7] Peter W. Sauer and M. A. Pai, " Power System Dynamics and Stability," *Prentice Hall*, 1998.

# CONTENTS

<b>List of Figures</b>	<b>vi</b>
<b>List of Tables</b>	<b>xiii</b>
<b>List of Symbols</b>	<b>xv</b>
<b>1 INTRODUCTION</b>	<b>1</b>
1.1 Facts Controllers	2
1.1.1 Static Var Compensator (SVC)	3
1.1.2 Thyristor Controlled Series Capacitor (TCSC)	3
1.1.3 Static Synchronous Compensator (STATCOM)	5
1.1.4 Static Synchronous Series Compensator (SSSC)	5
1.2 Modeling of Facts Devices	6
1.2.1 SVC Modeling	6
1.2.2 TCSC Modeling	7
1.2.3 STATCOM Modeling	8
1.2.4 SSSC Modeling	9
1.3 Placement Strategy of Facts Devices	9
1.4 Coordination of Facts Devices	13
1.5 Objectives and Scope of the Thesis	16
1.6 Outline of the Thesis	18
<b>2 MULTIMACHINE MODELING</b>	<b>20</b>
2.1 Model-I	21
2.1.1 Differential-Algebraic-Equation (DAE) for Model-I	23
2.1.2 Linerization of DAE for Model-I	29
2.2 Model-II	32
2.3 Development of the MATLAB Software Program	33
2.4 Case Study with System Model-I	34
2.5 Conclusions	35

<b>3</b>	<b>MODELING AND INCORPORATION OF FACTS DEVICES IN MULTIMACHINE SYSTEMS</b>	<b>36</b>
3.1	Static Var Compensator	36
3.1.1	State Equations of SVC with Controller	40
3.1.2	Interpretation of SVC Operation in Load Flow	42
3.1.3	Case Study	42
3.2	Thyristor Controlled Series Capacitor	44
3.2.1	Operating Modes	45
3.2.2	Controller Model	46
3.2.3	Incorporation of TCSC in Multimachine Power System	47
3.3	Static Synchronous Compensator	51
3.3.1	Comparison of STATCOM and SVC Characteristics	52
3.3.2	Fundamental Concepts of STATCOM	54
3.3.3	Inverter Configuration	55
3.3.4	STATCOM Modeling	58
3.3.5	State Feedback Controller with Integral Control	61
3.3.6	Incorporation of STATCOM in Multimachine System	63
3.4	Static Synchronous Series Compensator	64
3.4.1	Principle of SSSC	65
3.4.2	Modeling of SSSC	68
3.4.3	Incorporation of State Feedback Controller with Integral Control in SSSC Model	72
3.4.4	Incorporation of SSSC in Multimachine System	74
3.5	Incorporation of Multiple Facts Devices	76
3.6	Conclusions	77
<b>4</b>	<b>PLACEMENT STRATEGY OF FACTS DEVICES</b>	<b>78</b>
4.1	Line Flow Index Approach	79
4.2	Voltage Phasors Approach (VPA)	81
4.3	Proposed Strategy for Placement of Facts Devices	83
4.3.1	Six Bus Test System	84
4.3.2	Nine Bus WSCC Test System	87

4.3.3	Ten Machines, 39-Bus System	90
4.3.4	Sixteen Machines, 68-Bus System	94
4.4	Critical Path Identification at Maximum Loading Condition	98
4.4.1	Six Bus System	99
4.4.2	Nine Bus System	102
4.4.3	Ten Machines, 39-Bus System	104
4.4.4	Sixteen Machines, 68-Bus System	107
4.5	Placement of Facts Devices with Contingency Considerations	107
4.6	Placement Strategy for Multiple Devices	111
4.7	Conclusions	113
<b>5</b>	<b>SMALL SIGNAL ANALYSIS OF THE PLACEMENT STRATEGY</b>	<b>115</b>
5.1	Nine Bus System	116
5.1.1	Base Case Loading Condition	116
5.1.2	Maximum Loading Condition	118
5.2	Sixteen Machines 68-Bus System	124
5.2.1	Base Case Loading	124
5.2.2	Maximum Loading Condition	125
5.3	Eigenvalue Analysis Using STATCOM and SSSC	132
5.3.1	Nine-Bus System	132
5.3.2	Sixty Eight Bus System	133
5.3.3	Eigenvalue Analysis with SSSC for 68-Bus System	137
5.4	Conclusions	140
<b>6</b>	<b>COORDINATED CONTROL OF FACTS DEVICES</b>	<b>141</b>
6.1	Root Loci Method for Design of Individual Facts Controllers	142
6.2	Determination of “best” TCSC Controller (without SVC)	143
6.2.1	Base Case Loading Condition	144
6.2.2	100% Loading Condition (Mid-loading condition)	146
6.2.3	Maximum Loading Condition	147
6.3	Determination of “best” SVC Controller (without TCSC)	158
6.3.1	Base Case Loading Condition	158

6.3.2	Mid-Loading Condition	159
6.3.3	Maximum loading condition	159
6.4	Determination of Coordinated “best” SVC-TCSC Parameters	160
6.4.1	Different Loading Conditions	171
6.5	Determination of “best” TCSC Parameters for Different Compensation Levels at Maximum Loading Condition	172
6.6	Determination of “best” SVC-TCSC Parameters for Different Compensation Levels at Maximum Loading Condition	173
6.7	Discussion and General Observations	180
6.8	Conclusions	181
<b>7</b>	<b>CONCLUSIONS</b>	<b>183</b>
7.1	General Conclusions	183
7.1.1	Extended Voltage Phasors Approach (EVPA)- A Novel Placement Strategy	183
7.1.2	Development of General Purpose MATLAB Program	184
7.1.3	Mathematical Modeling and Incorporation of FACTS Devices in the Developed MATLAB Program	184
7.1.4	Analysis of EPVA Using Developed MATLAB Program	185
7.1.5	Coordinated Control of FACTS Devices	185
7.2	Scope for Future Work	186
	<b>REFERENCES</b>	<b>187</b>
	<b>APPENDICES</b>	
A	Multimachine Modeling	201
B	Calculation of Initial Conditions	212
C	System Data for WSCC 3-Machines, 9-Bus System	215
D	SVC Modeling and System Parameters	217
E	Details of TCSC Modeling	222
F	STATCOM Modeling	230



G	SSSC Modeling	246
H	Incorporation of Multiple Facts Devices	261
I	System Data for 6-Bus System	263
J	System Data for WSCC 3-Machines, 9-Bus System	265
K	System Data for 10-Machines, 39-Bus System	267
L	System Data for 16-Machines, 68-Bus System	275
M	APTP and RPTP for 68-Bus System at Maximum Loading Condition with SVC at Bus 40	291
N	Eigenvalues for 68-Bus System at Base Case Loading Shown in Three Columns	296
O	TCSC Characteristic with Different Values of $X_c$	297

## LIST OF FIGURES

2.1	A general m-machines, n-bus system	21
2.2	Synchronous machine two-axis model dynamic circuit	22
2.3	IEEE Type-I exciter model	22
2.4	Interconnection of synchronous machine dynamic circuit and the rest of the network	26
2.5	Generalized load electrical dynamic circuit	27
2.6	Static exciter model	33
2.7	WSCC 3-machines, 9-bus system	34
3.1	Simplified one line diagram of SVC	37
3.2	Control characteristic of SVC	38
3.3	Graphical operation of SVC for given system conditions	39
3.4	SVC block diagram	40
3.5	WSCC system with SVC at bus 4	43
3.6	TCSC module	44
3.7	Blocked and Bypassed operating modes of TCSC	45
3.8	Vernier operating modes of TCSC with partial thyristor conduction	45
3.9	Equivalent reactance $X_{TCSC}$ for TCSC	47
3.10	TCSC representation	47
3.11	TCSC power controller	49
3.12	Block diagram of a typical STATCOM	51

3.13	Typical voltage versus current characteristics of STATCOM and SVC	52
3.14	Typical voltage vs. reactive power characteristics of STATCOM and SVC	53
3.15	Voltage-source inverter scheme for STATCOM	54
3.16	Vector diagram of STATCOM operation with losses	55
3.17	Basic six-pulse voltage-source inverter	56
3.18	Modular structure for 48-pulse STATCOM inverter	57
3.19	Equivalent representation of a GTO-diode combination	57
3.20	Equivalent representation of a 48-pulse inverter (a) ac side, (b) dc side	58
3.21	Flow of current in dc side	60
3.22	Series compensation of two-machine system using capacitor and its phasor diagram	66
3.23	Series compensation of two-machine system using SSSC and its phasor diagram	66
3.24	Transmitted power-angle curve for capacitor and SSSC	67
3.25	Block diagram of SSSC	69
3.26	Equivalent representation of a 48-pulse inverter (i) ac side for phase a (ii) dc side	69
3.27	Current flow in dc side	71
4.1	Voltage phasor diagram for a two bus system	81
4.2	Schematic diagram of six-bus test system	84
4.3	LFIs of various line for 6-bus system at base case loading condition	85
4.4	Voltage profile of 6-bus system at base case loading condition	85
4.5	TPSI for APTPs and RPTPs at base case loading condition	86

4.6	Schematic diagram of the 9-bus test system	87
4.7	LFIs of various line for the 9-bus system at base case loading condition	88
4.8	Voltage profile of the 9-bus system at base case loading condition	88
4.9	TPSI for APTP and RPTP at base case loading condition	89
4.10	Schematic diagram of 10-machines, 39-bus system	90
4.11	LFIs of various line for the 39-bus system at base case loading condition	92
4.12	Voltage profile of 39-bus system at base case loading condition	93
4.13	TPSI of APTPs and RPTPs for base case loading condition of 39-bus system	93
4.14	Schematic diagram of 16-machines, 68-bus system	95
4.15	LFIs of various lines for the 68-bus system at base case loading condition	96
4.16	Voltage profile of the 68-bus system at base case loading condition	97
4.17	TPSI of APTPs and RPTPs for base case loading condition of the 68-bus system	97
4.18	LFIs for various lines of the 6-bus system at maximum loading condition	99
4.19	Voltage profile of the 6-bus system at maximum loading condition	100
4.20	TPSI for APTP and RPTP of the 6-bus system at maximum loading condition	101
4.21	Voltage profile of the 6-bus system with SVC at either bus 6 or bus 5 at maximum loadability condition	101
4.22	LFIs for various line of the 9-bus system at maximum loadability condition	102
4.23	Voltage profile of the 9-bus system at maximum loadability condition	102

4.24	TPSI for the 9-bus system at maximum loading condition	103
4.25	LFIs for various lines of the 39-bus system at maximum loading condition	105
4.26	Voltage profile of the 39-bus system at maximum loading condition	106
4.27	TPSI for APTPs and RPTPs at maximum loading condition for 39-bus system	106
4.28	LFIs for the 68-bus system at maximum loading condition	108
4.29	Voltage profile of the 68-bus system at maximum loading condition	109
4.30	TPSI for APTPs and RPTPs for the 68-bus system at maximum loading condition	109
4.31	TPSI for the 68-bus system with SVC at bus 40	112
5.1	Typical TCSC characteristic	116
5.2	Voltage profile of the 9-bus system at base case loading with and without TCSC	117
5.3	Real and reactive power flow over lines with and without TCSC at base case loading condition	118
5.4	Voltage profile of the 9-bus system without and with FACTS devices at maximum loading condition	119
5.5	Step response of the 9-bus system at maximum loading condition	121
5.6	Voltage profile of 9-bus system at maximum loading condition with SVC and with SVC-TCSC both	122
5.7	Voltage profile of 68-bus system at base case loading condition with and without TCSC	126
5.8	Voltage profile of the 68-bus system at maximum loading condition	127
5.9	Step response of the 68-bus system at maximum loading condition	128

5.10	Voltage profile of the 68-bus system at maximum loading condition	129
5.11	Step response of the 68-bus system with SVC-TCSC	131
5.12	Step Response of the 9-bus system at maximum loading condition	134
5.13	Step response of the 68-bus system at maximum and extreme loading conditions	138
5.14	Step response of 68-bus system with and without SSSC at maximum loading condition	139
6.1	Root loci of controller and interarea modes and their corresponding modal damping for varying TCSC $K_I$ ( $K_P = 0$ ) for base case of the 9-bus system with TCSC alone	148
6.2	Root loci of controller and interarea modes and their corresponding modal damping for varying TCSC $K_P$ ( $K_I = 12.4$ ) for base case of the 9-bus system with TCSC alone	149
6.3	Step response with “best” controller parameters and two arbitrary set of controller parameters for base case of the 9-bus system (TCSC alone)	150
6.4	Root loci of controller and interarea modes and their corresponding modal damping for varying TCSC $K_I$ ( $K_P = 0$ ) for mid-loading case of the 9-bus system with TCSC alone	151
6.5	Root loci of sensitive modes and their corresponding modal damping for varying TCSC $K_I$ ( $K_P = 12.1$ ) for mid-loading case of the 9-bus system with TCSC alone	152
6.6	Step response with “best” controller parameters and two other arbitrary set of controller parameters for mid-loading case of the 9-bus system (TCSC alone)	153

6.7	Root loci of controller and interarea modes and their corresponding modal damping for varying TCSC $K_I$ ( $K_P = 0$ ) for maximum loading case of the 9-bus system with TCSC alone	154
6.8	Root loci of controller and interarea modes and their corresponding modal damping for varying TCSC $K_I$ ( $K_P = 12.1$ ) for maximum loading case of the 9-bus system with TCSC alone	155
6.9	Step response with “best” controller parameters and two other arbitrary set of controller parameters for maximum loading case of the 9-bus system (TCSC alone)	156
6.10	Root loci of interarea and controller modes and their corresponding modal damping for varying SVC $K_I$ ( $K_P = 0$ ) for base case of the 9-bus system with SVC alone	161
6.11	Root loci of controller and interarea modes and their corresponding modal damping for varying SVC $K_P$ ( $K_I = 5.9$ ) for base case of the 9-bus system with SVC alone	162
6.12	Step response with “best” and two other arbitrary set of controller parameters for base case of the 9-bus system (SVC alone)	163
6.13	Root loci of controller and interarea modes and their corresponding modal damping for varying SVC $K_I$ ( $K_P = 0$ ) for mid-loading condition of the 9-bus system with SVC alone	164
6.14	Root loci of controller and interarea modes and their corresponding modal damping for varying SVC $K_P$ ( $K_I = 20$ ) for mid-loading condition of the 9-bus system with SVC alone	165
6.15	Step response for “best” controller parameters and two other arbitrary set of controller parameters for mid-loading condition of the 9-bus system (SVC alone)	166

6.16	Root loci of controller and interarea modes and their corresponding modal damping for varying SVC $K_I$ ( $K_P = 0$ ) for maximum loading condition of the 9-bus system with SVC alone	167
6.17	Root loci of controller and interarea modes and their corresponding modal damping for varying SVC $K_P$ ( $K_I = 60$ ) for maximum loading condition of the 9-bus system with SVC alone	168
6.18	Step response with “best” controller parameters and two other arbitrary set of controller parameters for maximum loading condition of the 9-bus system (SVC alone)	169
6.19	Root loci of interarea and controller modes and their corresponding modal damping for varying TCSC $K_I$ ( $K_P = 0$ ) for maximum loading condition of the 9-bus system with SVC-TCSC combine	174
6.20	Root loci of interarea and controller modes and their corresponding modal damping for varying TCSC $K_P$ ( $K_I = 12.8$ ) for maximum loading condition of the 9-bus system with SVC-TCSC combine	175
6.21	Step response for “best” controller parameters and two other arbitrary set of controller parameters for maximum loading condition of the 9-bus system (SVC-TCSC combine)	176



## LIST OF TABLES

2.1	Eigenvalues of WSCC system	35
3.1	Eigenvalues of WSCC system with SVC	43
4.1	Active and Reactive transmission paths for the 6-bus system at base case loading condition	86
4.2	Active and Reactive transmission paths for the 9-bus system at base case loading condition	89
4.3	Corrected voltage drops for reactive power transmission path R4	91
4.4	Corrected voltage drops for active power transmission path A48	98
4.5	Active and Reactive transmission paths for 6-bus system at maximum loading condition	100
4.6	Active and Reactive transmission paths for the 9-bus system at maximum loading condition	103
4.7	Line outages and critical segments for the 68-bus system at base case loading	111
4.8	FACTS devices needed for various systems	112
4.9	Corrected voltage drop in different line segments of path A52	113
5.1	FACTS devices needed for various systems	115
5.2	Eigenvalues with and without TCSC for the 9-bus system at base case loading condition	117
5.3	Eigenvalues of the 9-bus system at maximum loading condition	119
5.4	Eigenvalues of the 9-bus system at maximum loading condition	122
5.5	Eigenvalues of the 9-bus system at base case loading	123
5.6	Eigenvalues of the 9-bus system for extreme loading condition with SVC at bus 5	124

5.7	Eigenvalues for the 68-bus system at base case loading without and with TCSC	125
5.8	Eigenvalues of the 68-bus system at maximum loading condition	127
5.9	Eigenvalues with TCSC alone and with SVC-TCSC at maximum loading condition	129
5.10	Eigenvalues of the 68-bus system at base case loading with floating SVC	130
5.11	Eigenvalues of the 68-bus system	131
5.12	Eigenvalues of the 9-bus system at maximum loading condition	133
5.13	Eigenvalues of the 9-bus system	135
5.14	Eigenvalues of the 68-bus system at maximum loading condition	136
5.15	Eigenvalues of the 68-bus system with SSSC at maximum loading conditions	139
6.1	Eigenvalues with no FACTS device connected at different loading conditions for the 9-bus system	145
6.2	System Eigenvalues with “best” TCSC controller parameters at different loading conditions	157
6.3	System eigenvalues with “best” SVC controller parameters at different loading conditions	170
6.4	System eigenvalues with coordinated SVC-TCSC controller parameters at different loading conditions	177
6.5	TCSC alone at maximum loading condition with different compensation level	178
6.6	SVC-TCSC at maximum loading condition with different compensation level	179

## LIST OF SYMBOLS

$X_d$	Direct axis synchronous reactance (pu)
$X_q$	Quadrature axis synchronous reactance (pu)
$X'_d$	Direct axis transient reactance (pu)
$X'_q$	Quadrature axis transient reactance (pu)
$T'_{do}$	Direct axis transient open circuit time constant (sec.)
$T'_{qo}$	Quadrature axis transient open circuit time constant (sec.)
$H$	Inertia constant (MWs/MVA)
$D$	Damping constant
$E_{fd}$	Voltage proportional to field voltage
$V_{ref}$	Terminal voltage reference setting
$K_A$	Regulator gain (pu)
$T_A$	Regulator amplifier time constant (sec.)
$K_E$	Exciter gain (pu)
$T_E$	Exciter time constant (sec.)
$K_F$	Regulator stabilizing circuit gain (pu)
$T_F$	Regulator stabilizing circuit time constant (sec.)
$\delta$	Generator rotor angle
$\Delta$	Incremental change
APTP	Active Power Transmission Path
RPTP	Reactive Power Transmission Path

## INTRODUCTION

A power system is a complex network comprising numerous generators, transmission lines, transformers and variety of loads. Due to the economic as well as environmental problems associated with adding new transmission lines to keep pace with the growing loads and generation, the major task facing utility industry of today is the proper and efficient utilization of the existing transmission system. One of the approaches adopted for efficient utilization involves the use of power electronics technology.

With the growing demand of electrical power, the existing transmission lines get increasingly overloaded. This increased loading of transmission lines has lead to various problems associated with stability and maintenance of appropriate voltage levels across a system. A reliable solution of these problems can be achieved with the help of FACTS (Flexible Alternating Current Transmission System) devices, which may be connected in series, shunt or in a combination of series and shunt. FACTS devices include a host of fast, reliable solid state controllers such as Static Var Compensator (SVC), Thyristor Controlled Series Capacitor (TCSC), Static Synchronous Compensator (STATCOM), Thyristor Controlled Braking Resistor (TCBR), Thyristor Controlled Phase Shifting Transformer (TCPST), Static Synchronous Series Compensator (SSSC) and Unified Power Flow Controller (UPFC) [1]. However, these devices are effective only when they are placed at carefully determined locations.

There may further be situations where more than one FACTS device is employed in the system for tasks such as voltage stabilization, stability enhancement etc. Their collaborative interaction can play an important role in improving power transfer capability of the network and overall power system stability - both steady state and transient.

After a careful study of several existing techniques, an attempt has been made to evolve a simple strategy for placement of FACTS devices in a multimachine environment in this thesis. A general purpose interactive MATLAB program has been developed for

small signal analysis of multimachine system. Modeling of SVC, TCSC, STATCOM and SSSC is done and the system stability analyzed using the above FACTS devices. Finally, an attempt has also been made to examine the interaction of FACTS devices (SVC and TCSC) and their impact on the system stability utilizing the proposed placement strategy.

A brief review of FACTS controllers (SVC, TCSC, STATCOM and SSSC), their modeling, placement strategies and coordination of different FACTS devices are discussed below.

## 1.1 FACTS CONTROLLERS

The power flow over a transmission line depends mainly on three important parameters, namely voltage magnitude of the buses, impedance of the transmission line and phase angle between buses. The FACTS devices control one or more of the above parameters to improve system performance. As FACTS devices are fabricated using solid state controllers, their response is fast and accurate. Thus these devices can be utilized to improve the voltage profile of the system, enhance transmission capability of the network, augment system stability and achieve several other objectives [1]. IEEE definition of FACTS and FACTS Controller are given as [1]

***Flexible AC Transmission System (FACTS):** Alternating current transmission systems incorporating power electronics based and other static controllers to enhance controllability and increase power transfer capability.*

***FACTS Controller:** A power electronics based system and other static equipment that provides control of one or more AC transmission system parameters.*

In general, FACTS controllers can be divided in following categories

- Series controllers (TCSC, SSSC)
- Shunt controllers (SVC, STATCOM)
- Combined series-series controllers (Interline Power Flow Controller)
- Combined series-shunt controller (Unified Power Flow Controller)

In this thesis we shall concentrate only on the first two types of devices. A brief review of shunt and series devices such as SVC, TCSC, STATCOM and SSSC is presented in next sub-section.

### **1.1.1 Static Var Compensator (SVC)**

According to IEEE-CIGRE co-definition [1], a static var compensator is *a Static var generator whose output is varied so as to maintain or control specific parameters (e.g. voltage) of the electric power system.*

SVC is a first generation FACTS device that is already in operation at various places in the world. In its simplest form it uses a thyristor controlled reactor (TCR) in conjunction with a fixed capacitor (FC) or thyristor switched capacitor (TSC). A pair of opposite poled thyristors are connected in series with a fixed inductor to form a TCR module while the thyristors are connected in series with a capacitor to form a TSC module. An SVC can control the voltage magnitude at the required bus thereby improving the voltage profile of the system. The primary task of an SVC is to maintain the voltage of a particular bus by means of reactive power compensation (obtained by varying the firing angle of the thyristors). It can also provide increased damping to power oscillations and enhance power flow over a line by using auxiliary signals such as line active power, line reactive power, line current, computed internal frequency etc [2, 3].

### **1.1.2 Thyristor Controlled Series Capacitor (TCSC)**

A TCSC is *a capacitive reactance compensator, which consists of a series capacitor bank shunted by a thyristor controlled reactor in order to provide a smoothly variable series capacitive reactance* [1].

Even though a TCSC in the normal operating range is mainly capacitive, but it can also be used in an inductive mode. The power flow over a transmission line can be increased by controlled series compensation with minimum risk of subsynchronous resonance (SSR) [1]. TCSC is a second generation FACTS controller, which controls the

impedance of the line in which it is connected by varying the firing angle of the thyristors. A TCSC module comprises a series capacitor that is connected in parallel to a thyristor controlled reactor (TCR). A TCR includes a pair of anti-parallel thyristors that are connected in series with an inductor. In a TCSC, a metal oxide varistor (MOV) along with a bypass breaker is connected in parallel to the fixed capacitor for overvoltage protection. A complete compensation system may be made up of several of these modules.

The TCSC has three basic modes of operation

- Thyristor valve bypassed mode
- Thyristor valve blocked mode
- Vernier control mode

In the bypassed mode thyristors are gated for full conduction and the current flow in the reactor is continuous and sinusoidal. In this case the net reactance is slightly inductive because the susceptance of reactor is larger than that of the capacitor. This mode is mainly used for protecting the capacitor against the overvoltages (during transient overcurrents in the line). In the inserted mode with thyristor blocked, no current flows through the valve as the gate pulses are suppressed. In this mode, the TCSC reactance is the same as that of the fixed capacitor. This mode is also termed as waiting mode. In vernier control, thyristors are gated in such a manner that a controlled amount of inductive current can circulate through the capacitor thereby increasing effective capacitive/inductive reactance of the module. The thyristor bypass mode is used to provide control and protective measures. The breaker is generally provided to remove TCSC from service when there are internal TCSC failures.

Initial experience with TCSC installation has been favorable. A TCSC has been installed on the American Electric Power (AEP) 345 kV system in 1991 and another on the Western Area Power Administration (WAPA) 230 kV system in northeastern Arizona at the Kayenta substation in 1992. A third TCSC has been connected to the BPA 500 kV system at Slatt in 1993 for power flow control and improvement of system performance.

### 1.1.3 Static Synchronous Compensator (STATCOM)

*A STATCOM is a static synchronous generator operated as a shunt connected static var compensator whose capacitive or inductive output current can be controlled independent of the ac system voltage [1].*

A STATCOM is a solid state switching converter capable of generating or absorbing independently controllable real and reactive power at its output terminals, when it is fed from an energy source or an energy storage device of appropriate rating. A STATCOM incorporates a voltage source inverter (VSI) that produces a set of three phase ac output voltages, each of which is in phase with, and coupled to the corresponding ac system voltage via a relatively small reactance. This small reactance is usually provided by the per phase leakage reactance of the coupling transformer. The VSI is driven by a dc storage capacitor. By regulating the magnitude of the output voltage produced, the reactive power exchange between STATCOM and the ac system can be controlled. That is, if the amplitude of the output voltage is increased above that of the ac system voltage, then the current flows through the reactance from the STATCOM to the ac system, and the STATCOM generates reactive (capacitive) power for the ac system. On the other hand, if the amplitude of the output voltage is decreased below that of the ac system, then the reactive current flows from the ac system to STATCOM, and the STATCOM absorbs the reactive (inductive) power. If the output voltage is equal to the ac system voltage, the reactive power exchange is zero [1, 4, 6].

The first high-power STATCOM in the United States was commissioned in late 1995 at the Sullivan substation of the Tennessee Valley Authority (TVA).

### 1.1.4 Static Synchronous Series Compensator (SSSC)

*An SSSC is a static synchronous generator operated without an external electric energy source as a series compensator whose output voltage is in quadrature with, and controllable independently of, the line current for the purpose of increasing or decreasing the overall reactive voltage drop across the line and thereby controlling the*



*transmitted electric power. The SSSC may include transiently rated energy source or energy absorbing device to enhance the dynamic behavior of the power system by additional temporary real power compensation, to increase or decrease momentarily, the overall real voltage drop across the line [1].*

An SSSC incorporates a solid state voltage source inverter that injects an almost sinusoidal voltage of variable magnitude in series with a transmission line. The SSSC has the same structure as that of a STATCOM except that the coupling transformer of an SSSC is connected in series with the transmission line. The injected voltage is mainly in quadrature with the line current. A small part of the injected voltage, which is in phase with the line current, provides the losses in the inverter. Most of the injected voltage, which is in quadrature with the line current, emulates a series inductance or a series capacitance thereby altering the transmission line series reactance. This emulated reactance, which can be altered by varying the magnitude of injected voltage, favorably influences the electric power flow in the transmission line [7-8].

## **1.2 MODELING OF FACTS DEVICES**

### **1.2.1 SVC Modeling**

As SVC is the first generation FACTS device, a vast literature is available on this device and its applications [3]. However a brief literature review on SVC modeling is presented here.

An exhaustive information on modeling of SVC for load flow, harmonic analysis, stability and transient overvoltage studies has been provided in [5]. The general SVC model proposed in [5] is modified in [9] to include the control system delays. In [5, 9] TCR dynamics has been ignored. SVC has also been represented by various transfer functions [10, 11]. Detailed dynamic modeling of SVC for damping torque analysis is presented in [2]. A simplified model of SVC is presented in [12, 13]. Various SVC models for power flow simulation with proper representation of limits and SVC slope are presented in [14]. Dynamic models of SVC with modular structure are also presented in [14].

### 1.2.2 TCSC Modeling

TCSC controller design based on linearized model of the power system around a given nominal operating point is given in [15]. In [16-17] TCSC model of [15] has been used for enhancement of power system stability. The pole placement technique is utilized for calculating the controller feedback gains. Optimum location for installation of TCSC based on damping enhancement criterion is proposed using residue method. Reference [18] describes TCSC model and its controls (constant line power controller and constant angle controller) in a tutorial manner. Steady state model of TCSC has been described in [19].

Several TCSC models have been developed utilizing sampled data approach [20-23]. A discrete time domain TCSC model based on the linearized behavior of the state transition equation that can predict the shift in zero-crossings of the line current (or capacitor voltage) precisely is proposed in [20]. This model captures the system transient behavior very accurately. A method for computing the eigenvalues of the system in discrete time domain is also presented in [21]. However the model developed in [21] does not present a stand alone TCSC model. The system equations are developed with and without representing the thyristor switching through Poincare map. This approach requires sampling of full state at every sampling instant which is impractical for large power systems. Another model based on sampled data approach is described in [22]. Poincare map is also utilized in [24] to analyze the stability of two synchronization schemes for TCSC.

In [23] the TCSC dynamics is described at the switching instants and then converted into a continuous time model. This model assumes the line current as the forcing function of the TCSC performance equation and therefore is an independent quantity.

The models developed in [20-23] predict the system behavior very well and also offer an analytical basis for control design. However the model derivation is relatively complicated and the model structure has no clear relation to the system configuration. The models also do not interface well with the standard phasor-based models of the generator dynamics. A quasi state TCSC model based on phasor dynamics approach is

presented in [24]. The phasor dynamic model of TCSC is based on time varying Fourier coefficients, which capture the phasor dynamics of the TCSC. As the model is modular, it can be incorporated easily with other power system components.

### 1.2.3 STATCOM Modeling

In broad spectrum the STATCOM utilizes either multilevel [25-29] or multi-pulse [30-31] voltage source inverter configurations. The multilevel inverter usually synthesizes a staircase voltage wave from several levels of dc voltage source, typically obtained from capacitor voltage sources. As the number of level increases, the synthesized staircase wave approaches the sinusoidal wave resulting in reduced harmonic distortions. A multi-pulse inverter also generates a staircase wave closely resembling a sine wave by connecting a number of 6-pulse inverters through transformers. Usually switches of these inverters are synchronized with the ac bus voltage in which the firing of each switch is displaced by a constant amount from the zero crossing of the ac bus voltage. A multi-pulse inverter can also implement PWM switching technique for power transfer applications [32]. The mathematical model for 12-pulse STATCOM is derived in [30] and nonlinear state feedback control strategy has been used for the control of reactive power. The development and installation of a  $\pm 100$  MVAR STATCOM for the Tennessee Valley Authority (TVA) at the Sullivan substation in North-Eastern Tennessee is presented in [33]. The operation of this STATCOM is presented in [34]. The application of STATCOM for enhancement of power transfer in long lines is presented in [35]. A case study has also been presented to show the superiority of STATCOM over other shunt reactive compensation schemes. In [31] the model developed in [30] is utilized and a closed loop reactive current controller for the control of voltage at the mid-point of a long transmission line is proposed. It is reported that a fuzzy logic PI controller overcomes the problem of oscillatory instability.

#### **1.2.4 SSSC Modeling**

The design and control of 48-pulse SSSC is presented in [36, 37]. The investigations are carried out on IEEE first benchmark model for SSR studies to evaluate the performance of SSSC during balanced and unbalanced faults. The results of small signal analysis are validated using PSCAD/ EMTDC software. References [7-8] present basic theory, characteristics and modeling technique of 24-pulse SSSC using Electromagnetic Simulation Package (EMTP). Some results of TNA simulation studies carried out with SSSC hardware model are also presented. An EMTP model of a series connected solid state synchronous voltage source is presented in [38]. This is used to control and modulate the power flow of long transmission line.

### **1.3 PLACEMENT STRATEGY OF FACTS DEVICES**

For optimum use of generation and transmission resources and to enhance system angle and voltage stabilities, placement of a FACTS device at proper locations is crucial. Placing a high rating FACTS device at an inappropriate location may not be quite effective in improving the performance of the system. On the other hand, even a device of small rating, when placed at an appropriate location, can be greatly beneficial. Hence, however good the control strategy may be, an optimum performance can be achieved only when the FACTS device is strategically placed. A brief review of the placement of FACTS devices is presented below.

The placement of Static Var Compensators for transient stability enhancement is discussed in [39]. It is reported that in a transmission line the location of load and the relative inertia of the generators have a significant influence on the placement of the SVC for best stability enhancement. Also, in general, the best location from transient stability considerations is not the same as the optimal location for minimizing losses in steady state, and hence a compromise is necessary. A criterion based on machine acceleration for determining the location of a Static Var Compensator for transient stability improvement is presented in [40].

Transfer function residue technique for finding suitable locations for Static Var Compensators (SVC) is presented in [41] to demonstrate the efficacy of the proposed

technique for a two-area system. Residue method together with modal sensitivities is applied in [42] to determine the location, feedback signal and controller design of TCSC for improving the damping of the inter-area oscillations of a 3-area, 6-machine system. Modal controllability and observability has been used in [43] to determine the effective locations for TCSC damping controller.

Voltage stability analysis of large power systems using modal analysis technique has been proposed in [44]. The applicability of the approach is presented for a 3700 bus test system. Modal analysis through bus, branch and generator participation factors provide useful information, which can be utilized for placement of a FACTS device [45]. Bus participation factors have been utilized for determination of the most suitable sites in [46].

Various optimization techniques have also been used for determination of suitable location for FACTS device to improve the voltage profile and damping of the system. A hybrid optimization scheme using the simulated annealing and Lagrange multiplier technique for optimal SVC placement and voltage stability enhancement is presented in [47]. This optimization method incorporates all system constraints and nonlinearities. Genetic algorithm has been used to find optimal location of series FACTS devices based on system loadability, the real power losses and the maximum power exchange between a producer-consumer pair in [48]. A systematic method of worst case identification of reactive power margin and the most vulnerable busbar by incorporating genetic algorithm (GA) and nonlinear programming is proposed in [49]. This most vulnerable busbar could be the probable place for the placement a FACTS device.

Simulated annealing method has been used for contingency constrained optimal VAR source planning in large power system in [50]. The solution methodology determines the location, type, size and the settings of the VAR sources at different loading conditions. The methodology is applied for IEEE-30 bus system and Tai-Power Company system comprising 358 buses and 439 branches. A computer package based on extended simulated annealing technique and the  $\epsilon$ -constraint method for multiobjective VAR planning in a large scale power systems is presented in [51]. In [52-53] an eigensolution free method of reduced order modal analysis to select the location of FACTS based stabilizers is presented.

Several indices have been proposed in the literature for placement of FACTS devices. A method of identifying the critical bus based on voltage stability index is proposed in [54]. The bus with highest index is the critical bus in the network. This method does not consider the operating conditions of the system equipment e.g. the VAR limit of the generators etc. In [55] two methods (relative voltage change method and sensitivity method) for determination of weak buses and segments in a power transmission network are presented. A scalar index termed as Location Index for Effective Damping (LIED) based on modal controllability for finding the suitable location of SVC and variable series capacitor has been proposed in [56]. In [57] Damping Torque Analysis (DTA) index is presented and compared with various indices such as LIED [56], residue index [41], participation index [58] etc.

A voltage stability indicator based on the changes in the Jacobian submatrix is proposed in [59]. The changes are observed as the partial derivative of the reactive power with respect to the voltage at the load busbars. In [60] static voltage stability margin index is proposed, which is based on the sensitivity of the Jacobian matrix. The voltage stability margin index determines whether a system is stable or not. Also the busbars with smaller value of voltage stability margin index are considered to be critical from voltage stability viewpoint. An analytical method for identification of weak segment of a power system from voltage stability viewpoint is presented in [61]. The proposed method is compared with three established methods [54, 59-60] and shows its superiority over these established methods. Identification of critical path from voltage stability viewpoint has been proposed in [62].

Voltage Collapse Proximity Indicator (VCPI) has been used for identification of the weak buses in [63]. These weak buses are then utilized to enhance the system security margin using goal attainment method based on simulated annealing approach. A static voltage stability index based on minimum singular value of the power flow Jacobian to find out critical buses from voltage instability point of view has been proposed in [64-65].

Generator reactive power sensitivities with respect to reactive compensation for choosing reactive compensation locations to improve system steady state stability is proposed in [66]. The effectiveness of the proposed strategy is demonstrated for Saudi

Consolidated Electric Company (SCECO)-Central Power System operating at light load condition. In [67] a method for locating SVC is proposed using voltage sensitivity calculations for 39-bus New England system. Results for Wale and Hale 6-bus system and IEEE 30-bus system with L-index and V-Q sensitivity for four different corrective schemes, viz., transmission path, reactive compensation, load shedding and generation voltage and reactive path schemes are presented in [68]. A fast and efficient algorithm for placement of SVC in a power system for small signal stability improvement is presented in [69].

Linear programming has been used to gain insight of the impact of FACTS devices on the secure-economic operation of power system. It was found that the location of the FACTS device has an important influence on the system loadability, power exchange capability and system vulnerability to line outage [70].

In [71] it has been demonstrated that significant benefits in the dynamic stability improvement of power systems can be obtained by reactive power modulation in response to a local control signal derived from bus frequency. The effect of reactive power modulation is dependent on the location of SVC in a multimachine system. A simple method based on eigenvalue sensitivity is proposed for the prediction of location of SVC for improving the dynamic stability of a multimachine system. The effect of static compensation on voltage stability boundary is studied in [72]. Sensitivity method has been used for reactive support allocation whereas minimum singular value of Jacobian has been used as indicator of stability margin [72]. A tool based on the eigenvalue sensitivity to study the location and controller design of controllable series capacitors for power system electromechanical oscillation is presented in [73].

A theory based on equal angle criterion to improve power system damping by the application of SVC is proposed in [74]. The location of SVC is proposed on the basis of P- $\delta$  curve. The best SVC location to increase the damping is the one where a SVC would have the largest effect on the system P- $\delta$  curve.

Tangent vector has also been used to identify the critical bus [75]. The sensitivity matrices are also proposed on the basis of the critical bus for control action determination to avoid voltage collapse situation. The results are demonstrated for IEEE-300 bus test system with and without reactive power limit considerations.

In [76], a methodology for the calculation of the eXtreme Loading Condition (XLC) of power system using secant method is proposed. The XLC is reached when any one of the load buses reaches its maximum value. The bus where the load has reached its maximal value is viewed as the weakest from voltage stability view point. This bus can be considered for further remedial actions.

Determination of location of FACTS devices is a planning strategy. Extensive literature is available on the reactive power planning which utilizes various techniques such as zero-one implicit enumerative method [77], linear programming based decomposition method [78], mixed integer programming [79], unified approach for P and Q optimization [80], capability chart of the power system [81]. An expert system based algorithm for VAR planning is presented in [82]. Two expert system modules have been used. The first one analyzes the operating condition and the second one suggests the control actions for the existing VAR controllers, and location and sizes of new VAR controllers to be installed. This approach has been applied for IEEE-30 bus system.

An algorithm for identifying bus clusters (control areas) based on controllability and observability of the reactive power voltage dynamics ( $\partial Q/\partial V$ ) and real power angle dynamics ( $\partial P/\partial \theta$ ) is proposed in [83]. These areas can emerge as suitable locations for placing the compensation devices. A methodology to analyze the effect of FACTS devices on the transmission charges and on the production costs is presented in [84]. It has been demonstrated that installation of FACTS devices changes the transmission charges for each wheeling agent. Therefore both transmission owners and transmission users should take in to account the impact of FACTS device on transmission charges [84].

Various guidelines for placement of FACTS devices for attaining different objectives such as prevention of loop flows, creation of an electronic fence and ensuring economic operation are given in [85].

#### 1.4 COORDINATION OF FACTS DEVICES

In a practical power system, there could be number of different FACTS devices installed, which may cause interaction between them. This is more likely to be true in



foreseeable future in the deregulated environment. These multiple FACTS devices have the potential to interact with each other. This interaction may either deteriorate or enhance system stability depending upon the chosen controls and their placement. Hence there is a need to study the interaction between the FACTS devices.

Linear techniques for the control design of multiple SVCs along a transmission line have been used in [86]. Different voltage control strategies have been investigated and it has been found that centralized control strategy and its performance is superior to the traditional individual bus voltage control strategy. However the control strategy proposed is heavily dependent on telecommunicated data and redundancy must be provided for adequate reliability. It has also been found that the telecommunication delays (upto 50ms) in the remote signal feedback does not cause adverse effects on the dynamic performance of the system.

A fuzzy modeling approach to a coordinated control of voltage and reactive power in order to enhance voltage security of power system is presented in [87]. The results of the proposed approach shows that coordinated control of available voltage control devices leads to more secure system operating condition. The proposed approach uses combination of heuristic rules and linear equations.

The potential of control interaction between a proposed TCSC and an existing SVC in New York state's 345kV and 765kV transmission system is studied in [88]. The results indicate that a control interaction exists between the voltage input PSDC (Power Swing Damping Control) of the TCSC, the series compensated ac system resonance and the SVC controls. The study reveals that there is a need of a high frequency filter on the PSDC input signal. The study also shows that using synthesized angle difference input signal, no interaction exists between the PSDC of TCSC, series compensated ac network resonance and the SVC.

Two methods based on decentralized optimal control and pole placement for determining globally coordinated settings of PSS and FACTS devices' supplementary signals are presented in [89]. Three FACTS devices SVC, TCSC and Phase Shifter are considered in 13-machines, 77 bus equivalent system for the Southern Brazil Interconnected Network. The proposed approach does not explicitly consider robustness as a design requirement.

The damping of inter-area and local electromechanical oscillation modes using controllable series capacitor (TCSC) and controllable shunt capacitor (SVC) is presented in [90]. It has been found that a TCSC and an SVC do not have the same effect on damping of the local modes. It is shown that TCSC exhibits more effective damping than SVC for inter-area modes.

An approach based on the combined static/dynamic procedure is proposed in [91]. This approach uses continuation power flow, an optimal power flow and an eigenvalue analysis package for identifying the most effective FACTS controllers, their locations, types and ratings that increase the asset utilization of power system. The proposed method is tested on a system composed of 131 buses, 29 generators and 2 HVdc links. Using this approach 3 new SVCs and 2 new TCSCs were proposed. The study also reveals that a cooperative control action between the proposed SVC and TCSC devices is an efficient solution to solve the inter-area stability problem. The SVCs sustained the system voltages, avoiding the voltage collapse situation, while the TCSC devices supplied the necessary synchronizing torque to maintain electromechanical stability of the system. The study also shows that in a large network, with several embedded SVCs, no control interaction occurs if the SVCs are connected through high transfer impedance. It has found that in stiff ac systems, no interaction is found regardless of the electrical distance between the devices. However under low short circuit capacity condition, the SVC controllers experience a strong interaction.

An integrated methodology (FACTS-Optimal Power Flow) for assessing the behavior of FACTS controllers within the framework of economic power system studies is presented in [92]. The non-linear TCSC, IPC and UPFC models are incorporated directly in the Hessian-Jacobian matrix of Newton's method. The FACTS-OPF algorithm uses multiplier method and determines the level of active power to be regulated by a FACTS device such that it leads to more economical solution [92].

The coordinated control action of a TCSC and TCPAR (Thyristor Controlled Phase Angle Regulator) to increase power transfer and system damping using modal control theory is proposed in [93]. In [94] a Coordinated Damping Optimal (CDO) controller to design and implement multiple TCSC devices in a transmission network of interconnected power system is proposed. The proposed CDO controller shows its

effectiveness to damp inter-area oscillation and to enhance power system damping during large disturbances. The CDO controllers are validated using real time simulation studies using PSCAD/RTDC software packages.

Global parameter setting method for power damping control of multi-FACTS devices is presented in [95]. In NETOMAC (Network Torsion Machine Control) simulation program non-linear optimization technique has been used for minimizing overall power swings under transient conditions. With all nonlinearities considered, the relevant control parameters of FACTS and PSS (Power System Stabilizer) can be determined. The setting procedure is such that it avoids all possible negative interactions among FACTS controllers and achieves maximum damping effects. The proposed method is demonstrated on a 3-area interconnected power system in which a TCSC, an SVC and three PSS are in operation. The proposed method is complex and requires the full information of the system, but it shows that a coordinated setting of FACTS controllers is necessary to improve system stability [95].

A comprehensive annotated bibliography of FACTS devices modeling, placement, control, coordination including a list of major FACTS installations in the world is presented in [96].

## **1.5 OBJECTIVES AND SCOPE OF THE THESIS**

It clearly emerges from the study of the available literature on the FACTS devices that a proper placement strategy must precede the installation of any such device to obtain optimum system performance.

The techniques for determining the best location of FACTS devices can be classified in the four following categories

- (i) Jacobian based sensitivity methodologies [72, 44]
- (ii) Non-Jacobian based techniques [61, 62]
- (iii) Eigenanalysis based methods [42, 43]
- (iv) Optimization and Artificial Intelligence based techniques [47-50]

Placement techniques (iii) and (iv) are complex, detailed and computationally time intensive but are certainly accurate. Techniques (i) and (ii) are comparatively simpler and are shown to be reasonably accurate even though they do not consider system dynamics as in (iii) and system nonlinearities as in (iv). Between (i) and (ii) the non-Jacobian based techniques are simpler and less time consuming. The main objective of this thesis is therefore chosen to evolve an efficient non-Jacobian placement strategy, which is less time consuming yet accurate.

Once the location of a FACTS device is chosen, its performance can be evaluated. A study of the implication of adding various devices in multimachine environment requires an appropriate mathematical model of the system and FACTS devices. Commercial packages such as PEALS (Program for Eigenvalue Analysis of Large Systems), EPRI-ETMSP (Extended Transient/Midterm Stability Program), EPRI-LTSP (Long Term Stability Program), PSS/E (PTI's Power System Simulator for Engineers) exist for the analysis of a power system, although these are not so easily available in educational institutions. Further there is a need for a versatile small signal stability program which offers the flexibility of modeling different FACTS devices both individually as well as in different combinations. For this purpose a comprehensive general purpose program is required. For convenience this program may be developed in MATLAB on the same lines as given in [97]. The methodology presented in [97] is restrictive and must be extended to incorporate various FACTS devices and their controls to varying levels of complexity such that it can be used to study both small signal stability and voltage stability of an electric power system. The developed program then may be used for the determination of best possible location using various indices. Finally, to be at ease with the optimal placement of two or more FACTS controllers in a multimachine power system, the control interaction between these devices must also be studied.

Based on the above discussion, the objectives of the thesis are

1. To develop a methodology for placement of FACTS devices

2. To develop a general versatile MATLAB software package, which can incorporate various FACTS devices in multimachine environment for small signal stability analysis.
3. To examine the developed placement methodology for FACTS devices with the software package developed
4. To study the impact of the coordinated control of FACTS devices on the system performance.

## 1.6 OUTLINE OF THE THESIS

In Chapter 2, a multimachine model is developed using MATLAB (version 5.3) [98] on the same lines as given in [97]. The developed MATLAB software package for multimachine system is interactive and general in nature. The results obtained through the developed package are compared with the published result [97] for the 9-bus WSCC system. It has been found that both the results match very closely.

In Chapter 3, various FACTS device models such as SVC, TCSC, STATCOM and SSSC are developed. The models are incorporated in the developed MATLAB program in modular fashion. Multiple FACTS device incorporation in multimachine environment is also shown in Chapter 3.

Chapter 4 deals with the proposed placement strategy of FACTS device in multimachine environment. A novel technique called EVPA (Extended Voltage Phasors Approach) is proposed. The performance of EVPA is evaluated for four systems (6-bus, 9-bus, 39-bus and 68-bus system) at various loading conditions. The results thus obtained for various systems at different loading conditions are compared with established Line Flow Index Method [61]. The performance of EVPA is also evaluated for various system contingencies. Placement strategy for multiple devices using EVPA is also discussed in Chapter 4.

In Chapter 5, a small signal analysis of above mentioned four systems is done using EVPA technique at various loading conditions. The developed MATLAB program is used for small signal stability analysis. The results of the small signal stability are validated through step response investigations.

Chapter 6 deals with the study of coordinated control of FACTS devices. The coordinated control SVC and TCSC are studied for the 9-bus system at various loading conditions. The interaction between SVC and TCSC has also been studied with varying levels of series compensation. Root loci, modal analysis methods and step response studies have been used to determine the controller parameters and to visualize the impact of coordinated control of FACTS devices on system stability.

The thesis concludes in Chapter 7, which outlines major contributions and also suggests scope of future work in this area.

## MULTIMACHINE MODELING

A study of the implication of adding various devices in multimachine environment requires an appropriate mathematical model of the system and FACTS devices. There are commercial packages such as PSCAD/EMTDC and EMTP for transient simulation, PEALS (Program for Eigenvalue Analysis of Large Systems), EPRI-ETMSP (Extended Transient/Midterm Stability Program), EPRI-LTSP (Long Term Stability Program), PSS/E (PTI's Power System Simulator for Engineers) available for the analysis of a power system. However to get insight into modeling of multimachine power system, a comprehensive dynamic model of multimachine power system is developed in this chapter on the same lines as given in [97] using MATLAB 5.3. This multimachine dynamic model can be used to study both small signal stability and voltage stability of an electric power system.

The overall system model and the corresponding MATLAB program development consists of two stages

- 1) Development of multimachine system model
- 2) Development of FACTS device models and their integration in the multimachine system model

Stage 1 modeling is discussed in this chapter while stage 2 modeling is presented in Chapter 3.

The multimachine system model with two-axis representation of each machine can be developed with two types of exciter models

- Rotating exciter
- Static exciter

A detailed modeling of multimachine system with rotating exciter (IEEE type-I) is presented first. It is referred as Model-I. Thereafter the necessary modifications to incorporate static exciters in the overall system model are outlined in Model II.

The methodology describes dynamic modeling of a general m-machine, n-bus system. Based on this methodology, a small signal stability program has been developed using MATLAB 5.3. The program developed is general and interactive. The results of the developed MATLAB program are correlated with the results published in [97].

## 2.1 MODEL-I

A general m-machine, n-bus system is depicted in Fig. 2.1. In this figure, 1 to m are generator buses while m+1 to n are load buses. Bus 1 is assumed to be the slack bus. In this model, a machine is represented by a two-axis model and the excitation system is chosen as the IEEE type-I rotating exciter. This modeling utilizes original Park's transformation [100]. Two-axis synchronous machine model dynamic circuit and IEEE type-I exciter model are shown in Figs. 2.2 and 2.3 respectively.

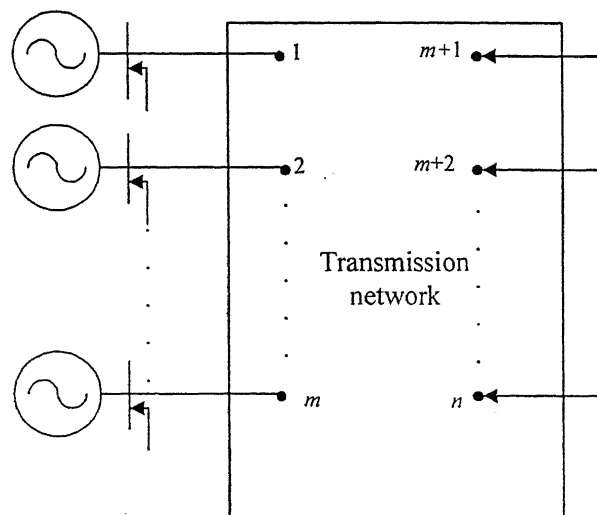
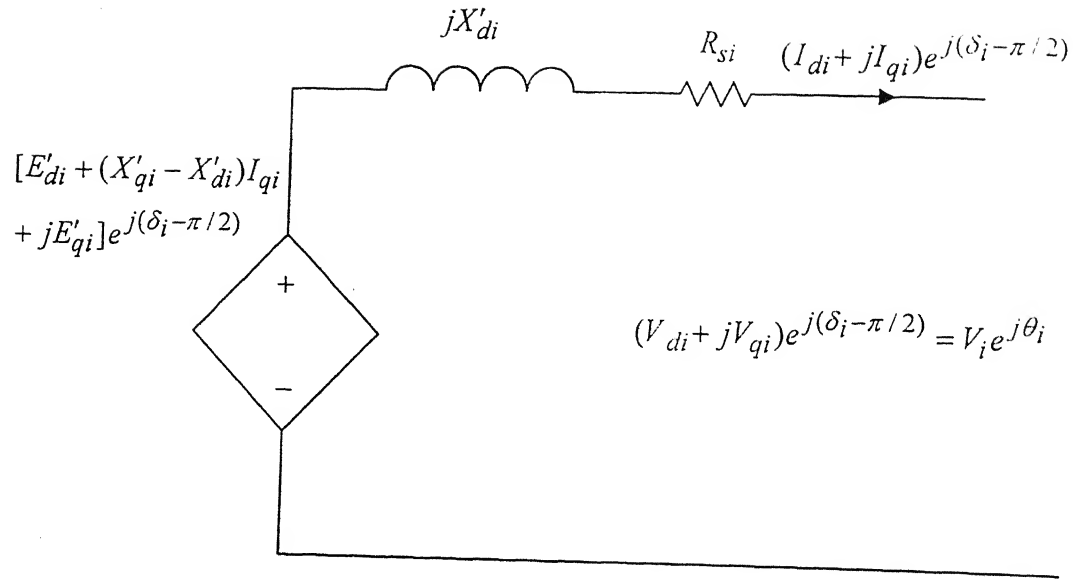
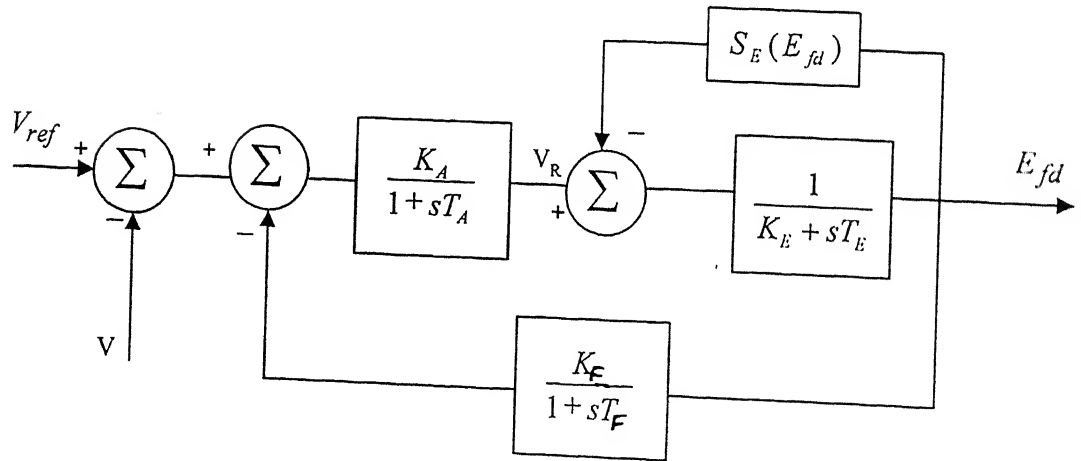


Fig. 2.1 A general m-machines, n-bus system





**Fig. 2.2** Synchronous machine two-axis model dynamic circuit ( $i = 1, 2, \dots, m$ )



**Fig. 2.3** IEEE Type-I exciter model

### 2.1.1 Differential-Algebraic-Equation (DAE) for Model -I

The Differential-algebraic equation model consists of

- Differential equations pertaining to machine and exciter dynamics
- Algebraic equations corresponding to the stator and network equations

As the model contains both differential and algebraic equations, therefore it is referred as Differential-Algebraic Equation (DAE) Model.

Two-axis model of the synchronous machine has been developed with following assumptions

- Subtransient reactances and saturation are negligible.
- Turbine-governor dynamics are negligible.
- The limiting constraints on exciter input voltage  $V_{Ri}$  are not present.
- The damping term is linear, i.e.,  $T_{F\omega i} = D_i(\omega_i - \omega_s)$ , where  $D_i$  and  $\omega_i$  are damping constant and speed of machine  $i$  respectively and  $\omega_s$  is the synchronous speed. This assumption is normally considered valid only for small deviations about an operating point.

Various differential-algebraic equations for m-machine, n-bus system with IEEE type-I exciter are [97]

#### *Differential equations*

$$\frac{d\delta_i}{dt} = \omega_i - \omega_s \quad i = 1, 2, \dots, m \quad (2.1)$$

$$\frac{d\omega_i}{dt} = \frac{T_{Mi}}{M_i} - \frac{[E'_{qi} - X'_{di}I_{di}]I_{qi}}{M_i} - \frac{[E'_{di} + X'_{qi}I_{qi}]I_{di}}{M_i} - \frac{D_i(\omega_i - \omega_s)}{M_i} \quad i = 1, 2, \dots, m \quad (2.2)$$

$$\frac{dE'_{qi}}{dt} = \frac{-E'_{qi}}{T'_{doi}} - \frac{(X_{di} - X'_{di})I_{di}}{T'_{doi}} + \frac{E_{fdi}}{T'_{doi}} \quad i = 1, 2, \dots, m \quad (2.3)$$

$$\frac{dE'_{di}}{dt} = \frac{-E'_{di}}{T'_{qoi}} + \frac{(X_{qi} - X'_{qi})I_{qi}}{T'_{qoi}} \quad i = 1, 2, \dots, m \quad (2.4)$$

$$\frac{dE_{fdi}}{dt} = \frac{-K_{Ei} + S_E(E_{fdi})}{T_{Ei}} E_{fdi} + \frac{V_{Ri}}{T_{Ei}} \quad i = 1, 2, \dots, m \quad (2.5)$$

$$\frac{dV_{Ri}}{dt} = \frac{-V_{Ri}}{T_{Ai}} + \frac{K_{Ai}R_{Fi}}{T_{Ai}} - \frac{K_{Ai}K_{Fi}}{T_{Ai}T_{Fi}} E_{fdi} + \frac{K_{Ai}(V_{refi} - V_i)}{T_{Ai}} \quad i = 1, 2, \dots, m \quad (2.6)$$

$$\frac{dR_{Fi}}{dt} = \frac{-R_{Fi}}{T_{Fi}} + \frac{K_{Fi}E_{fdi}}{(T_{Fi})^2} \quad i = 1, 2, \dots, m \quad (2.7)$$

Equations (2.1-2.4) pertain to the two-axis model of synchronous machine while (2.5-2.7) are differential equations for IEEE type-I exciter.

### ***Algebraic equations***

The algebraic equations consist of stator algebraic equations and network equations. The stator algebraic equation directly follows from the dynamic equivalent of circuit of Fig. 2.2. Machine-Network transformation is given in Appendix A.1.

### Stator algebraic equation

$$0 = V_i e^{j\theta_i} + (R_{si} + jX'_{di})(I_{di} + jI_{qi})e^{j(\delta_i - \pi/2)} - [E'_{di} + (X'_{qi} - X'_{di})I_{qi} + jE'_{qi}]e^{j(\delta_i - \pi/2)} \quad i = 1, 2, \dots, m \quad (2.8)$$

Separating into real and imaginary parts we get

$$E'_{di} - V_i \sin(\delta_i - \theta_i) - R_{si}I_{di} + X'_{qi}I_{qi} = 0 \quad i = 1, 2, \dots, m \quad (2.9)$$

$$E'_{qi} - V_i \cos(\delta_i - \theta_i) - R_{si}I_{qi} - X'_{di}I_{di} = 0 \quad i = 1, 2, \dots, m \quad (2.10)$$

These algebraic equations can be represented as a current dependent voltage source at the generator buses as shown in Fig. 2.2.

### ***Network equations***

The synchronous machine dynamic circuit, together with the static network and the loads, and generalized load electrical dynamic circuit are shown in Figs. 2.4 and 2.5 respectively. The network equations in complex form are

### Generator buses

$$P_{Gi} + jQ_{Gi} \triangleq V_i e^{j\theta_i} (I_{di} - jI_{qi})e^{-j(\delta_i - \pi/2)} + P_{Li}(V_i) + jQ_{Li}(V_i) \\ = \sum_{k=1}^n V_i V_k Y_{ik} e^{j(\theta_i - \theta_k - \alpha_{ik})} \quad i = 1, 2, \dots, m \quad (2.11)$$

where  $P_{Gi} + jQ_{Gi}$  is the complex power 'injected' into bus  $i$  by the generator.

### Load buses

$$P_{Li}(V_i) + jQ_{Li}(V_i) = \sum_{k=1}^n V_i V_k Y_{ik} e^{j(\theta_i - \theta_k - \alpha_{ik})} \quad i = m+1, \dots, n \quad (2.12)$$

where  $P_{Li}(V_i) + jQ_{Li}(V_i)$  are complex power supplied at the load buses. This power is voltage dependent.

Equations (2.11) and (2.12) are the real and reactive power balance equations at all the  $n$  buses. Equation (2.11) shows the interaction of the algebraic variables and the state variables  $\delta_i$ ,  $E'_{qi}$ , and  $E'_{di}$ . In (2.12)  $P_{Li}$  and  $Q_{Li}$  are treated as “injected” powers, this implies that  $P_{Li}$  and  $Q_{Li}$  will be negative for passive load.

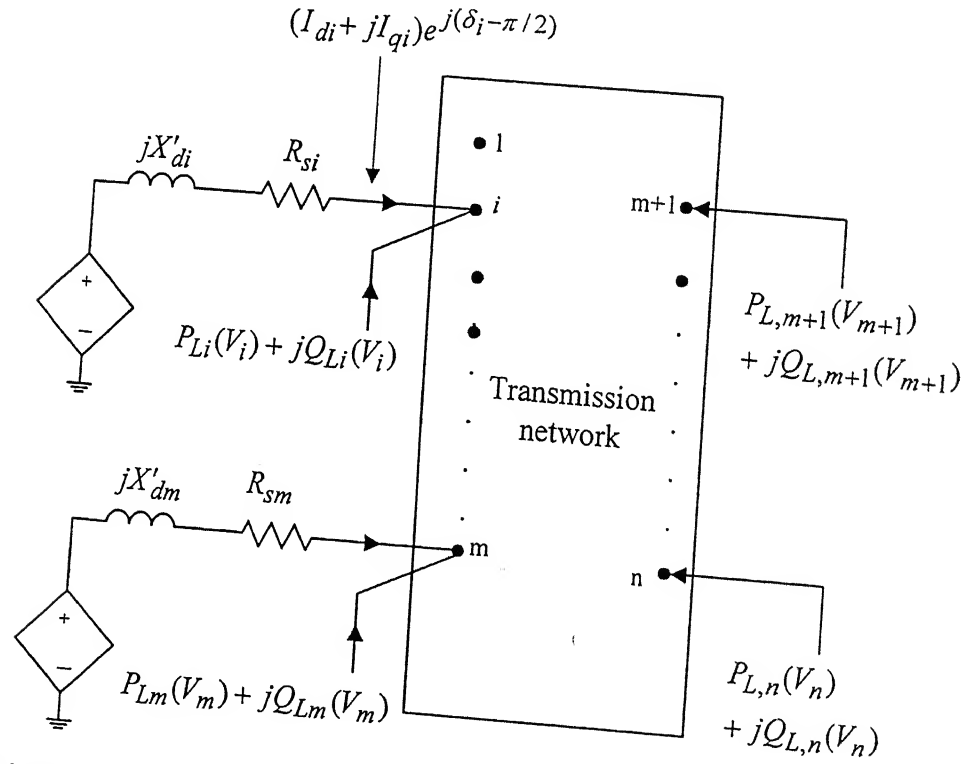


**Fig. 2.4** Interconnection of synchronous machine dynamic circuit and the rest of the network

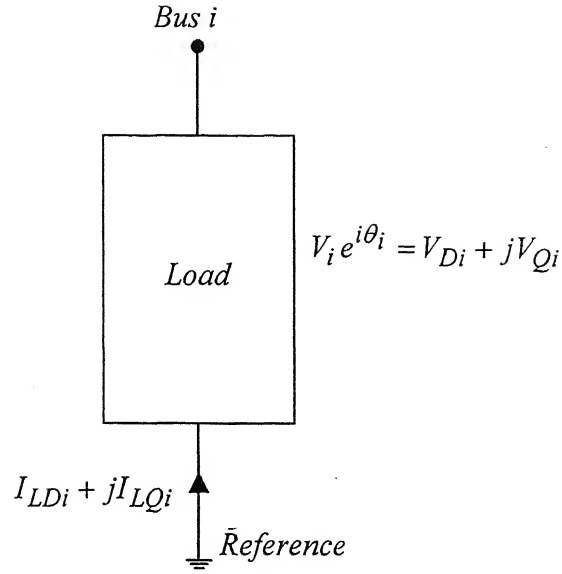


**Fig. 2.5** Generalized load electrical dynamic circuit

Separating (2.11) and (2.12) into real and imaginary parts yields the following

$$\begin{aligned}
 & I_{di}V_i \sin(\delta_i - \theta_i) + I_{qi}V_i \cos(\delta_i - \theta_i) + P_{Li}(V_i) \\
 & - \sum_{k=1}^n V_i V_k Y_{ik} \cos(\theta_i - \theta_k - \alpha_{ik}) = 0 \quad i = 1, 2, \dots, m
 \end{aligned} \tag{2.13}$$

$$\begin{aligned}
 & I_{di}V_i \cos(\delta_i - \theta_i) - I_{qi}V_i \sin(\delta_i - \theta_i) + Q_{Li}(V_i) \\
 & - \sum_{k=1}^n V_i V_k Y_{ik} \sin(\theta_i - \theta_k - \alpha_{ik}) = 0 \quad i = 1, 2, \dots, m
 \end{aligned} \tag{2.14}$$

$$P_{Li}(V_i) - \sum_{k=1}^n V_i V_k Y_{ik} \cos(\theta_i - \theta_k - \alpha_{ik}) = 0 \quad i = m+1, \dots, n \tag{2.15}$$

$$Q_{Li}(V_i) - \sum_{k=1}^n V_i V_k Y_{ik} \sin(\theta_i - \theta_k - \alpha_{ik}) = 0 \quad i = m+1, \dots, n \tag{2.16}$$

Thus, there are in all

- (i) Seven differential equations (2.1-2.7) for each machine, i.e., a total of  $7m$  differential equations for  $m$  machines.
- (ii) One complex stator algebraic equation (2.8) comprising two algebraic equations. (2.9-2.10) for each machine, i.e., a total of  $2m$  algebraic equations.
- (iii) One complex network equation. (2.11-2.12) comprising two algebraic equations each at each network bus, i.e., a total of  $2n$  algebraic equations.

Thus, there are  $7m+2m+2n$  equations with  $X = [X_1^t, \dots, X_m^t]^t$  as the 'state vector' where  $X_i = [\delta_i \quad \omega_i \quad E'_{qi} \quad E'_{di} \quad E_{fdi} \quad V_{Ri} \quad R_{Fi}]^t$  for each machine.

$y = [I_{d-q}^t \quad V^t \quad \theta^t]^t$  is the set of algebraic variables, where

$$I_{d-q} = [I_{d1} \quad I_{q1} \dots I_{dm} \quad I_{qm}]^t; \quad V = [V_1 \quad V_2 \dots V_n]^t;$$

$$\theta = [\theta_1 \quad \theta_2 \dots \theta_n]^t; \quad \tilde{V} = [\tilde{V}_1 \quad \tilde{V}_2 \dots \tilde{V}_n]^t$$

where  $\tilde{V}$  is the complex bus voltage vector comprising  $\tilde{V}_g$  and  $\tilde{V}_l$ . Where  $\tilde{V}_g$  is generator bus voltage vector and  $\tilde{V}_l$  is load bus voltage vector. The set of net injected generator currents is given by  $I_g = I_{d-q}$ .

Therefore (2.1-2.7) together with stator algebraic equations (2.9) and (2.10) and network equations (2.13- 2.16) form a set of differential-algebraic equations (DAE) of the form

$$\dot{X} = f(X, y, U) \tag{2.17}$$

$$0 = g(X, y) \tag{2.18}$$

where  $U = [U_1^t, \dots, U_m^t]^t$ . Note that  $U_i, i = 1, \dots, m$  is associated with machine  $i$  and is given by  $U_i = [\omega_s \ T_{Mi} \ V_{refi}]^t$ .

Equations (2.17) and (2.18) can be rewritten as

$$\dot{X} = f_o(X, I_{d-q}, \tilde{V}, U) \quad (2.19)$$

$$I_{d-q} = h(X, \tilde{V}) \quad (2.20)$$

$$0 = g_o(X, I_{d-q}, \tilde{V}) \quad (2.21)$$

Substituting (2.20) in (2.19) and (2.21) gives

$$\dot{X} = f_1(X, \tilde{V}, U) \quad (2.22)$$

$$0 = g_1(X, \tilde{V}) \quad (2.23)$$

Equation (2.23) is in the *power-balance* form because power at each network bus is equated. This is the differential-algebraic equation (DAE) analytical model with the network algebraic variables in the polar form. This form is preferred because in load-flow equations the voltages are generally in polar form. Another form in which DAE model can be developed is current balance form where the nodal set of equations is utilized. This is written as current balance form.

$$\tilde{I} = \tilde{Y}_N \tilde{V}$$

where  $\tilde{Y}_N$  is the  $n \times n$  bus admittance matrix of the network,  $\tilde{I}$  is the net injected current vector and  $\tilde{V}$  is the bus voltage vector. Depending on the manner in which  $\tilde{I}$  is expressed, the equation can take different forms.

### 2.1.2 Linearization of DAE for Model-I

Differential equations (2.1-2.7) are linearized and expressed in matrix form as



$$\Delta \dot{X}_i = A_{1i} \Delta X_i + A_{2i} \Delta I_{gi} + A_{3i} \Delta V_{gi} + E_i \Delta U_i \quad i = 1, 2, \dots, m \quad (2.24)$$

$$\text{where, } \Delta I_{gi} = \begin{bmatrix} \Delta I_{di} \\ \Delta I_{qi} \end{bmatrix}; \quad \Delta V_{gi} = \begin{bmatrix} \Delta \theta_i \\ \Delta V_i \end{bmatrix}; \quad \text{and} \quad \Delta U_i = \begin{bmatrix} \Delta T_{Mi} \\ \Delta V_{ref i} \end{bmatrix}$$

For m-machine system, (2.24) can be expressed as

$$\Delta \dot{X} = A_1 \Delta X + A_2 \Delta I_g + A_3 \Delta V_g + E \Delta U \quad (2.25)$$

Various matrices in (2.24) and (2.25) are described in Appendix A.2.

Linearization of (2.9) and (2.10) yields

$$0 = B_{1i} \Delta X_i + B_{2i} \Delta I_{gi} + B_{3i} \Delta V_{gi} \quad i = 1, 2, \dots, m \quad (2.26)$$

combining above m equations we get

$$0 = B_1 \Delta X + B_2 \Delta I_g + B_3 \Delta V_g \quad (2.27)$$

where  $B_1$ ,  $B_2$  and  $B_3$  are block diagonal matrices. Details of (2.26) are given in Appendix A.2.

Linearization of (2.13) and (2.14) yields

$$0 = C_1 \Delta X + C_2 \Delta I_g + C_3 \Delta V_g + C_4 \Delta V_l + \Delta S_{Lg}(V) \quad (2.28)$$

where  $C_1$  and  $C_2$  the block diagonal matrices and  $C_3$  and  $C_4$  are defined in Appendix A.2.

Linearizing (2.15) and (2.16), which pertain to load buses yields

$$0 = \Delta S_{Li}(V) + D_1 \Delta V_g + D_2 \Delta V_l \quad (2.29)$$

where  $D_1$  and  $D_2$  are matrices as defined in Appendix A.2.

Equations (2.25), (2.27), (2.28) and (2.29) together constitute the DAE model for multimachine system.

After elimination of  $\Delta I_g$  from (2.25), (2.27) and (2.28), Equation (2.29) is combined to yield the following

$$\begin{bmatrix} \Delta \dot{X} \\ 0 \\ 0 \end{bmatrix} = \begin{bmatrix} A_{1mod} & A_{2mod} & A_{3mod} \\ K_2 & K_1 & C_4 \\ G_1 & D_1 & D_2 \end{bmatrix} \begin{bmatrix} \Delta X \\ \Delta V_g \\ \Delta V_l \end{bmatrix} + \begin{bmatrix} 0 \\ \Delta S_{Lg} \\ \Delta S_{Ll} \end{bmatrix} + \begin{bmatrix} E \\ 0 \\ 0 \end{bmatrix} \Delta U \quad (2.30)$$

Various matrices are defined in Appendix A.2.

The variables in the vector  $\Delta V = [\Delta V_g \ \Delta V_l]^t$  are not in proper load flow format and hence reordering is done. The variables are reordered in the vector  $\Delta V = [\Delta V_g \ \Delta V_l]^t$  such that the new vector is  $[\Delta z^t \mid \Delta v^t] = [\Delta \theta_1, \Delta V_1, \dots, \Delta V_m \mid \Delta \theta_2, \Delta \theta_3, \dots, \Delta \theta_n, \Delta V_{m+1}, \dots, \Delta V_n]$ . Here  $\Delta v$  represents those variables appearing in the standard load flow equations and  $\Delta z$ , the remaining ones in  $\Delta V$ . Similarly, the variables in  $[\Delta S_{Lg} \ \Delta S_{Ll}]^t$  are reordered as  $[\Delta P_{L1}, \Delta Q_{L1}, \dots, \Delta Q_{Lm} \mid \Delta P_{L2}, \Delta P_{L3}, \dots, \Delta P_{Ln}, \Delta Q_{Lm+1}, \dots, \Delta Q_{Ln}] = [\Delta S_1^t \mid \Delta S_2^t]$

Since angles are expressed individually and not as difference with respect to a reference machine angle, (2.30) will always result in a zero eigenvalue. Hence DAE model for multimachine system after reordering is as given by (2.31).

$$\begin{bmatrix} \Delta \dot{X} \\ 0 \\ 0 \end{bmatrix} = \begin{bmatrix} A_{1mod} & A_{2new} & A_{3new} \\ K_2 & K_{1new} & C_{4new} \\ G_1 & D_{1new} & D_{2new} \end{bmatrix} \begin{bmatrix} \Delta X \\ \Delta z \\ \Delta v \end{bmatrix} + \begin{bmatrix} 0 \\ \Delta S_1 \\ \Delta S_2 \end{bmatrix} + \begin{bmatrix} E \\ 0 \\ 0 \end{bmatrix} \Delta U \quad (2.31)$$

This DAE model allows voltage dependency for the loads in the vectors  $\Delta S_1$  and  $\Delta S_2$ . For the constant power case, both  $\Delta S_1$  and  $\Delta S_2$  are equal to zero. Then (2.31) can be rewritten as

$$\begin{bmatrix} \Delta \dot{X} \\ 0 \\ 0 \end{bmatrix} = \begin{bmatrix} A_{1mod} & A_{2new} & A_{3new} \\ K_2 & K_{1new} & C_{4new} \\ G_1 & D_{1new} & D_{2new} \end{bmatrix} \begin{bmatrix} \Delta X \\ \Delta z \\ \Delta v \end{bmatrix} + \begin{bmatrix} E \\ 0 \\ 0 \end{bmatrix} \Delta U \quad (2.32)$$

where  $D_{2new}$  is the load flow Jacobian  $J_{LF}$  and

$$J_{AE} = \begin{bmatrix} K_{1new} & C_{4new} \\ D_{1new} & D_{2new} \end{bmatrix}$$

is the algebraic Jacobian.

The system matrix  $A_{sys}$  can be obtained as

$$\Delta \dot{X} = A_{sys} \Delta X + E \Delta U \quad (2.33)$$

where

$$A_{sys} = A_{1mod} - [A_{2new} \quad A_{3new}] [J_{AE}]^{-1} \begin{bmatrix} K_2 \\ G_1 \end{bmatrix}$$

This DAE model for multimachine system can be used for studying steady state stability, voltage stability and low frequency electromechanical oscillations.

## 2.2 MODEL-II

In this the machine is modeled as two-axis synchronous machine as before while the exciter is represented by a static exciter as shown in Fig. 2.6. The equations pertaining to synchronous machine are same as (2.1-2.4) whereas, the exciter is modeled as given in (2.34).

$$T_{Ai} \left( \frac{dE_{fdi}}{dt} \right) = -E_{fdi} + K_{Ai} (V_{refi} - V_i) \quad i = 1, 2, \dots, m \quad (2.34)$$

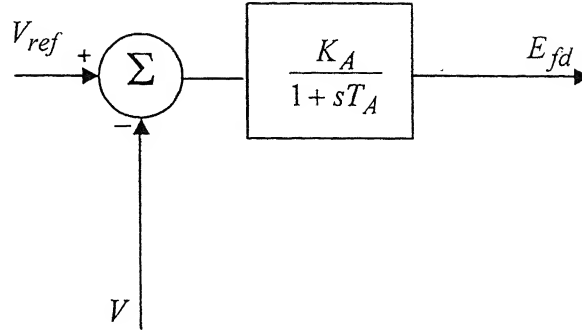


**Fig. 2.6** Static exciter model

In this case when the machine is equipped with static exciter instead of IEEE type-I rotating exciter, (2.5-2.7) are replaced by (2.34). Hence there will be  $5m$  state variables. Remaining procedure is same as that adopted with IEEE type-I exciter system.

### 2.3 DEVELOPMENT OF THE MATLAB SOFTWARE PROGRAM

MATLAB is a high-performance language for technical computing. It integrates computation, visualization and programming in an easy-to-use environment where problems and solutions are expressed in familiar mathematical notations. MATLAB features a family of application-specific solutions called toolboxes. Toolboxes are comprehensive collections of MATLAB functions that can be used to solve particular class of problems. MATLAB is a high-level matrix/array language with control flow statements, functions, data structures, input/output, and object-oriented programming features. MATLAB does not require dimensioning of matrices. It includes high-level commands for two-dimensional and three-dimensional data visualization. Graphical User Interface (GUI) can also be built with MATLAB.

Based on the methodology described in Section 2.1.1, a small signal stability program has been developed using MATLAB version 5.3. The developed small signal stability program is general, interactive and includes error identification procedures. As MATLAB does not require dimensioning and the developed small signal stability

program is general, it can be utilized to analyze small signal stability of large electric power systems. A dialog box of the developed program is shown in Appendix A.3.

## 2.4 CASE STUDY WITH SYSTEM MODEL-I

In order to ensure that the developed small signal stability program gives satisfactory results, eigenvalue analysis is performed for the Western System Coordinating Council (WSCC) 9-bus system (Fig. 2.7). This WSCC system comprises three generators and nine buses. Loads are connected at buses 5, 6 and 8 as shown in Fig. 2.7. At base case loading condition of the system, the generator 2 and 3 are supplying 163MW and 85MW power respectively. The base MVA is 100, and system frequency is 60 Hz. Calculation of initial condition for multimachine system is described in Appendix B.1. The system data and converged load-flow data at the base case loading condition are given in Appendix C. Table 2.1 shows the eigenvalues of WSCC system. Column 1 of Table 2.1 shows the eigenvalues reported in [97] while column 2 depicts the eigenvalues obtained from developed MATLAB program. It is evident that eigenvalues obtained from developed MATLAB program correlate very well with those reported in [97]. This validates the developed MATLAB program.

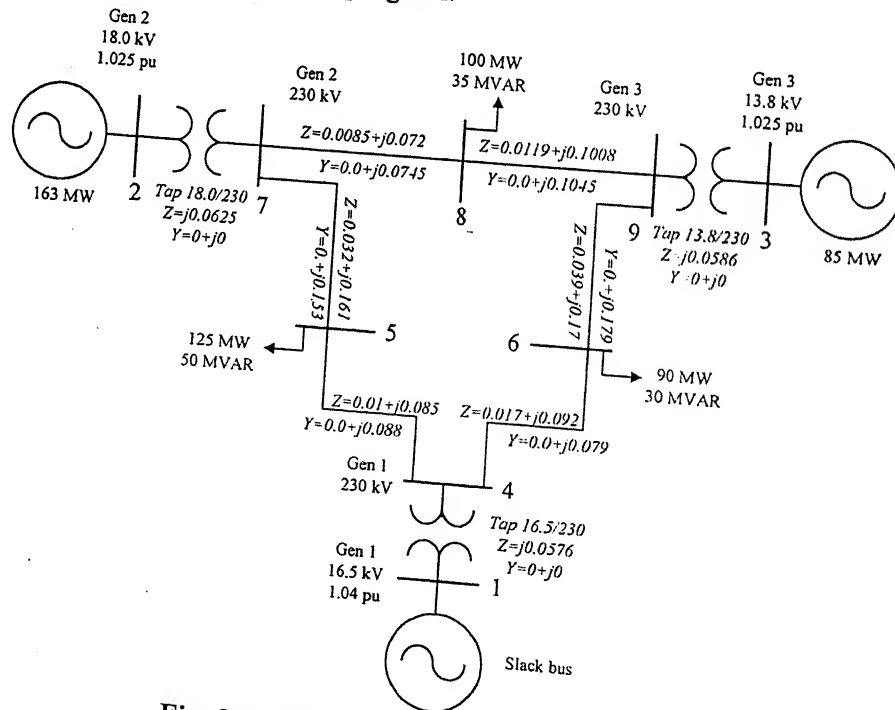


Fig. 2.7 WSCC 3-machines, 9-bus system

**Table 2.1** Eigenvalues of WSCC system

Eigenvalues from [97]	Eigenvalues from developed MATLAB program
$-0.7209 \pm j12.7486$	$-0.7198 \pm j12.7456$
$-0.1908 \pm j8.3672$	$-0.1906 \pm j8.3660$
$-5.4875 \pm j7.9487$	$-5.6867 \pm j7.9663$
$-5.3236 \pm j7.9220$	$-5.3644 \pm j7.9311$
$-5.2218 \pm j7.8161$	$-5.2287 \pm j7.8263$
$-5.1761$	$-5.1779$
$-3.3995$	$-3.3993$
$-0.4445 \pm j1.2104$	$-0.4513 \pm j1.1997$
$-0.4394 \pm j0.7392$	$-0.4481 \pm j0.7291$
$-0.4260 \pm j0.4960$	$-0.4366 \pm j0.4868$
$-0.0000$	$-0.0000$
$-0.0000$	$-0.0000$
$-3.2258$	$-3.2258$

## 2.5 CONCLUSIONS

In this chapter, a comprehensive dynamic models of multimachine power system has been developed using MATLAB 5.3 to study both small signal stability and voltage stability of an electric power system. This program has provision to incorporate both static and rotating exciters. The program developed is general, interactive in nature and posses error detection features. The results of the developed MATLAB program are correlated with the results published in [97]. The program works satisfactorily for 39-bus New England System and 68-bus system [98]. The results related to these systems are presented in subsequent chapters.

The most important feature of this program is that it is modular and can incorporate Flexible Alternating Current Transmission System (FACTS) devices such as Static VAR Compensator (SVC), Thyristor Controlled Series Capacitor (TCSC), Static Compensator (STATCOM), Static Synchronous Series Capacitor (SSSC) etc. as reported in subsequent chapters.

## MODELING AND INCORPORATION OF FACTS DEVICES IN MULTIMACHINE SYSTEMS

This chapter deals with modeling of FACTS devices and their incorporation in the multimachine system model developed in Chapter 2. FACTS devices use solid state inverters for power flow control at the transmission level [99]. FACTS devices such as Static Var Compensator (SVC) and Thyristor Controlled Series Capacitor (TCSC), are realized using thyristors and passive devices. A new generation of FACTS devices are based on the self commutated Voltage Source Inverters (VSI) using Gate-Turn Off (GTO) thyristor technology. It includes Static Synchronous Compensator (STATCOM), Static Synchronous Series Capacitor (SSSC), VSI-based Static Phase Shifter (SPS), Unified Power Flow Controller (UPFC) and Energy Systems with VSI-interface.

This chapter deals with the modeling of four key FACTS devices viz. SVC, TCSC, STATCOM and SSSC. The modeling of each device is presented in an independent section. Each section briefly describes the characteristics of the device, behavioral equations of the device, its associated control and its incorporation into the multimachine system model developed in Chapter 2. A general and interactive MATLAB program is developed incorporating each of the four FACTS devices into multimachine system model. This chapter also presents the incorporation of multiple FACTS devices e.g. SVC-TCSC, STATCOM-TCSC into the above multimachine system model.

### 3.1 STATIC VAR COMPENSATOR

Static Var Compensators are shunt connected static generators and/or absorbers whose outputs are varied so as to control specific parameters of the electric power system. The term “static” is used as SVCs have no moving or rotating main components. SVCs have been extensively employed in power systems since 1970s.

There are several configurations of the SVC possible, the most common ones being

- (i) FC-TCR (Fixed Capacitor-Thyristor Controlled Reactor)
- (ii) TSC-TCR (Thyristor switched Capacitor-Thyristor Controlled Reactor)

In its simplest form SVC is composed of FC-TCR configuration as shown in Fig. 3.1. The SVC is connected to a coupling transformer that is connected directly to the ac bus whose voltage is to be regulated. The effective reactance of the FC-TCR is varied by firing angle control of the thyristors. The firing angle can be controlled through a PI controller in such a way that the voltage of the bus where the SVC is connected is maintained at the desired reference value.

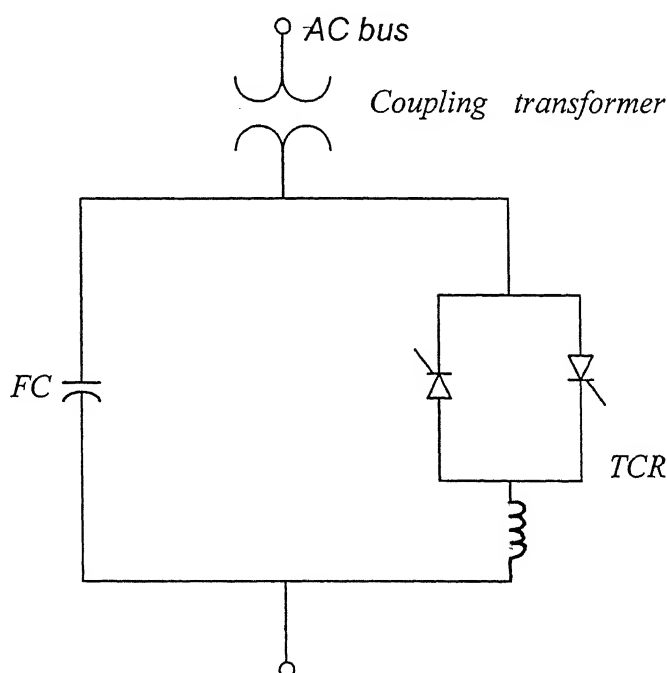


**Fig. 3.1** Simplified one line diagram of SVC

The SVC control characteristic is shown in Fig. 3.2. This plots the ac bus voltage at the point where the SVC is connected against variation in SVC current ( $I_{SVC}$ ). It can be seen that ac system voltage varies linearly with slope  $K$  from the reference setting  $V_{ref}$ . This characteristic is also called the droop characteristic as it indicates the droop in voltage due to current drawn. Composite SVC and power system characteristics are



depicted in Fig. 3.3. Three power system characteristics are considered. The middle characteristic represents nominal system condition, and is assumed to intersect the SVC characteristic at point  $A$  where  $V = V_{ref}$  and  $I_{SVC}$  is zero. If the bus voltage falls below  $V_{ref}$  due to increase in system load level, the SVC holds the voltage at  $V_3$  that would otherwise drop to  $V_2$  without SVC. In this case the SVC must become more capacitive to raise the voltage. If, on the other hand, the voltage rises above  $V_{ref}$  possibly due to a decrease in system loading, the system voltage will increase to  $V_1$  without SVC. With the SVC, the operating point moves to point  $B$ . The SVC regulates the system voltage to  $V_4$  by absorbing inductive current  $I_1$ . In this case the SVC becomes inductive to lower the voltage to the desired value. Outside the control range the SVC acts like a fixed capacitor or fixed inductor.

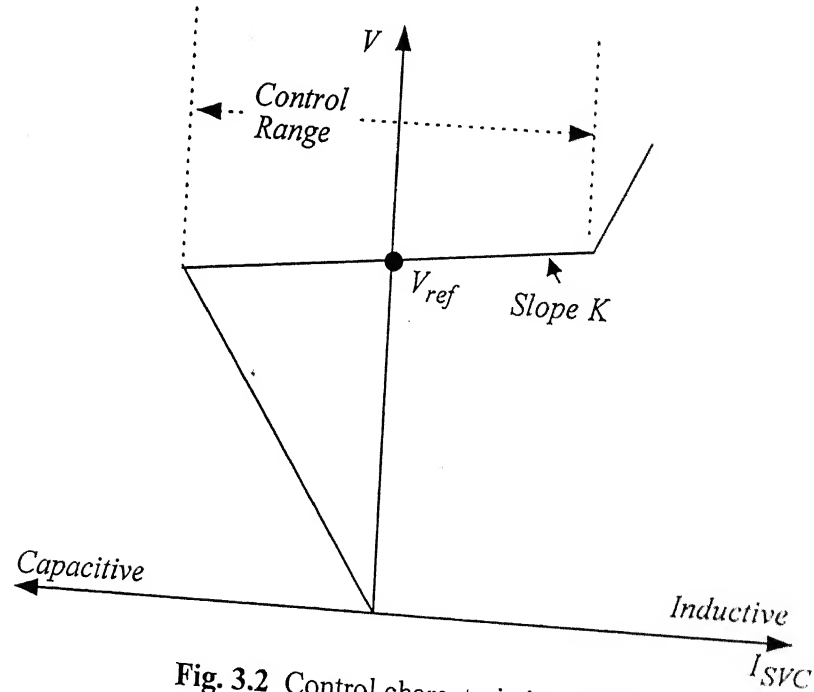
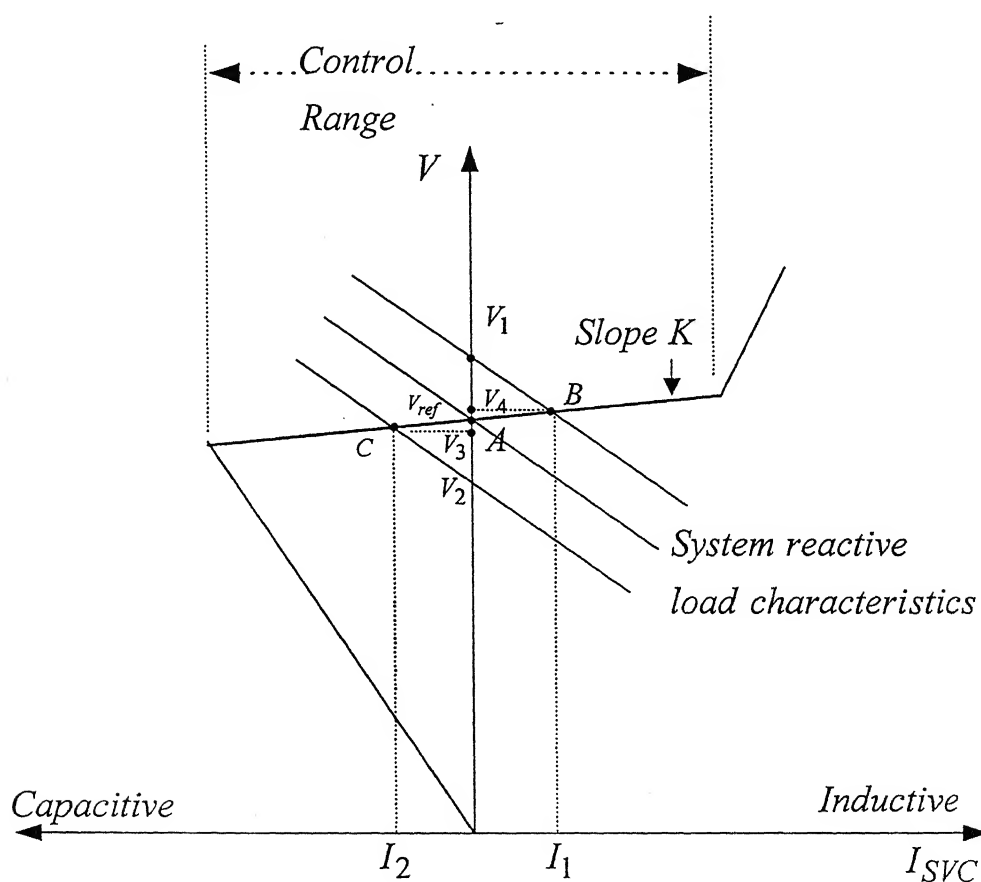


Fig. 3.2 Control characteristic of SVC

The block diagram of SVC is shown in Fig. 3.4. In this diagram the SVC is represented by a variable susceptance  $B_{SVC}$ . The TCR dynamics are ignored and only the SVC controller dynamics are considered. The droop characteristic is modeled by a

constant  $K$ . Time constants for both voltage and current measurement circuits are assumed to be equal to  $T_m$ . The voltage regulator is modeled as a proportional plus integral (PI) controller. The output of the SVC controller is  $B_{ref,SVC}$  and it represents the desired susceptance. This susceptance gets implemented at the SVC terminals after a firing delay which is represented by the time constant  $T_c$ . Typically  $T_c$  is  $1/4^{th}$  of a cycle. The susceptance of the SVC is  $B_{SVC}$  which is also a state variable denoted as  $X_{3SVC}$ . The voltage at the SVC bus,  $V_{SVC}$ , is multiplied by the negative of the susceptance to get the current injected  $I_{SVC}$  into the system. Various parameters of the SVC are given in Appendix D.2.



**Fig. 3.3** Graphical operation of SVC for given system conditions

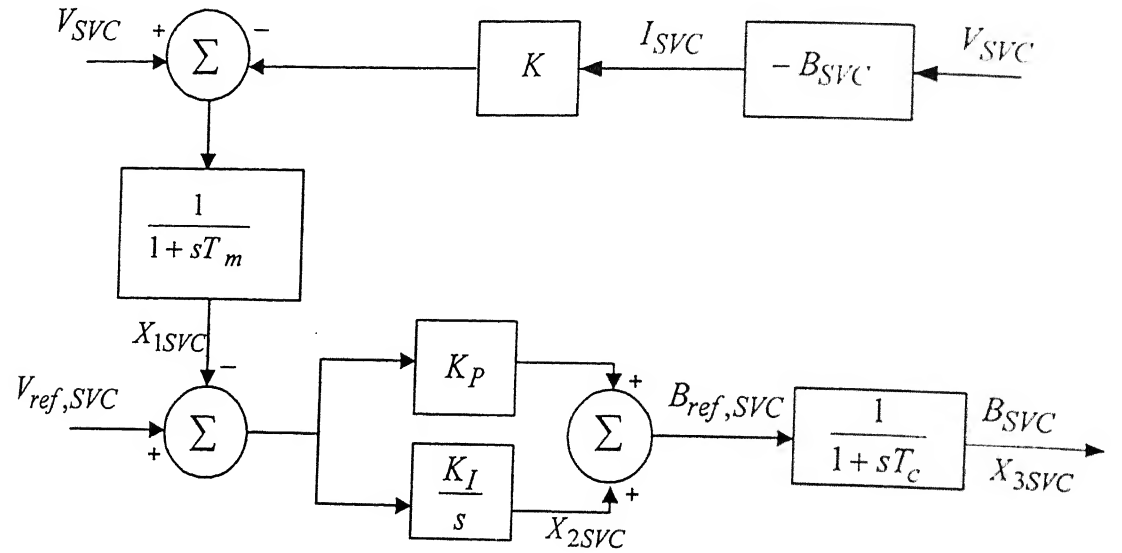


Fig. 3.4 SVC block diagram

### 3.1.1 State Equations of SVC with Controller

#### Linearized State Equations of SVC

The state equations of the SVC can be written as [13]

$$\dot{X}_{1SVC} = \frac{1}{T_m} [V_{SVC}(1 + K X_{3SVC}) - X_{1SVC}] \quad (3.1)$$

$$\dot{X}_{2SVC} = K_I (V_{ref,SVC} - X_{1SVC}) \quad (3.2)$$

$$\dot{X}_{3SVC} = \frac{1}{T_c} [X_{2SVC} + K_P (V_{ref,SVC} - X_{1SVC}) - X_{3SVC}] \quad (3.3)$$

The reactive power  $Q_{SVC}$  supplied by the SVC can be written as

$$Q_{SVC} = V_{SVC}^2 X_{3SVC} \quad (3.4)$$

Linearization of (3.1-3.4) yields

$$\Delta \dot{X}_{1SVC} = \frac{1}{T_m} [\Delta V_{SVC} (1 + K X_{3SVC0}) + V_{SVC0} K \Delta X_{3SVC} - \Delta X_{1SVC}] \quad (3.5)$$

$$\Delta \dot{X}_{2SVC} = K_I (\Delta V_{ref,SVC} - \Delta X_{1SVC}) \quad (3.6)$$

$$\Delta \dot{X}_{3SVC} = \frac{1}{T_c} [\Delta X_{2SVC} + K_P (\Delta V_{ref,SVC} - \Delta X_{1SVC}) - \Delta X_{3SVC}] \quad (3.7)$$

$$\Delta Q_{SVC} = 2 V_{SVC0} \Delta V_{SVC} X_{3SVC0} + V_{SVC0}^2 \Delta X_{3SVC} \quad (3.8)$$

where “ $\Delta$ ” denotes perturbed value and subscript “ $o$ ” denotes the nominal value.

The above equations are linearized, reordered and then expressed as

$$\begin{bmatrix} \Delta \dot{X} \\ \Delta \dot{X}_{SVC} \\ 0 \\ 0 \end{bmatrix} = \begin{bmatrix} A_{1mod} & P_{1svc} & A_{2new} & A_{3new} \\ P_{2svc} & A_{SVC} & P_{3svc} & B_{svcnew} \\ K_2 & P_{4svc} & K_{1new} & C_{4new} \\ G_1 & D_{SVC} & D_{1new\_svc} & D_{2new\_svc} \end{bmatrix} \begin{bmatrix} \Delta X \\ \Delta X_{SVC} \\ \Delta z \\ \Delta v \end{bmatrix} + \begin{bmatrix} E \\ 0 \\ 0 \\ 0 \end{bmatrix} \Delta U \quad (3.9)$$

Equation (3.9) can be written as

$$\Delta \dot{X}_{sys-svc} = A_{sys-svc} \Delta X_{sys-svc} + E_{SVC} \Delta U \quad (3.10)$$

Then the eigenvalues of system with SVC can be computed. Details of SVC modeling are given in Appendix D.1.

### 3.1.2 Interpretation of SVC Operation in Load Flow

In load flow studies, the bus where SVC is connected is treated as a PV bus. In practice SVC becomes capacitive as the bus voltage starts falling. The FC-TCR model of an SVC has been shown in Fig. 3.1. Suppose SVC has to supply  $\pm 10$  MVAR. Then FC-TCR type SVC can be thought of as having fixed capacitance of 10 MVAR and a variable inductance having value from 0 to 20 MVAR. When the inductive reactive power of the SVC is in this range, the SVC acts like a PV bus and the voltage of the SVC bus remains at prespecified voltage. However, if the susceptance limits are violated, the SVC acts like a PQ bus.

### 3.1.3 Case Study

The above technique has been applied to a modification of the 9 bus WSCC system. IN this new system a bus 4 has been created and arbitrarily placed midway between buses 6 and 8. [13]. An SVC is connected to this bus as shown in Fig. 3.5. As a result of inserting the SVC bus, the buses are renumbered. The machines are equipped with static exciter. Thus there are five state variables for each machine. The system data, SVC data and converged load flow data of the system at base operating condition with SVC is given in Appendix D.2.

A MATLAB program is developed which can incorporate multiple SVCs. The developed MATLAB program is general and interactive. Table 3.1 shows the eigenvalues with the developed MATLAB program and that reported in [13]. It can be seen that the eigenvalues obtained using the developed MATLAB program are closely following the reported eigenvalues in [13].

Apart from conventional voltage controller, auxiliary controller can be added to the SVC to enhance system damping. Many signals like line active power, line reactive power, computed internal frequency has been used as auxiliary feedback signal. This auxiliary controller can be added in the similar fashion [13].

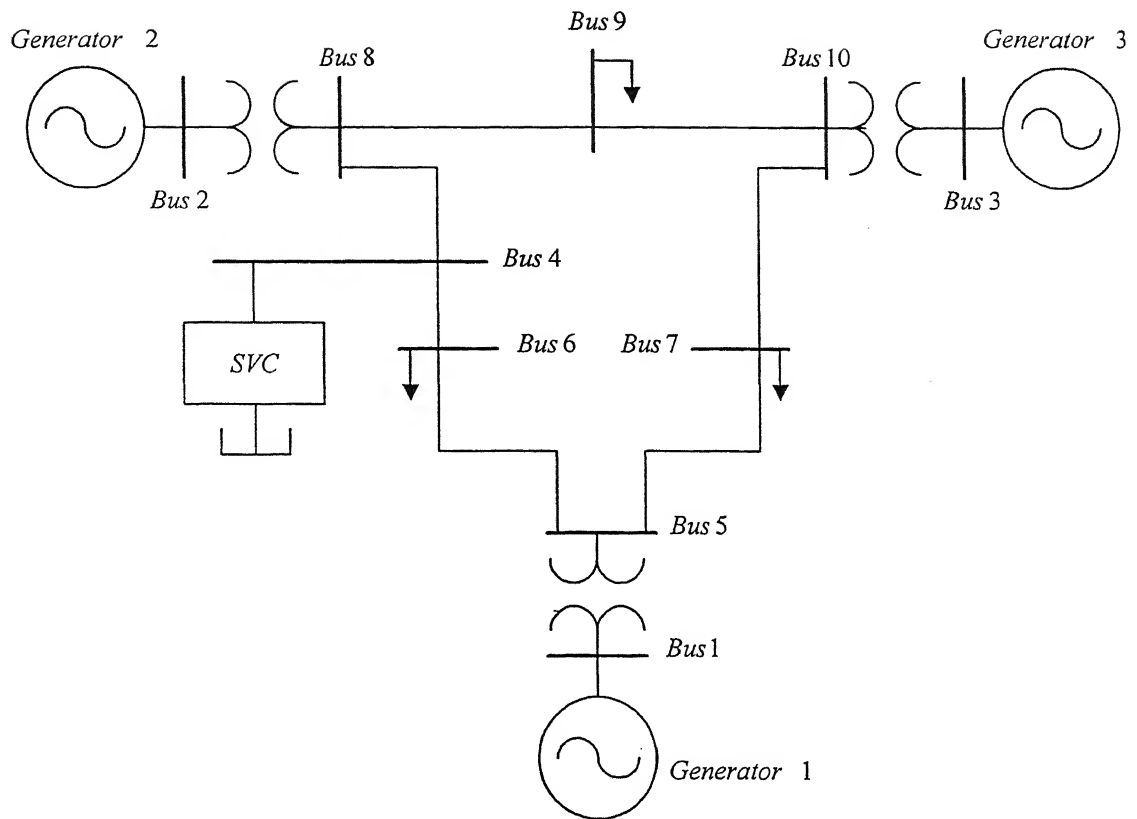


**Fig. 3.5** WSCC system with SVC at bus 4

**Table 3.1** Eigenvalues of WSCC system with SVC

From [13]	From developed MATLAB program
- 78.4325	- 78.4309
$-10.2417 \pm j26.2143$	$-10.2421 \pm j26.2120$
$-0.8432 \pm j12.7698$	$-0.8424 \pm j12.7669$
$-0.2677 \pm j8.4245$	$-0.2674 \pm j8.4233$
$-4.6918 \pm j1.3196$	$-4.6989 \pm j1.3187$
$-3.8082 \pm j1.5021$	$-3.8089 \pm j1.5006$
$-2.6818 \pm j2.0672$	$-2.6815 \pm j2.0675$
-1.7352	-1.7356
-0.0000	-0.0000
-0.1365	-0.1365
-0.8871	-0.8867
-3.2258	-3.2258

### 3.2 THYRISTOR CONTROLLED SERIES CAPACITOR

Thyristor Controlled Series Capacitor (TCSC) provides powerful means of controlling and increasing power transfer level of a system by varying the apparent impedance of a specific transmission line. A TCSC can be utilized in a planned way for contingencies to enhance power system stability. Using TCSC, it is possible to operate stably at power levels well beyond those for which the system was originally intended without endangering system stability [101]. Apart from this, TCSC is also being used to mitigate SSR (Sub Synchronous Resonance) [21, 24]. A TCSC module comprises of a series capacitor, a pair of anti-parallel thyristors with inductor in parallel path, a metal-oxide varistor (MOV) for over voltage protection and a bypass breaker as shown in Fig. 3.6.

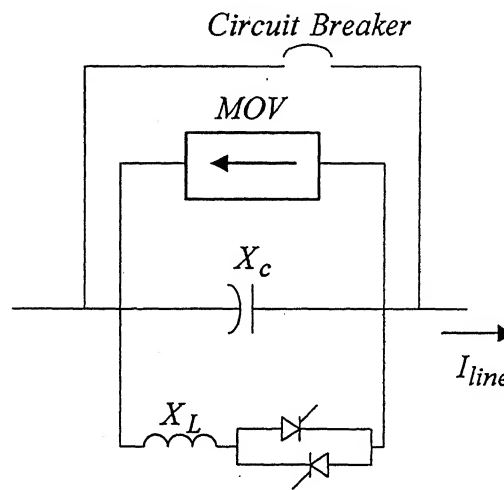


**Fig. 3.6** TCSC module

TCSCs are in service for quite some time now. They have been installed on Southern California Edison (SCE) 500 kV system in 1985 to mitigate SSR, on American Electric Power (AEP) 345 kV system in 1991 for power flow control, on Western Area Power Administration (WAPA) 230 kV system in 1992 with many control features for improving system performance. On BPA 500 kV system in 1993, a multi-module TCSC has been installed.

### 3.2.1 Operating Modes

TCSC can operate in three modes. They are

- (1) Thyristor blocked (no gating and zero thyristor conduction)
- (2) Thyristor bypassed (continuous gating and full thyristor conduction)
- (3) Vernier operation with phase control of gating signals

These are shown in Figs. 3.7 and 3.8.

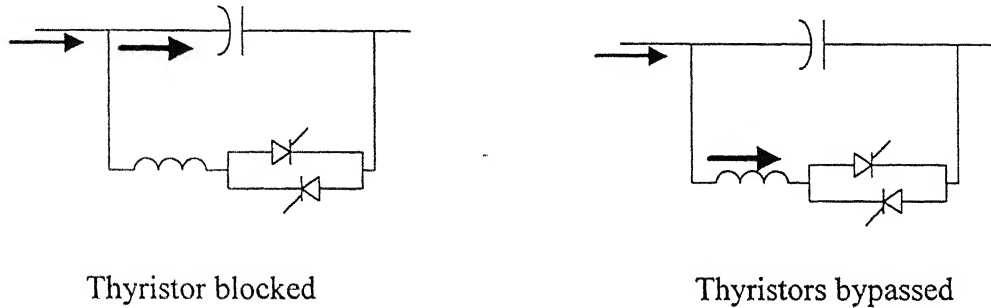


**Fig. 3.7** Blocked and Bypassed operating modes of TCSC

In case of blocked operating mode, the TCSC net impedance is just capacitive reactance. In case of bypass mode, as the thyristors are fully conducting, most of the line current flows through thyristors and hence TCSC has small net inductive reactance.

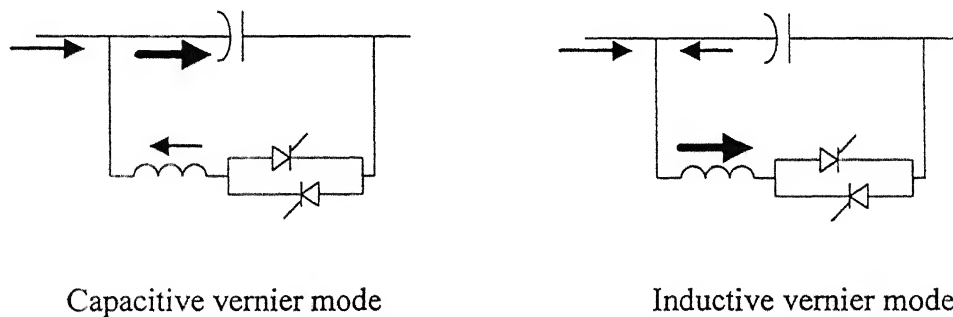


**Fig. 3.8** Vernier operating modes of TCSC with partial thyristor conduction

In vernier control, thyristors are conducted in such a manner that a controlled amount of inductive current can circulate through the capacitor thereby increasing effective capacitive /inductive reactance of the module. Bold and thick arrow shows direction of circulating current in Figs. 3.7-3.8.



The breaker removes the TCSC from service when there are internal TCSC failures, whereas thyristor bypass mode is used to provide control and protective measures.

### 3.2.2 Controller Model

The structure of the TCSC is the same as that of a FC-TCR type SVC. The equivalent impedance of the TCSC can be modeled using the following equation [19].

$$X_{TCSC} = X_c \left[ 1 - \frac{\kappa}{\kappa^2 - 1} \frac{\sigma + \sin \sigma}{\pi} + \frac{4\kappa^2 \cos^2(\sigma/2)}{\pi(\kappa^2 - 1)^2} \left( \kappa \tan \frac{\kappa \sigma}{2} - \tan \frac{\sigma}{2} \right) \right] \quad (3.11)$$

where

$\alpha$  = Firing angle delay (after forward valve voltage)

$\sigma$  = Conduction angle =  $2(\pi - \alpha)$  and

$\kappa$  = TCSC ratio =  $\sqrt{X_c/X_L}$

For a typical TCSC ratio,  $\kappa = 10$ , Fig. 3.9 shows values of  $X_{TCSC}$  for different values of firing angle  $\alpha$ . Different values of  $\kappa$  yield different resonance points. As shown in Fig. 3.9; resonance occurs for firing angle  $151.5^\circ$ . The device can be continuously controlled in the capacitive or inductive zone by varying firing angle in a predetermined fashion thus avoiding steady state resonance region.

As a TCSC is connected in series with transmission line, the resonant point must be avoided to prevent harmonic problems and large internal currents that may damage the controller. Operation of this controller “close” to the resonant point is not practical in steady state either, as this may induce substantial harmonics in the line current [19]. Also the steady state TCSC operation in the inductive region is equivalent to reducing the transmission system capability [19]. Hence, the steady state limits for the firing angle can be defined as  $\alpha_r < \alpha < 180^\circ$ . Firing angle  $\alpha_r$  corresponds to resonant point.

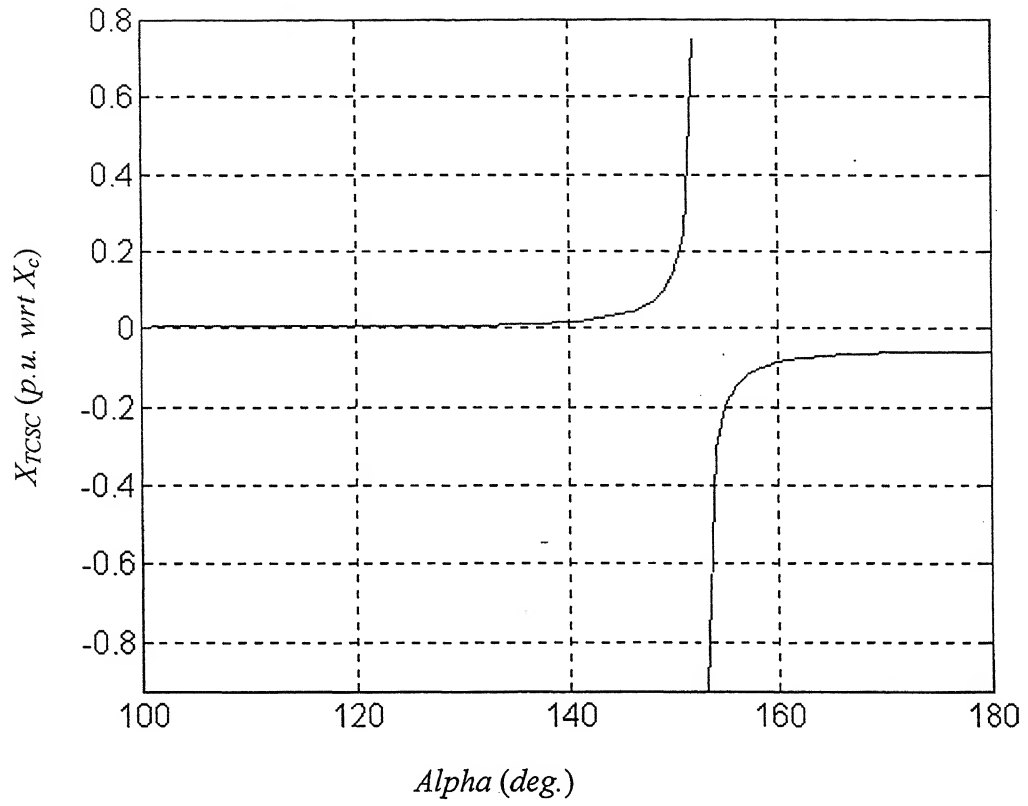


Fig. 3.9 Equivalent reactance  $X_{TCSC}$  for TCSC

### 3.2.3 Incorporation of TCSC in Multimachine Power System

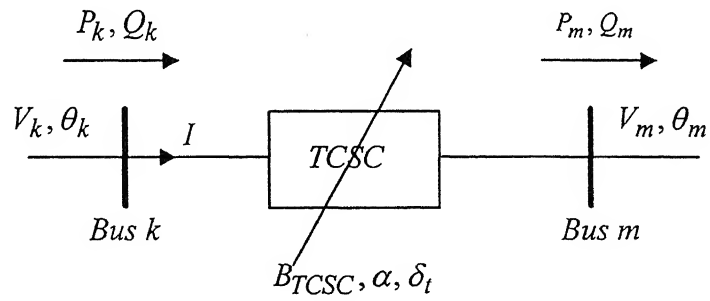


Fig. 3.10 TCSC representation

Let a TCSC be connected between bus k and bus m as shown in Fig. 3.10. It has been assumed that the controller is lossless. The power-balance equation and  $B_{TCSC}$  are given as [19]

$$P_k = V_k V_m B_{TCSC} \sin(\theta_k - \theta_m) \quad (3.12)$$

$$Q_k = V_k^2 B_{TCSC} - V_k V_m B_{TCSC} \cos(\theta_k - \theta_m) \quad (3.13)$$

$$P_m = V_k V_m B_{TCSC} \sin(\theta_m - \theta_k) \quad (3.14)$$

$$Q_m = V_m^2 B_{TCSC} - V_k V_m B_{TCSC} \cos(\theta_m - \theta_k) \quad (3.15)$$

$$\begin{aligned} B_{TCSC} = & -\pi(\kappa^4 - 2\kappa^2 + 1) \cos \kappa(\pi - \alpha) / [X_c(\pi \kappa^4 \cos \kappa(\pi - \alpha) \\ & - \pi \cos \kappa(\pi - \alpha) - 2\kappa^4 \alpha \cos \kappa(\pi - \alpha) \\ & + 2\alpha \kappa^2 \cos \kappa(\pi - \alpha) - \kappa^4 \sin 2\alpha \cos \kappa(\pi - \alpha) \\ & + \kappa^2 \sin 2\alpha \cos \kappa(\pi - \alpha) - 4\kappa^3 \cos^2 \alpha \sin \kappa(\pi - \alpha) \\ & - 4\kappa^2 \cos \alpha \sin \alpha \cos \kappa(\pi - \alpha))] \end{aligned} \quad (3.16)$$

Equation (3.16) is obtained from (3.11).

There are number of control strategies for TCSC [19]

- Reactance Control:  $B_{set} - B_{TCSC} = 0$
- Power Control:  $P_{set} - P = 0$
- Current Control:  $I_{set} - I = 0$
- Transmission angle control:  $\delta_{set} - \delta = 0$

where the subscript “set” indicates set point.

Any of the above mentioned control strategies can be used to achieve the objectives of TCSC. Of these, the power control strategy has been used here, the block diagram of which is shown in Fig. 3.11.

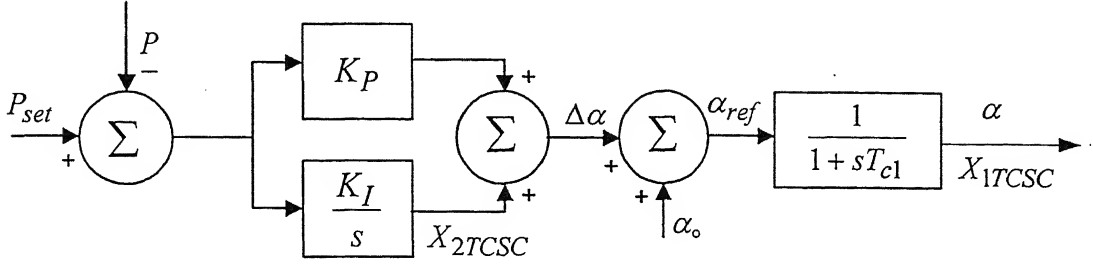


**Fig. 3.11** TCSC power controller

The line power is monitored and compared to desired power  $P_{set}$ . The error is fed to proportional-integral (PI) controller. The output of PI controller is fed through a first order block to get the desired  $\alpha$ . The controller equations are given as

$$X_{2TCSC} = \frac{K_I}{s} (P_{set} - P) \quad (3.17)$$

$$\dot{X}_{2TCSC} = K_I P_{set} - K_I P \quad (3.18)$$

$$\dot{X}_{1TCSC} = \frac{-X_{1TCSC}}{T_{cl}} + \frac{X_{2TCSC}}{T_{cl}} + \frac{K_P P_{set}}{T_{cl}} - \frac{K_P P}{T_{cl}} + \frac{\alpha_o}{T_{cl}} \quad (3.19)$$

In order to get the linearized model of TCSC, (3.12-3.16), (3.18) and (3.19) are linearized. The linearized TCSC model in matrix notation can be written as

$$\Delta \dot{X}_{TCSC} = A_{TCSC} \Delta X_{TCSC} + B_{TCSC} \begin{bmatrix} \Delta \theta_k \\ \Delta V_k \\ \Delta \theta_m \\ \Delta V_m \end{bmatrix} \quad (3.20)$$

where  $\Delta X_{TCSC} = \begin{bmatrix} \Delta X_{1TCSC} \\ \Delta X_{2TCSC} \end{bmatrix}$

$$\begin{bmatrix} \Delta P_k \\ \Delta Q_k \\ \Delta P_m \\ \Delta Q_m \end{bmatrix} = C_{TCSC} \Delta X_{1TCSC} + D_{TCSC} \begin{bmatrix} \Delta \theta_k \\ \Delta V_k \\ \Delta \theta_m \\ \Delta V_m \end{bmatrix} \quad (3.21)$$

Details of (3.20) and (3.21) are given in Appendices E.2 and E.3 respectively.

Incorporation of (3.20), (3.21) and (2.30) gives DAE model of multimachine system with TCSC incorporated in the system. After reordering, final form of DAE model with TCSC is given as

$$\begin{bmatrix} \Delta \dot{X} \\ \Delta \dot{X}_{TCSC} \\ 0 \\ 0 \end{bmatrix} = \begin{bmatrix} A_{1mod} & P_{1tcsc} & A_{2new} & A_{3new} \\ P_{2tcsc} & A_{TCSC} & B_{tcsc1new} & B_{tcscnew} \\ K_2 & P_{4tcsc} & K_{1new} & C_{4new} \\ G_1 & C_{TCSC} & D_{1new\_tcsc} & D_{2new-tcsc} \end{bmatrix} \begin{bmatrix} \Delta X \\ \Delta X_{TCSC} \\ \Delta z \\ \Delta v \end{bmatrix} + \begin{bmatrix} E \\ 0 \\ 0 \end{bmatrix} \Delta U \quad (3.22)$$

Equation (3.22) can be written as

$$\Delta \dot{X}_{SYS-TCSC} = A_{SYS-TCSC} \Delta X_{SYS-TCSC} + E_{TCSC} \Delta U \quad (3.23)$$

Details of (3.22) and (3.23) are given in Appendix E.2.

Then the eigenvalues of multi-machine system with TCSC can be computed.

### 3.3 STATIC SYNCHRONOUS COMPENSATOR

The Static Synchronous Compensator (STATCOM) has been earlier known as Static Condensor (STATCON) or Advanced Static Var Compensator (ASVC) or Self-Commutated Static Var Compensator. A STATCOM is a shunt connected reactive compensation device, whose output can be varied so as to control specific parameters of electric power system. The STATCOM typically consists of a dc to ac inverter employing solid state switching devices and a set of inverter controls as shown in Fig. 3.12.

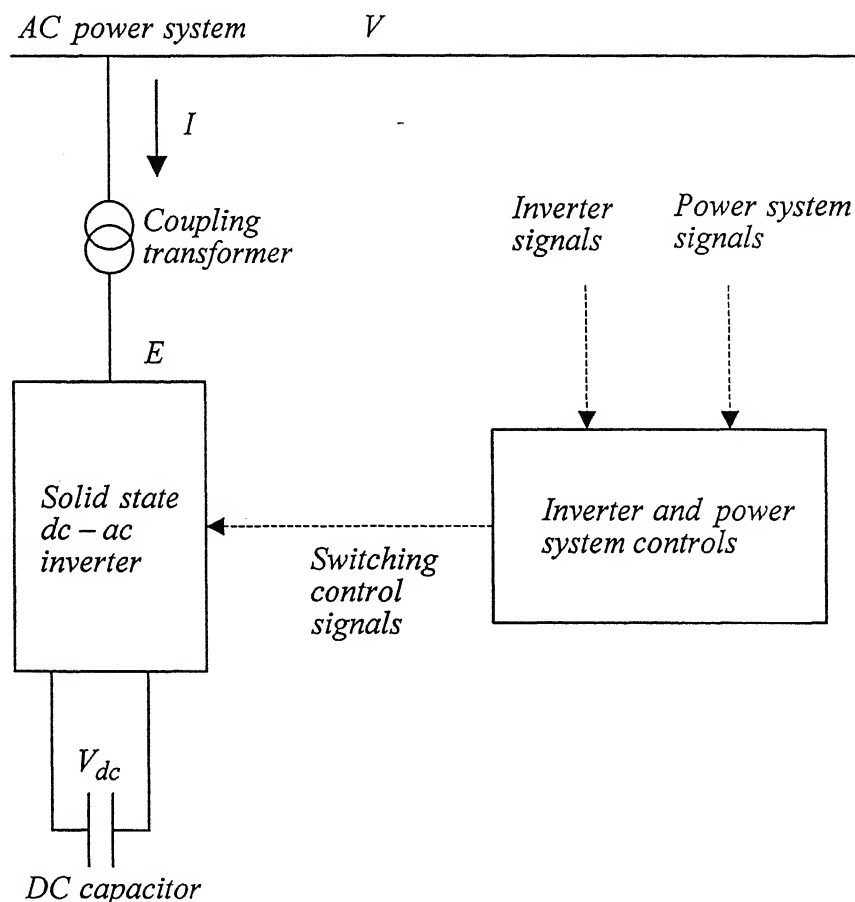


**Fig. 3.12** Block diagram of a typical STATCOM

The STATCOM provides operating characteristics similar to a rotating synchronous compensator (condenser), but it has no rotating components. The power

electronic characteristic of STATCOM provides rapid controllability of the three phase voltages, both in magnitude and phase angle, at the point of connection in the power system.

### 3.3.1 Comparison of STATCOM and SVC Characteristics

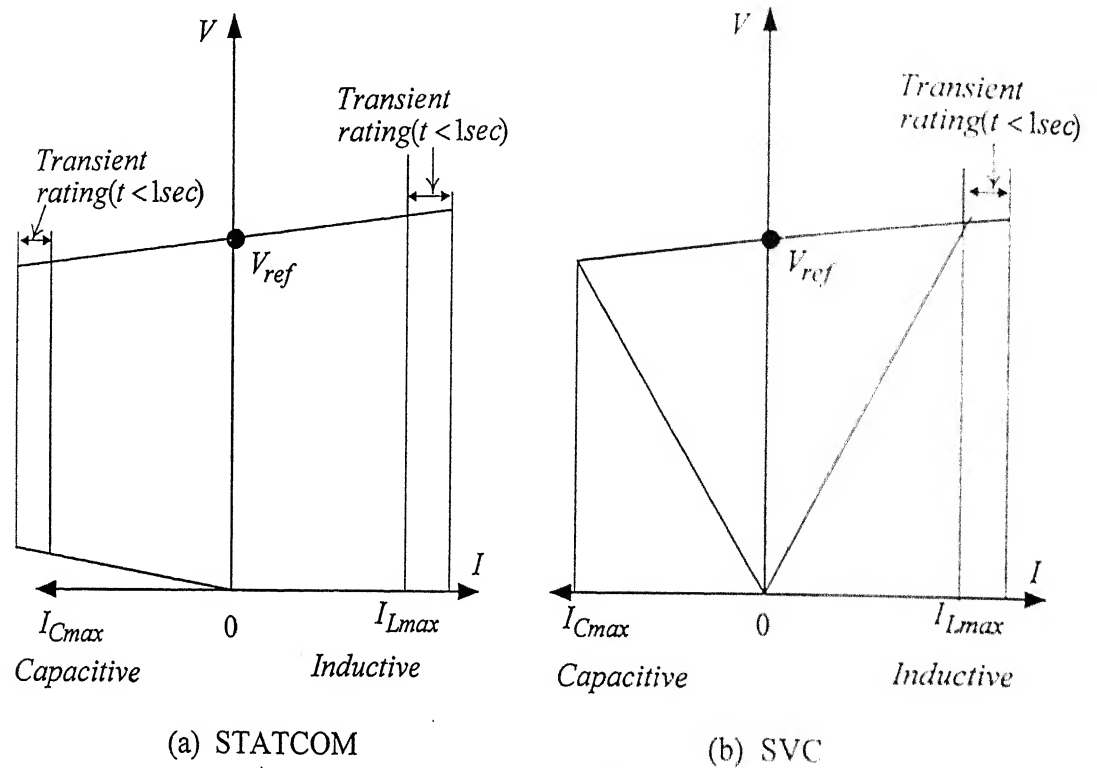


**Fig. 3.13** Typical voltage versus current characteristics of STATCOM and SVC

Typical operating voltage-current characteristics of STATCOM and SVC are shown in Fig. 3.13. The STATCOM is able to maintain virtually constant voltage at its point of connection to the power system by generating and absorbing reactive power within its control range. As evident from Fig. 3.13, the STATCOM can provide capacitive and reactive output currents over the rated maximum capacitive and inductive current range independent of the system voltage. This is in contrast to an SVC which can only supply linearly decreasing output current with declining system voltage. The inherent characteristic makes the STATCOM more robust and effective than SVC in controlling specific parameters of the electric power system to enhance stability

performance. Fig. 3.13 also illustrates that the STATCOM, depending on its specification and the characteristic of the power electronic components used, may have an increased transient rating in both capacitive and inductive operating regions. Conventional SVC is only capable of increased transient rating in inductive output range. The STATCOM is able to provide reactive output linearly decreasing with system voltage, whereas the SVC reactive output decreases by the square of this voltage as shown in Fig. 3.14.

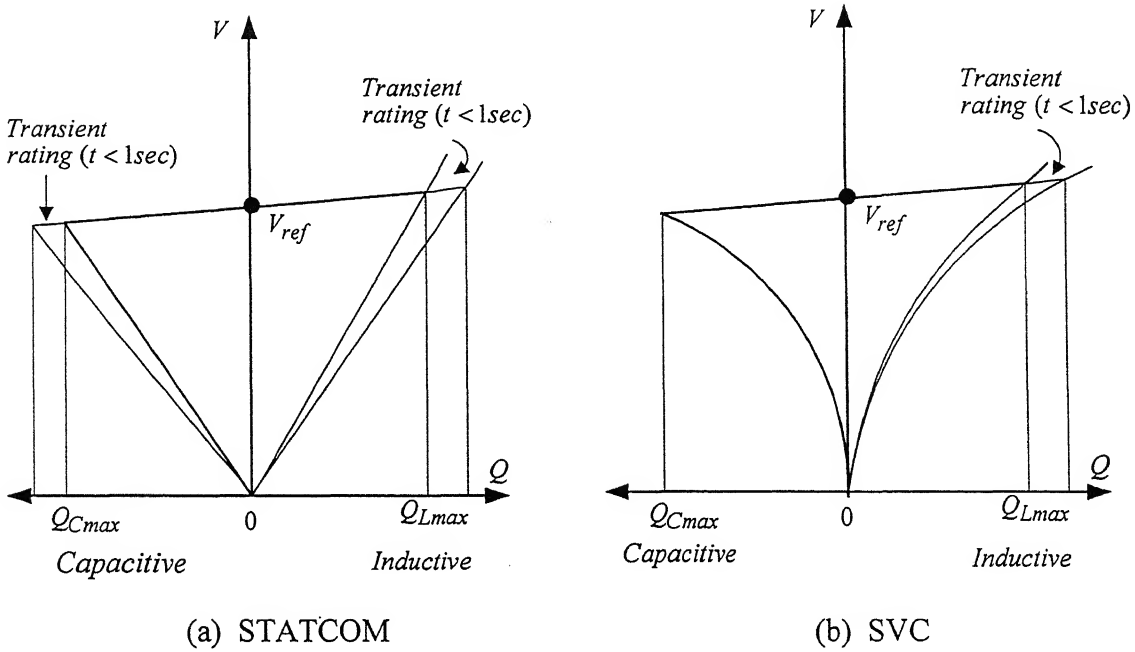


**Fig. 3.14** Typical voltage vs. reactive power characteristics of STATCOM and SVC

The ideal behavior of the STATCOM is equivalent to that of a voltage source behind a reactance whose magnitude can be controlled in a rapid manner. This is different from the characteristic of an SVC whose behavior is equivalent to a voltage controlled shunt susceptance depending upon the system voltage at the connection point. The STATCOM can deliver rated current over the full voltage range like a rotating synchronous compensator.



### 3.3.2 Fundamental Concepts of STATCOM

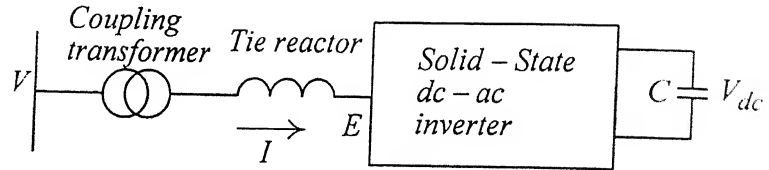
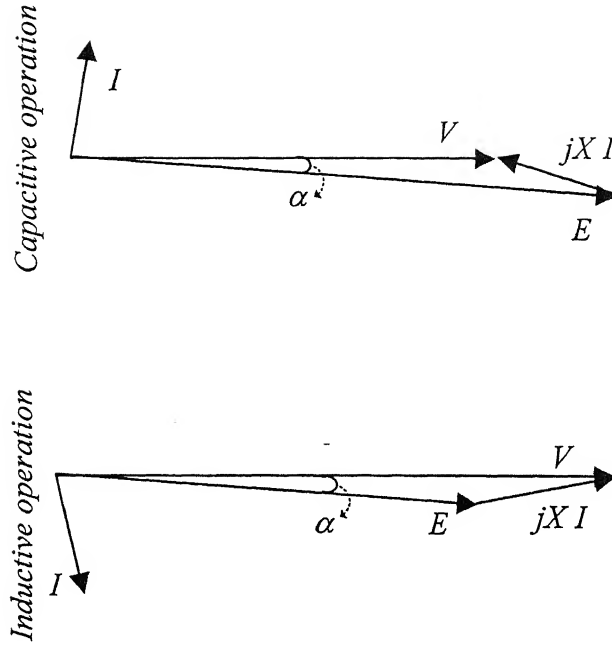


Fig. 3.15 Voltage-source inverter scheme for STATCOM

The basic voltage-source inverter scheme for reactive power generation/absorption is shown in Fig. 3.15. The dc input voltage  $V_{dc}$  to the STATCOM is provided by a dc storage capacitor  $C$ . From this the inverter produces a set of controllable three phase output voltages ( $E$ ) at the fundamental frequency of the ac system. Each output voltage is in phase with, and coupled to corresponding ac system voltage ( $V$ ) via a relatively small (0.1-0.15 p.u.) reactance ( $X$ ) that is usually the per phase leakage reactance of the coupling transformer and tie reactor on its own base. Tie reactor represents various transformers required to form the multi-pulse waveform output from the VSI. By varying the amplitude of the output voltages produced, the reactive power exchange between the inverter and ac system can be controlled as illustrated in Fig. 3.16. If the amplitude  $|E|$  of the output voltage phasor ( $E$ ) is increased above the amplitude  $V$  of the ac system voltage phasor ( $V$ ), then the current phasor leads the voltage phasor and current flows from inverter to the ac system. In this case inverter generates capacitive reactive power. If the amplitude of the output voltage phasor is decreased below that of the ac system voltage phasor, then the reactive power flows from the ac system to the inverter, and the inverter absorbs reactive (inductive) power from the ac system. However, if the amplitude of the output voltage of the inverter is equal to that of the ac system voltage, the reactive power exchange is zero between the power system and STATCOM. Fig. 3.16 shows capacitive and inductive operation of STATCOM with losses.



**Fig. 3.16** Vector diagram of STATCOM operation with losses

### 3.3.3 Inverter Configuration

In its simplest form, an inverter contains six self-commutated semiconductor switches,  $S_1 - S_6$ , each composed of a GTO (Gate Turn Off) thyristor in reverse parallel with a diode as shown in Fig. 3.17. This arrangement is termed as two level, six-pulse inverter. These diodes are also called as feedback diodes because they maintain the continuity of load current flow. As every load has some inductance or capacitance (in this case power system is inductive in nature), the load current does not reverse at the same instant as the load voltage. The diodes connected in anti-parallel carry the load current till it becomes zero (negative current when the load voltage is positive).

In practice, the elementary six-pulse inverter can not meet practical harmonic requirements either for the output voltages or for the input capacitor current. However, by combining a number of six pulse inverters into a multi-pulse structure (and/or using

appropriate pulse width modulation techniques or multi-level inverters), the output voltage distortion and capacitor ripple current can be theoretically reduced to any degree.

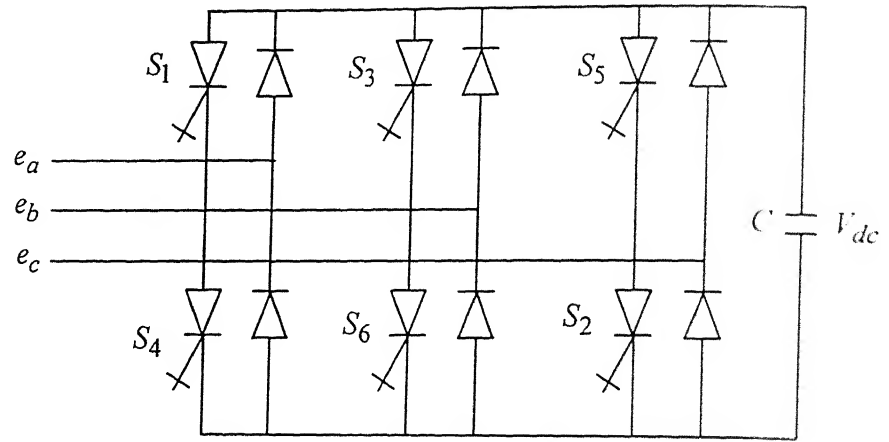


Fig. 3.17 Basic six-pulse voltage-source inverter

Thus, a STATCOM employing an ideal voltage source inverter, generates sinusoidal output voltages and draws sinusoidal reactive current from the ac system with zero average input current from the dc capacitor. In practice, due to system unbalance and other imperfections as well as economic considerations, these ideal conditions are not achieved, but can be approximated quite satisfactorily by inverter structures of sufficiently high pulse number (24 or higher).

Furthermore in a practical inverter, the semiconductor switches are not lossless and therefore the energy stored in the dc capacitor would be used up for meeting the internal losses. However, these losses can be supplied from the ac system by making the output voltages of the inverter lag the ac system voltage by a small angle. In this way the inverter absorbs a small amount of real power from the ac system to meet its internal losses and keep the capacitor voltage at the desired level.

In this chapter, a 48-pulse inverter has been modeled. The design criterion of the 48-pulse inverter is given in detail in [36, 37]. A modular structure of the 48-pulse inverter is shown in Fig. 3.18. The ac side of the 48-pulse inverter is modeled as a voltage source in series with its internal impedance and dc side by a current source in parallel with dc capacitor and a resistance ( $R_{off} + R_{on}$ ). The resistances  $R_{on}$ ,  $R_{off}$  and a switch represents equivalent GTO-diode combination as shown in Fig. 3.19. As  $R_{on} \ll R_{off}$ ,

the impedance appearing across terminals  $A$ - $B$  can be approximated to  $R_{on}$  when switch  $S$  is ON, and it becomes equal to  $R_{off}$  when switch  $S$  is OFF. The 48-pulse inverter is connected to the system bus through an interfacing (coupling) transformer as shown in Fig. 3.18.

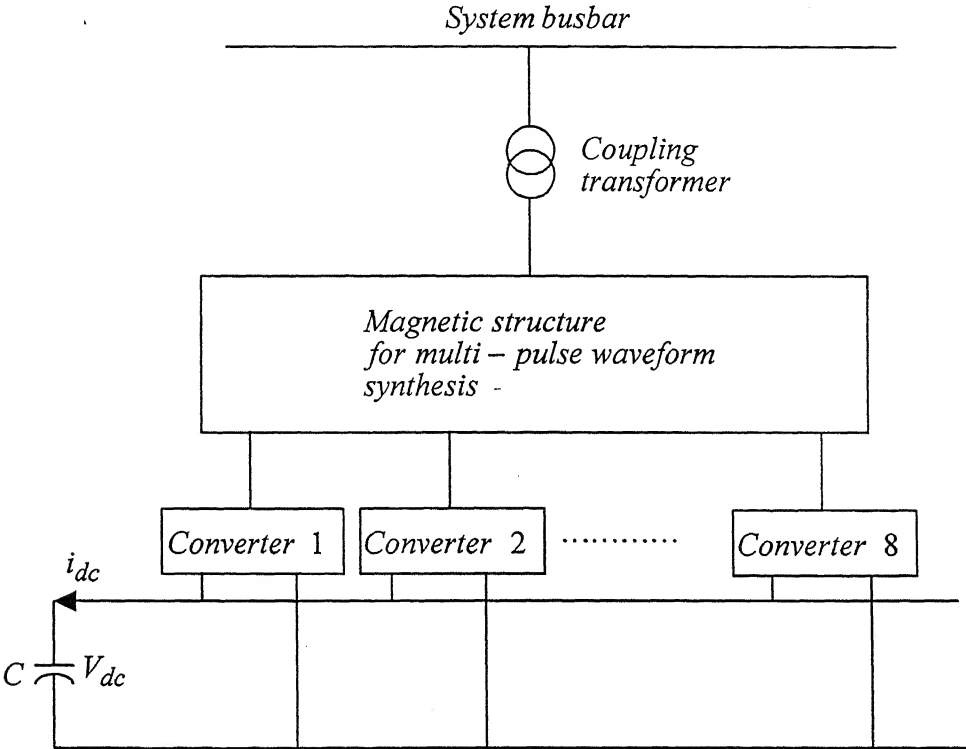


**Fig. 3.18** Modular structure for 48-pulse STATCOM inverter

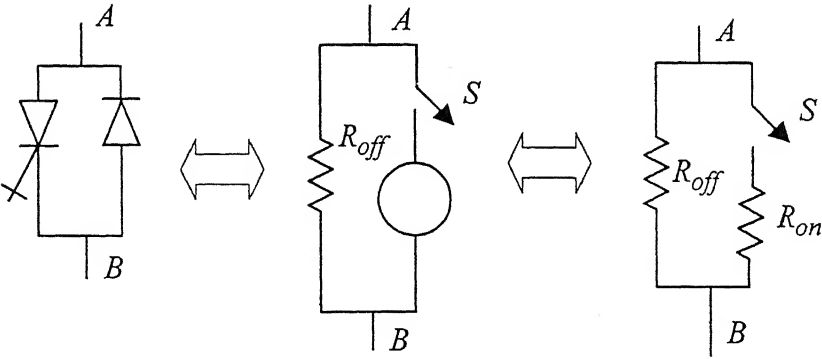


**Fig. 3.19** Equivalent representation of a GTO-diode combination

The equivalent circuit of the 48-pulse inverter is shown in Fig. 3.20 [36, 37]. In this figure  $L_{st}$  and  $R_{st}$  are referred magnetic circuit leakage inductance and inverter resistance respectively.  $R_{dc} = (R_{off} + R_{on})/24$  ( as there are 24 legs) and  $C_{dc}$  is the capacitance of the dc storage capacitor.

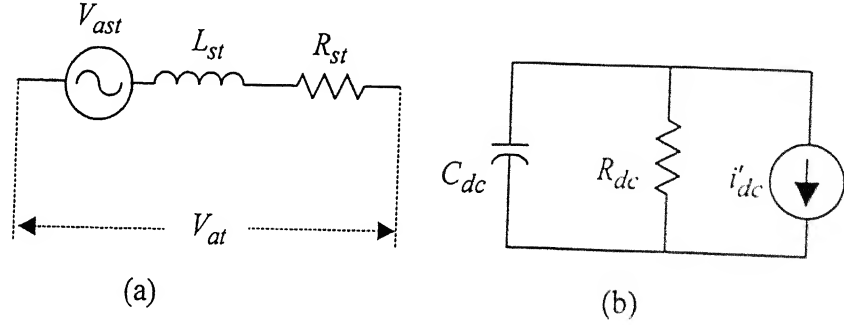


**Fig. 3.20** Equivalent representation of a 48-pulse inverter (a) ac side, (b) dc side

### 3.3.4 STATCOM Modeling

To derive 48-pulse STATCOM modeling, equivalent representation of Fig. 3.20 is considered with the following assumptions.

- The fundamental components of the injected voltage  $V_{ast}$ ,  $V_{bst}$  and  $V_{cst}$  are considered. The lowest order harmonic components for a 48-step inverter are 47<sup>th</sup> and 49<sup>th</sup>. As they have very small magnitudes, their effects have been neglected.
- The three phase voltages  $V_{ast}$ ,  $V_{bst}$  and  $V_{cst}$  are balanced.

Here subscripts 'ast', 'bst' and 'cst' represents the three phases a, b and c respectively.

With the above assumptions, the STATCOM dynamic equations for the three phases can be written as

$$L_{st} \frac{d}{dt} i_{ast} = V_{at} - V_{ast} - R_{st} i_{ast} \quad (3.24)$$

$$L_{st} \frac{d}{dt} i_{bst} = V_{bt} - V_{bst} - R_{st} i_{bst} \quad (3.25)$$

$$L_{st} \frac{d}{dt} i_{cst} = V_{ct} - V_{cst} - R_{st} i_{cst} \quad (3.26)$$

where  $i_{ast}$ ,  $i_{bst}$  and  $i_{cst}$  are the currents flowing in the three phases connected to the STATCOM.

The fundamental components of the STATCOM voltage are given by the following equations [36, 37].

$$V_{ast} = \sigma \frac{16\sqrt{3}}{\pi} V_{dc} \sin(\omega t + \alpha + \theta_t) \quad (3.27)$$

$$V_{bst} = \sigma \frac{16\sqrt{3}}{\pi} V_{dc} \sin(\omega t + \alpha + \theta_t - \frac{2\pi}{3}) \quad (3.28)$$

$$V_{cst} = \sigma \frac{16\sqrt{3}}{\pi} V_{dc} \sin(\omega t + \alpha + \theta_t + \frac{2\pi}{3}) \quad (3.29)$$

where  $\sigma$  is the primary to secondary turns ratio of the interfacing transformer,  $\alpha$  is the small angle between STATCOM output voltage and ac system bus voltage (angle between E and V in Fig. 3.16) and  $\theta_t$  is the angle associated with the ac system bus where the STATCOM is connected. The instantaneous 3- $\phi$  ac bus voltages are given by

$$V_{at} = V_m \sin(\omega t + \theta_t) \quad (3.30)$$

$$V_{bt} = V_m \sin(\omega t + \theta_t - \frac{2\pi}{3}) \quad (3.31)$$

$$V_{ct} = V_m \sin(\omega t + \theta_t + \frac{2\pi}{3}) \quad (3.32)$$

where  $V_m = \sqrt{2} V_{ph}$

Fig. 3.20 (b) is redrawn and is shown in Fig. 3.21. The dc capacitor dynamics is governed by the following equations

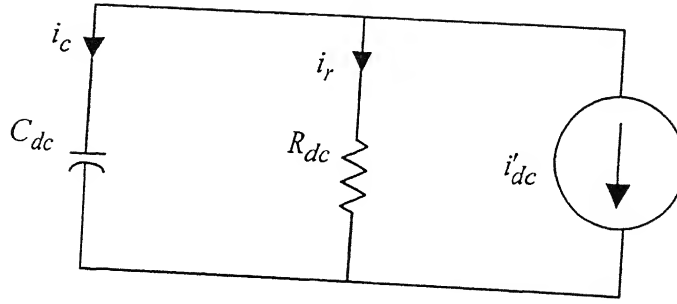


Fig. 3.21 Flow of current in dc side

$$i'_{dc} = -(i_c + i_r) = -\left(\frac{V_{dc}}{R_{dc}} + C_{dc} \frac{d}{dt} V_{dc}\right) \quad (3.33)$$

or

$$\frac{d}{dt} V_{dc} = -\frac{V_{dc}}{C_{dc} R_{dc}} - \frac{i'_{dc}}{C_{dc}} \quad (3.34)$$

The current source  $i'_{dc}$  is given as [36, 37]

$$i'_{dc} = -\sigma \frac{16\sqrt{3}}{\pi} \left[ \sin(\omega t + \alpha + \theta_t) i_{ast} + \sin\left(\omega t + \alpha + \theta_t - \frac{2\pi}{3}\right) i_{bst} + \sin\left(\omega t + \alpha + \theta_t + \frac{2\pi}{3}\right) i_{cst} \right] \quad (3.35)$$

In compact form, the STATCOM model can then be written as

$$\Delta \dot{\mathbf{X}}_{stcom} = \mathbf{L}_{1stcom} \Delta \mathbf{X}_{stcom} + \mathbf{L}_{2stcom} \Delta \alpha + \mathbf{L}_{3stcom} \Delta V_{st} \quad (3.36)$$

Details of (3.36) are given in Appendix F.1.

### 3.3.5 State Feedback Controller with Integral Control

A state feedback controller with integral control is designed for the STATCOM to achieve to regulate the ac bus voltage. The state feedback controller with integral control is of the following form

$$v = \int (V_{dc} - V_{dcref}) dt$$

i.e.

$$\dot{v} = e = V_{dc} - V_{dcref} \quad (3.37)$$

Since  $V_{dcref}$  is constant, Linearizing (3.37) we get

$$\Delta \dot{v} = \Delta V_{dc} \quad (3.38)$$

The combined state-space model of the STATCOM and controller is

$$\begin{bmatrix} \Delta \dot{X}_{stcom} \\ \Delta \dot{v} \end{bmatrix} = \begin{bmatrix} L_{1stcom} & 0 \\ E_{cont} & 0 \end{bmatrix} \begin{bmatrix} \Delta X_{stcom} \\ \Delta v \end{bmatrix} + \begin{bmatrix} L_{2stcom} \\ 0 \end{bmatrix} [\Delta \alpha] + \begin{bmatrix} L_{3stcom} \\ 0 \end{bmatrix} [\Delta V_{st}] \quad (3.39)$$

where  $E_{cont} = [0 \ 0 \ 1]$

We can then rewrite (3.39) as

$$\Delta \dot{X}_{stat} = A_{onst} \Delta X_{stat} + B_{onst} \Delta \alpha + V_{onst} \Delta V_{st} \quad (3.40)$$

In addition to the integral control, a state feedback controller is designed to obtain  $\Delta \alpha$ .

The state feedback is of the form

$$\Delta \alpha = -[\rho_1 \ \rho_2 \ \rho_3 \ \rho_4] [\Delta X_{stat}]$$

i.e.



$$\Delta\alpha = -K_{onst} \Delta X_{stat} \quad (3.41)$$

Incorporation of (3.41) into (3.40) gives

$$\begin{aligned} \Delta \dot{X}_{stat} &= A_{onst} \Delta X_{stat} + B_{onst} (-K_{onst}) \Delta X_{stat} + V_{onst} \Delta V_{st} \\ \text{i.e.} \\ \Delta \dot{X}_{stat} &= A_{stnew} \Delta X_{stat} + V_{onst} \Delta V_{st} \end{aligned} \quad (3.42)$$

In (3.42),  $A_{stnew}$  is  $4 \times 4$  matrix and  $V_{onst}$  is  $4 \times 2$  matrix.

The complex power given by the STATCOM to the system can be written as

$$P_{stcom} + jQ_{stcom} = \tilde{V}_t \tilde{i}_{stcom}^* \quad (3.43)$$

In (3.43)  $P_{stcom}$  and  $Q_{stcom}$  are the real and reactive power given or absorbed by the STATCOM depending on the angle between  $V$  and  $E$  (Fig. 3.16). Also  $P_{stcom}$  is very small;  $\tilde{V}_t$  is the complex bus voltage where the STATCOM is connected and  $i_{stcom}$  is the current flowing in the STATCOM branch. The STATCOM branch current  $i_{stcom}$  is resolved in DQ components as

$$\tilde{i}_{stcom} = i_{Dst} + j i_{Qst} \quad (3.44)$$

After simplification, (3.43) can be written as

$$P_{stcom} + jQ_{stcom} = V_t e^{j\theta_t} \left( \frac{V_{st} e^{j(\alpha+\theta_t)} - V_t e^{j\theta_t}}{R_{st} + jX_{st}} \right)^* \quad (3.45)$$

After linearization, (3.45) can be written in matrix form as

$$\begin{bmatrix} \Delta P_{stcom} \\ \Delta Q_{stcom} \end{bmatrix} = N_{1mod} \Delta X_{stat} + N_2 \Delta V_{st} \quad (3.46)$$

Details of (3.46) are given in Appendix F.2.

### 3.3.6 Incorporation of STATCOM in Multimachine System

The STATCOM model is given by (3.42) and (3.46) and these equations can be incorporated in the DAE multimachine model. Addition of power balance (3.46) of STATCOM in the multimachine system modifies  $D_{2new}$  of (2.32). Equations (2.15) and (2.16) get modified as shown below when STATCOM is connected in the system at specified load buses.

$$P_{stcom i} + P_{Li}(V_i) - \sum_{k=1}^n V_i V_k Y_{ik} \cos(\theta_i - \theta_k - \alpha_{ik}) = 0 \quad i = m+1, \dots, n \quad (3.47)$$

$$Q_{stcom i} + Q_{Li}(V_i) - \sum_{k=1}^n V_i V_k Y_{ik} \sin(\theta_i - \theta_k - \alpha_{ik}) = 0 \quad i = m+1, \dots, n \quad (3.48)$$

Equation (3.49) is obtained after linearization of (3.47) and (3.48) on the same lines as done before.

$$N_{2new} \Delta V_l + N_{1mod} \Delta X_{stat} + D_1 \Delta V_g + D_2 \Delta V_l = 0 \quad (3.49)$$

where  $N_{2new}$  incorporates  $N_2$  and has identical dimension as  $D_2$ .

Equation (3.49) can be rewritten as

$$N_{1mod} \Delta X_{stat} + D_1 \Delta V_g + D_{2stat} \Delta V_l = 0 \quad (3.50)$$

where  $D_{2stat} = N_{2new} + D_2$

Equations (3.42) and (3.50) are added to (2.30) and then reordered to get final form as

$$\begin{bmatrix} \Delta \dot{X} \\ \Delta \dot{X}_{stat} \\ 0 \\ 0 \end{bmatrix} = \begin{bmatrix} A_{1mod} & P_{1stat} & A_{2new} & A_{3new} \\ P_{2stat} & A_{stnew} & B_{stat1new} & B_{statnew} \\ K_2 & P_{3stat} & K_{1new} & C_{4new} \\ G_1 & N_{1mod} & D_{1new\_stat} & D_{2new\_stat} \end{bmatrix} \begin{bmatrix} \Delta X \\ \Delta X_{stat} \\ \Delta z \\ \Delta v \end{bmatrix} + \begin{bmatrix} E \\ 0 \\ 0 \\ 0 \end{bmatrix} \Delta U \quad (3.51)$$

Equation (3.51) can be written as

$$\Delta \dot{X}_{sys\_statcom} = A_{sys\_statcom} \Delta X_{sys\_statcom} + E_{stat} \Delta U \quad (3.52)$$

Various matrices of (3.52) are defined in Appendix F.3. Using (3.52) eigenvalues of the system with STATCOM can be computed.

### 3.4 STATIC SYNCHRONOUS SERIES COMPENSATOR

Static Series Synchronous Compensator (SSSC) is also known as Solid State Series Compensator. It is a series compensation device, which employs a voltage source inverter (VSI) that is fed by a dc storage capacitor. The VSI can be used for shunt reactive power compensation (STATCOM), series reactive power compensation (SSSC) and transmission angle adjustment. A combination of STATCOM and SSSC is called as

Unified Power Flow Controller (UPFC).

This section describes fundamental principles and characteristics, modeling of SSSC in multimachine system and a case study of WSCC system with SSSC connected in the system.

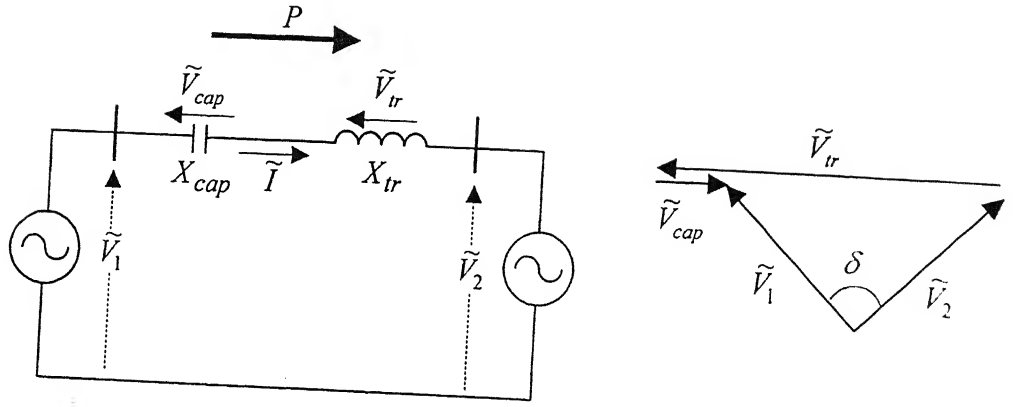
### 3.4.1 Principle of SSSC

Fig. 3.22 shows a two-machine system, in which series compensating device is a series capacitor. The Series capacitor decreases effective reactive line impedance. In other words, series capacitor increases the voltage across the impedance of the transmission line, thereby increasing the line current and the power flow over the line. The same series compensation can be achieved, if the capacitor is replaced by a synchronous ac voltage source, whose output precisely matches the voltage of the series capacitor ( $\tilde{V}_{sssc} = \tilde{V}_{cap} = -j X_{cap} \tilde{I}$ ) as shown in Fig. 3.23. The phasor diagrams for two machine system compensated by capacitor and SSSC respectively are also shown in Figs. 3.22 and 3.23.

In Fig. 3.23,  $\tilde{V}_{sssc}$  is the injected voltage by VSI through interfacing transformer and is given as

$$\tilde{V}_{sssc} = \beta \tilde{I} e^{-j90^\circ} \quad (3.53)$$

Where  $\tilde{I}$  is line current and  $\beta$  is proportionality constant. Equation (3.53) shows that injected voltage by SSSC must be in quadrature (lagging) with the line current for capacitive mode. The output voltage from VSI can be reversed by simple control action to make it lead or lag the line current by  $90^\circ$ . In the inductive mode, the injected voltage decreases the voltage across the inductive line impedance and thus the series compensation has same effect as if the reactive line impedance has been increased.



**Fig. 3.22** Series compensation of two-machine system using capacitor and its phasor diagram

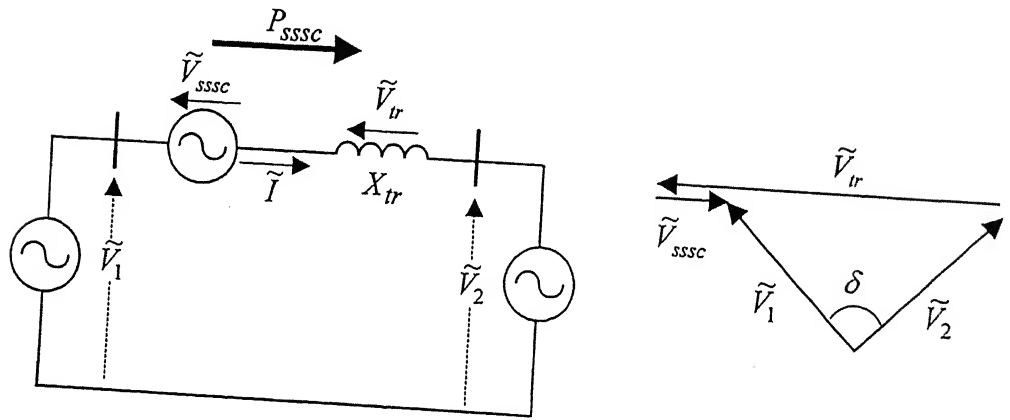


**Fig. 3.23** Series compensation of two-machine system using SSSC and its phasor diagram

SSSC injects the voltage in series with the line irrespective of the line current. Let the injected voltage be redefined as

$$\tilde{V}_{sssc} = V_{sssc} \{ \tilde{I} / |\tilde{I}| \} e^{\mp j90^\circ} \text{ and } V_{sssc} = |\tilde{V}_{sssc}|$$

The power flow equation in this case can be written as

$$P_{sssc} = \frac{V^2}{X_{tr}} \sin \delta + \frac{V}{X_{tr}} V_{sssc} \cos(\delta/2) \quad (3.54)$$

where  $V_1 = V_2 = V$  and  $\delta = \delta_1 - \delta_2$ .

Similarly power flow for the case when capacitor is being used for series compensation (Fig. 3.22) is

$$P = \frac{V^2}{X_{tr}(1-s)} \sin \delta \quad (3.55)$$

where.  $s = \frac{X_{cap}}{X_{tr}}$

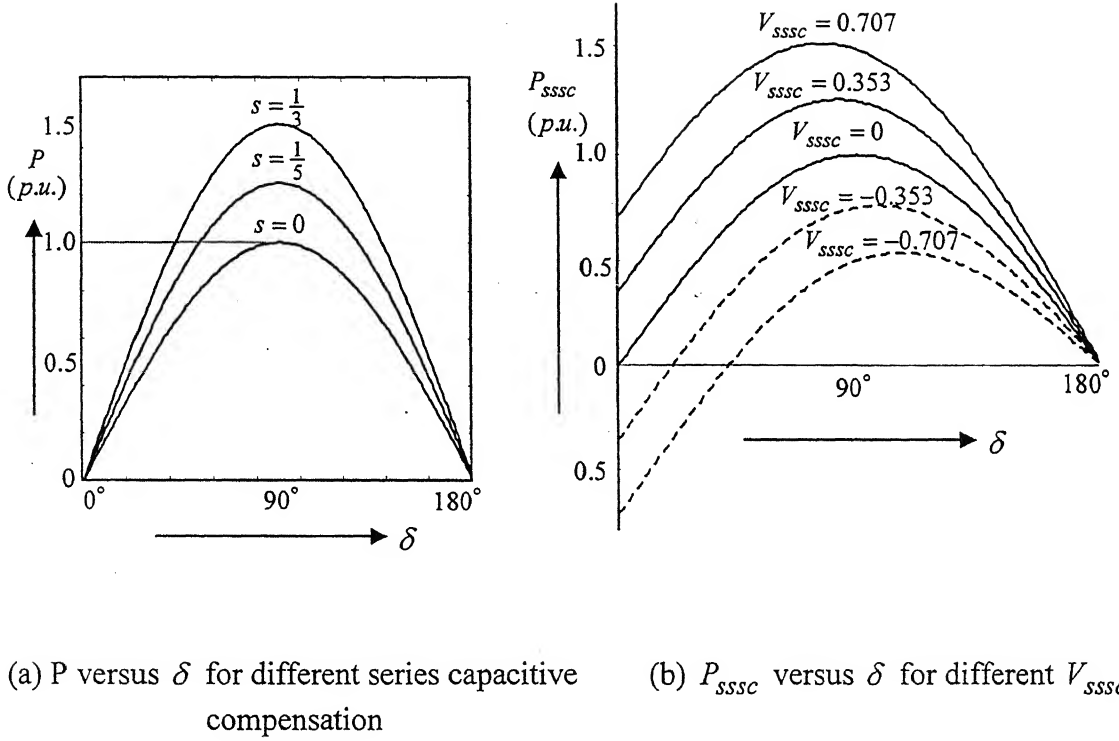


**Fig. 3.24** Transmitted power-angle curve for capacitor and SSSC

The power-angle characteristics for series capacitor and SSSC are shown in Fig. 3.24. In this figure,  $V_{sssc}$  is so chosen that it gives the same maximum power as the

series capacitor for the corresponding  $s$  ( $s = X_{cap}/X_{tr}$ ). It is evident from Fig. 3.24 that at a given  $\delta$ , the series capacitor increases the transmitted power by a fixed percentage of uncompensated power whereas SSSC increases it by a fixed fraction of maximum power transmitted by the uncompensated line.

There are various advantages of SSSC listed in [7]. Some of them are as follows:

- SSSC increases the transmitted power by a fraction of the maximum that can be transmitted by uncompensated line, independently of  $\delta$  in the range  $0 \leq \delta \leq 90^\circ$ .
- SSSC can reverse the power flow over a line by reversing the polarity of the injected voltage and making the injected voltage larger than the voltage impressed across the uncompensated line.
- SSSC has wider control range than the series capacitor type compensation of the same VA rating.
- SSSC can exchange both active and reactive power with the ac system by controlling the angular position of the injected voltage with respect to line current.
- SSSC can keep the effective  $X_{tr}/R$  ratio high by providing compensation for line resistance and line reactance independently of the degree of series compensation.
- SSSC can be extremely effective in damping of power oscillations.
- SSSC can not form series resonant circuit with the inductive line impedance to initiate Subsynchronous Resonance (SSR) i.e. SSSC is immune to SSR. As SSSC has very fast response, it can be very effective in damping of subsynchronous oscillations.

### 3.4.2 Modeling of SSSC

A schematic diagram of SSSC is shown in Fig. 3.25. It is evident from this figure that the main difference between STATCOM and SSSC is in the connection of these devices to the power system. A STATCOM is connected to power system in shunt at a bus whereas an SSSC is connected in series with the transmission line as shown in Fig.

3.25. Both STATCOM and SSSC, produce compensating voltage through VSI. Therefore there is not much difference in the modeling approach.

In this thesis, a 48-step inverter base SSSC is considered. Configuration, model and assumptions of the 48-step inverter have been discussed in detail in previous section pertaining to STATCOM therefore are not being repeated here. The SSSC model has been developed as independent unit and can be connected between any two buses. The equivalent circuit of 48-pulse inverter is shown in Fig. 3.26.

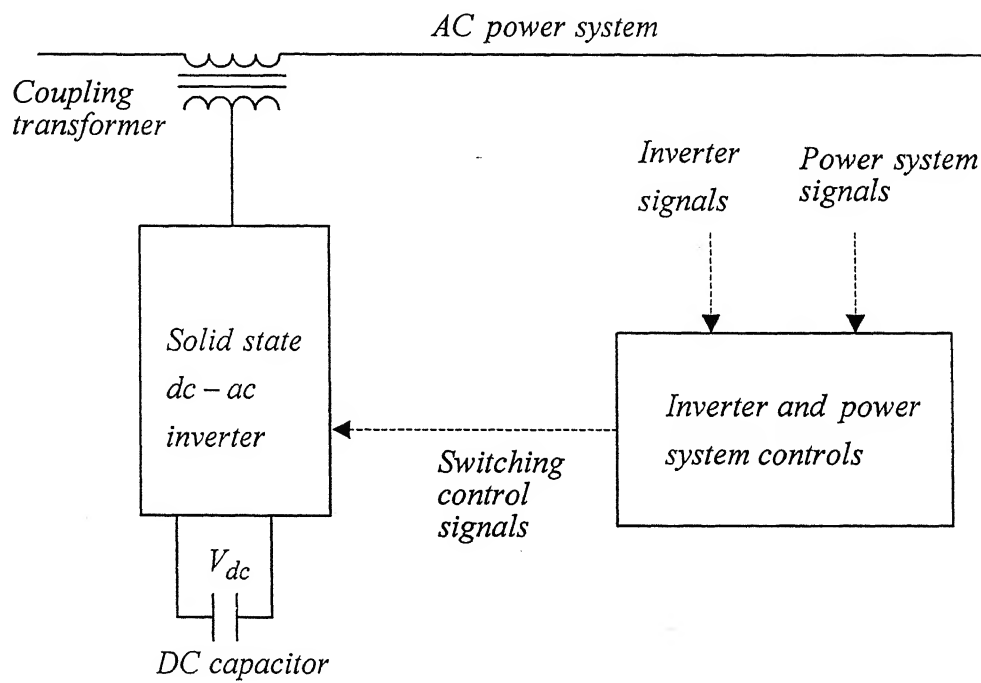


Fig. 3.25 Block diagram of SSSC

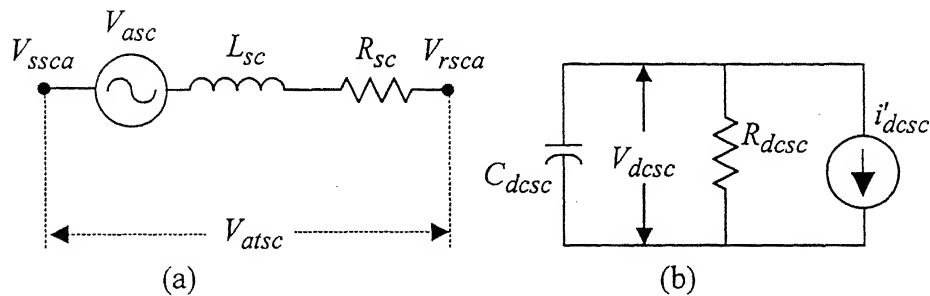


Fig. 3.26 Equivalent representation of a 48-pulse inverter  
(i) ac side for phase a (ii) dc side



In Fig. 3.26,  $L_{sc}$  and  $R_{sc}$  are referred leakage inductance and resistance of coupling transformer and magnetic circuit of voltage source inverter,  $V_{asc}$  is the SSSC output of phase a,  $V_{atsc}$  is the net voltage across SSSC in phase a,  $V_{ssca}$  and  $V_{rsca}$  are the sending end and receiving end voltages of phase a, and  $C_{dcsc}$  and  $R_{dcsc}$  are capacitance of dc storage capacitor and inverter resistance respectively.

The model has been derived using same assumptions as taken for STATCOM i.e.

- The fundamental components of  $V_{asc}$ ,  $V_{bsc}$  and  $V_{csc}$  are considered and harmonics are neglected.
- The three phase voltages  $V_{asc}$ ,  $V_{bsc}$  and  $V_{csc}$  are balanced.

With above assumptions, the SSSC dynamic equations for the three phases can be written as

$$L_{sc} \frac{d}{dt} i_{asc} = V_{atsc} - V_{asc} - R_{sc} i_{asc} \quad (3.56)$$

$$L_{sc} \frac{d}{dt} i_{bsc} = V_{btsc} - V_{bsc} - R_{sc} i_{bsc} \quad (3.57)$$

$$L_{sc} \frac{d}{dt} i_{csc} = V_{ctsc} - V_{csc} - R_{sc} i_{csc} \quad (3.58)$$

where  $i_{asc}$ ,  $i_{bsc}$  and  $i_{csc}$  are the line currents flowing in the three phases through SSSC. The fundamental components of SSSC sending end voltage are given by the following equations [36, 37].

$$V_{asc} = \mu \frac{16\sqrt{3}}{\pi} V_{dcsc} \sin(\omega t + \theta_f) \quad (3.59)$$

$$V_{bsc} = \mu \frac{16\sqrt{3}}{\pi} V_{dcsc} \sin(\omega t + \theta_f - \frac{2\pi}{3}) \quad (3.60)$$

$$V_{csc} = \mu \frac{16\sqrt{3}}{\pi} V_{dcsc} \sin(\omega t + \theta_f + \frac{2\pi}{3}) \quad (3.61)$$

where  $\mu$  is the primary to secondary turns ratio of the interfacing transformer and  $\theta_f$  is the angle of the injected voltage of SSSC.

The instantaneous 3- $\phi$  sending end ac bus voltages are given by

$$V_{ssca} = V_m \sin(\omega t + \theta_s) \quad (3.62)$$

$$V_{sscb} = V_m \sin(\omega t + \theta_s - \frac{2\pi}{3}) \quad (3.63)$$

$$V_{sscc} = V_m \sin(\omega t + \theta_s + \frac{2\pi}{3}) \quad (3.64)$$

where  $V_m = \sqrt{2} V_{ph}$  and  $\theta_s$  is the sending end bus voltage angle. Similarly instantaneous 3- $\phi$  receiving end ac bus voltages can be written. Fig. 3.20 is redrawn and is shown in Fig. 3.27. The dc capacitor dynamics is governed by the following equations

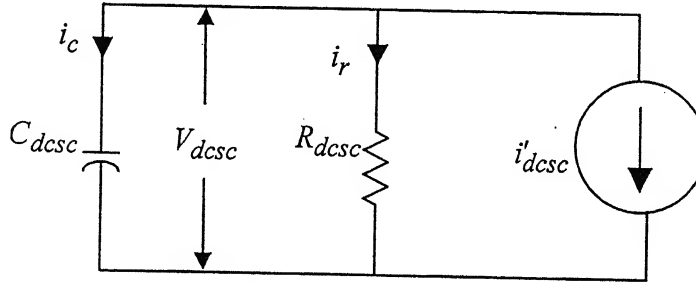


Fig. 3.27 Current flow in dc side

$$i'_{dcsc} = -(i_c + i_r) = -\left( \frac{V_{dcsc}}{R_{dcsc}} + C_{dcsc} \frac{d}{dt} V_{dcsc} \right) \quad (3.65)$$

or

$$\frac{d}{dt} V_{dcsc} = -\frac{V_{dcsc}}{C_{dcsc} R_{dcsc}} - \frac{i'_{dcsc}}{C_{dcsc}} \quad (3.66)$$

The current source  $i'_{dcsc}$  is given as [36, 37]

$$i'_{dcsc} = -\mu \frac{16\sqrt{3}}{\pi} \left[ \sin(\omega t + \theta_f) i_{asc} + \sin\left(\omega t + \theta_f - \frac{2\pi}{3}\right) i_{bsc} + \sin\left(\omega t + \theta_f + \frac{2\pi}{3}\right) i_{csc} \right] \quad (3.67)$$

The procedure adopted in STATCOM is repeated and the following equation is obtained in matrix notation

$$\Delta \dot{X}_{sc} = M_{1ssc} \Delta X_{sc} + M_{2ssc} \Delta \theta_f + M_{3ssc} \Delta V_{ssc} \quad (3.68)$$

Equation (3.68) represents state-space model of SSSC without controller. Various matrices of (3.68) are defined in Appendix G.1.

### 3.4.3 Incorporation of State Feedback Controller with Integral Control in SSSC Model

As already discussed, SSSC should inject the voltage in quadrature with line current to enhance power transfer capacity of the transmission line. The injected voltage is directly proportional to dc capacitor voltage. So, to control the injected voltage, the dc capacitor voltage should be regulated. The dc capacitor voltage can regulate the injected voltage, which can be achieved by changing  $\theta_f$  (angle of the injected voltage). This is done by a controller. The integral feedback controller has been chosen here.

The state feedback controller with integral control is of the following form

$$\sigma_{ssc} = \int (V_{dcsc} - V_{dcscref}) dt$$

i.e.

$$\dot{\sigma}_{ssc} = er = V_{dcsc} - V_{dcscref} \quad (3.69)$$

where  $V_{dcref}$  is the desired voltage on the dc side and is constant. Thus linearizing (3.69) we get

$$\Delta \dot{\sigma}_{ssc} = \Delta V_{dcsc} \quad (3.70)$$

The combined state-space model of the SSSC and integral feedback controller is

$$\begin{bmatrix} \Delta \dot{X}_{sc} \\ \Delta \dot{\sigma}_{ssc} \end{bmatrix} = \begin{bmatrix} \mathbf{M}_{1ssc} & 0 \\ E_{int} & 0 \end{bmatrix} \begin{bmatrix} \Delta X_{sc} \\ \Delta \sigma_{ssc} \end{bmatrix} + \begin{bmatrix} \mathbf{M}_{2ssc} \\ 0 \end{bmatrix} [\Delta \theta_f] + \begin{bmatrix} \mathbf{M}_{3ssc} \\ 0 \end{bmatrix} [\Delta V_{ssc}] \quad (3.71)$$

where  $E_{int} = [0 \ 0 \ 1]$

Equation (3.71) is rewritten as

$$\Delta \dot{X}_{sssc} = \mathbf{A}_{onssc} \Delta X_{sssc} + \mathbf{B}_{onssc} \Delta \theta_f + \mathbf{V}_{onssc} \Delta V_{ssc} \quad (3.72)$$

where

$$\Delta X_{sssc} = [\Delta X_{sc} \ \Delta \sigma_{ssc}]^t, \quad \mathbf{A}_{onssc} = \begin{bmatrix} \mathbf{M}_{1ssc} & 0 \\ E_{int} & 0 \end{bmatrix}$$

$$\mathbf{B}_{onssc} = \begin{bmatrix} \mathbf{M}_{2ssc} \\ 0 \end{bmatrix} \text{ and } \mathbf{V}_{onssc} = \begin{bmatrix} \mathbf{M}_{3ssc} \\ 0 \end{bmatrix}$$

In addition, a state feedback controller is used to compute  $\Delta \theta_f$ . This is given by

$$\Delta \theta_f = -[\rho_{s1} \ \rho_{s2} \ \rho_{s3} \ \rho_{s4}] [\Delta X_{sssc}],$$

i.e.

$$\Delta \theta_f = -\mathbf{K}_{onssc} \Delta X_{sssc} \quad (3.73)$$

Incorporation of (3.73) into (3.72) gives

$$\Delta \dot{X}_{SSC} = A_{onssc} \Delta X_{SSC} + B_{onssc} (-K_{onssc}) \Delta X_{SSC} + V_{onssc} \Delta V_{SSC}$$

i.e.

$$\Delta \dot{X}_{SSC} = A_{SSCnew} \Delta X_{SSC} + V_{onssc} \Delta V_{SSC} \quad (3.74)$$

$$\text{where } A_{SSCnew} = A_{onssc} - B_{onssc} K_{onssc}$$

In (3.74),  $A_{SSCnew}$  and  $V_{onssc}$  are  $4 \times 4$  matrices.

The power equation for SSSC can be written in matrix form as

$$\begin{bmatrix} \Delta P_{SSC} \\ \Delta Q_{SSC} \\ \Delta P_{rsc} \\ \Delta Q_{rsc} \end{bmatrix} = A_{SSSC1} \Delta X_{SSC} + A_{SSSC2} \Delta V_{SSC} \quad (3.75)$$

Details of (3.75) are given in Appendix G.2.

#### 3.4.4 Incorporation of SSSC in Multimachine System

Equations (3.74) and (3.75) are the linearized equations of the SSSC and can be incorporated in the DAE multimachine model. Addition of (3.75) of SSSC in the multimachine system modifies  $D_{2new}$  of (2.32). In order to get the power balance equation with SSSC in the multimachine system, (3.75) is added to (2.15) and (2.16). Hence when SSSC is connected in the system between specified load buses, (2.15) and (2.16) get modified as shown below

$$P_{sssc\ i} + P_{Li}(V_i) - \sum_{k=1}^n V_i V_k Y_{ik} \cos(\theta_i - \theta_k - \alpha_{ik}) = 0 \quad i = m+1, \dots, n \quad (3.76)$$

$$Q_{sssc\ i} + Q_{Li}(V_i) - \sum_{k=1}^n V_i V_k Y_{ik} \sin(\theta_i - \theta_k - \alpha_{ik}) = 0 \quad i = m+1, \dots, n \quad (3.77)$$

Equation (3.78) is obtained after linearization of (3.76) and (3.77) on the same lines as done before

$$A_{sssc1} \Delta X_{sssc} + D_1 \Delta V_g + D_{2sssc} \Delta V_l = 0 \quad (3.78)$$

Details of (3.78) are given in Appendix G.2.

Equations (3.74) and (3.78) are added to (2.30) and then reordered to get final form as

$$\begin{bmatrix} \Delta \dot{X} \\ \Delta \dot{X}_{sssc} \\ 0 \\ 0 \end{bmatrix} = \begin{bmatrix} A_{1mod} & P_{1sssc} & A_{2new} & A_{3new} \\ P_{2sssc} & A_{ssscnew} & B_{sssc1new} & B_{ssscnew} \\ K_2 & P_{3sssc} & K_{1new} & C_{4new} \\ G_1 & A_{sssc1} & D_{1new\_sssc} & D_{2new\_sssc} \end{bmatrix} \begin{bmatrix} \Delta X \\ \Delta X_{sssc} \\ \Delta z \\ \Delta v \end{bmatrix} + \begin{bmatrix} E \\ 0 \\ 0 \\ 0 \end{bmatrix} \Delta U \quad (3.79)$$

Equation (3.79) can be written as

$$\Delta \dot{X}_{sys\_sssc} = A_{sys\_sssc} \Delta X_{sys\_sssc} + E_{sssc} \Delta U \quad (3.80)$$

Details of (3.80) are given in Appendix G Sec. G.3. Using (3.80), eigenvalues of the system with SSSC can be computed.

### 3.5 INCORPORATION OF MULTIPLE FACTS DEVICES

Incorporation of multiple FACTS devices can be done on the same lines as described for various FACTS devices. The models of various FACTS devices are developed on independent basis as done in Sections 3.1-3.4 for various FACTS devices. For example when SVC-TCSC combination is required to be incorporated in multimachine model of the system, following equation in matrix form will emerge

$$\begin{bmatrix} \Delta \dot{X} \\ \Delta \dot{X}_{SVC} \\ \Delta \dot{X}_{TCSC} \\ 0 \\ 0 \end{bmatrix} = \begin{bmatrix} A_{1mod} & P_{1svc} & P_{1tcsc} & A_{2new} & A_{3new} \\ P_{2svc} & A_{SVC} & tcsv1 & B_{svclnew} & B_{svcnnew} \\ P_{2tcsc} & tcsv2 & A_{TCSC} & B_{tcscclnew} & B_{tcscnnew} \\ K_2 & P_{4svc} & P_{4tcsc} & K_{1new} & C_{4new} \\ G_1 & D_{SVC} & C_{TCSC} & D_{1newsvtc} & D_{2newsvtc} \end{bmatrix} \begin{bmatrix} \Delta X \\ \Delta X_{SVC} \\ \Delta X_{TCSC} \\ 0 \\ 0 \end{bmatrix} + \begin{bmatrix} E \\ 0 \\ 0 \\ 0 \\ 0 \end{bmatrix} \Delta U \quad (3.81)$$

Equation (3.81) can be written as

$$\Delta \dot{X}_{SVTC} = A_{SVTC} \Delta X_{SVTC} + E_{SVTC} \Delta U \quad (3.82)$$

Details of (3.82) are given in Appendix H.1.

Similarly STATCOM-TCSC combination can also be incorporated in the multimachine model.

### **3.6 CONCLUSIONS**

In this chapter modeling of various FACTS devices, viz., SVC, TCSC, STATCOM and SSSC using power balance formulation is presented. These developed modules of FACTS devices are modular in nature and can incorporate any type of controller with varying complexity. This chapter also describes methodology for incorporating the FACTS devices into multimachine model developed in Chapter 2. The methodology is general hence any number and any type of FACTS device can be incorporated in the multimachine model. Incorporation of multiple FACTS devices into multimachine model has also been described in this chapter. These models are utilized in subsequent chapters to assess the small signal stability of various power systems using the proposed placement methodology. Using these modules the interaction between two FACTS devices is also studied in subsequent chapters.



## PLACEMENT STRATEGY OF FACTS DEVICES

Due to ever increasing load demand and reduced rights of way, modern power transmission systems are forced to carry increasingly more power over long distances. Consequently, the transmission system becomes more stressed, which in turn, makes the system more vulnerable to stability and security problems [60, 54, 59, 61, 102, 104, 55, 46]. There are several cases of voltage instability leading to voltage collapse in France, Belgium, United States, Japan, and in Ontario Hydro system in Canada [55]. The need of the hour is, therefore, to operate the high power transmission grid in a way that it is able to carry more power (ideally close to its thermal limit) over long distance without sacrificing its stability and security margins. The above task can only be accomplished when there is proper fast control over power flow in a transmission system. With the emergence of high power semiconductor switches, a number of control devices under the generic name of Flexible AC Transmission System (FACTS) have come under active consideration to achieve the above objective.

FACTS controllers, by virtue of their fast controllability, are expected to maintain the stability and security margin of highly stressed power systems. A number of control strategies for FACTS controllers have been suggested in literature for this purpose [1, 99]. However, to achieve the optimum performance of these controllers, proper placement of controlling devices in the grid is as important as an effective control strategy. Hence, it is imperative that proper placement strategy must precede the installation of any such device to obtain optimum performance.

There are several indices/methods proposed in literature for placement of FACTS devices from voltage stability/small signal stability viewpoint [60, 54, 59, 61, 102, 104, 55, 46, 83, 56, 47, 57, 91]. Various techniques such as Residue method [55, 91], Bus participation factor [46], Control area algorithm [83], Location Index for Effective Damping (LIED) [56], Hybrid optimization technique [47], Damping index [57] have been used for placement of FACTS devices. Weak lines/buses based on voltage stability

considerations have been proposed in [60, 54, 59, 61, 55] that could be probable locations for placing a FACTS device

In this chapter a very simple method of identifying most critical segment is proposed using an extension of Voltage Phasors Approach (VPA), henceforth called as Extended Voltage Phasors Approach (EVPA). The results of EVPA are compared with Line Flow Index (LFI) Method [61]. LFI identifies exact location and cause of the voltage collapse (whether due to real or reactive power loading) by identifying critical lines instead of critical buses and also it does not require computation of the Jacobian matrix.

#### 4.1 LINE FLOW INDEX APPROACH

The method for Line Flow Index (LFI) computation is well documented in [61]. The method is compared with the methods developed in [60, 54, 59]. In this method the power flow over a line is examined from either direction, i.e., power flowing from sending end (node  $i$ ) to receiving end (node  $i+1$ ) and vice versa. This leads to four different equations, two for the real power and two for the reactive power. Each of these equations can be utilized to determine a condition that can indicate the critical lines/buses. This methodology is discussed below.

Let  $r_i$  and  $X_i$  be the resistance and reactance respectively of the line joining buses  $i$  and  $j$ ;  $P_i$  and  $Q_i$  represent real and reactive power flowing from node  $i$ ;  $P_r$  and  $Q_r$  represent real and reactive power entering into node  $i+1$ . Then the real power  $P_r$  entering at the receiving end of a bus is given by

$$P_r = P_i - \frac{r_i(P_i^2 + Q_i^2)}{V_i^2} \quad (4.1)$$

where  $V_i$  is the voltage of node  $i$ .

Rearranging the above equation, the value of  $P_i$  can be calculated from the roots of the following quadratic equation:

$$\frac{r_i}{V_i^2} P_i^2 - P_i + P_r + \frac{r_i}{V_i^2} Q_i^2 = 0 \quad (4.2)$$

Since  $P_i$  must be real, the following condition obtained from the above equation, must be satisfied for ensuring voltage stability.

$$1 - 4 \frac{r_i}{V_i^2} \left( P_r + \frac{r_i}{V_i^2} Q_i^2 \right) \geq 0 \quad (4.3)$$

The second term in the left-hand side of (4.3) is the Line Flow Index of Sending end Real Power (LFISP). Proceeding similarly and using expressions for real and reactive powers, the Line Flow Indices of Receiving end Real Power (LFIRP), Sending End Reactive Power (LFISQ) and Receiving End Reactive Power (LFIRQ), can be found out as

$$\text{LFISP:} \quad 4 \frac{r_i}{V_i^2} \left( P_r + \frac{r_i}{V_i^2} Q_i^2 \right) \quad (4.4)$$

$$\text{LFIRP:} \quad 4 \frac{r_i}{V_{i+1}^2} \left( -P_i + \frac{r_i}{V_{i+1}^2} Q_r^2 \right) \quad (4.5)$$

$$\text{LFISQ:} \quad 4 \frac{X_i}{V_i^2} \left( Q_r + \frac{X_i}{V_i^2} P_i^2 \right) \quad (4.6)$$

$$\text{LFIRQ:} \quad 4 \frac{X_i}{V_{i+1}^2} \left( -Q_i + \frac{X_i}{V_{i+1}^2} P_r^2 \right) \quad (4.7)$$

These Line Flow Indices are calculated for all the lines in the system and the lines with high value (close to 1.0) are considered as the critical lines. This is because when the indices become close to unity, the roots tend to become imaginary. The receiving end bus of the critical line is identified as the weakest bus from the voltage stability point of view [61].

## 4.2 VOLTAGE PHASORS APPROACH (VPA)

Gubina et al. [62] presented Voltage Collapse Proximity Index (VCPI) using VPA. They have shown that voltage phasors contain sufficient information to determine voltage collapse proximity and it is possible to identify transmission paths to the most critical load buses with respect to the real or reactive power loading. The main advantage of this method is that it is computationally less intensive, as it does not require computation of Jacobian matrices. A brief outline of voltage phasors approach is given below for ready reference.

For a simple two bus system with bus 1 as generator bus and bus 2 as load bus, the critical condition for stable operation is reached when its Jacobian reaches singularity, i.e.

$$\det J = \frac{\partial P_2}{\partial \delta_2} \frac{\partial Q_2}{\partial V_2} - \frac{\partial P_2}{\partial V_2} \frac{\partial Q_2}{\partial \delta_2} = 0 \quad (4.8)$$

Equation (4.8) gives the condition for stable operating limit as [62]

$$0.5 V_1 = V_2 \cos \delta_{12} \quad (4.9)$$

where voltage phasors are denoted by  $\bar{V} = Ve^{j\delta}$ , P and Q are active and reactive powers respectively.

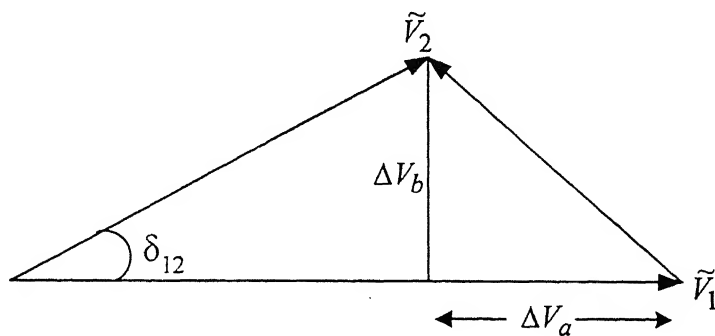


**Fig. 4.1** Voltage phasor diagram for a two bus system

Fig. 4.1 shows voltage phasor diagram for a simple two bus system. It is evident from this figure that  $V_2 \cos \delta_{12}$  in (4.9) corresponds to the projection of load bus phasor  $V_2$  on phasor  $V_1$  and voltage drop phasor  $\Delta V_a$  represents the difference between the above projection and the sending end voltage phasor  $V_1$ . Then the stability condition can be expressed in terms of phasors.

As the active power flow is strongly related to the angle variation, a transmission path with decreasing phase angles (voltage phase angles) can be identified. An Active Power Transmission Path (APTP) is defined as a sequence of connected buses with declining phase angles. An APTP starts from a generator bus with the highest phase angle value and ends at a load bus with lowest phase angle value.

Similarly, as the reactive power flow is strongly related to voltage magnitude variation, a transmission path with declining voltage magnitudes can be identified. A Reactive Power Transmission Path (RPTP) is defined as a sequence of connected buses with declining voltage magnitudes. A RPTP also starts from a generator bus with the highest voltage magnitude and ends at a load bus with lowest voltage magnitude. As the voltage collapse may occur at the load bus at the end of the identified transmission path, therefore all identified transmission paths (APTP and RPTP) are considered for voltage collapse location and identification.

A voltage stability index termed Transmission Path Stability Index (TPSI) has been proposed [62], which is defined as the difference between the halved generator phasor magnitude and the corrected voltage drop along a transmission path

$$TPSI = 0.5 V_g - \Delta V'_a \quad (4.10)$$

where  $V_g$  is generator voltage phasor magnitude and  $\Delta V'_a$  is sum of corrected voltage drops along a transmission path. The TPSI index is expressed in per unit. When its value reaches zero, the power transfer on that transmission path becomes unstable due to voltage collapse [62].

TPSI is calculated for both active and reactive power transmission paths (APTPs and RPTPs respectively). Further VCPI is defined as minimum TPSI value of APTPs and

RPTPs. Minimum TPSI value for APTP/RPTP shows that voltage instability problem is due to active power loading or reactive power loading in the system.

#### 4.3 PROPOSED STRATEGY FOR PLACEMENT OF FACTS DEVICES

Both LFI and TPSI do not require calculation of Jacobian, hence these methods are computationally less intensive. LFI identifies critical lines instead of critical buses due to real/reactive power loading. LFIs for all lines in the system are computed and the line with highest values of LFI is identified as most critical. Since LFIs are calculated for each line in the system, four indices are required for each line.

VPA identifies the critical transmission path due to real/reactive power loading [62]. It is to be noted that while VPA identifies the critical path, it does not identify the critical segment. Hence there is a need for modification in the VPA approach for identification of critical segment. The investigation presented below shows that VPA technique can be suitably modified to identify the critical segment/bus of the system, which can be utilized for placement of a FACTS device. A close examination of VPA reveals that critical path identification is dependent on corrected voltage drop along a line segment. Hence, intuitively, the segment experiencing the maximum corrected voltage drop in the critical path may be construed as the optimum location for placing a FACTS device. This hypothesis is examined for various systems of different sizes at base case and maximum loading conditions (upto the non-convergence of load flow). Studies performed on these systems reveal that this hypothesis works accurately in all systems at different loading conditions. This hypothesis is now termed as Extended Voltage Phasors Approach (EPVA). Further the EPVA is computationally more efficient than LFI approach as it does not require four indices for each segment.

A close examination of the EVPA leads to the following interpretation. If TPSI is minimum for APTP, a series device may be placed in the most critical segment, similarly if TPSI is minimum for RPTP, a shunt device can be placed at the most critical bus.

This study has been done for four systems, viz. 6 bus [61], 9 bus [97], 39 bus [12] and 68 bus [98] systems at the original base case loading condition and maximum loading condition (beyond which load flow does not converge) when FACTS devices are not

connected. In all the system studies LFIs of transformers have been omitted as these are treated as device segments. This practice has been followed in an earlier paper [56].

The results of the four systems are compared with LFI approach and it is shown that EVPA is capable of identifying critical segment/bus due to active/reactive power loading. Moreover this method requires much less computation effort than LFI approach as it does not require four indices for each segment.

#### 4.3.1 Six Bus Test System

The schematic diagram of the 6-bus test system is shown in Fig. 4.2. The system data for 6-bus test system is given in Appendix I [61]. Dynamic data has been taken from [97, 45]. The 6-bus system comprises two generators connected at buses 1 and 2 respectively and loads at all other four buses. The load flow results at base case condition are also given in Appendix I. Both approaches, viz. LFI and Voltage Phasors Approach are applied to the system. Fig. 4.3 shows LFIs of various lines in the system at base case loading condition.

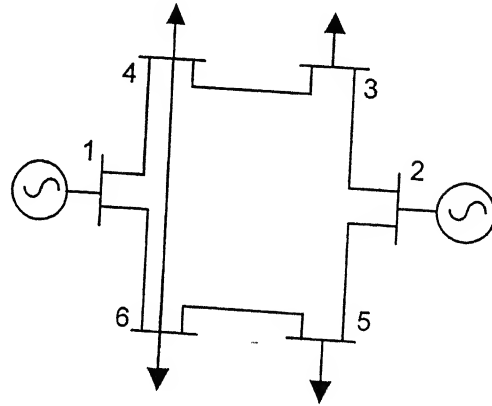
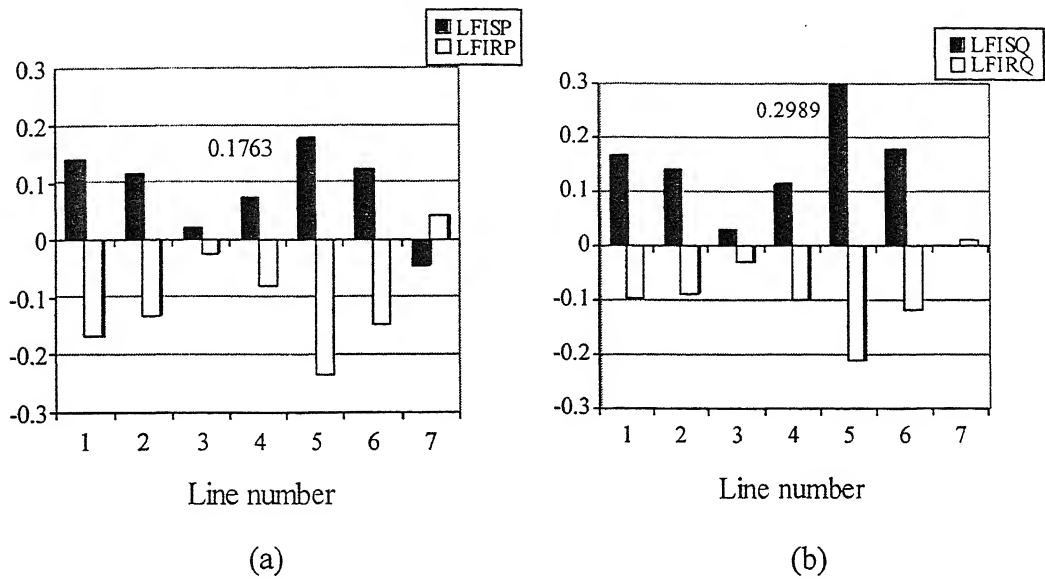


Fig. 4.2 Schematic diagram of six-bus test system

Various LFIs are tabulated and are given in Appendix I. Fig 4.3 (a) and Fig. 4.3 (b) show values of various LFIs for the 6-bus system. The maximum value in each graph is also indicated. It is clear from Fig. 4.3 that the LFISQ index of line 5 (segment 2-5) is maximum and therefore line 2-5 and bus 5 are most critical at base case loading condition. Thus from LFI approach line 2-5 and bus 5 are most suitable locations for

placing FACTS device. As the index of LFISQ is maximum, therefore it seems logical that a suitable shunt FACTS device need to be placed at bus 5 for voltage profile/stability improvement.



**Fig. 4.3** LFIs of various line for 6-bus system at base case loading condition

Fig. 4.4 shows the voltage profile of the 6-bus system at base case loading condition. It is clear that voltage of bus 5 is less than any other load bus in the system. Hence bus 5 can be the candidate bus for placement of a shunt device.

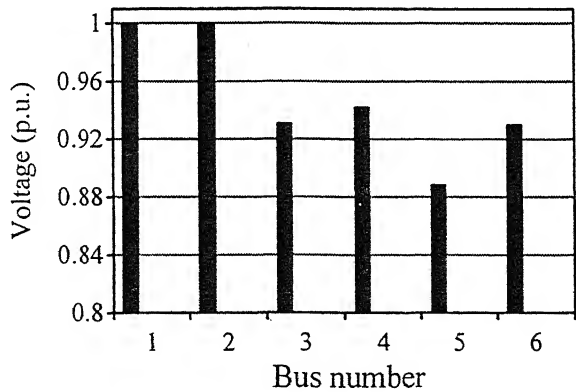


**Fig. 4.4** Voltage profile of 6-bus system at base case loading condition



The Voltage Phasor Approach requires identification of Active Power Transmission Path (APTP) and Reactive Power Transmission Path (RPTP) together with the computation of Transmission Path Stability Index (TPSI). The minimum value of TPSI for a particular APTP or RPTP signifies that that particular path is most critical. Various APTPs and RPTPs for the 6-bus system at base case loading condition are given in Table 4.1. In general, APTPs are written as A1, A2...., and RPTPs are written as R1, R2.... First bus in each APTP and RPTP indicates generator bus number e.g. A1 specified as (1-6) (6-5) indicates that this segment starts from generator 1. There are 5 active and 5 reactive paths as shown in Table 4.1. It is revealed in Table 4.1 that the system has same APTPs and RPTPs. Hence, same TPSI values are obtained as shown in Fig. 4.5.

**Table 4.1** Active and Reactive transmission paths for the 6-bus system at base case loading condition

Active Power Transmission Paths  
(APTP)

Path No.	Line connection from bus to bus
A1	(1-6) (6-5)
A2	(1-4) (4-3)
A3	(1-4) (4-6) (6-5)
A4	(2-5)
A5	(2-3)

Reactive Power Transmission Paths  
(RPTP)

Path No.	Line connection from bus to bus
R1	(1-6) (6-5)
R2	(1-4) (4-3)
R3	(1-4) (4-6) (6-5)
R4	(2-5)
R5	(2-3)

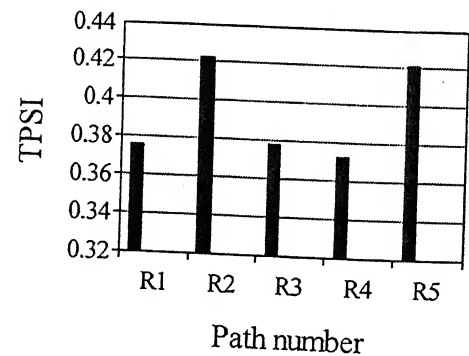
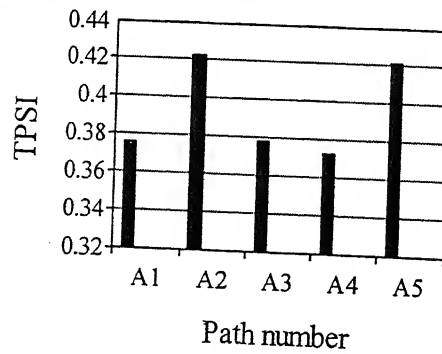


**Fig. 4.5** TPSI for APTPs and RPTPs at base case loading condition

Fig. 4.5 shows that TPSI for paths A4 and R4 are minimum. Table 4.1 shows that A4 and R4 corresponds to the line segment 2-5. Hence from the consideration of APTP and RPTP both line segment 2-5 and bus 5 are critical. The results of Extended Voltage Phasor Approach (EVPA) match with LFI approach. Hence for base case condition line segment 2-5 and bus 5 are appropriate places for placing a FACTS device. This result also correlates with that reported in [60].

### 4.3.2 Nine Bus WSCC Test System

The schematic diagram of nine bus WSCC test system [97] is shown in Fig. 4.6. System data at base case loading is shown in Appendix J.

Both VPA and LFI approaches are applied at base case loading condition of WSCC 9-bus system. Fig. 4.7 shows Line Flow Indices for various lines in the system. It is indicated from Fig. 4.7 that line number 6 (line segment 7-5) has the highest index value. Various LFIs are also listed in Appendix J. The maximum index is due to LFIRP (receiving end real power index), therefore a suitable series FACTS device needs to be placed in line 7-5.

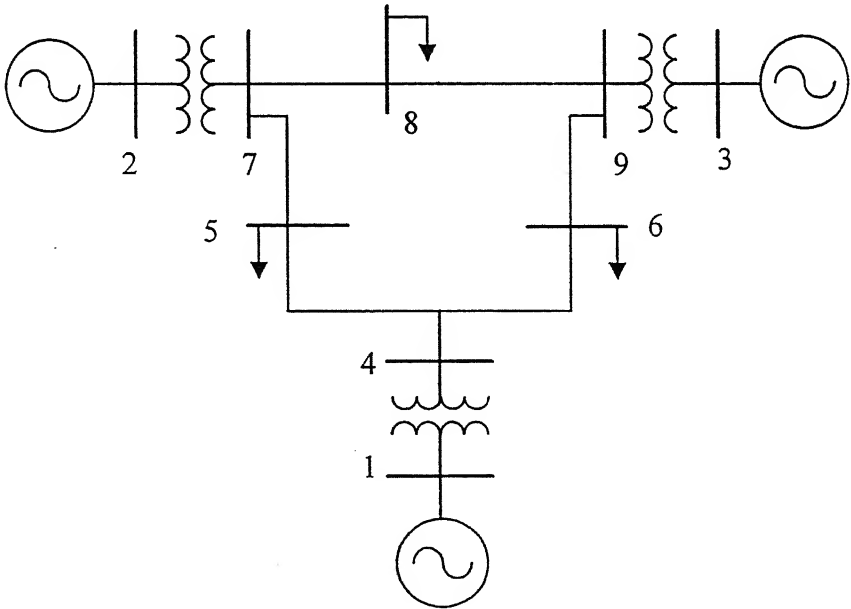


Fig. 4.6 Schematic diagram of the 9-bus test system

Fig. 4.8 shows the voltage profile of the 9-bus system at base case loading condition. It is evident from Fig. 4.8 that voltage profile of the system is quite good at base case loading condition. Therefore there is no need of connecting any shunt device in the system. LFI considerations also indicate that there is no need for shunt device.

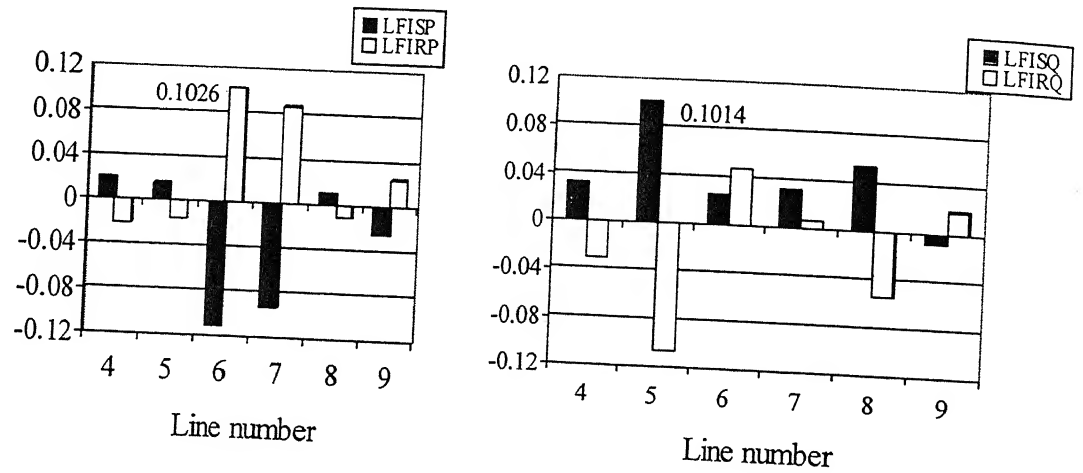


Fig. 4.7 LFIs of various line for the 9-bus system at base case loading condition

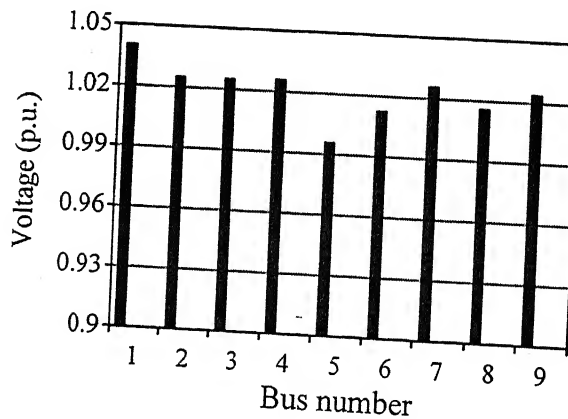
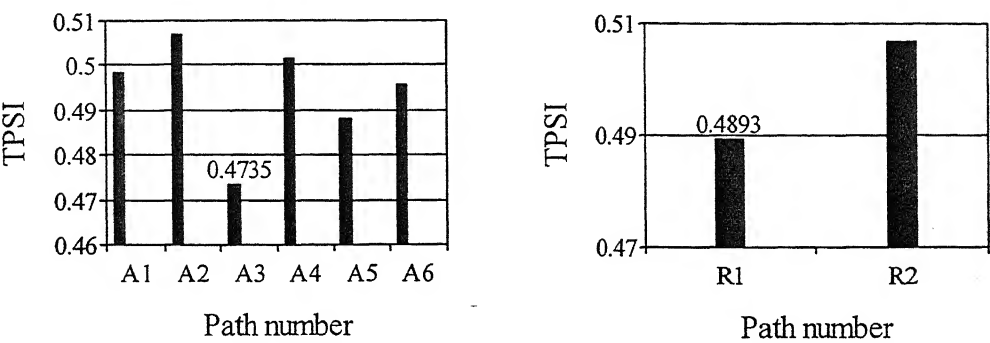


Fig. 4.8 Voltage profile of the 9-bus system at base case loading condition

Various APTPs and RPTPs for Extended Voltage Phasors Approach (EVPA) are shown in Table 4.2. Segments (1-4), (2-7) and (3-9) are transformer segments but as mentioned before they are ignored in the analysis. There are six active power transmission paths and two reactive power transmission paths.

Fig. 4.9 depicts that TPSI of path A3 is minimum. The path A3 corresponds to the line segment (7-5) as shown from Table 4.2. Hence the line segment 7-5 is critical. The results of Extended Voltage Phasors Approach (EVPA) are seen to match with that of LFI. Hence for base case condition the line segment 7-5 is the appropriate place for placing a series FACTS device.



**Fig. 4.9** TPSI for APTP and RPTP at base case loading condition

**Table 4.2** Active and Reactive transmission paths for the 9-bus system at base case loading condition

Active Power Transmission Paths (APTP)

Path No.	Line connection from bus to bus
A1	(1-4) (4-5)
A2	(1-4) (4-6)
A3	(2-7) (7-5)
A4	(2-7) (7-8)
A5	(3-9) (9-6)
A6	(3-9) (9-8)

Reactive Power Transmission Paths (RPTP)

Path No.	Line connection from bus to bus
R1	(1-4) (4-6)
R2	(1-4) (4-5)

### 4.3.3 Ten Machines, 39-Bus System

The schematic diagram of the 10-machines, 39-bus system is given in Fig. 4.10. The system data has been adopted from [12] and is tabulated in Appendix K. Both EVPA and LFI approach are applied to this system at base case loading condition. While Fig. 4.11 (a) depicts the real power indices LFISP and LFIRP, Fig. 4.11 (b) illustrates the reactive power indices LFISQ and LFIRQ. Fig. 4.11 shows Line Flow Indices for various lines in the system at base case loading condition. Lines 1-12 correspond to transformers and hence are not shown in the Fig. 4.11. Various LFIs in tabular form are given in Appendix K. It is demonstrated from Fig. 4.11, that line 33 (the line segment 18-19) has the highest index value, and therefore the line segment 19-18 and bus 18 are most critical from voltage stability viewpoint. This index is maximum for LFIRQ and therefore a shunt FACTS device is required in this case.

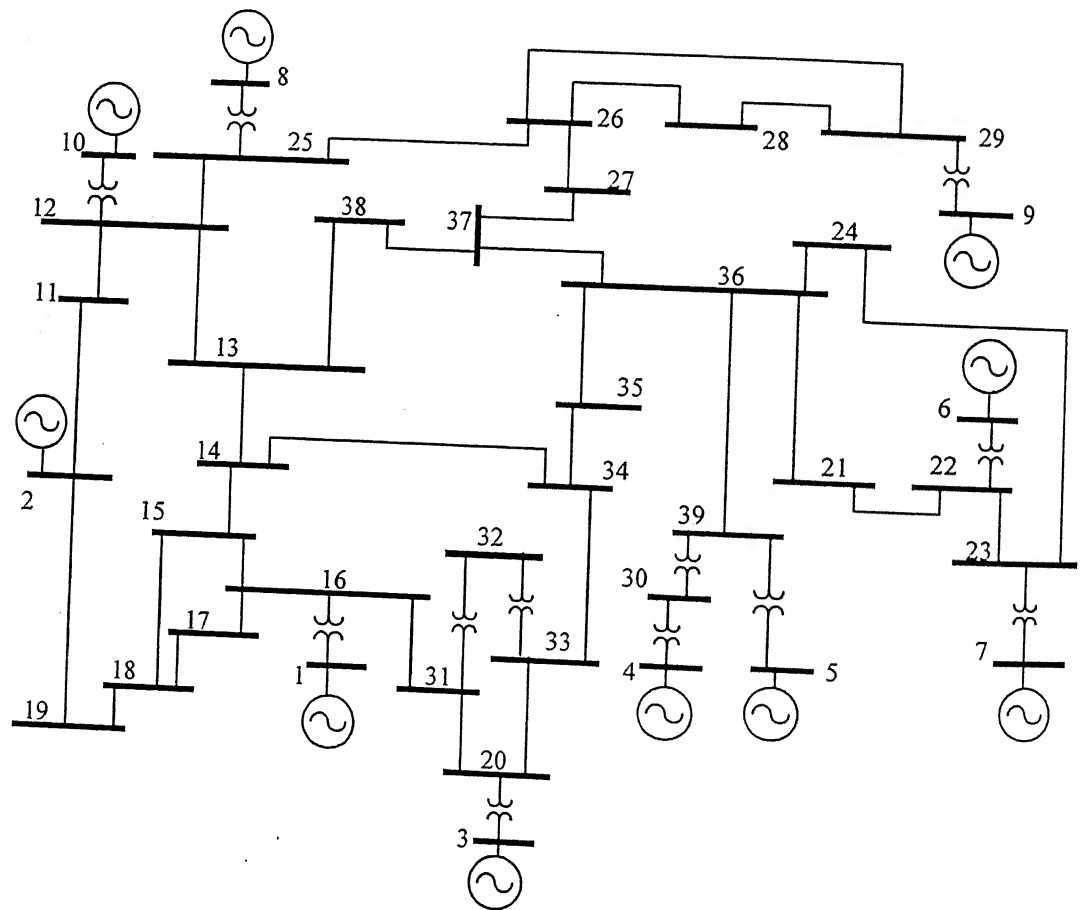


**Fig. 4.10** Schematic diagram of 10-machines, 39-bus system

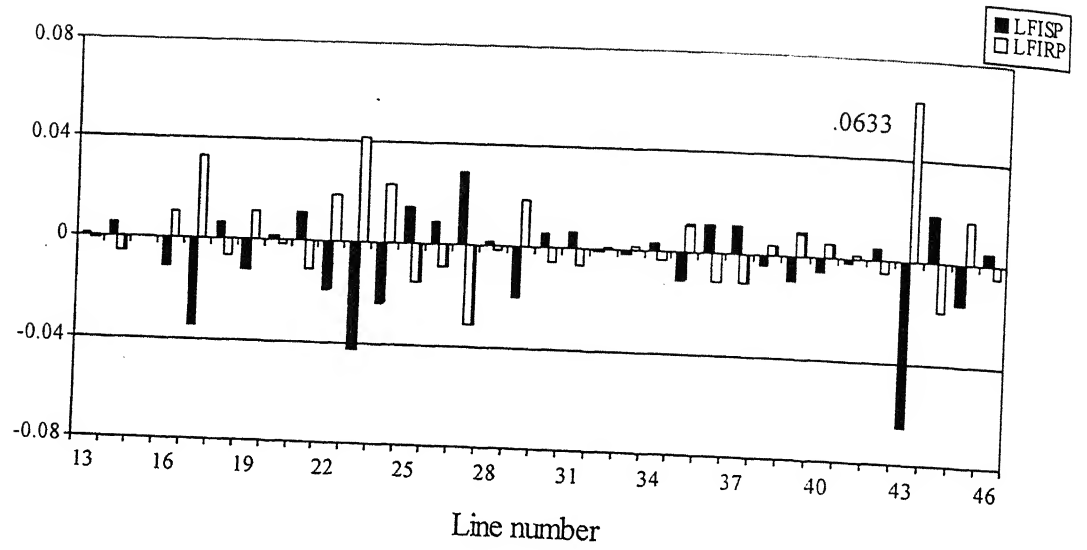
Fig. 4.12 shows voltage profile of the 39-bus system at base case loading condition. There are two zones where voltage dip is more as compared to other buses. The First zone is from bus 13 to bus 18 and the second zone is from bus 31 to bus 35. Placing a device in one or both zones will improve the voltage profile of the system. LFI shows that bus 18 is the most critical bus where a shunt device can be placed. Bus 18 belongs to first zone.

Extended Voltage Phasor Approach needs identification of APTP and RPTP for TPSI evaluation. Various APTP and RPTP are shown in Appendix K. Fig. 4.13 (a) and (b) show TPSI values for APTP and RPTP at base case loading condition respectively. In Fig. 4.13 (a) paths A13 and A14 have only transformers, hence zero values are shown for paths A13 and A14. Similarly in Fig. 4.13 (b) path R11 consists of only transformer and hence its value is also shown to be zero. A-close look at Fig. 4.13 (a) and (b) reveals that Active Power Transmission Path A4 (line segments (2-19), (19-18)) and Reactive Power Transmission Path R4 (line segments (2-19), (19-18) and (18-17)) have minimum values. Between these two paths R4 has minimum value of 0.4291. In the previous two studies of 6-bus system and 9-bus system, Voltage Phasors Approach identifies a critical path that is comprised of only one line segment. Hence this was considered for placement of the device. But in this case, there are three segments that constitute the critical path. Although all three line segments contribute to instability but the need is to identify the most critical segment in these three line segments.

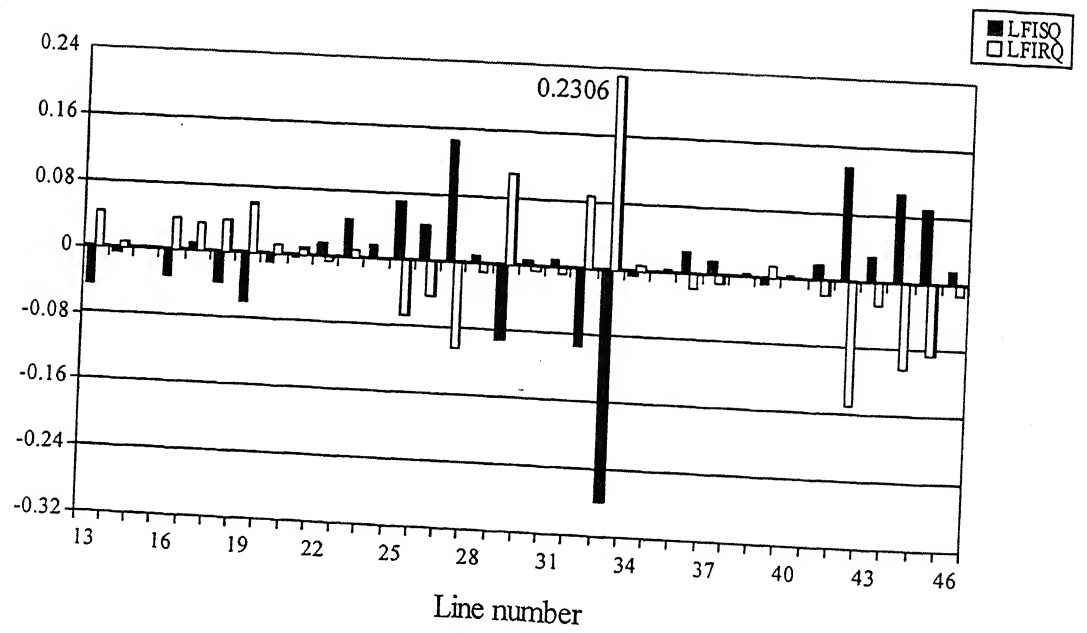
It is known that Transmission Path Stability Index (TPSI) is the summation of corrected voltage drops along a path [62]. It is therefore seems logical that the line segment with has the maximum value of corrected drop would be more critical than line segments. This hypothesis is now investigated in the subsequent studies. Corrected voltage drops for path R4 is shown in Table 4.3.

**Table 4.3** Corrected voltage drops for reactive power transmission path R4

Line segment	Corrected voltage drop
(2-19)	0.0229
<b>(19-18)</b>	<b>0.0623</b>
(18-17)	0.0007



(a)



(b)

**Fig. 4.11** LFIs of various line for the 39-bus system at base case loading condition

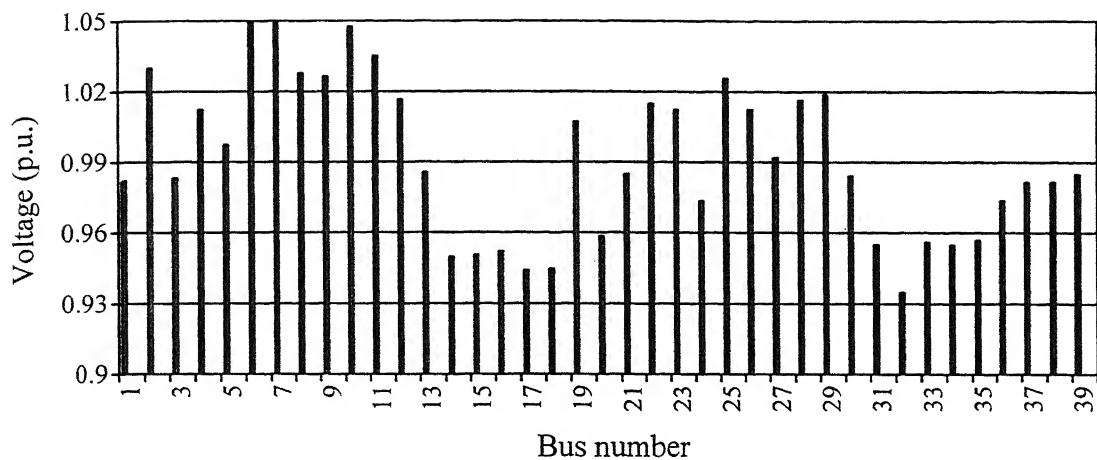
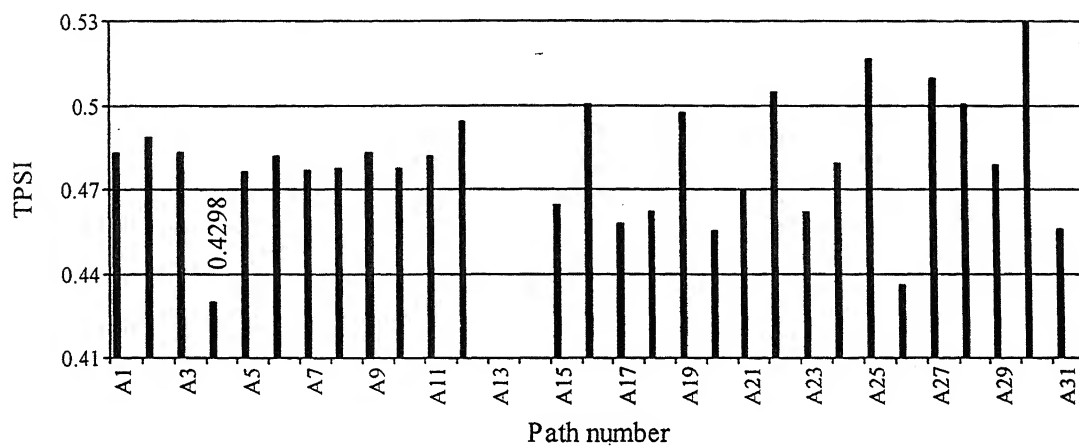
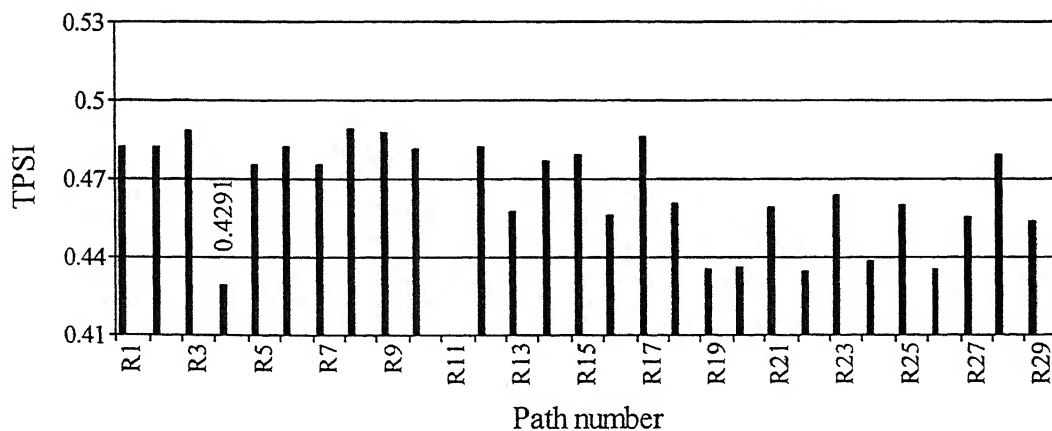


**Fig. 4.12** Voltage profile of the 39-bus system at base case loading condition



(a)



(b)

**Fig. 4.13** TPSI of APTPs and RPTPs for base case loading condition of 39-bus system



Table 4.3 indicates that line segment (19-18) is most critical followed by line segments (2-19) and (18-17) in that order. As the TPSI of RPTP 'R4' is minimum therefore a shunt device requirement emerges at bus 18. This result matches with that of LFI and also comes in first zone, as indicated by voltage profile of the system.

#### 4.3.4 Sixteen Machines, 68-Bus System

The schematic diagram of 16-machines, 68-bus system [98] is shown in Fig. 4.14. The system data is given in Appendix L. The procedure that has been outlined in Section 4.3.3 is applied to this 68-bus system. Fig. 4.15 (a) and (b) show the Line Flow Indices for various lines in the system at base case loading condition. In Fig. 4.15 (a) the maximum value for path 46 (line segment 60-30) is 0.2403 for LFIRP index, whereas Fig. 4.15 (b) shows a maximum value of 0.6502 for path 75 (line segment 41-40) corresponding to LFIRQ index. Hence from LFI criterion, the path 40-41 and bus 41 are critical.

Voltage profile of the 68-bus system shown in Fig. 4.16 at base case loading. This shows that voltage of bus 41 is quite high (0.9991 per unit) hence there is no need of any shunt device to be connected. This indicates a limitation of LFI technique for this study system.

After LFI approach, EVPA is applied to the 68-bus system at base case loading condition. Various APTPs and RPTPs are shown in Appendix L. Fig. 4.17 (a) and (b) show TPSI for APTP and RPTP. In Fig. 4.17 (a), paths A13 and A17 consist of only transformers and are therefore neglected. Similarly in Fig. 4.17 (b), paths R9 and R12 have only transformers and are also ignored. In Fig. 4.17 (a), minimum TPSI is for path A48 and in Fig. 4.17 (b), minimum value is for path R30. Between these two paths, the minimum value is obtained as 0.3312 for path A48. Thus Path A48 consists of line segments (14-41)(41-40)(40-48)(48-47)(47-65)(65-30)(30-60)(60-36)(36-37)(37-43)(43-44)(44-39). In this path segment (14-41) corresponds to a transformer, hence its corrected voltage is not considered in TPSI evaluation. Table 4.4 shows corrected voltage drops for different segments. Table 4.4 clearly shows that line segment (41-40) is most critical followed by path (30-60). As the path A48 is active power transmission path, a series

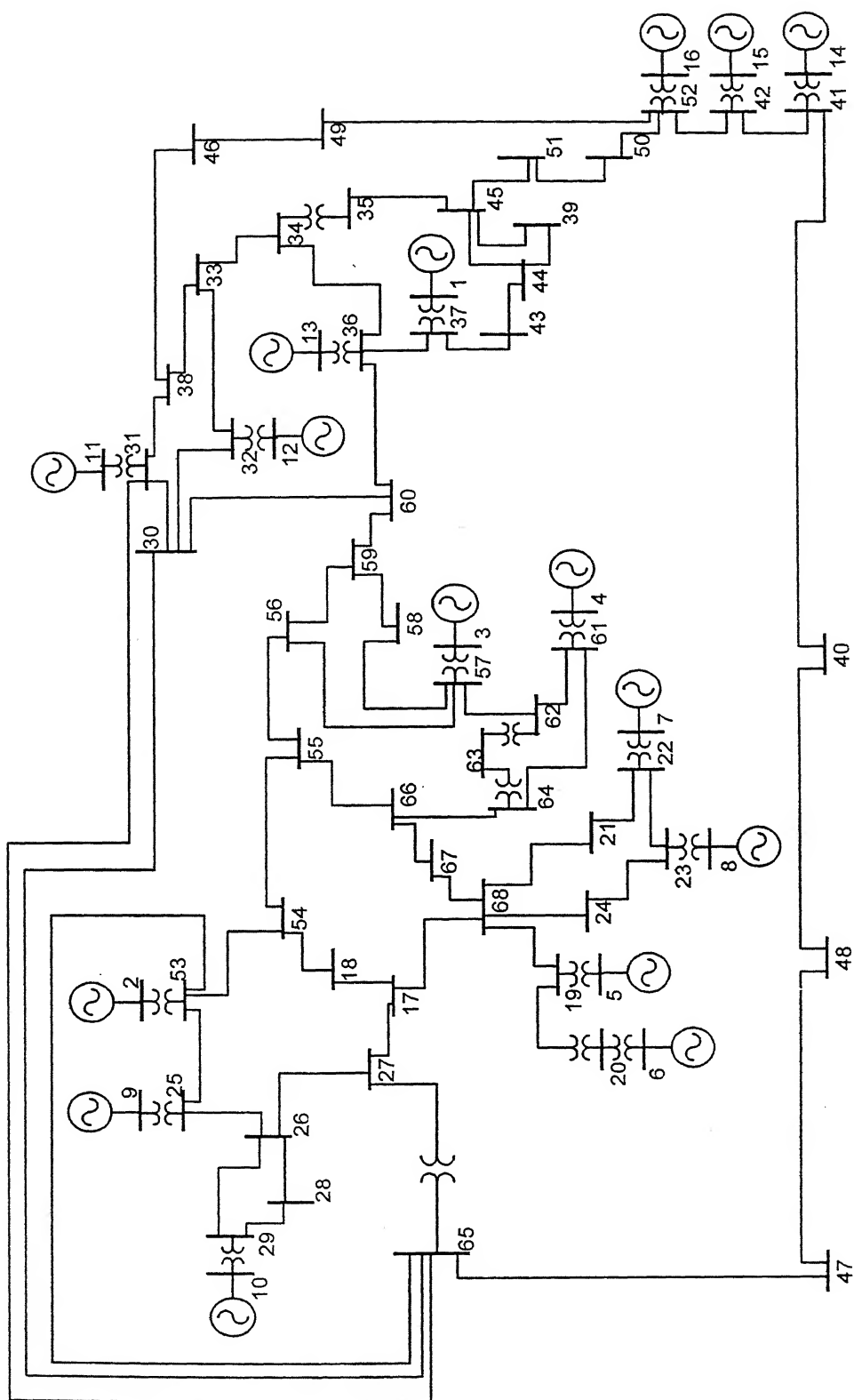
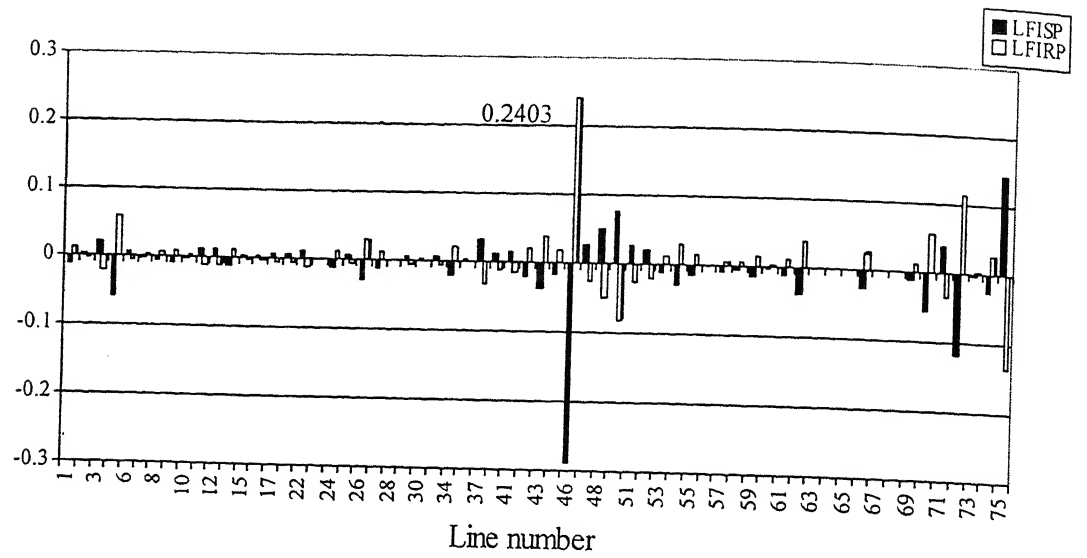
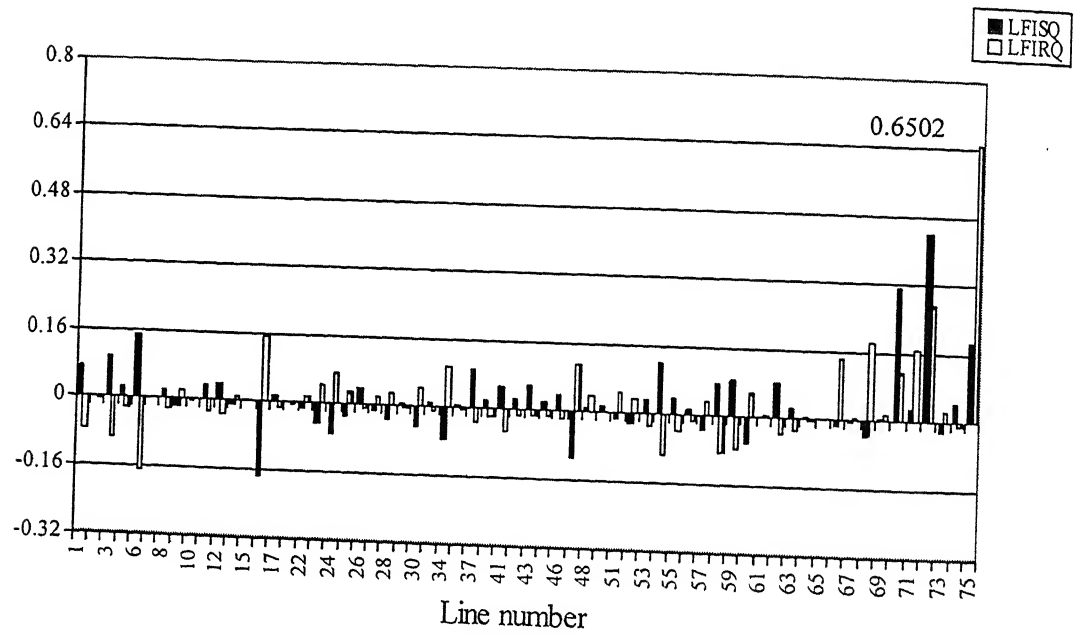


Fig. 4.14 Schematic diagram of 16-machines, 68-bus system



(a)



(b)

**Fig. 4.15** LFIs of various lines for the 68-bus system at base case loading condition

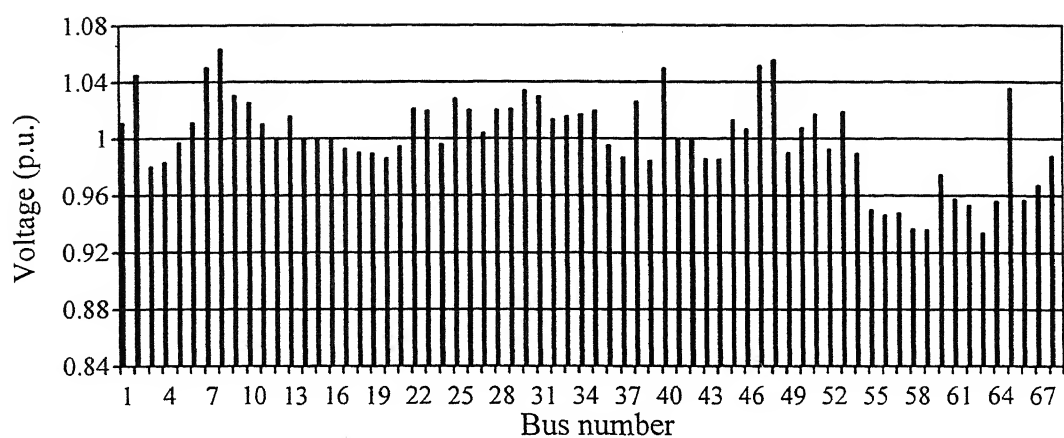
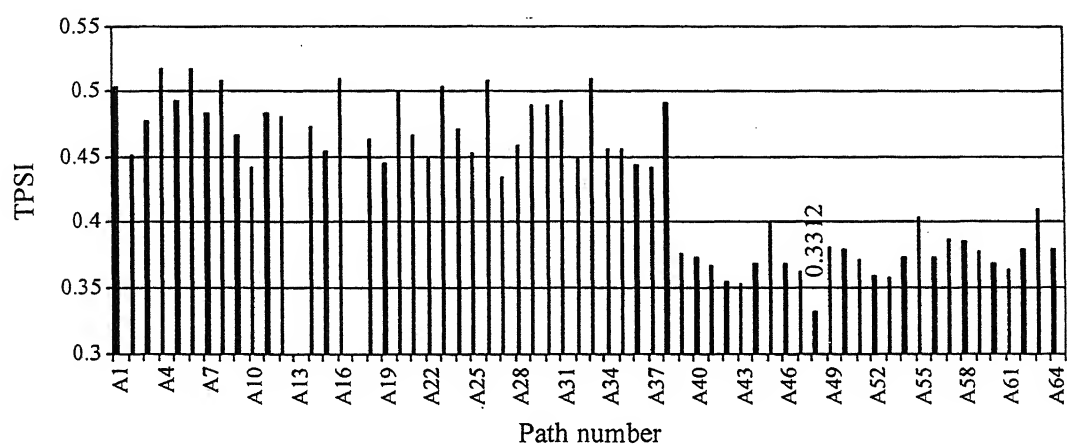
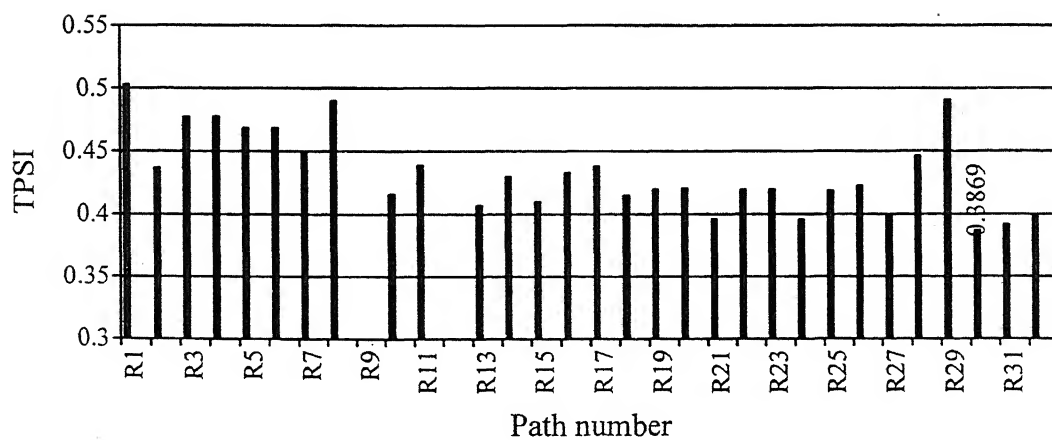


**Fig. 4.16** Voltage profile of the 68-bus system at base case loading condition



(a)



(b)

**Fig. 4.17** TPSI of APTPs and RPTPs for base case loading condition of the 68-bus system

**Table 4.4** Corrected voltage drops for active power transmission path A48

Line segment	Corrected voltage drop
<b>(41-40)</b>	<b>0.0862</b>
(40-48)	0.0003
(48-47)	0.0045
(47-65)	0.016
(65-30)	0.0016
(30-60)	0.0616
(60-36)	-0.0186
(36-37)	0.0145
(37-43)	0.0014
(43-44)	0.0001
(44-39)	0.0013

device will be more useful in the line segment (41-40). The Line segment (41-40) has also been shown critical by LFI. As the voltages of buses 40 and 41 are quite good, there is no need of voltage support at these buses. This is also indicated by EVPA as the minimum TPSI is obtained for Active Power Transmission Path and not for Reactive Power Transmission Path.

Based on the studies of 6-bus, 9-bus, 39-bus and 68-bus system, it can be said that Voltage Phasors Approach is able to identify not only the critical path and but critical line segment as well. It is also able to identify correctly whether the problem of voltage instability is due to active power or reactive power loading.

#### **4.4 CRITICAL PATH IDENTIFICATION AT MAXIMUM LOADING CONDITION**

In all the four systems studied at base case loading condition, the problem of voltage instability is not significant. Therefore it was decided to load the system to its maximum loadability limit and then identify the critical paths. The maximum loading of the system is found out using Newton Raphson Load Flow algorithm. The loading is increased in the same ratio of their base case loads and generation is increased according to the inertia of the generators [13].

#### 4.4.1 Six Bus System

The system loading is increased to 84.8% from base case loading. In a similar fashion LFIs are calculated for each line segment and are shown in Fig. 4.18. These show that the reactive power index LFISQ is maximum for line 5 (line segment 2-5). Therefore bus 5 can be the candidate location for placing a shunt FACTS device. Fig. 4.19 shows voltage profile of the system. It is observed that voltage of bus 5 is lowest among all buses and needs reactive power support. Hence a shunt compensation device at bus 5 can be placed to improve the voltage profile of the system.

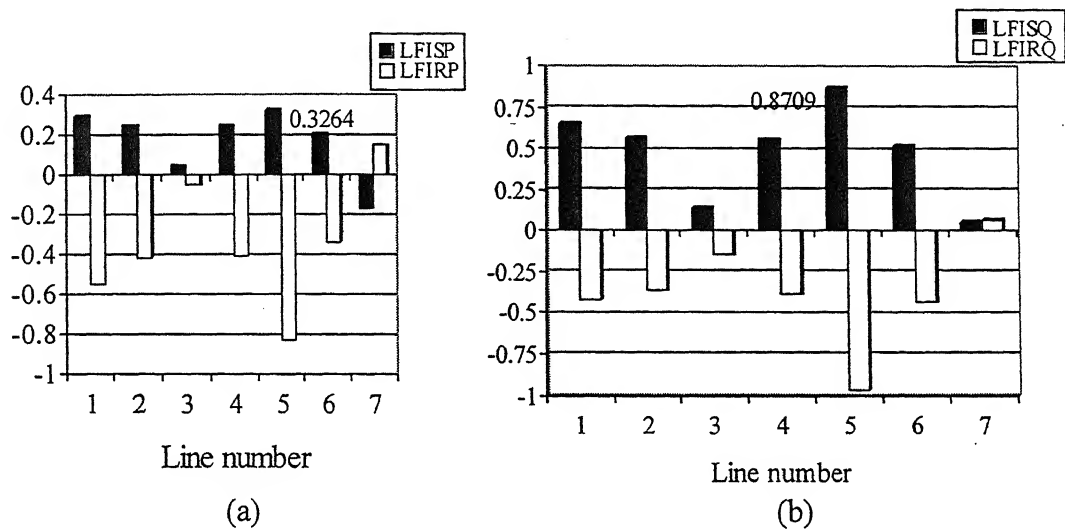


**Fig. 4.18** LFIs for various lines of the 6-bus system at maximum loading condition

At the maximum loading condition, APTP and RPTP are identified and then TPSI of each path is computed. It is noted that various APTPs and RPTPs are the same as given in Table 4.1 and are being repeated here for convenience.

TPSI for various paths is shown in Fig. 4.20. Since APTPs and RPTPs are identical at maximum loading condition, their TPSI are also same. Fig. 4.20 shows that TPSI is minimum for path A1 and R1 (line segments (1-6) and (6-5)). The corrected voltage drops of the line segment (1-6) is 0.2841 and for the line segment (6-5) is 0.1758. Thus from EVPA the line segment (1-6) is identified as the most critical segment. Thus bus 6 emerges as the candidate bus for placing a shunt device. On the other hand LFI identifies bus 5 as the most critical bus. It seems that the results obtained by EVPA and

LFI approaches are different but close examination of LFI and TPSI reveals that both buses 5 and 6 are weak buses. Fig. 4.21 is presented to validate the results obtained from LFI and EVPA.

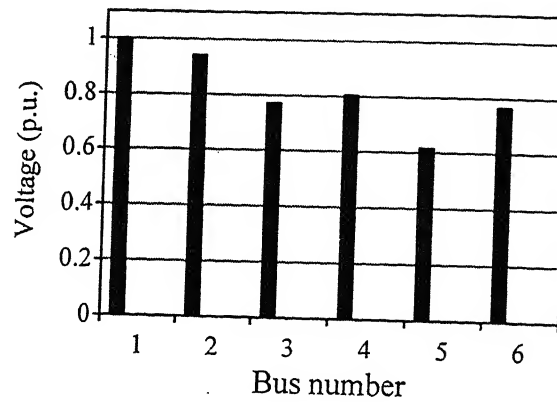


**Fig. 4.19** Voltage profile of 6-bus system at maximum loading condition

**Table 4.5** Active and Reactive transmission paths for the 6-bus system at maximum loading condition

Active Power Transmission Paths (APTP)

Path No.	Line connection From bus to bus
A1	(1-6) (6-5)
A2	(1-4) (4-3)
A4	(1-4) (4-6) (6-5)
A4	(2-5)
A5	(2-3)

Reactive Power Transmission Paths (RPTP)

Path No.	Line connection from bus to bus
R1	(1-6) (6-5)
R2	(1-4) (4-3)
R3	(1-4) (4-6) (6-5)
R4	(2-5)
R5	(2-3)

Fig. 4.21 shows the voltage profile of the system with a shunt device (SVC or STATCOM) placed either at bus 6 or at bus 5. It can be seen from Fig. 4.20 that with a shunt device at bus 6, the overall voltage profile is better than when a shunt device is placed at bus 5. This validates the result of EVPA.

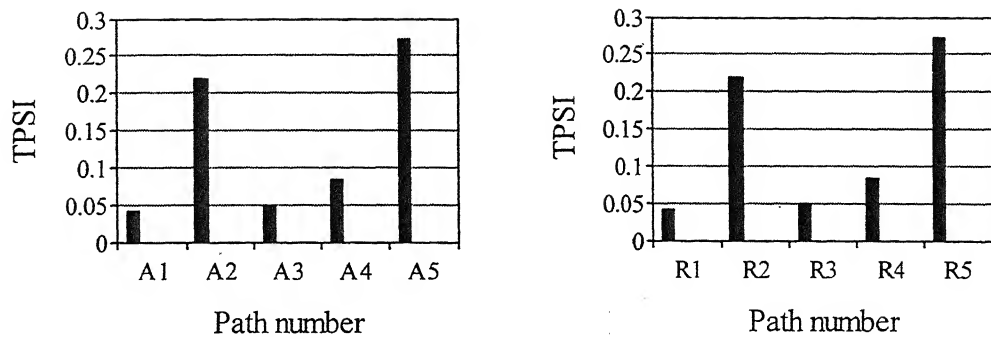


**Fig. 4.20** TPSI for APTP and RPTP of the 6-bus system at maximum loading condition

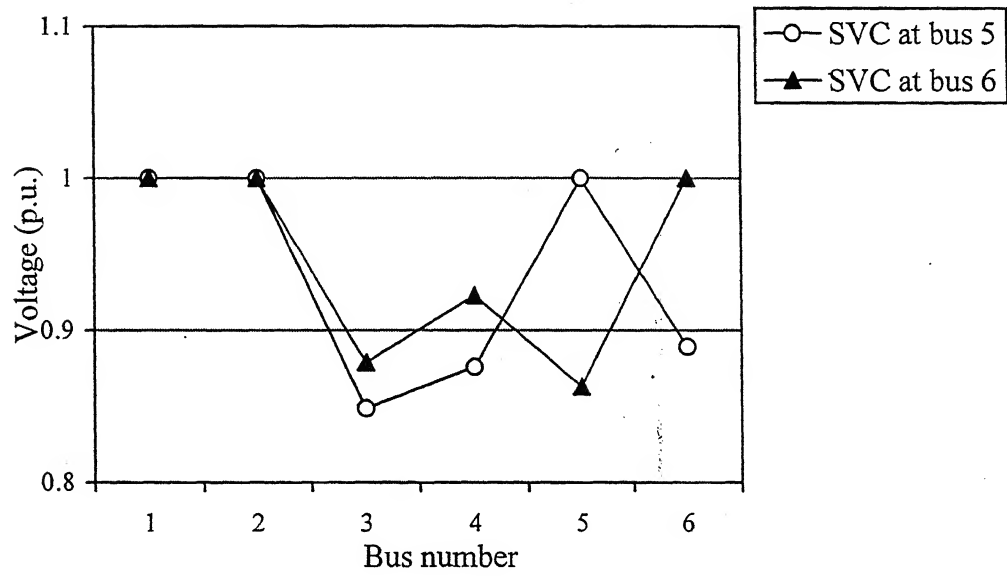


**Fig. 4.21** Voltage profile of the 6-bus system with SVC at either bus 6 or bus 5 at maximum loadability condition



#### 4.4.2 Nine Bus System

The system loading is increased by 143% over the base case loading. At this loading condition, Fig. 4.22 shows LFIs for various lines in the system. From Fig. 4.22 it is evident that LFIRQ for line number 6 (line segment 5-7) is maximum, therefore bus 5 appears to be an appropriate place for placing a shunt device. Fig. 4.23 shows voltage profile of 9-bus system at maximum loadability condition.

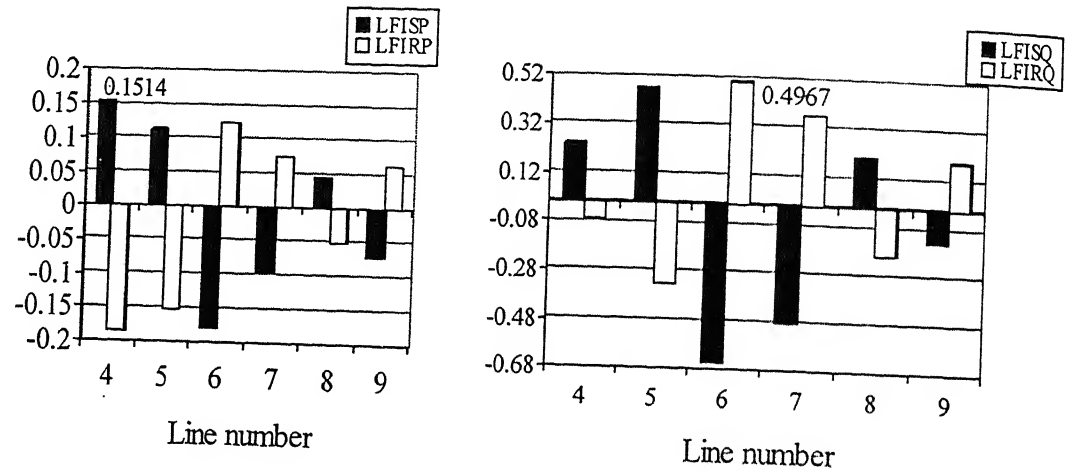


Fig. 4.22 LFIs for various line of the 9-bus system at maximum loadability condition

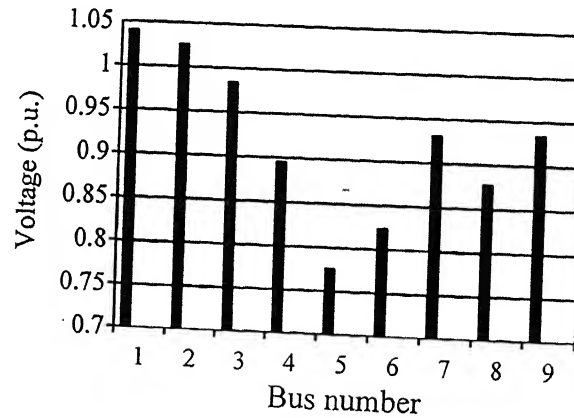


Fig. 4.23 Voltage profile of the 9-bus system at maximum loadability condition

From Fig. 4.23, it is clear that the voltage of bus 5 is the lowest among all the buses. Therefore bus 5 is the most appropriate place for placing a shunt compensator

device. Various APTP and RTPP for the 9-bus system at maximum loading condition are given in Table 4.6. It is once again seen that APTPs and RTPPs are the same at maximum loading condition. Fig. 4.24 shows the corresponding TPSIs for various paths. As mentioned earlier transformers are not considered in TPSI computations.

**Table 4.6** Active and Reactive transmission paths for the 9-bus system at maximum loading condition

Active Power Transmission Paths  
(APTP)

Path No.	Line connection from bus to bus
A1	(1-4) (4-5)
A2	(1-4) (4-6)
A3	(2-7) (7-5)
A4	(2-7) (7-8)
A5	(3-9) (9-6)
A6	(3-9) (9-8)

Reactive Power Transmission Paths  
(RTPP)

Path No.	Line connection from bus to bus
R1	(1-4) (4-5)
R2	(1-4) (4-6)
R3	(2-7) (7-5)
R4	(2-7) (7-8)
R5	(3-9) (9-6)
R6	(3-9) (9-8)

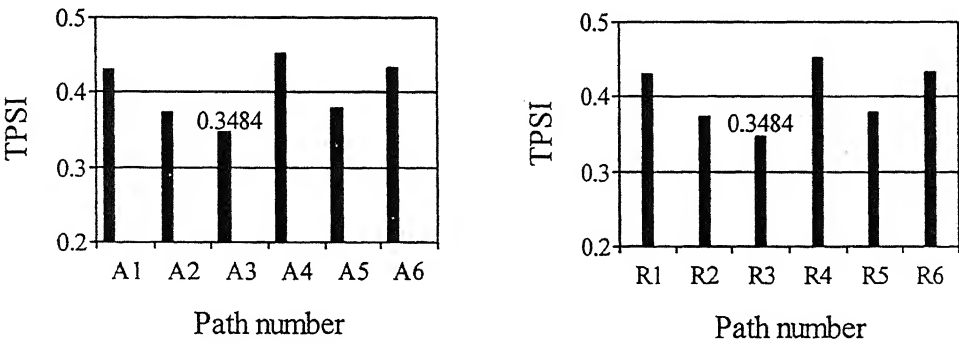


**Fig. 4.24** TPSI for the 9-bus system at maximum loading condition

It is seen that TPSIs for paths A3 and R3 are minimum. Now A3 and R3 have one line segment (7-5). Therefore bus 5 is most appropriate place for placing a shunt device.

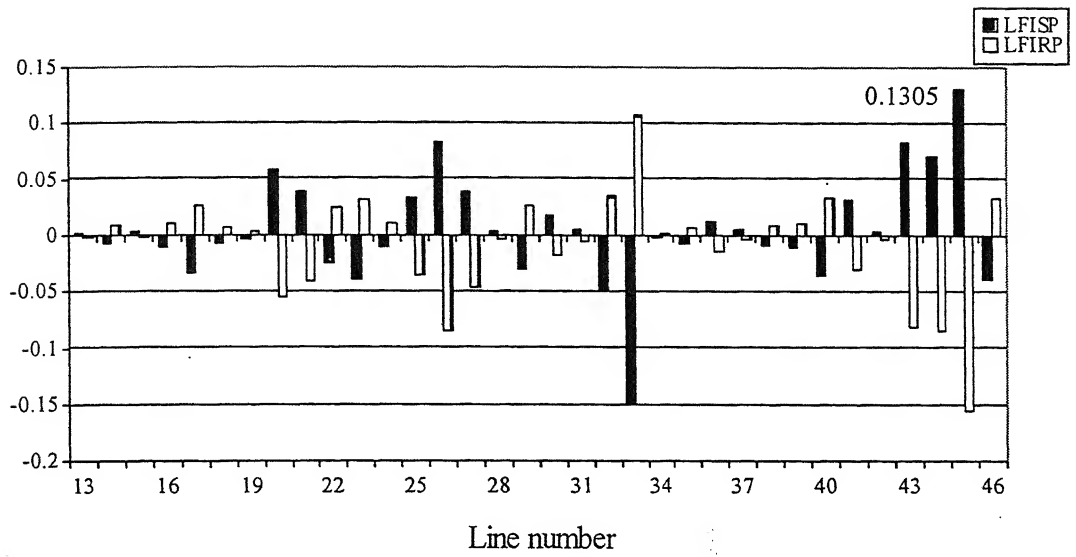
Thus in this case EVPA result matches with that of LFI approach. Hence bus 5 is the most appropriate location for placing a shunt FACTS device.

#### 4.4.3 Ten Machines, 39-Bus System

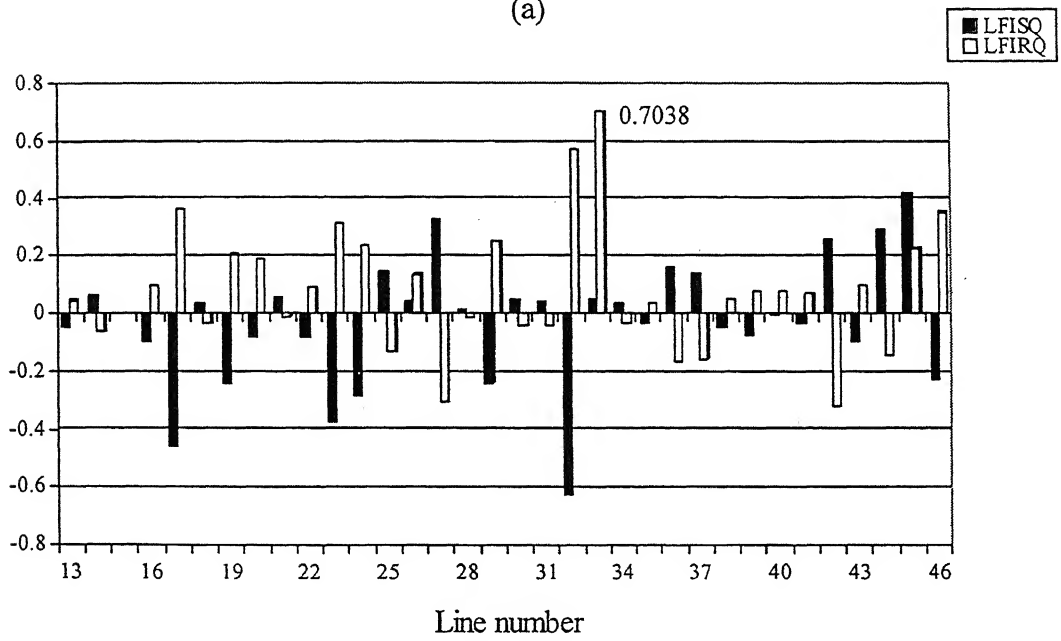
The system loading is increased by 67% over the base case loading. Again, LFI approach and EVPA are applied to the system at maximum loading condition. Fig. 4.25 shows LFIs for various lines at maximum loading condition of the system. In Fig. 4.25 (a) and (b), the maximum value is obtained as 0.7038 for LFIRQ path 33 corresponding to line segment (18-19). Therefore bus 18 is most critical from LFI point of view.

Fig. 4.26 shows voltage profile of the 39-bus system at maximum loading condition. It is noted that there are two zones which experiences large voltage dips. The first zone is from bus 13 to bus 18 and the second zone is from bus 31 to bus 35. Intuitively a shunt device must be connected in any one of these two zones to improve the voltage profile of the system. Bus 18 belongs to first zone and has the lowest voltage amongst all buses.

For EVPA, various APTs and RPTs are identified and are tabulated in Appendix K. Fig. 4.27 shows TPSI for various active and reactive paths. It can be seen from Fig. 4.27 (a) and 4.27 (b) that TPSI for RPTP 'R5' is minimum. R5 comprises two line segments (2-19) and (19-18). The corrected voltage drops for the line segment (2-19) is 0.1876 and for (19-18) is 0.2188. So the line segment (19-18) is more critical. As the TPSI index is minimum for RPTP, therefore a shunt device at bus 18 could be placed to improve voltage profile/stability of the system. Result of EVPA exactly matches with that of LFI approach.



(a)



(b)

**Fig. 4.25** LFIs for various lines of the 39-bus system at maximum loading condition

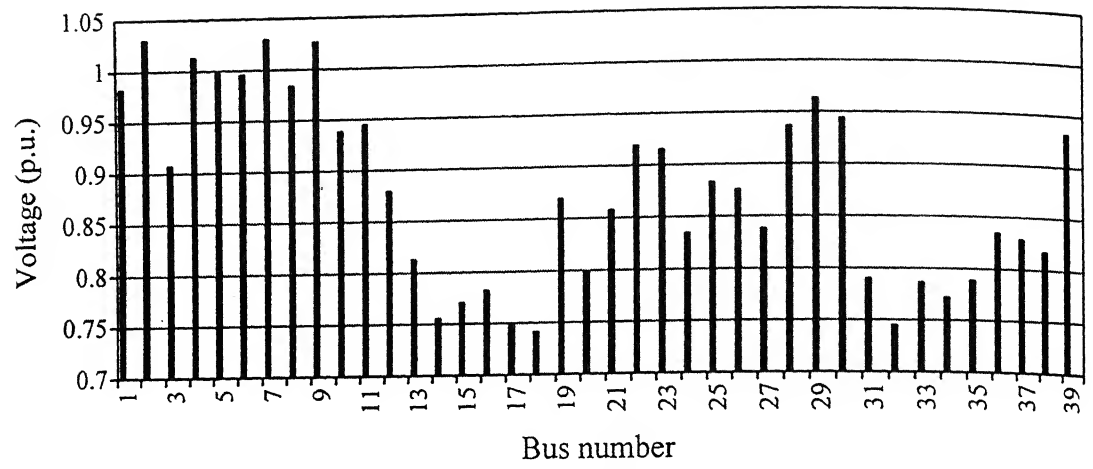


Fig. 4.26 Voltage profile of the 39-bus system at maximum loading condition

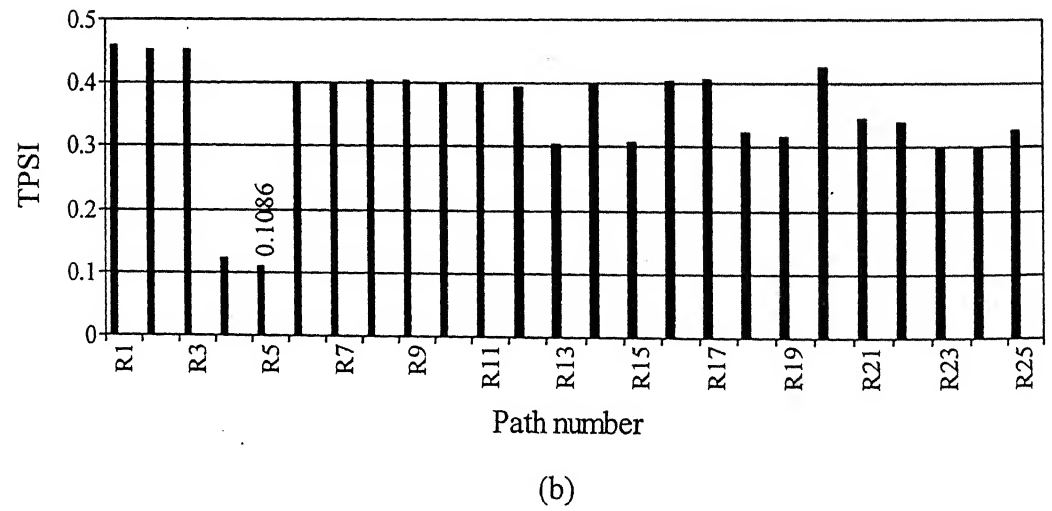
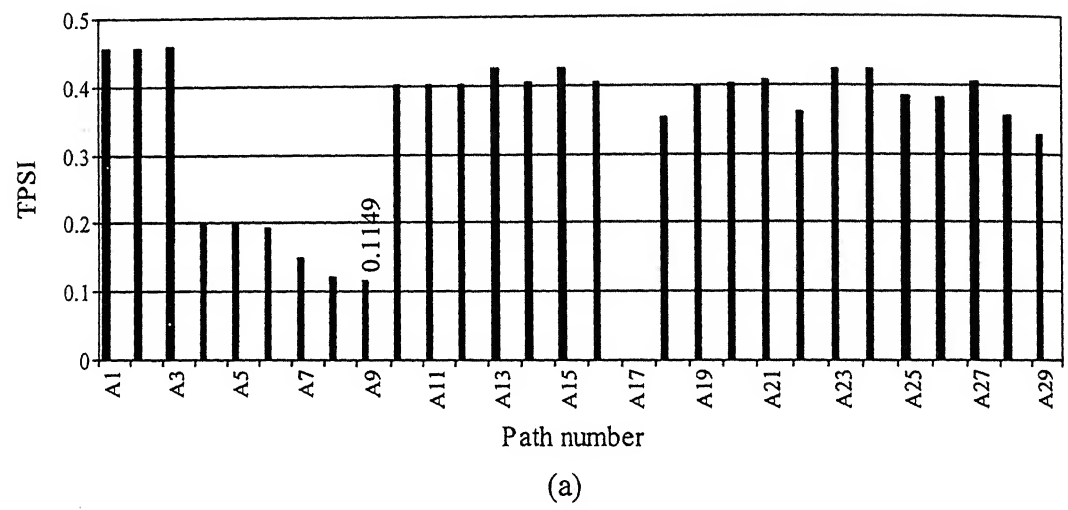


Fig. 4.27 TPSI for APTs and RPTs at maximum loading condition for 39-bus system

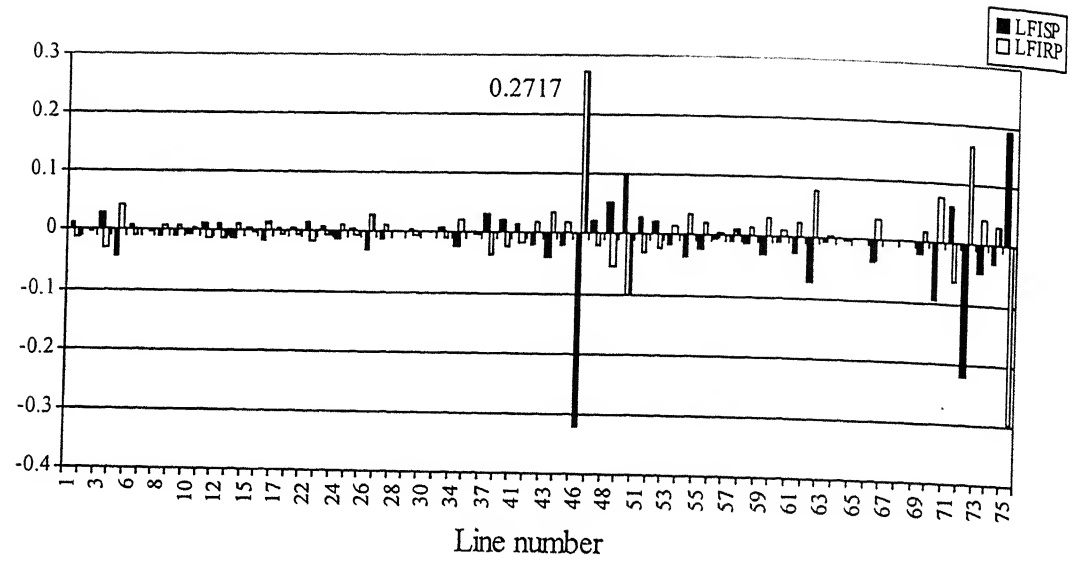
#### 4.4.4 Sixteen Machines, 68-Bus System

System loading is increased by 14% beyond base case loading. LFIs for the 68-bus system at maximum loading condition are shown in Fig. 4.28. It can be seen that line 75 (line segment 41-40) has maximum value for LFIRQ. Therefore bus 40 is most critical in this case. Fig. 4.29 shows voltage profile of the system at maximum loadability condition. It shows that voltage of bus 40 is minimum. Hence from intuitive reasoning a shunt compensating device should be placed at bus 40.

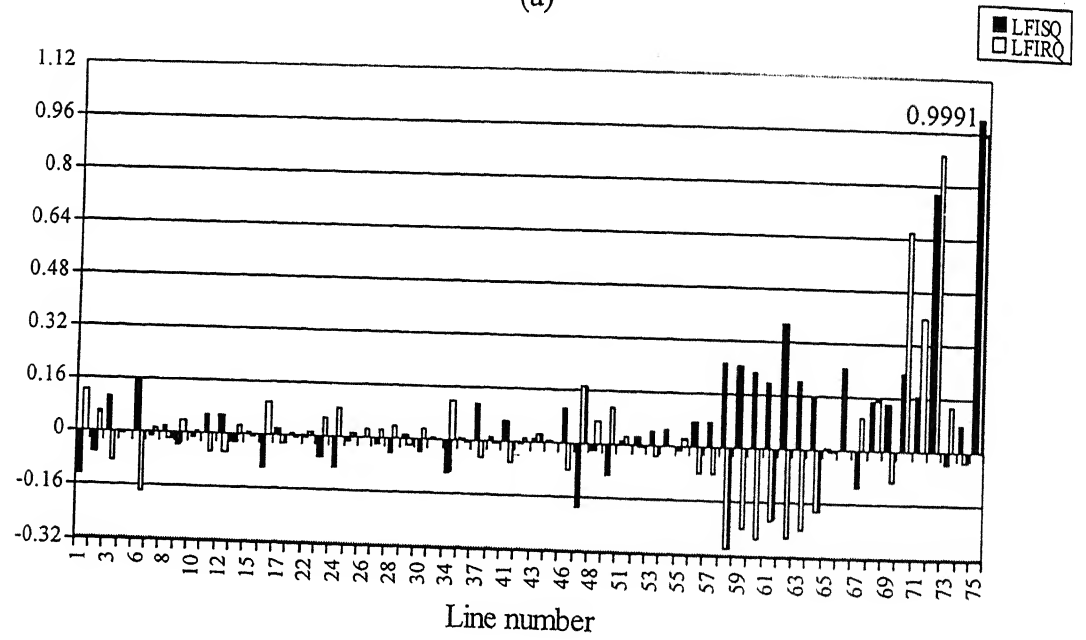
Various APTPs and RPTPs at maximum loading condition are tabulated in Appendix L. It is graphically depicted in Fig. 4.30. In Fig. 4.30(a), paths A14 and A18 consist of only transformers hence their TPSI values are taken as zero. It is seen from Fig. 4.30 (a) that path A50 has minimum TPSI value (0.0166). In Fig. 4.30 (b) since paths R13 and R15 comprise only transformers their TPSIs are considered to be zero. TPSI value for path R41 is minimum (-0.0301). Therefore for the 68-bus system at maximum loading condition, path R41 (the line segment 41-40) is most critical. As TPSI value is minimum for reactive transmission path, a shunt device at bus 40 should be placed to improve the voltage profile/stability of the system. Hence EVPA results matches exactly with that of LFI approach and also with the voltage profile analysis of the system.

#### 4.5 PLACEMENT OF FACTS DEVICES WITH CONTINGENCY CONSIDERATIONS

Since contingencies invariably occur in power systems, a proper placement strategy must consider realistic contingencies in the system. Although contingency analysis should be rigorous, it has been performed selectively in this study for representative contingencies to show their effect on placement strategy. In this study critical segments have been found using Voltage Phasors Approach for the 68-bus system at base case loading condition considering selected line outages. Mainly three types of contingencies are considered



(a)



(b)

Fig. 4.28 LFIs for the 68-bus system at maximum loading condition

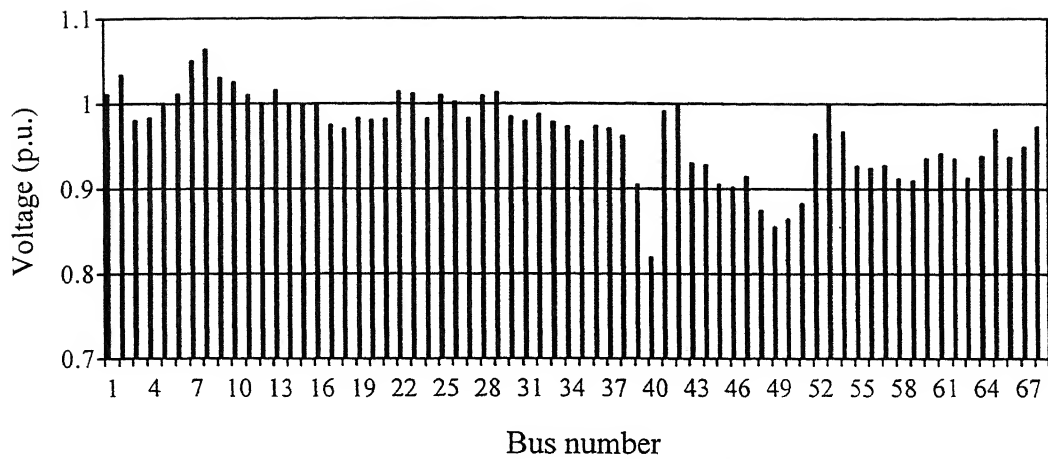
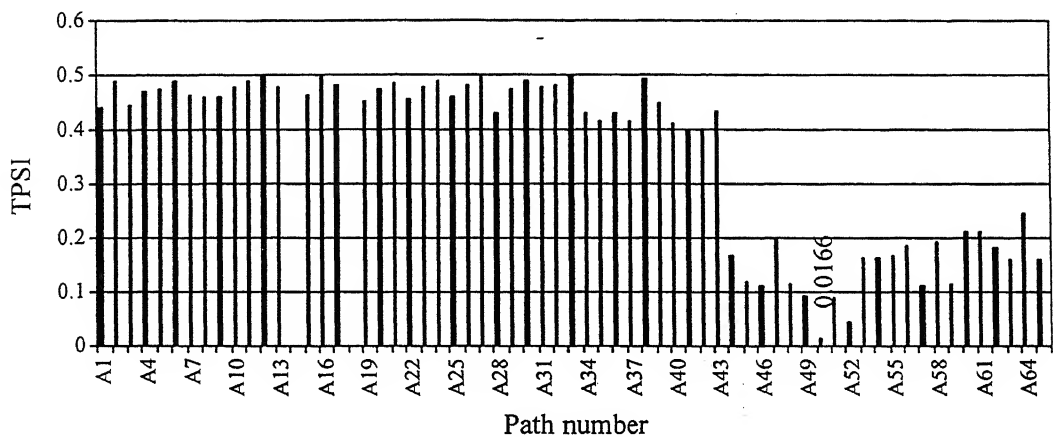
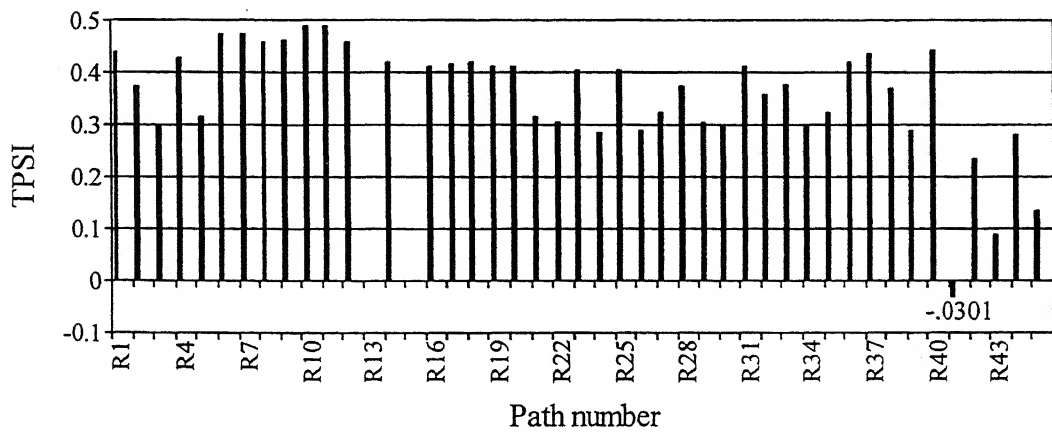


**Fig. 4.29** Voltage profile of the 68-bus system at maximum loading condition



(a)



(b)

**Fig. 4.30** TPSI for APTs and RPTs for the 68-bus system at maximum loading condition



- Line outages near high load buses
- Line outages of lines having high reactance values (long lines)
- Line outages of lines carrying high power

In this analysis generation rescheduling after line outages is not done. Only those cases are considered in which NRLF converge. In all, thirteen line outages have been considered as given below

- Lines near high loads: (59-60), (56-59), (58-59), (54-55), (55-56), (55-66), (66-67) and (68-67)
- High reactance lines: (26-29), (26-28) and (33-38)
- High power lines: (32-33) and (30-60)

The EVPA is applied in all these outage investigations. It was observed that the same line segment (41-40), which was critical in the healthy base case situation, remains critical in most of the contingencies cases. Table 4.7 shows various line outages considered and the EVPA results. In all these cases the Active Power Transmission Path (APTP) has been found as most critical one. In Table 4.7, the most critical segment is shown in bold letters. It can be seen from this table that the line segment (41-40) is most critical in eleven out of thirteen contingencies considered. Only in two contingency cases (line outages of (32-33) and (30-60)), it did not emerge as the most critical one. This study demonstrates that although it is imperative to install a FACTS device in line 41-40, which is the critical segment obtained from healthy base case system study, it may be desirable to connect an appropriate compensation device to augment the first suggested FACTS device.

This study also demonstrates that for a proper placement strategy, all realistically probable contingencies must be considered and appropriate remedial measures must be taken.

**Table 4.7** Line outages and critical segments for the 68-bus system at base case loading

Line outage	Critical Active Power Transmission Path
(26-28)	(14-41)(41-40)(40-48)(48-47)(47-65)(65-30)(30-60)(60-36) (36-37)(37-43)(43-44)(44-39)
(32-33)	(14-41)(41-42)(42-52)(52-49)(49-46)(46-38)(38-33)(33-34) (34-36)(36-37)(37-43)(43-44)
(30-60)	(14-41)(41-42)(42-52)(52-50)(50-51)(51-45)(45-39)
(54-55)	(14-41)(41-40)(40-48)(48-47)(46-65)(65-30)(30-60)(60-59)
(58-59)	(14-41)(41-40)(40-48)(48-47)(47-65)(65-30)(30-60)(60-36) (36-37)(37-43)(43-44)(44-39)
(59-60)	(14-41)(41-40)(40-48)(48-47)(47-65)(65-30)(30-60)(60-36) (36-37)(37-43)(43-44)(44-39)
(56-59)	(14-41)(41-40)(40-48)(48-47)(47-65)(65-30)(30-60)(60-59)
(68-67)	(14-41)(41-40)(40-48)(48-47)(47-65)(65-30)(30-60)(60-59)
(66-67)	(14-41)(41-40)(40-48)(48-47)(47-65)(65-30)(30-60)(60-36) (36-37)(37-43)(43-44)(44-39)
(55-56)	(14-41)(41-40)(40-48)(48-47)(47-65)(65-30)(30-60)(60-36) (36-37)(37-43)(43-44)(44-39)
(55-66)	(14-41)(41-40)(40-48)(48-47)(47-65)(65-30)(30-60)(60-36) (36-37)(37-43)(43-44)(44-39)
(26-29)	(14-41)(41-40)(40-48)(48-47)(47-65)(65-30)(30-60)(60-36) (36-37)(37-43)(43-44)(44-39)
(33-38)	(14-41)(41-40)(40-48)(48-47)(47-65)(65-30)(30-60)(60-36) (36-37)(37-43)(43-44)(44-39)

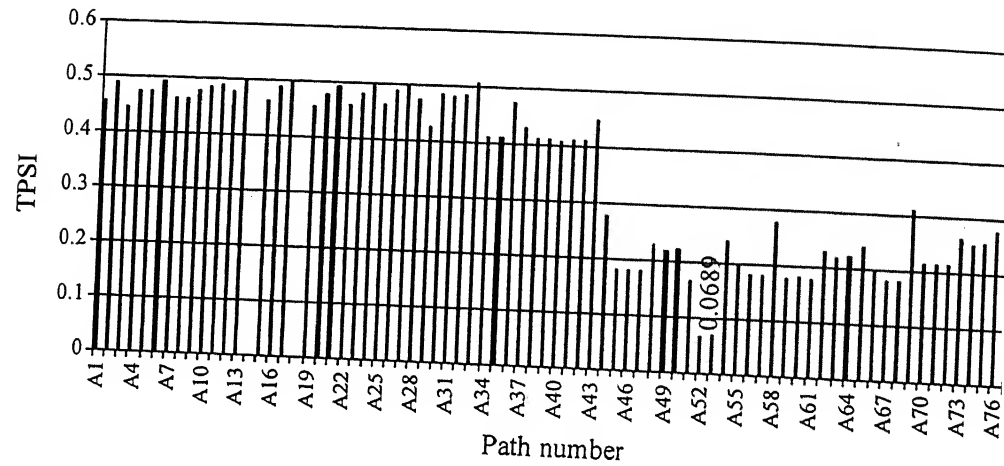
**4.6 PLACEMENT STRATEGY FOR MULTIPLE DEVICES**

In Sections 4.3 and 4.4 four systems have been considered at base case loading and maximum loading conditions for placement of FACTS devices. Table 4.8 summarizes the results obtained in sections 4.3 and 4.4. It can be observed from Table 4.8 that for the 6-bus and 39-bus systems shunt device is needed from base case to maximum loading condition, whereas the 9-bus and 68-bus systems need different devices at different loading conditions. As evident from Table 4.8, there is a need of shunt device at maximum loading condition for the 68-bus system. It is therefore decided to install an SVC at bus 40 as suggested from EVPA studies for the 68 bus system at maximum loading condition. EVPA studies are subsequently conducted to determine the need for any additional device after the placement of SVC at the maximum loading

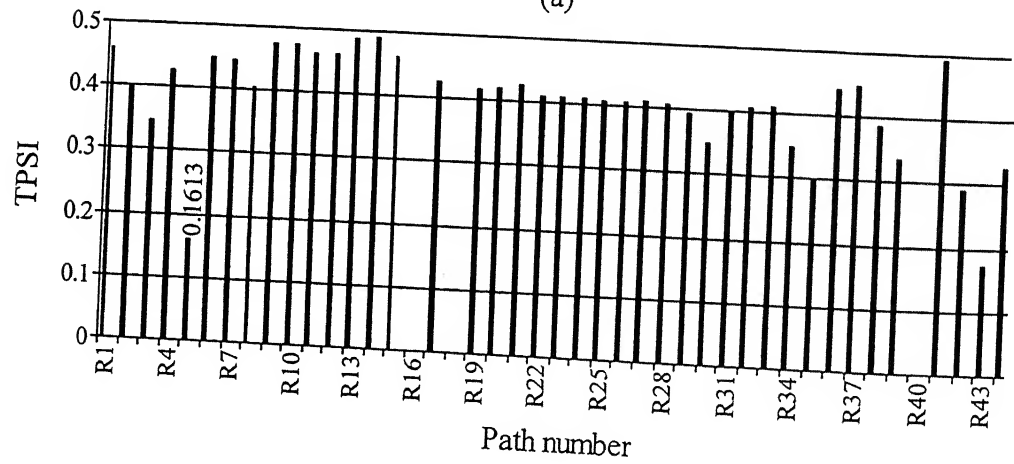
condition. Various APTPs and RPTPs are obtained are tabulated in graphically illustrated in Fig. 4.31.

**Table 4.8** FACTS devices needed for various systems

Type of system	Base case loading Condition	Maximum loading Condition
6-bus	Shunt	Shunt
9-bus	Series	Shunt
39-bus	Shunt	Shunt
68-bus	Series	Shunt



(a)



(b)

**Fig. 4.31** TPSI for the 68-bus system with SVC at bus 40

Paths A14 and A18 in Fig. 4.30 (a) and paths R16, R18 and R40 in Fig. 4.31(b) have only transformers, and hence their values are shown as zero. The Active Power Transmission Path A52 has minimum TPSI value. Table 4.9 shows the corrected voltage drops in different line segments of path A52 from where it is seen that the line segment (41-40) is most critical. Hence there is a need for a series device.

**Table 4.9** Corrected voltage drop in different line segments of path A52

Line segment	Corrected voltage drop
<b>(41-40)</b>	<b>0.3246</b>
(40-48)	0.01
(48-47)	-.001
(47-65)	.0005
(65-30)	.0028
(30-60)	.0647
(60-59)	.0352

This analysis shows that for the 68-bus system, apart from a shunt device connected at bus 40, a series device must also be connected in the line segment (41-40). It may be recalled that a series device was already indicated from EVPA studies at base case loading condition.

Hence it is recommended that for satisfactory operation both the devices must be connected in the system. Further investigation can be done on the same lines with both devices in the system to examine if the system is stable and whether the system voltage profile is acceptable. Any additional device must be adequately justified from both technical and economic considerations.

## 4.7 CONCLUSIONS

In this chapter a modification in the Voltage Phasors Approach is presented for easy identification of critical line segment from voltage stability consideration in the

power systems. These EVPA results are validated by LFI approach as well as voltage profile graphs of the system at base case loading and maximum loading conditions. EVPA is applied to four systems. In all these systems it has been found that EVPA approach is able to identify the critical path and the most critical segment correctly. It also identifies the cause of the problem as either due to active power or reactive power loading of the system. Corrective measures can then be taken for the most critical segment. There is no need to compute four indices for each line as is done in LFI approach. Therefore EVPA is computationally more efficient.

EVPA is applied to the 68-bus system at base case loading condition considering various contingencies in the system. It is found that in most cases the critical link obtained in healthy system study continues to remain critical, but in few cases some other line become more critical. A proper placement strategy must therefore consider the following:

- Different loading conditions
- Different probable contingencies
- Need for multiple devices

## SMALL SIGNAL ANALYSIS OF THE PLACEMENT STRATEGY

In the previous chapter, the placement strategy has been proposed by detailed analysis of various systems (6, 9, 39 and 68 bus systems) using Extended Voltage Phasors Approach (EVPA). The results of EVPA are compared with that of Line Flow Index (LFI) approach and voltage profiles of the systems. A proper placement strategy must ensure that once the device is placed in the system, its interaction with the system should improve overall system damping, voltage profile, etc. In this chapter it is investigated whether indeed the system performance improves when the devices are placed at these locations. The system performance is evaluated using the following three techniques:

- Eigenvalue analysis
- Voltage profile evaluation
- Step response

The validation of placement strategy has been performed on the 9-bus and 68-bus systems only.

As already observed in Chapter 4, both the 9-bus and 68-bus systems require different types of devices at different loading conditions. Table 5.1 repeats the results obtained from Chapter 4 for the 9-bus and the 68-bus systems for ready reference.

**Table 5.1** FACTS devices needed for various systems

Type of system	Base case loading condition	Maximum loading condition
9-bus	Series	Shunt
68-bus	Series	Shunt

## 5.1 NINE BUS SYSTEM

### 5.1.1 Base Case Loading Condition

At base case loading condition, the 9-bus system requires a series device. Table 5.2 shows eigenvalues both without and with TCSC connected between buses 7 and 5. Figure 5.1 repeats Fig. 3.9 of a TCSC characteristic that has a TCSC ratio of 10. The firing angle can be computed from Fig. 5.1 for a given compensation level. The compensation provided by TCSC is 50% for which the corresponding firing angle is  $160^\circ$ . Proportional gain ( $K_P$ ) and integral gain ( $K_I$ ) for TCSC controller are selected as 0.1 and 10 respectively. From Table 5.2 it is evident that damping of the interarea mode, the eigenvalues of which are given in bold letters, is improved after the connection of the TCSC in the system. Fig. 5.2 shows the voltage profile and Fig. 5.3 depicts real and reactive power flow over lines without and with the TCSC at the base case loading condition for the 9-bus system.

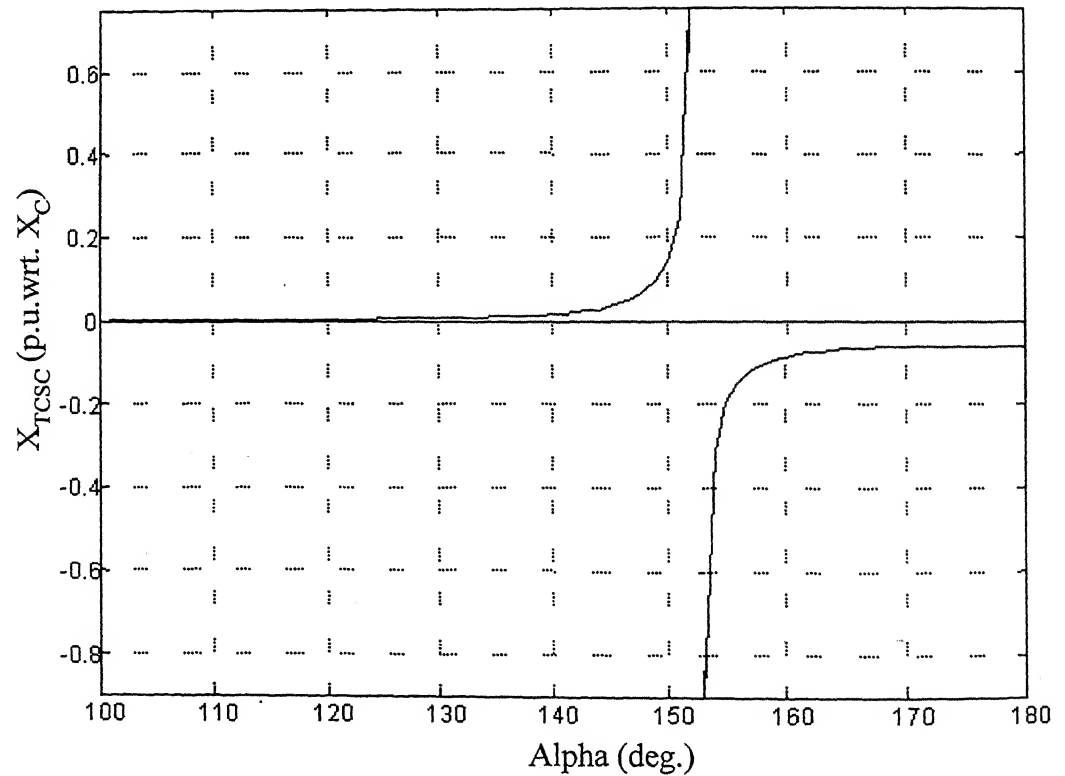
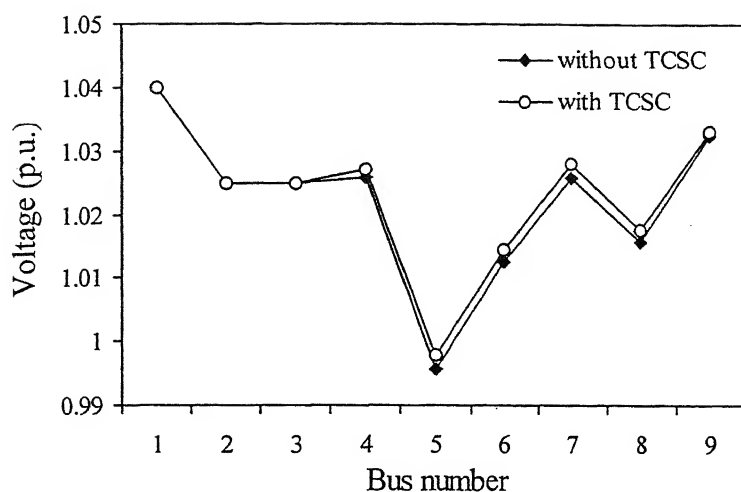


Fig. 5.1 Typical TCSC characteristic



**Fig. 5.2** Voltage profile of the 9-bus system at base case loading with and without TCSC

**Table 5.2** Eigenvalues with and without TCSC for the 9-bus system at base case loading condition

Without FACTS device	With TCSC
	-45.4983
$-0.7198 \pm 12.7456i$	$-0.7136 \pm 12.7660i$
<b><math>-0.1906 \pm 8.3660i</math></b>	<b><math>-1.4702 \pm 7.9159i</math></b>
$-5.6867 \pm 7.9663i$	$-5.7151 \pm 8.0302i$
$-5.3644 \pm 7.9311i$	$-5.3759 \pm 7.9573i$
$-5.2287 \pm 7.8263i$	$-5.2389 \pm 7.8670i$
-5.1779	-6.4486
-3.3993	-5.5485
	-4.8023
$-0.4513 \pm 1.1997i$	$-0.4490 \pm 0.8849i$
$-0.4481 \pm 0.7291i$	$-0.4238 \pm 0.5051i$
$-0.4366 \pm 0.4868i$	$-0.4407 \pm 0.3091i$
$0.0000 \pm 0.0000i$	$0.0000 \pm 0.0000i$
-3.2258	-3.2258

It is obvious from Figs. 5.2 and 5.3 that there is marginal improvement in the voltage profile of the system but a reasonable increase in the active and reactive power over line (7-5) after connecting TCSC in the system. This is further accompanied by a substantial enhancement in modal damping of the system.



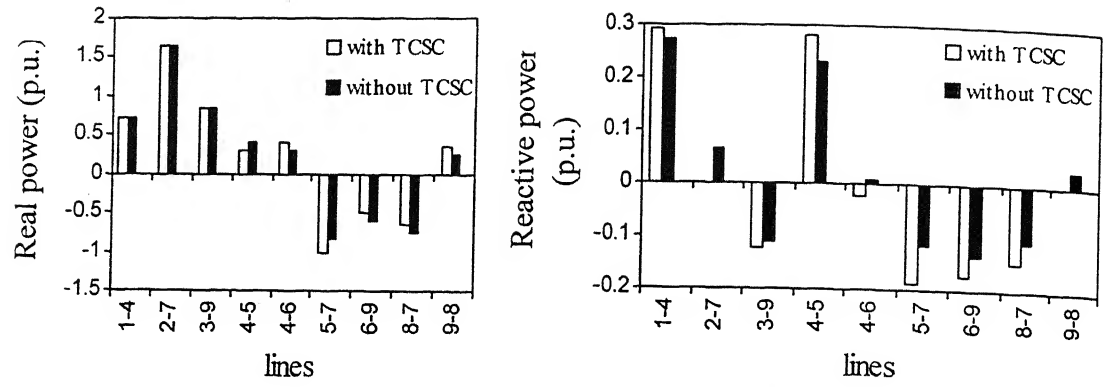


Fig. 5.3 Real and reactive power flow over lines with and without TCSC at base case loading condition

### 5.1.2 Maximum Loading Condition

At maximum loading condition, there is a need for a shunt device at bus 5. Table 5.3 shows eigenvalues of the 9-bus system at maximum loading condition for three different cases - without any FACTS device, with an SVC connected at bus 5 and with a TCSC connected between line (7-5). Whereas TCSC controller parameters are same as those used for base case loading condition, the SVC controller parameters are chosen as  $K_P = 0.3$  and  $K_I = 100$ .

Table 5.3 shows that without any FACTS device the system is unstable, where unstable eigenvalues are highlighted. However the system becomes stable when either SVC or TCSC are connected. Fig. 5.4 depicts voltage profile of the 9-bus system at maximum loading condition with and without any FACTS device. It is evident from Fig. 5.4 that voltage profile of the system with SVC connected at bus 5 is the best. Therefore at maximum loading condition, SVC should be connected at bus 5. This validates the EVPA result obtained in previous chapter.

In practice, the real power over a line or current signal is usually taken to examine the system performance. In the present context it is not possible to express power/current over a line in a straightforward manner because network is modeled by algebraic equations only. Therefore step response of output signal  $\Delta E_{fd}$  (small change in voltage proportional to field voltage) of the machine connected to bus 2 is taken for input signal

$\Delta V_{ref}$  (small change in terminal voltage reference setting). Figure 5.5 shows step response of the 9-bus system without any FACTS device connected in the system, with SVC connected at bus 5 and with TCSC connected between line (7-5). The step response shows that both SVC and TCSC, when connected, stabilize the system.

**Table 5.3** Eigenvalues of the 9-bus system at maximum loading condition

Without any FACTS device Device	With SVC	With TCSC
		-46.1753
-90.9053	-92.8398	-41.2866
-45.3014	-0.5511 ±50.3889i	-0.7151 ±12.3385i
-2.8938 ±12.3353i	-0.5840 ±12.6211i	-10.2041 ± 6.9092i
-10.8806 ± 5.8904i	-0.1256 ± 8.0372i	-5.4101 ± 7.9066i
-1.2151 ± 8.8486i	-9.8966 ± 7.0805i	-1.0760 ± 6.7042i
-6.3982 ± 7.4235i	-7.3482 ± 7.9374i	-7.5342
-7.1865	-5.2924 ± 7.8977i	-5.4913 ± 0.1888i
-5.1023	-5.3210	-4.8011
-2.1747	-3.9843	-0.4923 ± 1.0871i
-1.6763	-0.5010 ± 1.1119i	-1.9310
-0.7284 ± 0.3533i	-0.6142 ± 0.6468i	-0.8733 ± 0.2529i
<b>0.0229 ± 0.2268i</b>	-0.7376 ± 0.2042i	-0.5034
-0.0000 ± 0.0000i	-0.0000 ± 0.0000i	-0.0000 ± 0.0000i
-3.2258	-3.2258	-3.2258

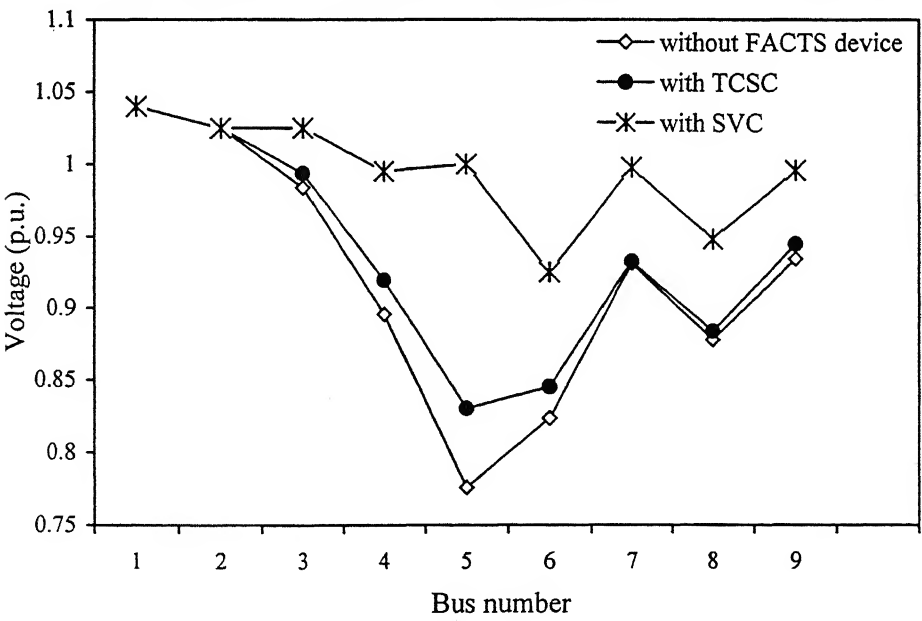


**Fig. 5.4** Voltage profile of the 9-bus system without and with FACTS devices at maximum loading condition

It is clear that TCSC is needed for base case loading condition and SVC is needed at maximum loading condition. Therefore a combination of both SVC and TCSC has been considered at maximum loading condition. The step response shows that a combination of both SVC and TCSC stabilizes the system much more effectively as compared to a single device. At base case loading condition SVC will remain floating and only TCSC will be active. Table 5.4 shows eigenvalues with SVC and with SVC-TCSC combination in the system. From Table 5.4 and Fig. 5.5, it can be observed that with SVC-TCSC the system overall damping and voltage profile improves further. The controller parameters for SVC and TCSC when used in combination are kept same when the devices are connected individually in the system. Figure 5.6 shows voltage profile of the system with SVC and with SVC-TCSC connected in the system. It is evident from Fig. 5.6 that there is a marginal improvement in voltage profile of the system when both SVC-TCSC are connected in the system. At base case loading condition, the system is stable. Therefore only SVC can serve the purpose of voltage profile improvement and stability enhancement. However if there is a need for power transfer improvement over the lines and further enhancement of system damping, a TCSC may be connected. With both TCSC and SVC in the system, the stability of the system improves so does the voltage profile. However the following considerations may restrict the installation of only one FACTS device (SVC) as opposed to the installation of a combination of SVC-TCSC:

- Restrictive overriding cost considerations
- EVPA suggests installation of a shunt device at maximum loading, which is more important in system operation as compared to base case loading.

In this situation the performance of SVC is evaluated for the following three conditions:

- Floating at base case condition
- Maximum loading condition (system loading condition without FACTS devices beyond which load flow does not converge)
- Extreme loading condition (system loading condition with FACTS devices beyond which load flow does not converge)

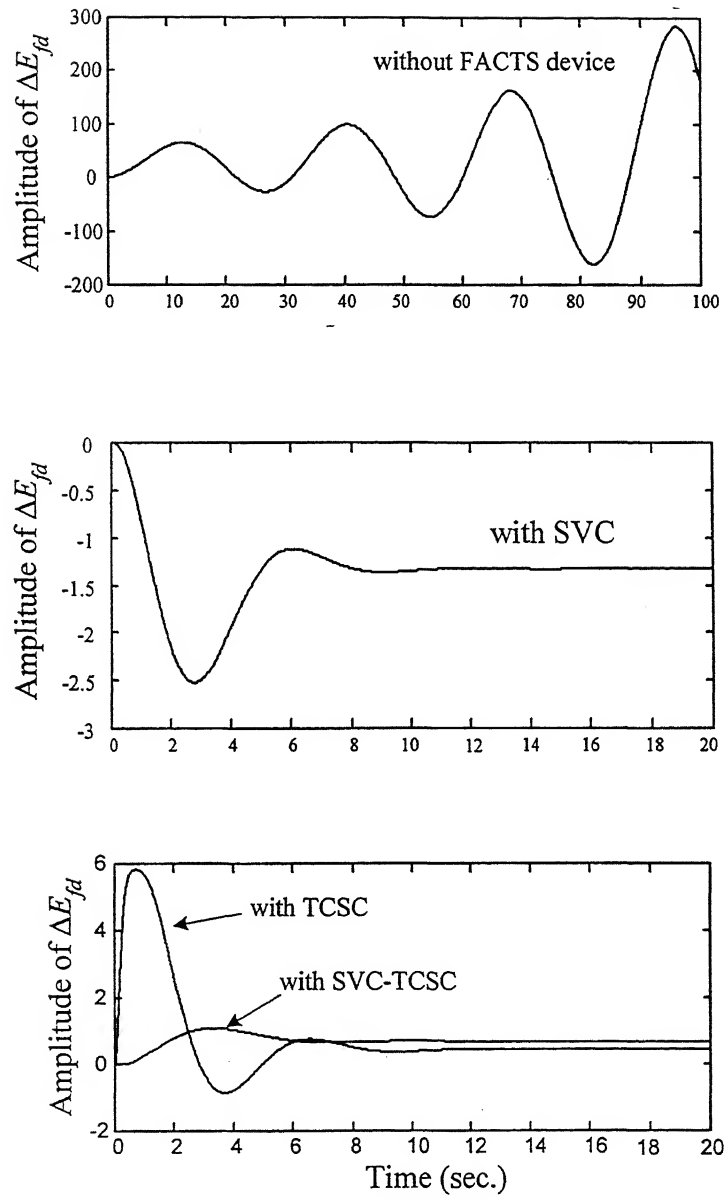


**Fig. 5.5** Step response of the 9-bus system at maximum loading condition

**Table 5.4** Eigenvalues of the 9-bus system at maximum loading condition

With SVC	With SVC-TCSC
	-73.2762
	-45.7923
-92.8398	-13.4003 ± 22.7099i
-0.5511 ± 50.3889i	-0.8122 ± 12.7828i
-0.5840 ± 12.6211i	-8.9940 ± 7.6013i
-0.1256 ± 8.0372i	-7.1699 ± 7.9906i
-9.8966 ± 7.0805i	-5.3159 ± 7.9089i
-7.3482 ± 7.9374i	-1.5319 ± 7.5468i
-5.2924 ± 7.8977i	-6.6072
-5.3210	-5.0487
-3.9843	-4.7690
-0.5010 ± 1.1119i	-0.4599 ± 0.9280i
-0.6142 ± 0.6468i	-0.6605 ± 0.4841i
-0.7376 ± 0.2042i	-1.0336
-0.0000 ± 0.0000i	-0.0000
-3.2258	-0.4012
	-0.1391
	-3.2258

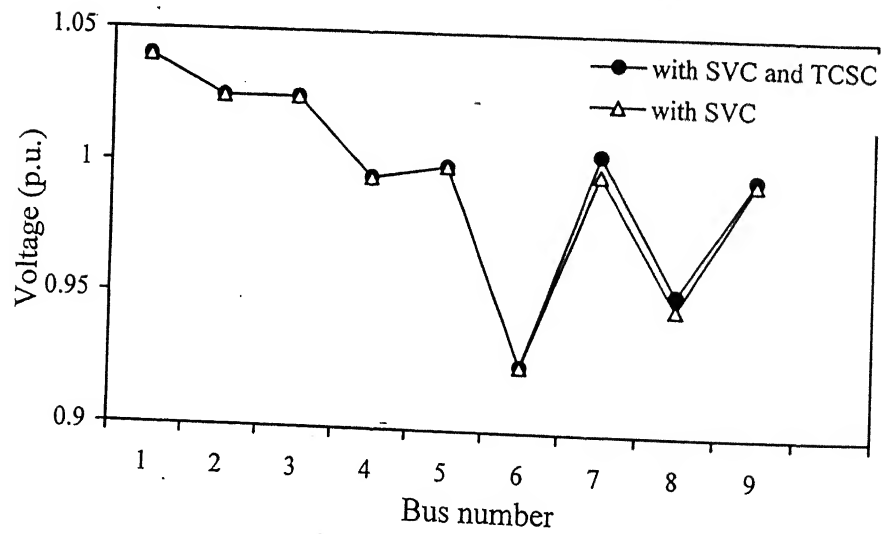


**Fig. 5.6** Voltage profile of 9-bus system at maximum loading condition with SVC and with SVC-TCSC both

**Table 5.5** Eigenvalues of the 9-bus system at base case loading

Without FACTS device	With SVC floating
	-75.1082
$-0.7198 \pm 12.7456i$	$-12.1101 \pm 25.5649i$
$-0.1906 \pm 8.3660i$	$-0.7100 \pm 12.7523i$
$-5.6867 \pm 7.9663i$	$-0.1882 \pm 8.3982i$
$-5.3644 \pm 7.9311i$	$-5.6853 \pm 7.9827i$
$-5.2287 \pm 7.8263i$	$-5.3645 \pm 7.9396i$
-5.1779	$-5.2350 \pm 7.8768i$
-3.3993	-5.2195
	-3.9818
$-0.4513 \pm 1.1997i$	$-0.4641 \pm 0.9617i$
$-0.4481 \pm 0.7291i$	$-0.4500 \pm 0.7205i$
$-0.4366 \pm 0.4868i$	$-0.4342 \pm 0.4847i$
$0.0000 \pm 0.0000i$	$-0.0000 \pm 0.000i$
-3.2258	-3.2258

Table 5.5 show eigenvalues at base case loading without any FACTS device and with floating SVC. The system remains stable with SVC in floating condition. As the system is inherently stable at base case loading condition, only SVC at bus 5 can serve the purpose of improving voltage profile as well as small signal stability of the system. Once the SVC is installed in the system, next step is to see how much more system can be loaded before being unstable. For this case, with SVC connected at bus 5, system loading and generation are again increased up to non-convergence of the load flow. It was found that with SVC in the system, the loading could be increased up to 250% beyond base case loading. It may be recalled that the net increase in system loading was 143% beyond base case loading without SVC. Table 5.6 shows eigenvalues with SVC connected at bus 5 for this extreme loading condition. At this condition although the system is stable, the system damping is poor as evident from Table 5.6. It is observed that although SVC is able to improve the voltage profile of the system, the improvement in system damping at maximum loading is not as much as that with TCSC. This performance of SVC is expected because SVC with voltage control alone is not expected

to contribute to system damping [2]. On the other hand, a TCSC directly enhance system damping.

**Table 5.6** Eigenvalues of the 9-bus system for extreme loading condition with SVC at bus 5

Maximum loading condition	Extreme loading condition
-92.8398	-124.86
$-0.5511 \pm 50.3889i$	-67.58
$-0.5840 \pm 12.6211i$	-48.63
$-0.1256 \pm 8.0372i$	$-16.34 \pm 10.96i$
$-9.8966 \pm 7.0805i$	$-0.35 \pm 11.45i$
$-7.3482 \pm 7.9374i$	<b><math>-0.03 \pm 8.09i</math></b>
$-5.2924 \pm 7.8977i$	$-6.03 \pm 8.10i$
-5.3210	-7.18
-3.9843	-5.87
$-0.5010 \pm 1.1119i$	-5.43
$-0.6142 \pm 0.6468i$	-5.65
$-0.7376 \pm 0.2042i$	-2.41
$-0.0000 \pm 0.0000i$	-2.01
-3.2258	$-0.25 \pm 0.59i$
	-0.81
	-0.35
	$-0.0000 \pm 0.0000i$
	-3.23

## 5.2 SIXTEEN MACHINES 68-BUS SYSTEM

### 5.2.1 Base Case Loading

At the base case loading of the 68-bus system, EVPA showed that from the viewpoint of voltage stability, line (41-40) is most critical. The most critical path was an Active Power Transmission Path and therefore there was a need for a series device. Table 5.7 shows the set of eigenvalues having damping less than 0.1 at base case loading without and with TCSC connected in the system. All eigenvalues that have damping more than 0.1 are listed in Appendix N. From Table 5.7, it is evident that there is a

marginal effect on the stability of the system with TCSC operating at 50% compensation level. This may be due to arbitrary choice of TCSC controller parameters of  $K_P = 0.1$  and  $K_I = 10$ . At base case loading condition, the system is inherently stable. Fig. 5.7 shows voltage profile of the system with and without TCSC. It is further seen that there is not much effect of TCSC on voltage profile of the system.

**Table 5.7** Eigenvalues for the 68-bus system at base case loading without and with TCSC

Eigenvalues without TCSC	Damping	Eigenvalues with TCSC	Damping
		$-42.3686 \pm 41.0541i$	0.7182
$-0.5851 \pm 12.0779i$	0.0484	$-0.5867 \pm 12.0673i$	0.0486
$-0.6511 \pm 10.1218i$	0.0642	$-0.6505 \pm 10.1217i$	0.0641
$-0.6223 \pm 9.9461i$	0.0624	$-0.6200 \pm 9.9480i$	0.0622
$-0.8185 \pm 9.8868i$	0.0825	$-0.8179 \pm 9.8868i$	0.0824
$-0.3904 \pm 8.5142i$	0.0458	$-0.3931 \pm 8.5131i$	0.0461
$-0.5008 \pm 8.3996i$	0.0595	$-0.5004 \pm 8.3983i$	0.0595
$-0.3803 \pm 8.0569i$	0.0471	$-0.3841 \pm 8.0153i$	0.0479
$-0.4687 \pm 7.7676i$	0.0602	$-0.4684 \pm 7.7682i$	0.0602
$-0.5217 \pm 7.4364i$	0.0700	$-0.5181 \pm 7.4248i$	0.0696
$-0.3820 \pm 7.0022i$	0.0545	$-0.3825 \pm 6.9968i$	0.0546
$-0.3886 \pm 6.5793i$	0.0590	$-0.3881 \pm 6.5793i$	0.0589
$-0.4544 \pm 4.9673i$	0.0911	$-0.4592 \pm 4.9217i$	0.0929
$-0.2848 \pm 4.1451i$	0.0685	$-0.2880 \pm 4.1442i$	0.0693
$-0.1931 \pm 3.3344i$	0.0578	$-0.1769 \pm 3.2335i$	0.0546

### 5.2.2 Maximum Loading Condition

The maximum loading beyond which the load flow does not converge is obtained when the load is increased by 14% from the base case loading. At this loading condition, EVPA indicates the need of a shunt device at bus 40. A TCSC has been suggested by EVPA at base case loading condition. Table 5.8 shows the eigenvalues with damping less than 0.1 without FACTS device, with SVC connected at bus 40 and with TCSC connected between buses 41-40 at maximum loading condition. It is seen that with SVC



the unstable mode having frequency (0.9411 rad/s) stabilizes and acquires a damping of 0.0284. However with TCSC the damping of the same mode increases significantly. SVC controller parameters are  $K_P = 0.0$  and  $K_I = 100.0$  and TCSC controller parameters are  $K_P = 0.1$  and  $K_I = 10$  (same as used at base case loading). From Table 5.8, it can be seen that both SVC and TCSC individually are able to stabilize the system.

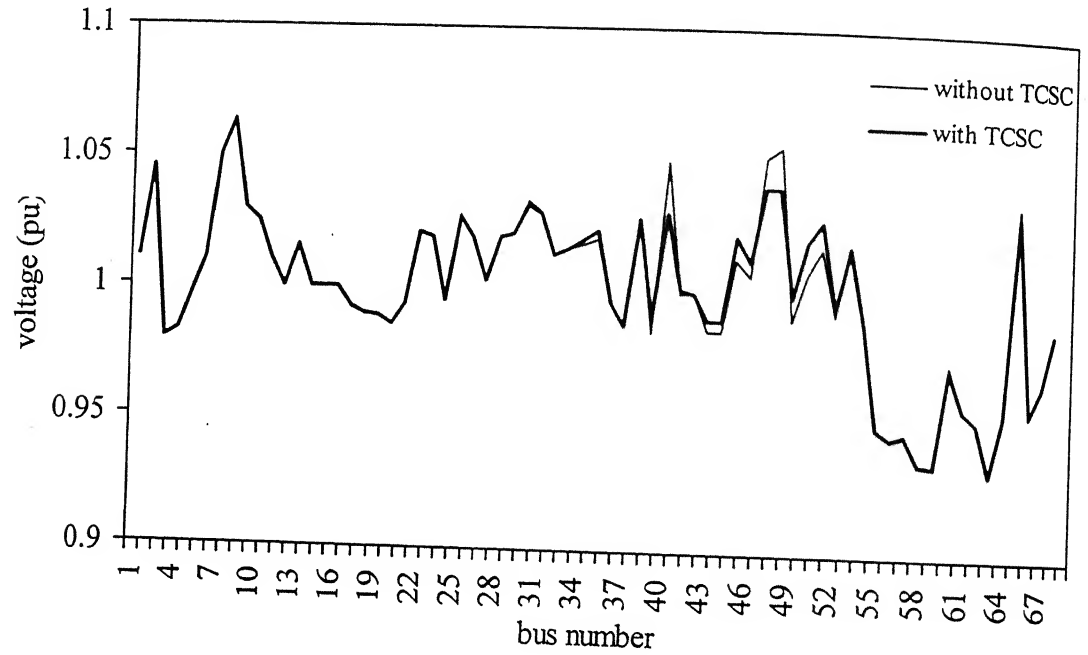


**Fig. 5.7** Voltage profile of 68-bus system at base case loading condition with and without TCSC

Figure 5.8 shows voltage profile of the 68-bus system at maximum loading condition with and without FACTS devices. It is seen that at some buses voltage is better with SVC in the system and at some other buses voltage is better with TCSC. It appears that for a good voltage profile SVC-TCSC combination should be used. More concrete conclusions can be drawn after looking at the step response of the system at maximum loading condition. Figure 5.9 depicts that although SVC alone is able to stabilize the system, response of individual TCSC is better than individual SVC. A combination of SVC-TCSC gives even better performance than TCSC or SVC alone.

**Table 5.8** Eigenvalues of the 68-bus system at maximum loading condition

Without FACTS device	With SVC	With TCSC
$-0.6143 \pm 11.8161i$	$-0.5979 \pm 11.9204i$	$-0.5974 \pm 11.9193i$
$-0.6466 \pm 10.1371i$	$-0.6405 \pm 10.1370i$	$-0.6412 \pm 10.1371i$
$-0.6762 \pm 9.8847i$	$-0.6334 \pm 9.9470i$	$-0.6390 \pm 9.9402i$
$-0.8014 \pm 9.9045i$	$-0.7952 \pm 9.9048i$	$-0.7959 \pm 9.9048i$
$-0.3827 \pm 8.4470i$	$-0.3840 \pm 8.4820i$	$-0.3891 \pm 8.4760i$
$-0.5052 \pm 8.4224i$	$-0.4980 \pm 8.4154i$	$-0.4986 \pm 8.4156i$
$-0.3906 \pm 7.9805i$	$-0.3797 \pm 8.0186i$	$-0.3830 \pm 7.9911i$
$-0.5053 \pm 7.4819i$	$-0.5060 \pm 7.4649i$	$-0.4442 \pm 7.7457i$
$-0.4468 \pm 7.7387i$	$-0.4439 \pm 7.7465i$	$-0.5020 \pm 7.4506i$
$-0.3765 \pm 6.9377i$	$-0.3741 \pm 6.9500i$	$-0.3749 \pm 6.9439i$
$-0.3850 \pm 6.5133i$	$-0.3842 \pm 6.5259i$	$-0.3846 \pm 6.5229i$
$-0.4368 \pm 4.8480i$	$-0.4369 \pm 4.8954i$	$-0.4481 \pm 4.8994i$
$-0.2762 \pm 4.0448i$	$-0.2772 \pm 4.0946i$	$-0.2798 \pm 4.0880i$
$-0.1545 \pm 2.8595i$	$-0.1656 \pm 3.0192i$	$-0.1637 \pm 2.9652i$
<b><math>0.0855 \pm 0.9411i</math></b>	<b><math>-0.0416 \pm 1.4673i</math></b>	<b><math>-0.1985 \pm 1.4865i</math></b>

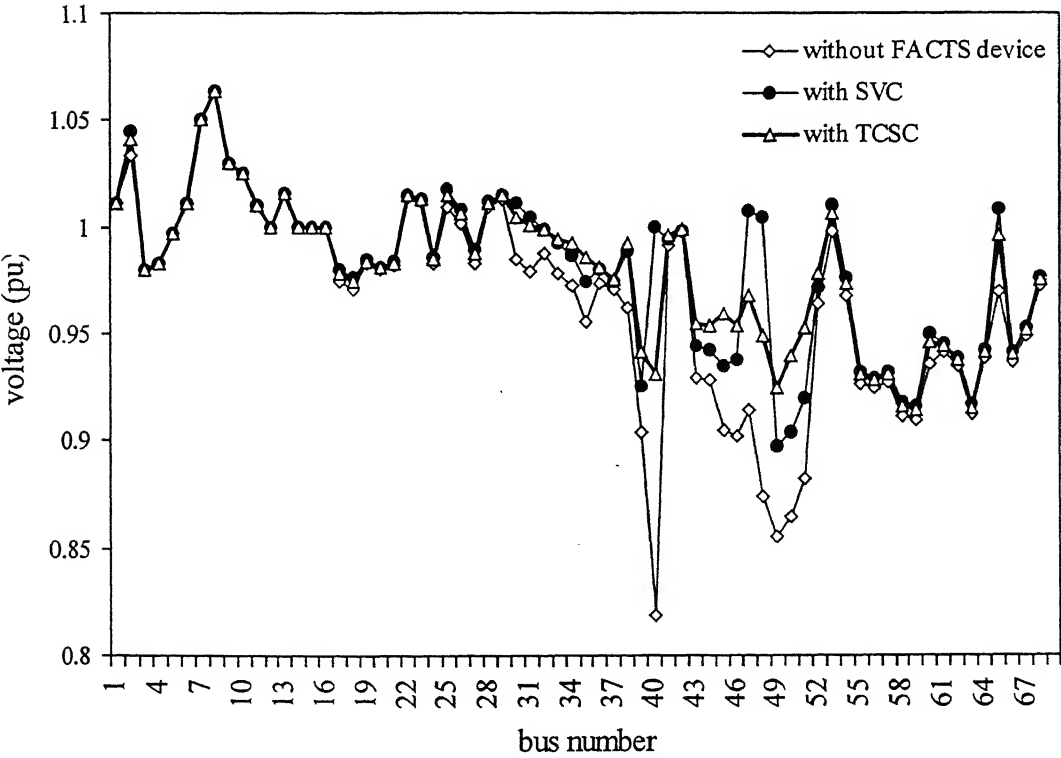


**Fig. 5.8** Voltage profile of the 68-bus system at maximum loading condition

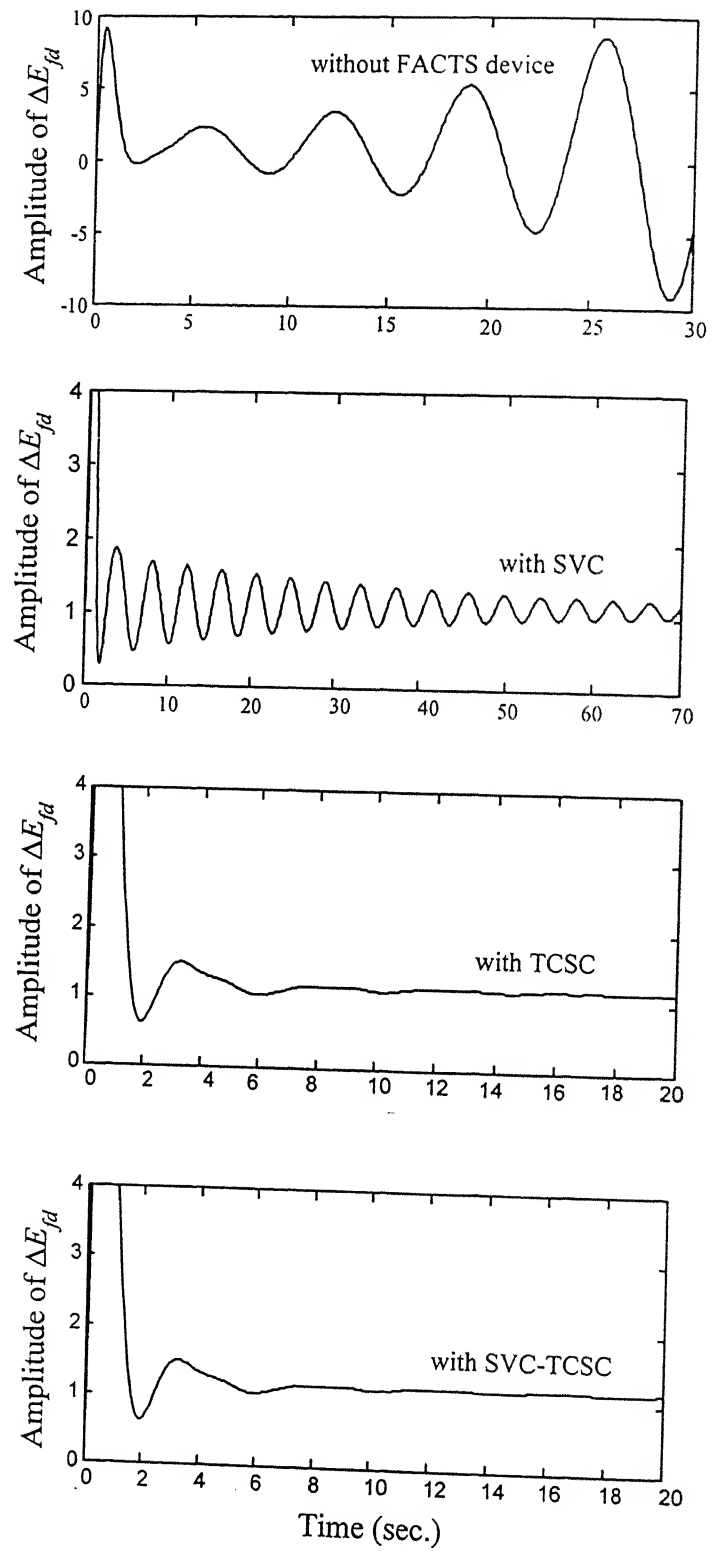


**Fig. 5.9** Step response of the 68-bus system at maximum loading condition

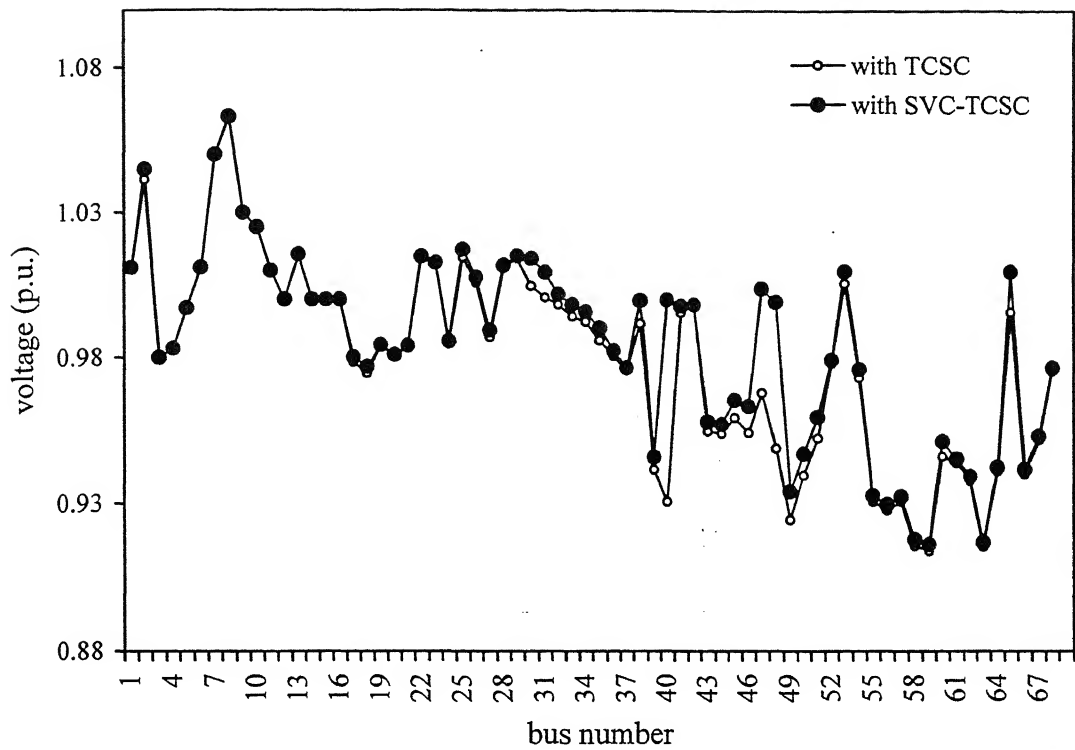


**Fig. 5.10** Voltage profile of the 68-bus system at maximum loading condition

**Table 5.9** Eigenvalues with TCSC alone and with SVC-TCSC at maximum loading condition

With TCSC	With SVC-TCSC
$-0.5974 \pm 11.9193i$	$-0.5953 \pm 11.9320i$
$-0.6412 \pm 10.1371i$	$-0.6403 \pm 10.1371i$
$-0.6390 \pm 9.9402i$	$-0.6333 \pm 9.9472i$
$-0.7959 \pm 9.9048i$	$-0.7950 \pm 9.9049i$
$-0.3891 \pm 8.4760i$	$-0.3894 \pm 8.4803i$
$-0.4986 \pm 8.4156i$	$-0.4976 \pm 8.4143i$
$-0.3830 \pm 7.9911i$	$-0.3818 \pm 7.9930i$
$-0.4442 \pm 7.7457i$	$-0.4438 \pm 7.7468i$
$-0.5020 \pm 7.4506i$	$-0.5017 \pm 7.4476i$
$-0.3749 \pm 6.9439i$	$-0.3747 \pm 6.9452i$
$-0.3846 \pm 6.5229i$	$-0.3848 \pm 6.5244i$
$-0.4481 \pm 4.8994i$	$-0.4483 \pm 4.9014i$
$-0.2798 \pm 4.0880i$	$-0.2804 \pm 4.0939i$
$-0.1637 \pm 2.9652i$	$-0.1634 \pm 2.9733i$
$-0.1985 \pm 1.4865i$	$-0.2038 \pm 1.5002i$

Voltage profile of the 68-bus system is shown in Fig. 5.10 also shows that SVC-TCSC gives much better voltage profile than when only TCSC is connected in the system. Eigenvalues with TCSC alone and with SVC-TCSC in the system at maximum loading condition are tabulated in Table 5.9.

As the voltage of bus 40 is quite high at base case loading, the SVC may remain floating. In that situation Table 5.10 shows eigenvalues without any FACTS device and with SVC-TCSC combination (but SVC floating) at base case loading condition.

**Table 5.10** Eigenvalues of the 68-bus system at base case loading with floating SVC

Without FACTS device	With SVC-TCSC
$-0.5851 \pm 12.0779i$	$-0.5868 \pm 12.0673i$
$-0.6511 \pm 10.1218i$	$-0.6505 \pm 10.1217i$
$-0.6223 \pm 9.9461i$	$-0.6199 \pm 9.9479i$
$-0.8185 \pm 9.8868i$	$-0.8179 \pm 9.8868i$
$-0.3904 \pm 8.5142i$	$-0.3933 \pm 8.5132i$
$-0.5008 \pm 8.3996i$	$-0.5004 \pm 8.3983i$
$-0.3803 \pm 8.0569i$	$-0.3839 \pm 8.0154i$
$-0.4687 \pm 7.7676i$	$-0.4684 \pm 7.7682i$
$-0.5217 \pm 7.4364i$	$-0.5181 \pm 7.4248i$
$-0.3820 \pm 7.0022i$	$-0.3825 \pm 6.9968i$
$-0.3886 \pm 6.5793i$	$-0.3883 \pm 6.5791i$
$-0.4544 \pm 4.9673i$	$-0.4592 \pm 4.9216i$
$-0.2848 \pm 4.1451i$	$-0.2885 \pm 4.1430i$
$-0.1931 \pm 3.3344i$	$-0.1770 \pm 3.2334i$

Again with SVC-TCSC connected in the system, loads and generations are increased up to non-convergence of load flow. This constitutes the extreme loading condition for the system considered. The maximum loading is obtained with 14% increase from base case in the absence of any FACTS device. However the extreme loading condition is realized with 21% increase from the base case loading. At this extreme loading condition, eigenvalues of 68-bus system are shown in Table 5.11. The eigenvalues show that with SVC-TCSC the system is stable at extreme loading condition but its damping is lower than when SVC-TCSC are at maximum loading condition. Same results are also depicted in Fig. 5.11.

**Table 5.11** Eigenvalues of the 68-bus system

With SVC-TCSC At maximum loading	With SVC-TCSC At extreme loading
$-0.5953 \pm 11.9320i$	$-0.6015 \pm 11.8407i$
$-0.6403 \pm 10.1371i$	$-0.6370 \pm 10.1441i$
$-0.6333 \pm 9.9472i$	$-0.6463 \pm 9.9316i$
$-0.7950 \pm 9.9049i$	$-0.7857 \pm 9.9127i$
$-0.3894 \pm 8.4803i$	$-0.3874 \pm 8.4496i$
$-0.4976 \pm 8.4143i$	$-0.4970 \pm 8.4227i$
$-0.3818 \pm 7.9930i$	$-0.3849 \pm 7.9710i$
$-0.4438 \pm 7.7468i$	$-0.4909 \pm 7.4556i$
$-0.5017 \pm 7.4476i$	$-0.4332 \pm 7.7316i$
$-0.3747 \pm 6.9452i$	$-0.3719 \pm 6.9103i$
$-0.3848 \pm 6.5244i$	$-0.3835 \pm 6.4922i$
$-0.4483 \pm 4.9014i$	$-0.4429 \pm 4.8821i$
$-0.2804 \pm 4.0939i$	$-0.2766 \pm 4.0587i$
$-0.1634 \pm 2.9733i$	$-0.1717 \pm 2.7896i$
$-0.2038 \pm 1.5002i$	$-0.0985 \pm 1.2248i$

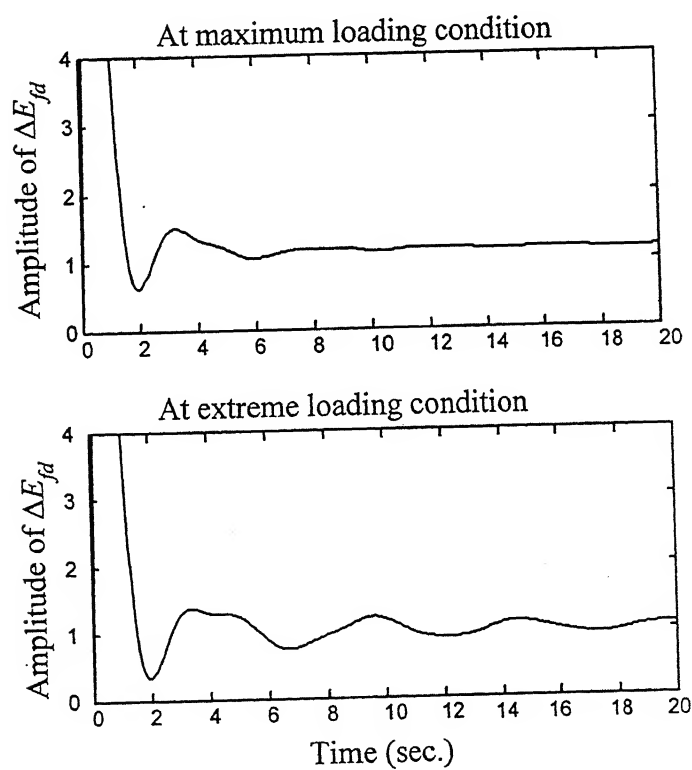


**Fig. 5.11** Step response of the 68-bus system with SVC-TCSC

### 5.3 EIGENVALUE ANALYSIS USING STATCOM AND SSSC

In the previous section, EVPA results were analyzed using SVC, TCSC and SVC-TCSC combination. In this section, EVPA results are analyzed using models of STATCOM and SSSC developed in Chapter 3. The STATCOM and SSSC models are dynamic models, which includes the dynamics of device components such as inductors and thyristors bridges etc. [36, 37]. Further both models are equipped with integral feedback controllers. On the other hand the models of SVC and TCSC do not include the representation of device components. Moreover the controllers in both SVC and TCSC are simple PI controllers. Hence no meaningful comparison can be done between the performance of SVC and STATCOM or TCSC and SSSC.

#### 5.3.1 Nine-Bus System

At maximum loading condition, it was observed that the 9-bus system needs a shunt compensator. The eigenvalues of the 9-bus system without any FACTS device, with STATCOM and with STATCOM-TCSC combined are shown in Table 5.12. It is seen from this table that the system is unstable without any FACTS device but is stable when a FACTS device is included in the system. The STATCOM data is taken from [36] and are given in Appendix N. The STATCOM controller parameters  $[K_1 \ K_2 \ K_3 \ K_4]$  are chosen as  $[-0.0684 \ 0.1020 \ 3.4603 \ -33.828]$ . These parameters are chosen using pole placement technique such that the STATCOM system has a desired response. Subsequently, the overall system stability associated with these parameters is studied. Step responses (output signal  $\Delta E_{fd}$  of the 2<sup>nd</sup> machine with input  $\Delta V_{ref}$  of the 2<sup>nd</sup> machine) of the 9-bus system without FACTS device, with STATCOM and with STATCOM-TCSC are shown in Fig. 5.12. The TCSC controller parameters are identical to those used in previous section i.e.  $K_P = 0.1$  and  $K_I = 10$ . As evident from Fig. 5.12, the combination of STATCOM-TCSC gives best response at maximum loading condition for the 9-bus system.

**Table 5.12** Eigenvalues of the 9-bus system at maximum loading condition

Without FACTS device	With STATCOM	With STATCOM-TCSC
	$-464.56 \pm 419.69i$	$-45.774$
$-90.9053$	$-0.66485 \pm 12.672i$	$-0.8161 \pm 12.783i$
$-45.3014$	$-0.1647 \pm 8.09i$	$-8.9938 \pm 7.6015i$
$-2.8938 \pm 12.3353i$	$-9.9045 \pm 7.0791i$	$-7.1694 \pm 7.9888i$
$-10.8806 \pm 5.8904i$	$-5.3161 \pm 7.8904i$	$-5.3007 \pm 7.894i$
$-1.2151 \pm 8.8486i$	$-7.3579 \pm 7.9372i$	$-1.5799 \pm 7.4243i$
$-6.3982 \pm 7.4235i$	$-5.349$	$-6.6066$
$-7.1865$	$-4.2192$	$-5.0667$
$-5.1023$	$-0.4638 \pm 0.92351i$	$-4.7661$
$-2.1747$	$-0.65201 \pm 0.61794i$	$-0.46495 \pm 0.98762i$
$-1.6763$	$-0.74475 \pm 0.16847i$	$-0.65953 \pm 0.48493i$
$-0.7284 \pm 0.3533i$	$-11.433 \pm 8.1141i$	$-1.0335$
<b><math>0.0229 \pm 0.2268i</math></b>	$-0.0000 \pm 0.0000i$	$-0.0000$
$-0.0000 \pm 0.0000i$	$-3.2258$	$-0.13909$
		$-0.40131$
		$-467.27 \pm 423.98i$
		$-10.838 \pm 8.3552i$
		$-3.2258$
$-3.2258$		

As discussed for the 9-bus system, a shunt device is more useful from voltage stability viewpoint. The performance of STATCOM is analyzed at extreme loading condition. From Table 5.13 it is noted that STATCOM is able to stabilize the system at the extreme loading condition. The STATCOM controller parameters are same as that used for maximum loading condition.

### 5.3.2 Sixty Eight Bus System

As discussed in Section 5.3.2, this system requires a combination of shunt and series device at maximum loading condition. Eigenvalues of 68-bus system without any FACTS device, with the STATCOM alone and with STATCOM-TCSC combine are tabulated in Table 5.14. The STATCOM is connected at bus 40 and TCSC is connected between buses 41-40. For the STATCOM connected alone at bus 40, the controller parameters  $[K_1 \ K_2 \ K_3 \ K_4]$  are chosen as  $[-0.0566 \ -0.1529 \ 6.4620 \ 35.5118]$ . The



STATCOM controller parameters are chosen using pole placement technique so that the overall system stabilizes. For the STATCOM-TCSC combination at maximum loading, the STATCOM controller parameters are selected as  $[-0.1959 \quad 0.0280 \quad -1.1779 \quad -104.9722]$  and  $K_P = 0.1$  and  $K_I = 10$  for TCSC controller. It is seen that the overall damping of system is best at maximum loading condition when STATCOM-TCSC combination are connected in the system. Even at extreme loading condition, the system remains stable with STATCOM-TCSC both connected in the system as shown in Table 5.14. However STATCOM controller parameters are modified to  $[-0.0812 \quad -0.1846 \quad 3.5072 \quad 6.8239]$  in order to get a stable response. The TCSC parameters at extreme loading condition are same as used at maximum loading condition.

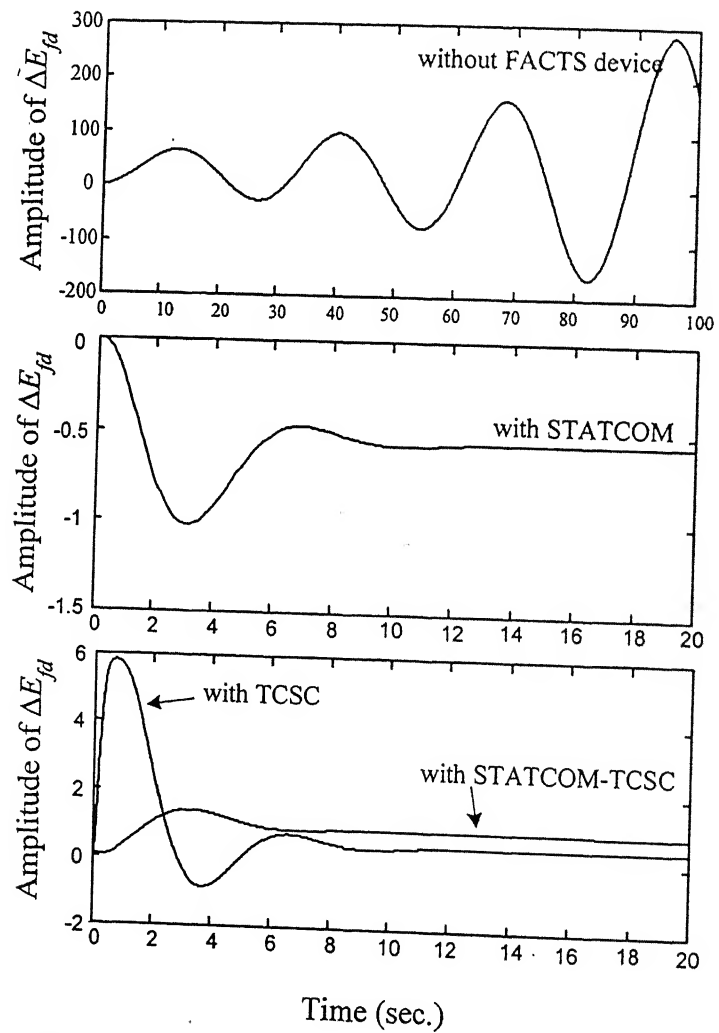


**Fig. 5.12** Step Response of the 9-bus system at maximum loading condition

**Table 5.13** Eigenvalues of the 9-bus system

With STATCOM at Maximum loading condition	With STATCOM at extreme loading condition
$-464.56 \pm 419.69i$	$-1000.4$
$-0.66485 \pm 12.672i$	$-124.86$
$-0.1647 \pm 8.09i$	$-199.76$
$-9.9045 \pm 7.0791i$	$-48.605$
$-5.3161 \pm 7.8904i$	$-0.76539 \pm 12.005i$
$-7.3579 \pm 7.9372i$	$-0.97051 \pm 9.2683i$
$-5.349$	$-6.1687 \pm 8.1431i$
$-4.2192$	$-20.045$
$-0.4638 \pm 0.92351i$	$-7.2378$
$-0.65201 \pm 0.61794i$	$-5.974$
$-0.74475 \pm 0.16847i$	$-5.4753$
$-11.433 \pm 8.1141i$	$-5.8454$
$-0.0000 \pm 0.0000i$	$-2.4099$
$-3.2258$	$-2.0318$
	$-1.0879$
	$-0.12318 \pm 0.59755i$
	$-0.35674$
	$-0.0000 \pm 0.0000i$
	$-9.986$
	$-3.2258$

**Table 5.14** Eigenvalues of the 68-bus system at maximum loading condition

Without FACTS device at maximum loading condition	With STATCOM at maximum loading condition	With STATCOM-TCSC at maximum loading condition	With STATCOM-TCSC at extreme loading condition
-0.6143 ± 11.8161i	-0.59762 ± 11.921i	-0.59514 ± 11.932i	-0.60118 ± 11.841i
-0.6466 ± 10.1371i	-0.64046 ± 10.137i	-0.6403 ± 10.137i	-0.63705 ± 10.144i
-0.6762 ± 9.8847i	-0.63363 ± 9.9464i	-0.63336 ± 9.9473i	-0.64641 ± 9.9317i
-0.8014 ± 9.9045i	-0.79525 ± 9.9049i	-0.79502 ± 9.9049i	-0.78565 ± 9.9127i
-0.3827 ± 8.4470i	-0.38541 ± 8.4823i	-0.38905 ± 8.4802i	-0.38675 ± 8.4495i
-0.5052 ± 8.4224i	-0.49799 ± 8.4152i	-0.49757 ± 8.4144i	-0.49701 ± 8.4228i
-0.3906 ± 7.9805i	-0.3796 ± 8.0208i	-0.38189 ± 7.9931i	-0.38485 ± 7.9711i
-0.5053 ± 7.4819i	-0.44393 ± 7.7465i	-0.44378 ± 7.7468i	-0.49081 ± 7.4558i
-0.4468 ± 7.7387i	-0.50597 ± 7.4649i	-0.5017 ± 7.4477i	-0.4332 ± 7.7317i
-0.3765 ± 6.9377i	-0.37415 ± 6.95i	-0.37456 ± 6.9453i	-0.3716 ± 6.9106i
-0.3850 ± 6.5133i	-0.38484 ± 6.5257i	-0.38453 ± 6.5246i	-0.38303 ± 6.4926i
-0.4368 ± 4.8480i	-0.44091 ± 4.9105i	-0.44833 ± 4.9014i	-0.44289 ± 4.8821i
-0.2762 ± 4.0448i	-0.27764 ± 4.0936i	-0.28004 ± 4.0947i	-0.27633 ± 4.0594i
-0.1545 ± 2.8595i	-0.17968 ± 3.0561i	-0.16319 ± 2.9737i	-0.17133 ± 2.7906i
<b>0.0855 ± 0.9411i</b>	<b>-0.045001 ± 1.5849i</b>	<b>-0.20408 ± 1.5001i</b>	<b>-0.099043 ± 1.2244i</b>

Figure 5.13 shows step response of the 68-bus system at maximum and extreme loading condition. It is seen that the step response with the STATCOM-TCSC combine at maximum loading gives best performance.

The STATCOM parameters in maximum loading condition do not give stable operation at extreme loading condition. Interestingly the STATCOM parameters resulting in stable system at extreme loading condition also do not provide stable operation at maximum loading condition. This shows a strong dependence of the STATCOM parameters on system loading. Hence a careful determination of the STATCOM parameters is necessary, which may ensure stable operation at all loading conditions. However this has not been attempted here.

### **5.3.3 Eigenvalue Analysis with SSSC for the 68-bus System**

The SSSC model is connected between buses 41 and 40 at maximum loading condition in the 68-bus system. The SSSC data is taken from [36] and is given in Appendix N. The compensation provided by the SSSC is 50%. The eigenvalues of 68-bus system at maximum loading condition with and without SSSC are tabulated in Table 5.15. It can be seen from Table 5.15 that the SSSC is able to stabilize the system. The SSSC controller parameters are chosen as  $[-0.045529 \ -0.041277 \ 3.7331 \ -0.19319]$ .

Further step response shown in Fig. 5.14 also depicts that SSSC stabilizes the system. No detailed analysis is done with SSSC model. The main purpose to present this study was to demonstrate the effectiveness of SSSC in stabilizing the overall system.

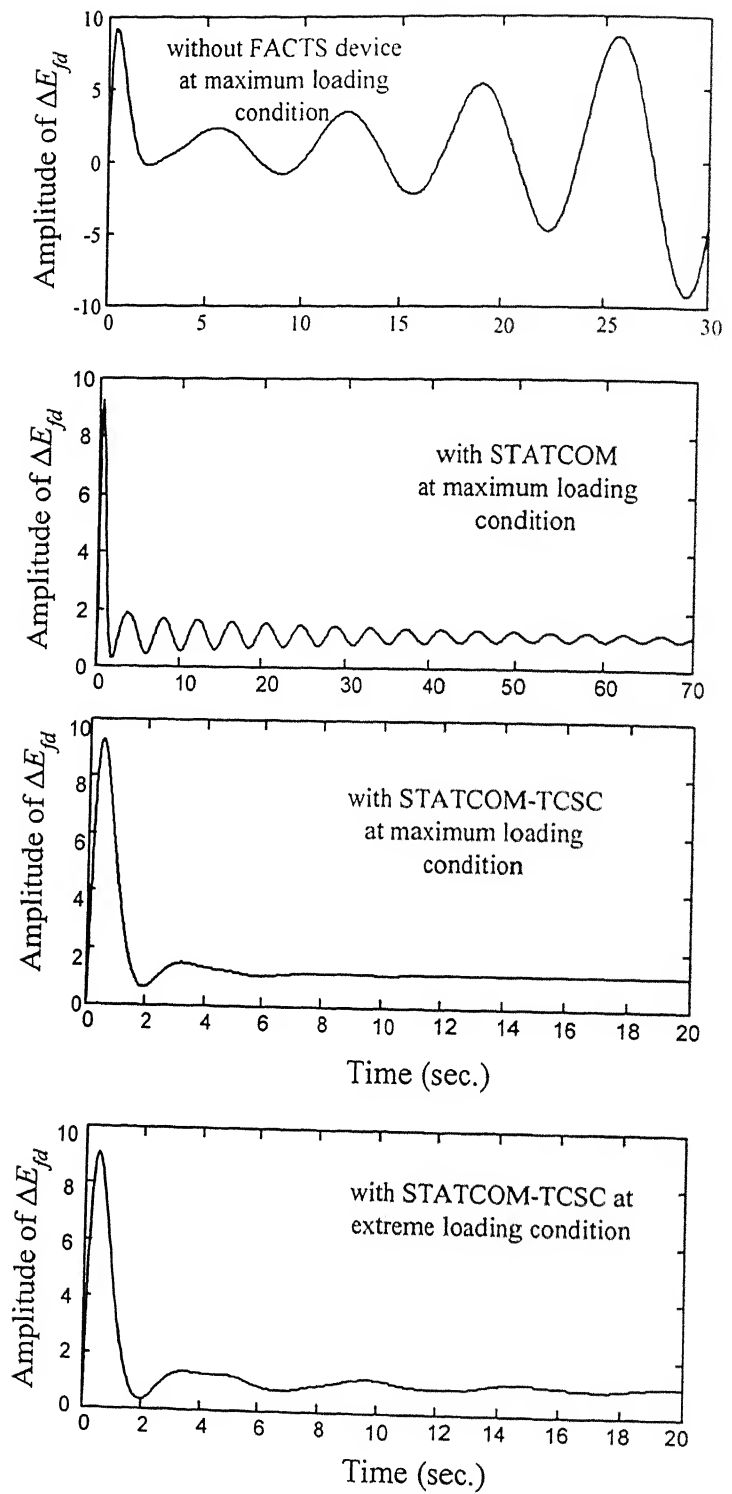


**Fig. 5.13** Step response of the 68-bus system at maximum and extreme loading conditions

**Table 5.15** Eigenvalues of the 68-bus system with SSSC at maximum loading conditions

Without FACTS device	With SSSC
	$-0.58413 \pm 12.007i$
$-0.6143 \pm 11.8161i$	$-0.64268 \pm 10.137i$
$-0.6466 \pm 10.1371i$	$-0.64679 \pm 9.9261i$
$-0.6762 \pm 9.8847i$	$-0.79742 \pm 9.9048i$
$-0.8014 \pm 9.9045i$	$-0.35595 \pm 8.4881i$
$-0.3827 \pm 8.4470i$	$-0.49977 \pm 8.4198i$
$-0.5052 \pm 8.4224i$	$-0.35929 \pm 8.221i$
$-0.3906 \pm 7.9805i$	$-0.44489 \pm 7.7436i$
$-0.5053 \pm 7.4819i$	$-0.51198 \pm 7.5023i$
$-0.4468 \pm 7.7387i$	$-0.36832 \pm 6.9795i$
$-0.3765 \pm 6.9377i$	$-0.37802 \pm 6.5701i$
$-0.3850 \pm 6.5133i$	$-0.36994 \pm 6.4773i$
$-0.4368 \pm 4.8480i$	$-0.34321 \pm 4.353i$
$-0.2762 \pm 4.0448i$	$-0.28059 \pm 4.0811i$
$-0.1545 \pm 2.8595i$	$-0.10297 \pm 2.4854i$
<b><math>0.0855 \pm 0.9411i</math></b>	<b><math>-0.15498 \pm 1.5604i</math></b>

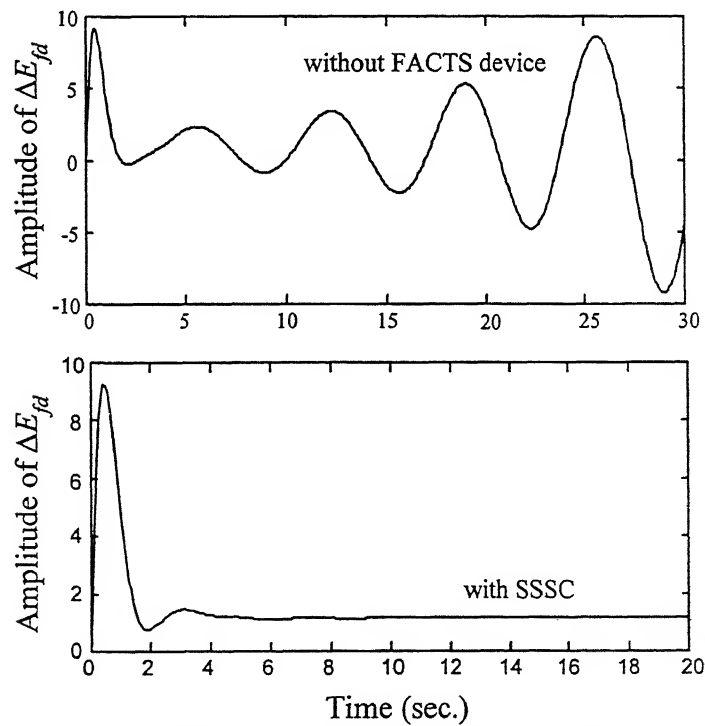


**Fig. 5.14** Step response of 68-bus system with and without SSSC at maximum loading condition

## 5.4 CONCLUSIONS

In this chapter, placement strategy using Extended Voltage Phasors Approach has been analyzed using various FACTS device models developed in Chapter 2. The EVPA results are analyzed using voltage profile analysis, small signal stability analysis and step response of the system. It is observed that the EVPA gives a clear identification of the place where a device should be placed. It may be noted here that these places may not be the optimal places from the viewpoint of system damping. However the EVPA gives optimal places from voltage stability viewpoint. The controller parameters are carefully chosen in such a way that system stability is improved, however there is a need of to know the complete range in which controller parameters can be chosen. This is illustrated in the next chapter.

## COORDINATED CONTROL OF FACTS DEVICES

Modern power systems are heading towards a deregulated environment. This will result in simultaneous installation of different FACTS devices in the system. A need therefore arises to examine possible control interaction amongst these devices. In this chapter studies are performed to gain an insight into the interaction between controllers of two FACTS devices which are electrically close to each other.

It is understood that the FACTS devices will normally be equipped with higher order controllers such as power swing damping controller, SSR damping controller etc. Still to develop an insight, the FACTS devices are assumed to be equipped with simple PI controller only.

The interaction is studied through the established technique of root loci analysis and the performance of the FACTS controllers derived is evaluated through step response studies. First the “best” PI controller of each device is obtained individually which provides a high degree of damping for all the sensitive modes (interarea modes and controller mode) simultaneously. Then the combined performance of the above two “best” controllers is investigated at different loading conditions to look for any interaction between the two controllers.

In this study the amount of series compensation is assumed to be completely controllable through a TCSC. In one of the investigations, the SVC-TCSC interaction is examined for a given set of system loads when the percent series compensation provided by the TCSC is varied.

The above studies are conducted on the 9-bus WSCC system [97]. Since FACTS devices are installed in power systems mainly for increasing the power transfer limit and improving the voltage profile of the system, the efficacy of FACTS controllers need to be studied at operating points close to stability limit. In this chapter the variation in “best”

---

**NOTE:** *In this Chapter, wherever the term “interarea mode” appears, kindly read it as “critical mode”.*

---



controller parameters is examined when operating conditions are varied from base case to maximum loading condition.

## 6.1 ROOT LOCI METHOD FOR DESIGN OF INDIVIDUAL FACTS CONTROLLERS

Each FACTS device is assumed to be equipped with a basic PI controller. The SVC has a PI voltage regulator with no auxiliary control whereas the TCSC has basic PI power controller with no other damping control.

Rigorous techniques exist for a global optimization of controller parameters such as genetic algorithm, performance indices based optimization and transient response based optimization. However, as the thrust of this chapter is not the design of FACTS controllers but examination of their interaction, a simple, though widely used, heuristic technique that combines root loci and step response analysis is employed to determine the “best” controller parameters in a ‘local sense’.

The procedure adopted for obtaining the controller parameters of the PI controller of this FACTS device is a two fold process as described below [2].

Step I: The proportional gain  $K_P$  is kept at zero and integral gain  $K_I$  is varied.

The value of  $K_I$  is chosen to provide a high degree of damping for all the sensitive modes simultaneously. These sensitive modes are the ‘interarea modes- a & b’ and ‘device controller modes’.

Step II: For the value of  $K_I$  chosen in step I,  $K_P$  is varied to determine the highest overall damping of the sensitive modes simultaneously.

The above combination of  $K_P$  and  $K_I$ , which imparts a high degree of damping to the sensitive modes simultaneously, is defined to be the “desirable” set of controller parameters. Further refinement of controller parameters is achieved through step response of the system and the parameters thus obtained are termed as the “best” set of controller parameters. This strategy is adopted for obtaining the “best” controller parameters of TCSC and SVC, individually, in the 9-bus system.

To study the variation of controller parameters of each FACTS device over a wide range of operating condition, following loading conditions are considered for the 9-bus system.

- Base case loading condition
- Mid-loading condition (where the loading is increased by 100% over the base case loading and generation is also increased in proportion to machine inertia).
- Maximum loading condition (beyond which load flow does not converge)

As suggested by EVPA method, the location for a TCSC is between buses 7-5 and the site for SVC is at bus 5 in the 9-bus system.

Table 6.1 shows eigenvalues with no FACTS device connected at different loading conditions for the 9-bus system. The following observations are made:

- Damping of the interarea mode ‘a’ increases with the increase in system loading. This can be attributed to the fact that loads contribute to system damping.
- Damping of the interarea mode ‘b’ increases until mid-loading condition and then decreases at maximum loading condition. The initial increase in damping is due to the contribution of loads but later decrease on further system loading is due to voltage instability.
- With the increase in system loading without FACTS device, the frequency of the interarea mode ‘b’ decreases from 8.36 rad/s to 2.3 rad/s implying a decrease in synchronizing torque.

## **6.2 DETERMINATION OF “BEST” TCSC CONTROLLER (WITHOUT SVC)**

As indicated in Table 5.2, the TCSC improved damping of one of the interarea modes while operating with a set of controller parameters, which were not the “best”. The “best” set of controller parameters are now determined for the TCSC PI controller through root loci and step response studies as indicated in Sec. 6.1. The TCSC is providing a nominal compensation of 50%. The SVC is not connected in the system.

### 6.2.1 Base Case Loading Condition

From the results of Chapter 5, the 9-bus system without any FACTS device is found to be stable at base case loading condition. This case is indicated in Table 5.2, which is reproduced in the 1<sup>st</sup> column of Table 6.1 for ease of reference. The eigenvalues show that there are two interarea modes - interarea mode 'a'(12.74 rad/s) and interarea mode 'b'(8.36 rad/s).

Fig. 6.1 shows root loci and damping of interarea modes as well as the TCSC controller modes with varying  $K_I$  ( $K_P = 0$ ) at base case loading condition. Fig. 6.1 (a) shows the modal damping of the controller and interarea modes while Fig. 6.1 (b) illustrates the root loci of controller modes and interarea modes. Three different pairs of graphs are presented in Fig. 6.1, one for each sensitive mode. The first pair corresponds to the controller mode and other two pairs of graphs correspond to the interarea modes. Unless otherwise stated all the root loci cum modal damping plots reported in this chapter also follow the same pattern. The graph illustrating the modal damping of FACTS controller modes actually indicate the minimum damping of the controller modes. Since in this case there is only one pair of complex conjugate mode, the minimum damping is basically equal to damping of either of the two complex conjugate modes. The range of  $K_I$  is varied from -1 to 100 (point 1 to 15, correspondingly). Roots for each individual point corresponding to a  $K_I$  is shown in Fig. 6.1 (b), while the modal damping corresponding to this  $K_I$  point is depicted in Fig. 6.1 (a). For instance  $K_I = 5$  corresponds to point 3 and its modal damping is +1 for the controller mode in Fig. 6.1 (a). It can be observed from Fig. 6.1 (a) that for  $K_I = 12.4$  (point 6), all the sensitive modes have high degree of damping. Therefore  $K_I = 12.4$  is chosen as the “desirable” value with  $K_P = 0$ . Now with this value of  $K_I$ ,  $K_P$  is varied over a wide range. The corresponding root loci of controller and interarea mode as well as the modal damping is shown in Fig. 6.2. Three pairs of figures are once again presented one for each relevant mode. It is evident from Fig. 6.2 that for  $K_P = -0.6$  ( $K_I = 12.4$ ), the overall damping of controller and interarea modes is maximum. Therefore the “desirable” values of  $K_P$  and  $K_I$  are selected as -0.6 and 12.4 respectively at base case loading.

**Table 6.1** Eigenvalues with no FACTS device connected at different loading conditions for the 9-bus system

Base case loading condition	Damping	Mid-loading Condition	Damping	Maximum loading condition	Damping	Remarks
				-90.9053	1.0000	
		-9.6793 ± 7.1148i	0.8057	-45.3014	1.0000	
<b>-0.7198 ± 12.7456i</b>	<b>0.0564</b>	<b>-0.7819 ± 12.5219i</b>	<b>0.0623</b>	<b>-2.8938 ± 12.3353i</b>	<b>0.2284</b>	Interarea mode 'a'
<b>-0.1906 ± 8.3660i</b>	<b>0.0228</b>	<b>-0.2150 ± 8.0167i</b>	<b>0.0268</b>	<b>0.0229 ± 0.2268i</b>	<b>-0.1005</b>	Interarea mode 'b'
-5.6867 ± 7.9663i	0.5810	-6.8870 ± 7.9402i	0.6552	-10.8806 ± 5.8904i	0.8794	
-5.3644 ± 7.9311i	0.5603	-5.2730 ± 7.7979i	0.5602	-1.2151 ± 8.8486i	0.1360	
-5.2287 ± 7.8263i	0.5555	-5.0537	1.0000	-6.3982 ± 7.4235i	0.6529	
-5.1779	1.0000	-3.2133	1.0000	-7.1865	1.0000	
-3.3993	1.0000	-0.3734 ± 1.5162i	0.2391	-5.1023	1.0000	
-0.4513 ± 1.1997i	0.3521	-0.5761 ± 0.6691i	0.6525	-2.1747	1.0000	
-0.4481 ± 0.7291i	0.5237	-0.7434 ± 0.3232i	0.9171	-1.6763	1.0000	
0.0000 ± 0.0000i	0.0000	-0.0000 ± 0.0000i	0.0000	-0.7284 ± 0.3533i	0.8997	
-3.2258	1.0000	-3.2258	1.0000	-0.0000 ± 0.0000i	0.0000	
<b>-0.4366 ± 0.4868i</b>				-3.2258	1.0000	

Validation and refinement of the controller parameters obtained through root loci technique is done through step response studies. In practice, line current or line power is usually taken to examine the system performance. In the present context it is not possible to express power/current over a line in a straightforward manner because network is modeled by algebraic equations only. Therefore the step response is shown for  $\Delta E'_d$  (small perturbation in voltage proportional to damper winding flux linkage) of machine connected at bus 2 with the input signal being  $\Delta V_{ref}$  (small perturbation in terminal voltage reference setting) of machine 2, both of which are state variables in the system model. It is expected that the system response with  $\Delta E'_d$  and  $\Delta V_{ref}$  will be indicative of the step response of line power/current signals. Fig. 6.3 shows step response of the system with the “best” controller parameters and two other set of arbitrary controller parameters. To clearly distinguish the three similar looking responses a zoomed version of these plots is presented in Fig. 6.3 (b). It is clear from Figs 6.3 (a) and (b) that parameters obtained as above from the root loci technique indeed give the “best” performance.

It is important to mention that the same signals  $\Delta E'_d$  and  $\Delta V_{ref}$  have been used in step response studies in all subsequent studies.

### 6.2.2 100% Loading Condition (Mid-loading condition)

In this case, loading of all the buses is increased by 100% over the base case loading. The generation is also increased according to the respective machine inertias. Again, the root loci of controller and interarea modes are plotted for different values of  $K_P$  and  $K_I$ . Fig. 6.4 shows the modal damping and root loci of different modes with varying  $K_I$ , keeping  $K_P = 0$ .

It is seen that for  $K_I = 12.1$ , the TCSC controller and the interarea modes have simultaneous high degree of damping. Therefore for  $K_P = 0$ ,  $K_I = 12.1$  is chosen as the “best” value. With this value of  $K_I$ , parameter  $K_P$  is varied. In this case, root loci for different modes are shown in Fig. 6.5. It can be observed that for  $K_P = -0.8$ , all the

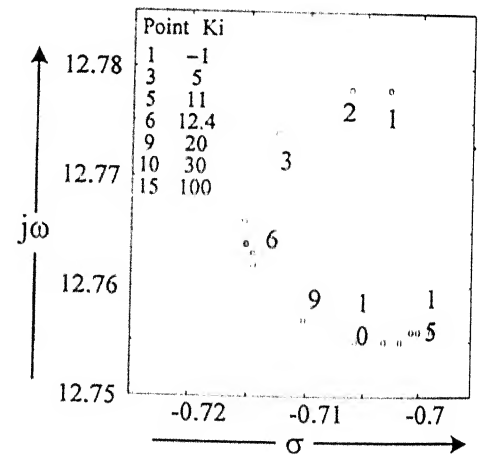
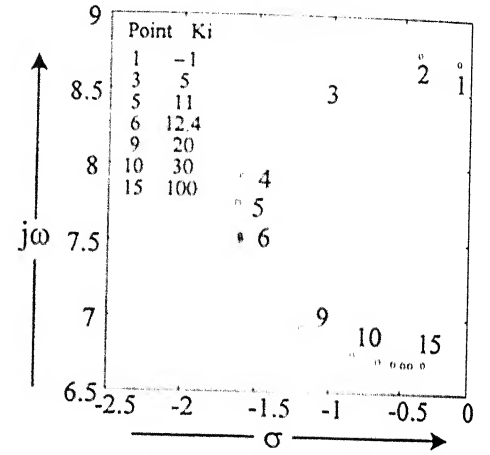
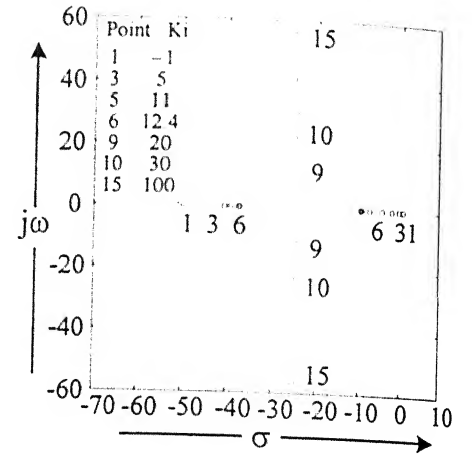
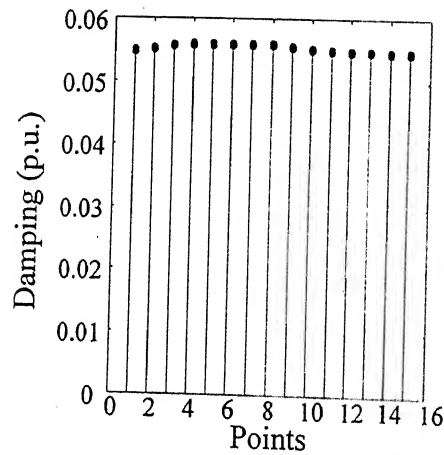
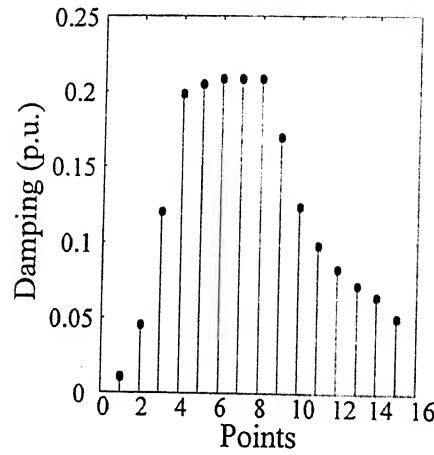
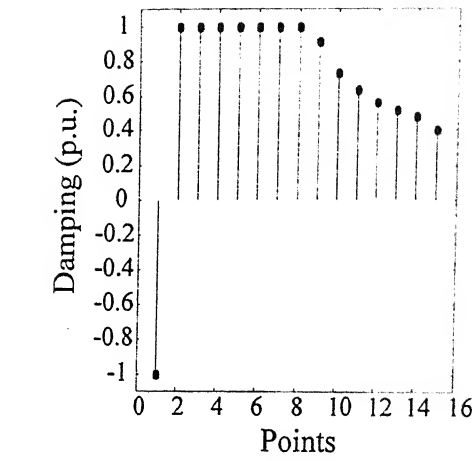
sensitive modes exhibit simultaneous high damping. Therefore,  $K_P = -0.8$  and  $K_I = 12.1$  are taken as the “desirable” values of TCSC controller for mid-loading condition. Further refinement of the controller parameters obtained from root loci studies is done through step response analysis. Fig. 6.6 shows the step response of 9-bus system for the “best” controller parameters and two other arbitrary sets of controller parameters at mid-loading condition. It is evident from step response also that the parameters selected above are indeed the “best” controller parameters for TCSC controller for mid-loading condition.

### 6.2.3 Maximum Loading Condition

In this case, with TCSC connected in the system, the loads are increased up to the point beyond which load flow does not converge. At this loading condition again, the root loci of controller and interarea modes are plotted on the same lines as described earlier. Fig. 6.7 shows modal damping and root loci of the three sensitive modes with varying  $K_I$  with  $K_P = 0$ . In this case a simultaneous high degree of modal damping of all sensitive modes is observed for  $K_I = 12.1$ . With this  $K_I$ , the  $K_P$  is varied over a wide range. Fig. 6.8 shows root loci and modal damping with varying  $K_P$ , keeping  $K_I = 12.1$  constant. The “desirable” value of  $K_P$  is found at  $-1.0$ . Thus, a high degree of damping for the sensitive modes is achieved simultaneously when  $K_P$  and  $K_I$  are  $-1.0$  and  $12.1$  respectively. The root loci results are subsequently validated by step response. In Fig. 6.9, step response for “best” controller parameters from root loci technique and two other arbitrary set of TCSC parameters is shown. It is seen that step response with selected values of TCSC controller parameters from root loci technique are indeed the “best”.

Table 6.2 shows system eigenvalues with “best” TCSC controller parameters obtained at different loading conditions (base, mid and the maximum) for the 9-bus system. Following observations can be made.

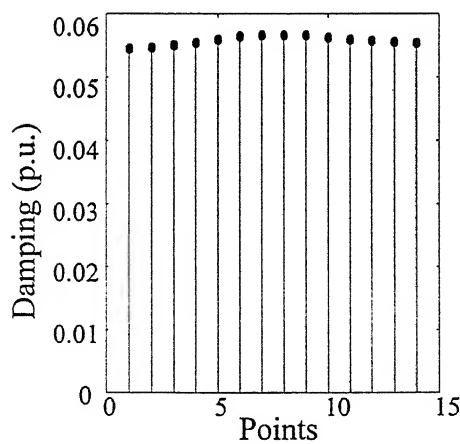
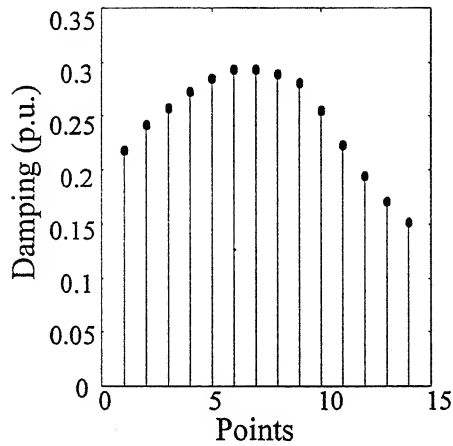
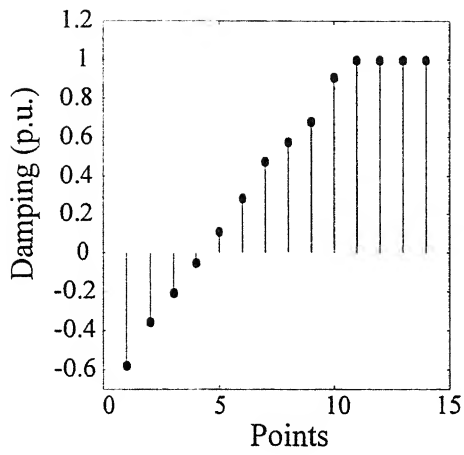
- The TCSC dramatically improves the damping of interarea mode ‘b’ from 2.3% to 29.2%. The imparted damping increases with the loading except in case of maximum loading condition in which case the damping drops to 25%.



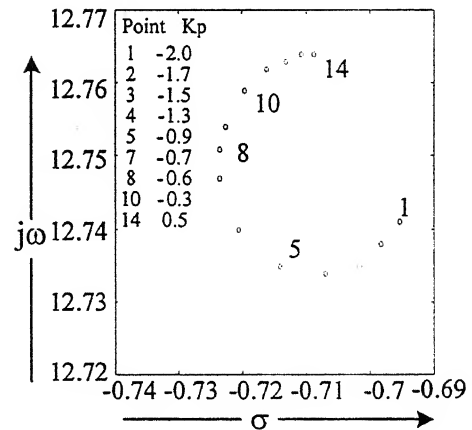
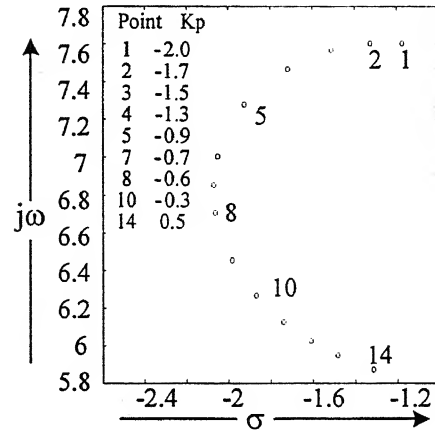
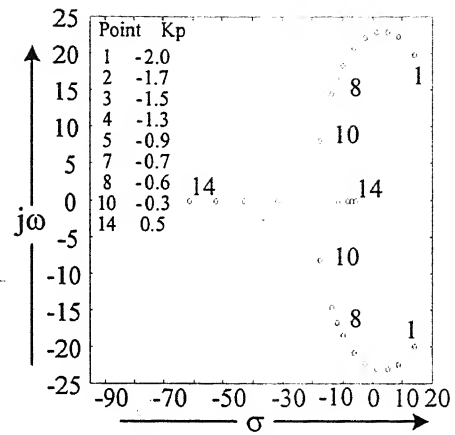
(a) Modal Damping

(b) Root loci

**Fig. 6.1** Root loci of controller and interarea modes and their corresponding modal damping for varying TCSC  $K_I$  ( $K_P = 0$ ) for base case of the 9-bus system with TCSC alone



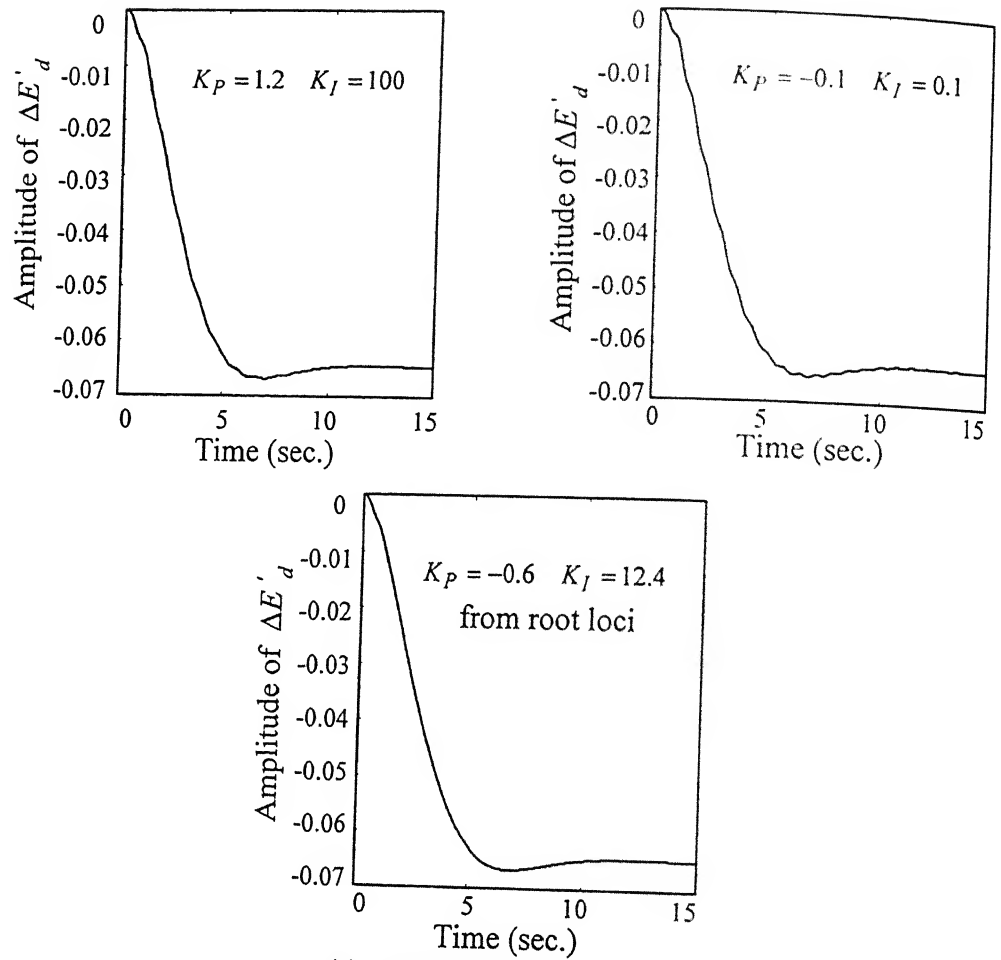
(a) Modal Damping



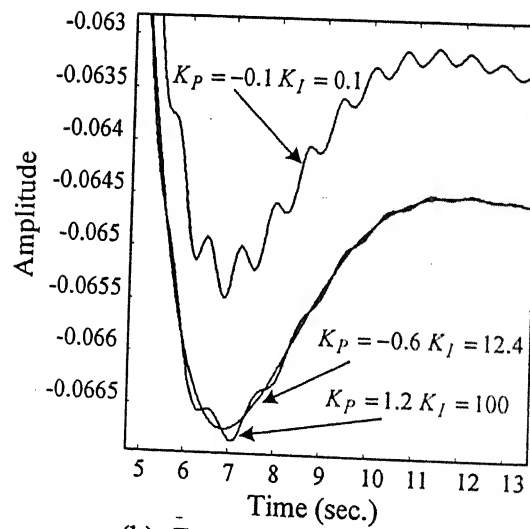
(b) Root loci

**Fig. 6.2** Root loci of controller and interarea modes and their corresponding modal damping for varying TCSC  $K_P$  ( $K_I = 12.4$ ) for base case of the 9-bus system with TCSC alone



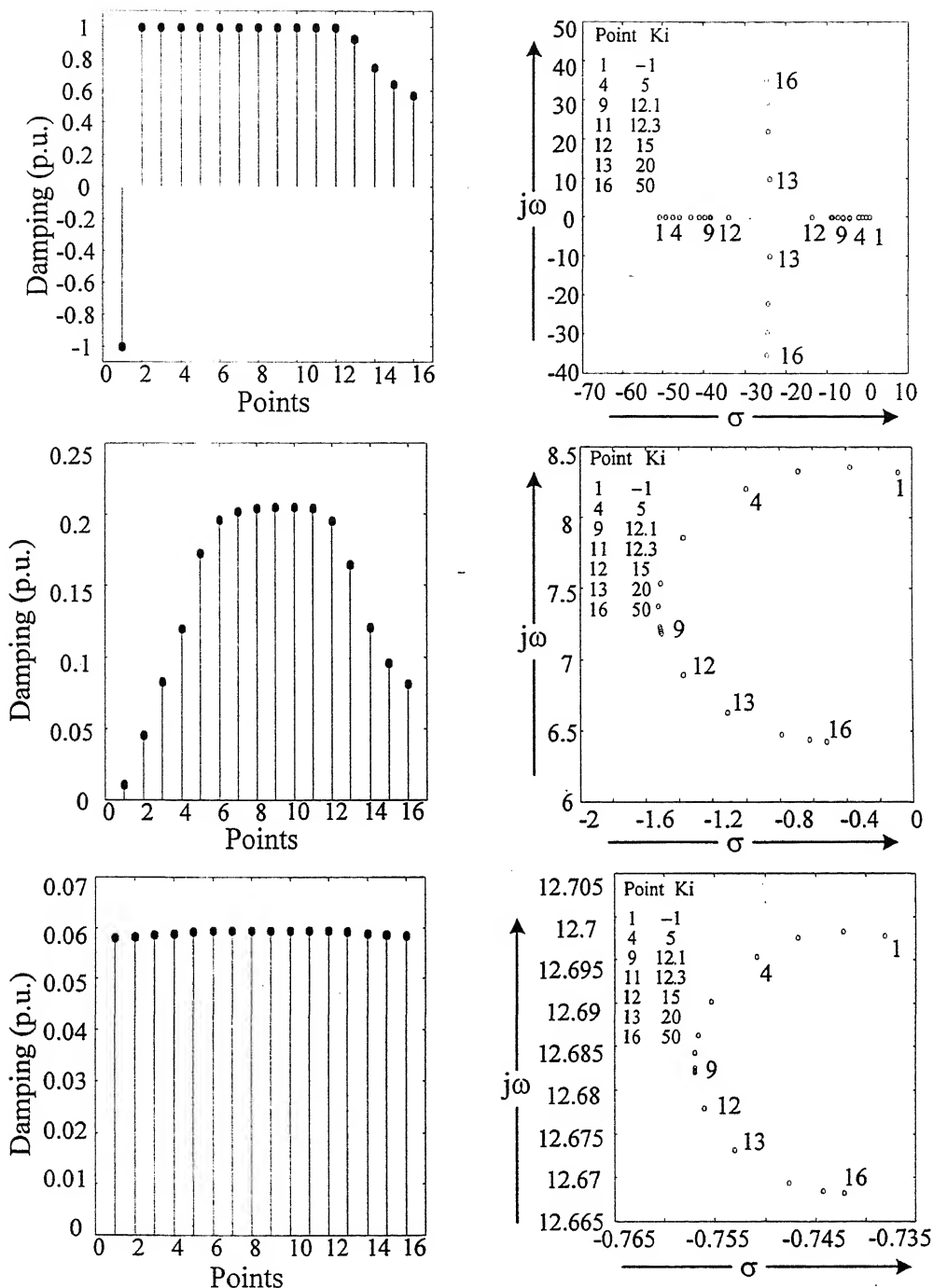


(a) Actual step response



(b) Zoomed response of (a)

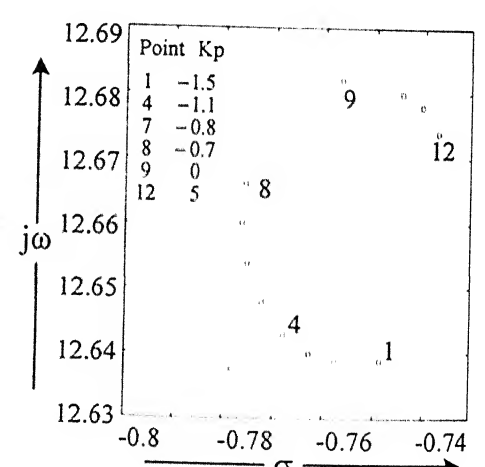
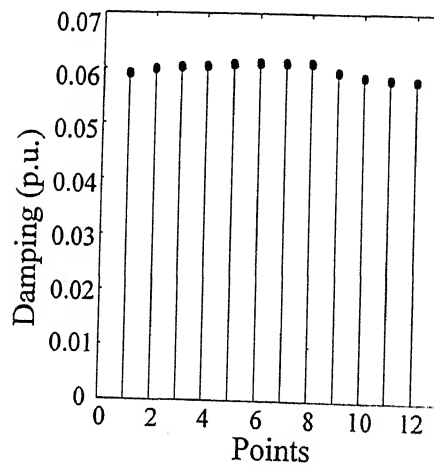
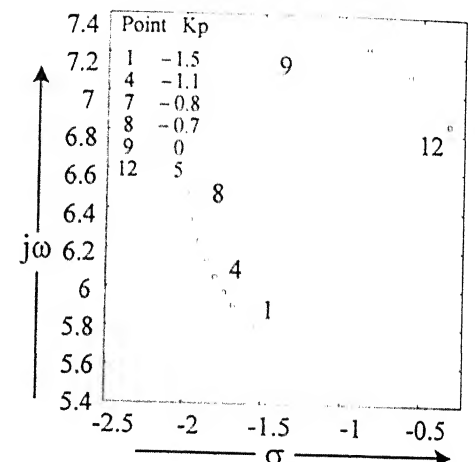
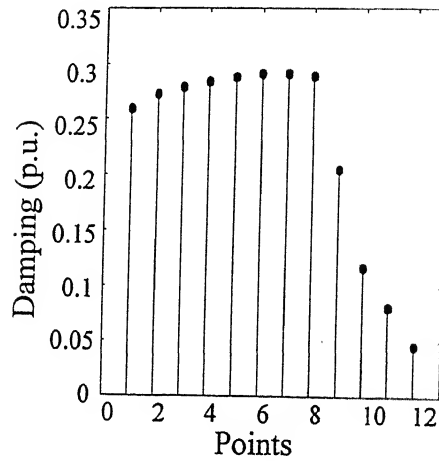
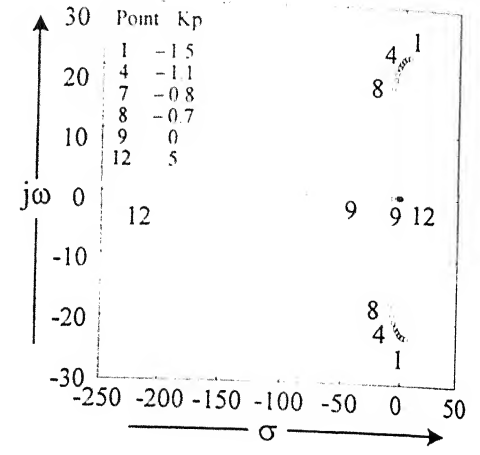
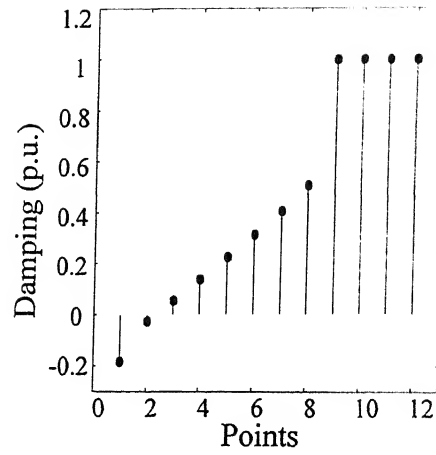
**Fig. 6.3** Step response with “best” controller parameters and two arbitrary set of controller parameters for base case of the 9-bus system (TCSC alone)



(a) Modal Damping

(b) Root loci

**Fig. 6.4** Root loci of controller and interarea modes and their corresponding modal damping for varying TCSC  $K_I$  ( $K_P = 0$ ) for mid-loading case of the 9-bus system with TCSC alone



(a) Modal Damping

(b) Root loci of interarea modes

**Fig. 6.5** Root loci of sensitive modes and their corresponding modal damping for varying TCSC  $K_I$  ( $K_P = 12.1$ ) for mid-loading case of the 9-bus system with TCSC alone

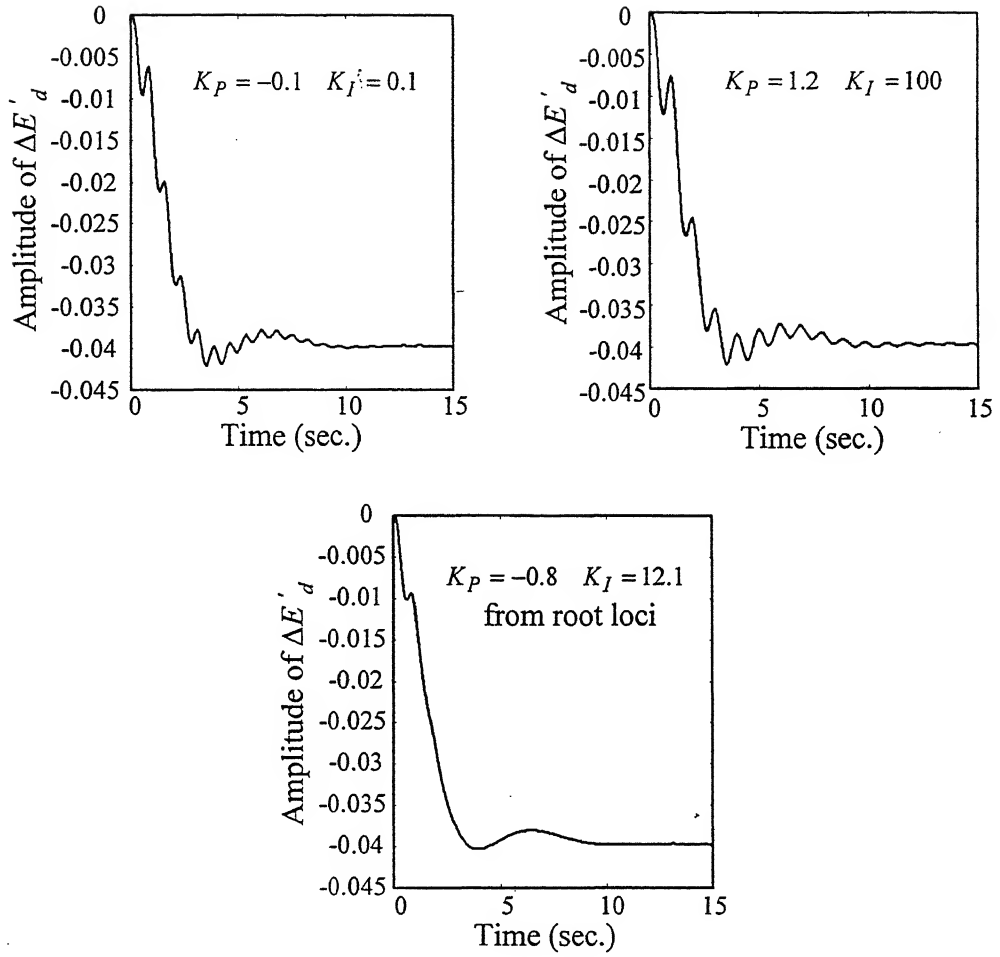


**Fig. 6.6** Step response with “best” controller parameters and two other arbitrary set of controller parameters for mid-loading case of the 9-bus system (TCSC alone)

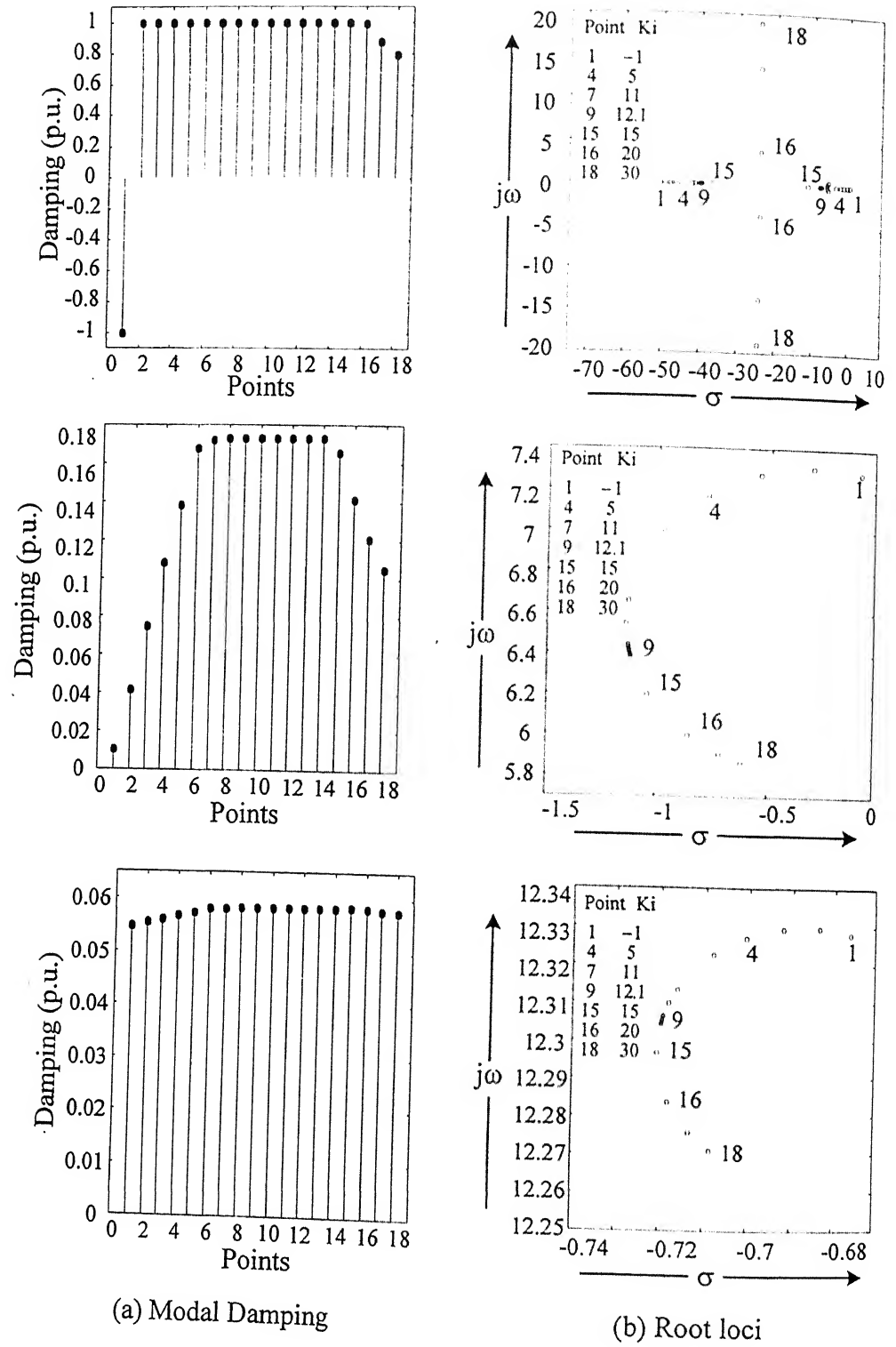


**Fig. 6.7** Root loci of controller and interarea modes and their corresponding modal damping for varying TCSC  $K_I$  ( $K_P = 0$ ) for maximum loading case of the 9-bus system with TCSC alone

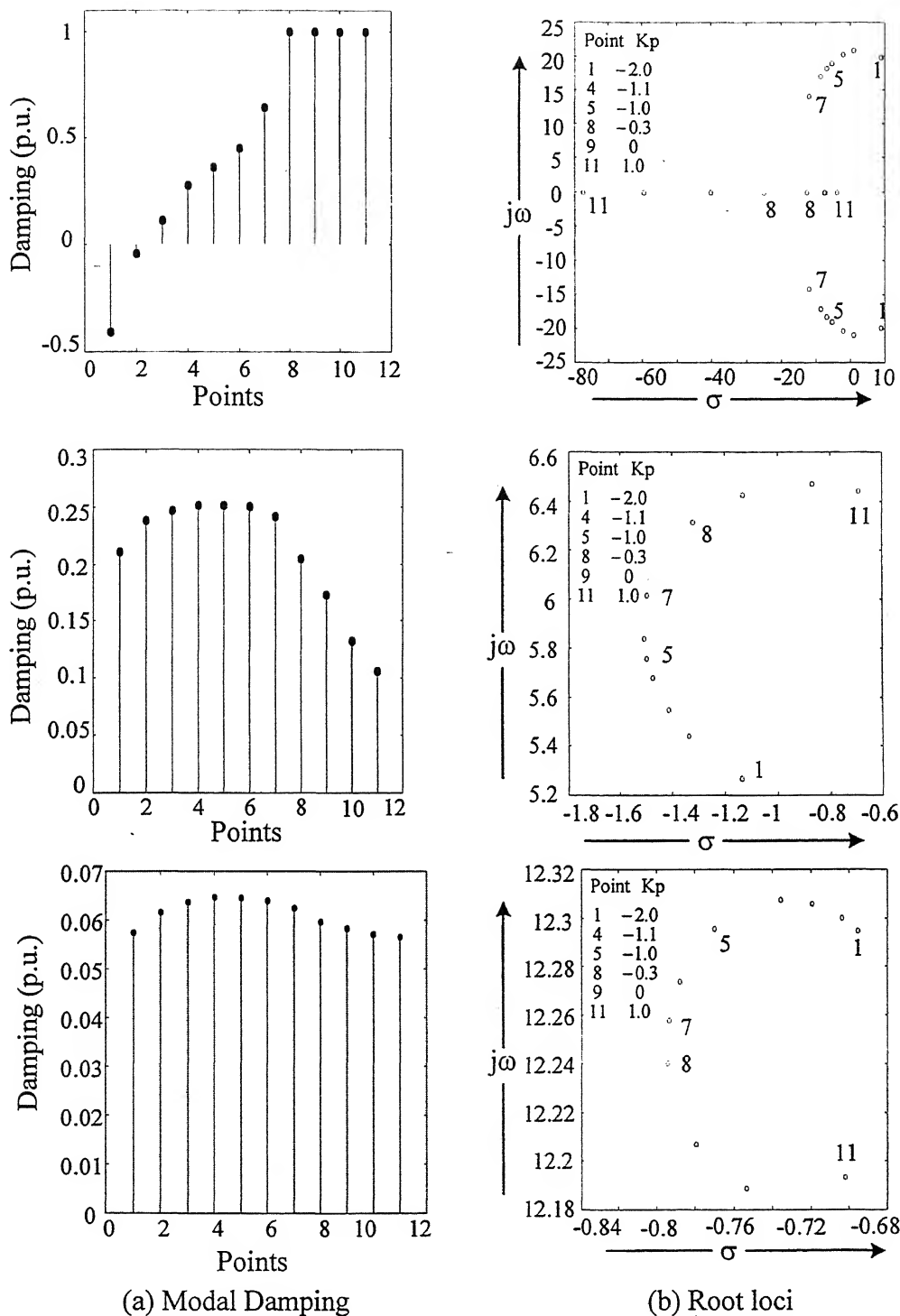


**Fig. 6.8** Root loci of controller and interarea modes and their corresponding modal damping for varying TCSC  $K_I$  ( $K_P = 12.1$ ) for maximum loading case of the 9-bus system with TCSC alone

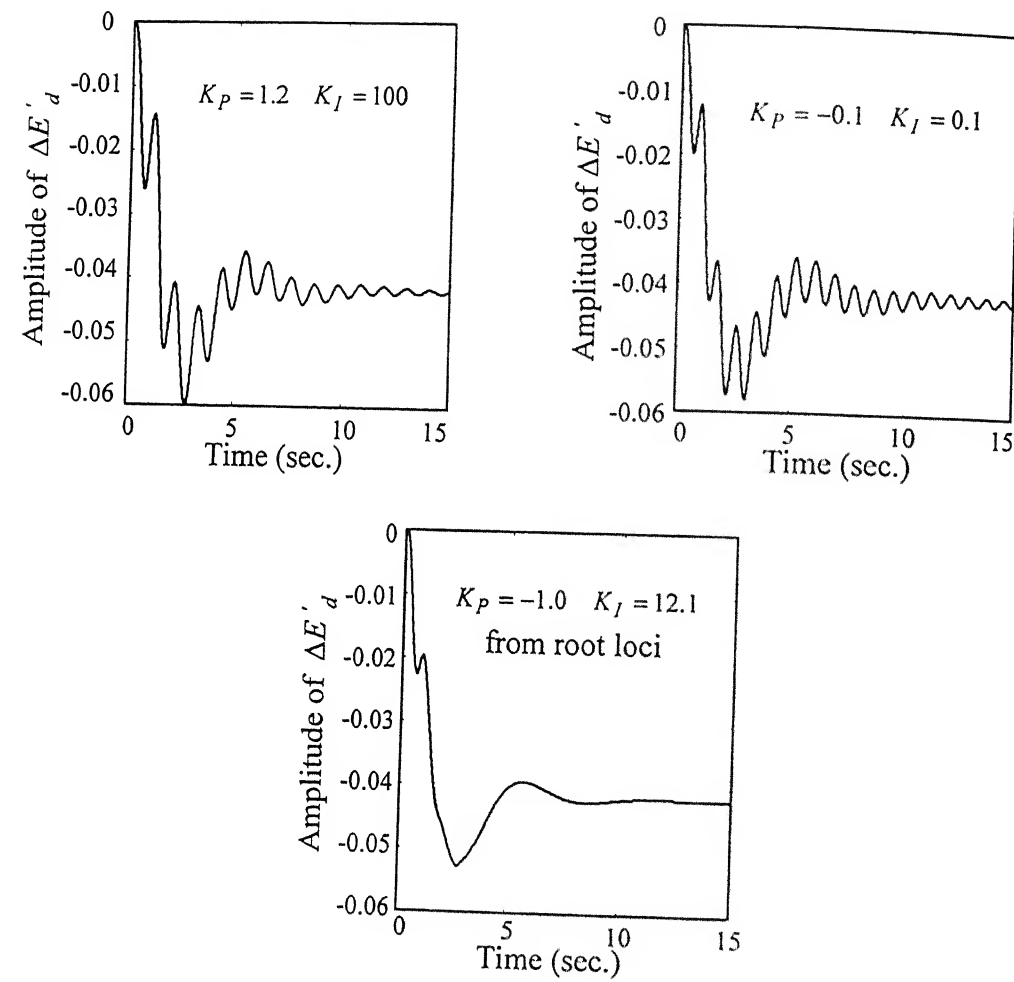


Fig. 6.9 Step response with “best” controller parameters and two other arbitrary set of controller parameters for maximum loading case of the 9-bus system (TCSC alone)

Table 6.2 System Eigenvalues with “best” TCSC controller parameters at different loading conditions

Base case loading Condition	Base case loading Condition With TCSC	Mid loading condition With TCSC	Maximum loading Condition With TCSC	Remarks
No FACTS device	$K_P = -0.6$ $K_I = 12.4$	$K_P = -0.8$ $K_I = 12.1$	$K_P = -1.0$ $K_I = 12.1$	
			-43.5417	
	-11.8088 ± 16.6991i	-8.4287 ± 18.7680i	-7.1032 ± 18.1840i	
-0.7198 ± 12.7456i (Damping=0.0564)	-0.7236 ± 12.7510i (Damping=0.0567)	-0.7764 ± 12.6601i (Damping=0.0612)	-0.7937 ± 12.2582i (Damping=0.0646)	Interarea mode 'a'
-0.1906 ± 8.3660 (Damping=0.0228)	-2.0723 ± 6.8541i (Damping=0.2894)	-1.9385 ± 6.3503i (Damping=0.2920)	-1.4972 ± 5.7564i (Damping=0.2517)	Interarea mode 'b'
-5.6867 ± 7.9663i	-5.7117 ± 8.0325i	-9.6713 ± 7.2732i	-10.2947 ± 6.8554i	
-5.3644 ± 7.9311i	-5.2386 ± 7.8683i	-6.8632 ± 8.0121i	-5.4260 ± 7.8333i	
-5.2287 ± 7.8263i	-5.3754 ± 7.9570i	-5.3091 ± 7.8662i	-7.3933	
-5.1779	-6.1023	-5.9747	-5.8324	
-3.3993	-4.8120	-4.6235	-4.7561	
-0.4513 ± 1.1997i	-0.4490 ± 0.8849i	-0.4638 ± 0.9475i	-1.9586	
-0.4481 ± 0.7291i	-0.4238 ± 0.5051i	-0.6575 ± 0.5263i	-0.4941 ± 1.0960i	
-0.4366 ± 0.4868i	-0.4407 ± 0.3091i	-1.0913	-0.8765 ± 0.2414i	
-0.0000 ± 0.0000i	-0.0000 ± 0.0000i	-0.5286	-0.5057	
-3.2258	-3.2258	-0.0000 ± 0.0000i	-0.0000 ± 0.0000i	
		-3.2258	-3.2258	

- With increased loading the frequency of interarea mode 'b' decreases implying a decline in synchronizing torque.
- The TCSC marginally enhances the damping of interarea mode 'a' from 5.6% to 6.4%.
- The "best" controller parameters do not undergo any significant change with the change in loading condition. This is when the TCSC is providing 50% nominal line compensation.

### 6.3 DETERMINATION OF "BEST" SVC CONTROLLER (WITHOUT TCSC)

#### 6.3.1 Base Case Loading Condition

The procedure for obtaining "best" SVC controller parameters is the same as that for TCSC controller. At base case loading with SVC connected at bus 5 alone in the system, the root loci of sensitive modes and corresponding modal damping are obtained. Fig. 6.10 shows the root loci and the modal damping of SVC controller and interarea modes with varying  $K_I$  and  $K_P = 0$ . While Fig. 6.11 shows root loci and modal damping with varying  $K_P$  ( $K_I = 5.9$ ). The modal damping of interarea mode 'a' (12.75rad/s) is not much affected and is therefore not shown in Figs. (6.10-6.11). It is to be noted that SVC has three controller modes. The modal damping shown in Fig. 6.10 (a) for SVC controller modes represents infact the overall minimum damping of these three SVC modes. From Figs. 6.10 and 6.11 it is evident that the desirable values for SVC controller parameters are  $K_P = 1$ ,  $K_I = 5.9$  for which all the sensitive modes have a high degree of damping simultaneously. Further refinement of these controller parameters has been done through the step response studies. Fig. 6.12 shows the step response of  $\Delta E'_d$  of machine 2 corresponding to a step input in  $\Delta V_{ref}$  of machine 2. The desirable SVC controller parameters obtained from root loci i.e.  $K_P = 1$ ,  $K_I = 5.9$  are refined to give the "best" parameters as  $K_P = 1$  and  $K_I = 20$  for which a reduced overshoot is witnessed.



### 6.3.2 Mid-Loading Condition

This mid-loading operating condition is the same as that used for the TCSC controller studies in Sec. 6.2.2. At this mid-loading condition the root loci and the modal damping of interarea modes and SVC controller modes are observed. Fig. 6.13 shows the root loci and the modal damping with varying  $K_I$  ( $K_P = 0$ ). It is for  $K_I = 20$ , the SVC controller modes and interarea modes simultaneously have a high degree of damping. With this  $K_I$ , the parameter  $K_P$  is varied. The root loci and modal damping of the SVC controller and interarea modes are shown in Fig. 6.14. It is noticed that for  $K_I = 20$  and  $K_P = 0.1$ , all the sensitive modes have a high degree of damping. The refinement of the above “desirable” SVC controller parameters  $K_I = 20$ ,  $K_P = 0.1$  is done through step response studies. It is found that indeed the “desirable” controller parameters obtained with root loci and modal damping give the “best” performance. The step response with the “best” SVC controller parameters along with two other arbitrary set of controller parameters are shown in Fig. 6.15.

### 6.3.3 Maximum Loading Condition

The maximum loading condition is the same as that used for TCSC in Sec. 6.2.3. At this maximum loading condition the root loci and modal damping of the SVC controller modes and interarea modes are observed on the same lines as done earlier. Fig. 6.16 shows the root loci and modal damping of the SVC controller modes and interarea modes with varying  $K_I$  ( $K_P = 0$ ). It is depicted in Fig. 6.16. It can be seen from this figure that for  $K_I = 60$ , all the sensitive modes have a high degree of damping. With this  $K_I$ , the parameter  $K_P$  is varied over a wide range and the root loci and the corresponding modal damping are plotted in Fig. 6.17. It can be observed from Fig. 6.17 that the overall damping of the sensitive modes is the highest for  $K_I = 60$  and  $K_P = 2$ . Further refinement of the “desirable” SVC controller parameters is done using step response of the system. As evident from Fig. 6.18, there are some oscillations present in all step responses for chosen and other controller parameters. These oscillations die quite

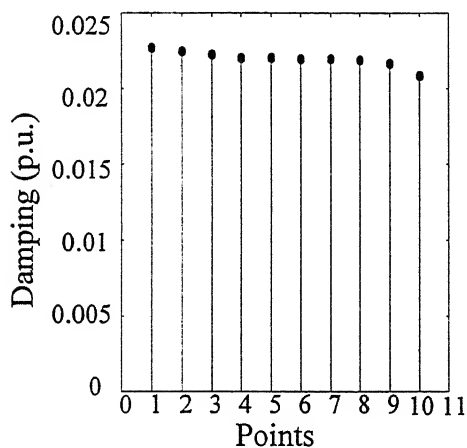
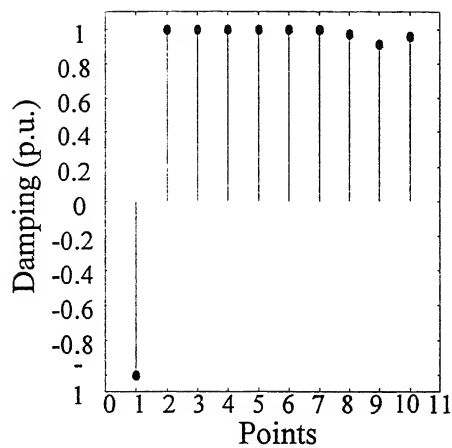
quickly. Since the controller gains should not be too high,  $K_P = 2$  and  $K_I = 60$  are taken to be the “best” parameters for SVC at maximum loading condition.

The “best” SVC controller parameters and the corresponding eigenvalues are shown in Table 6.3 for different loading conditions.

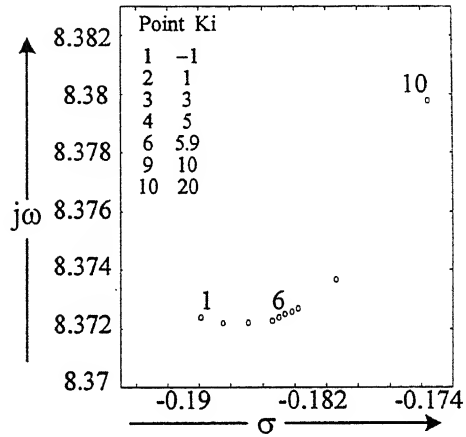
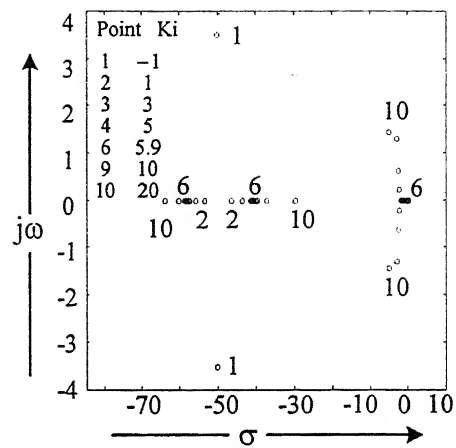
- The SVC does not improve the damping of both interarea modes ‘a’ and ‘b’ with the increase in system loading from base case to maximum loading case. Infact it reduces the damping of interarea mode ‘a’ from 5.6% to 4.3% and that of interarea mode ‘b’ from 2.3% to 1.1%.
- The “best” SVC controller parameters vary significantly with the change in loading condition.

#### **6.4 DETERMINATION OF COORDINATED “BEST” SVC-TCSC PARAMETERS**

For the 9-bus system at base case loading condition, Extended Voltage Phasors Approach (EVPA) indicated the line 7-5 as the most probable location for placing a series device. The system voltage profile shows that voltages of all buses are within range (more than 0.9 per unit). At maximum loading condition, however, EVPA shows that there is a need for a shunt device at bus 5. It may be recalled that in Chapter 5, that although two devices were indicated by EVPA, only SVC was recommended for the 9-bus system from voltage stability and economic considerations. However to investigate the control of coordinated FACTS devices both devices are assumed to be installed in the system. As two devices are needed from base case to maximum loading condition, an attempt has been made to investigate the coordinated control of these two FACTS devices for these loading conditions. The SVC is connected at bus 5 and a TCSC that provides 50% compensation is connected between buses 7-5.

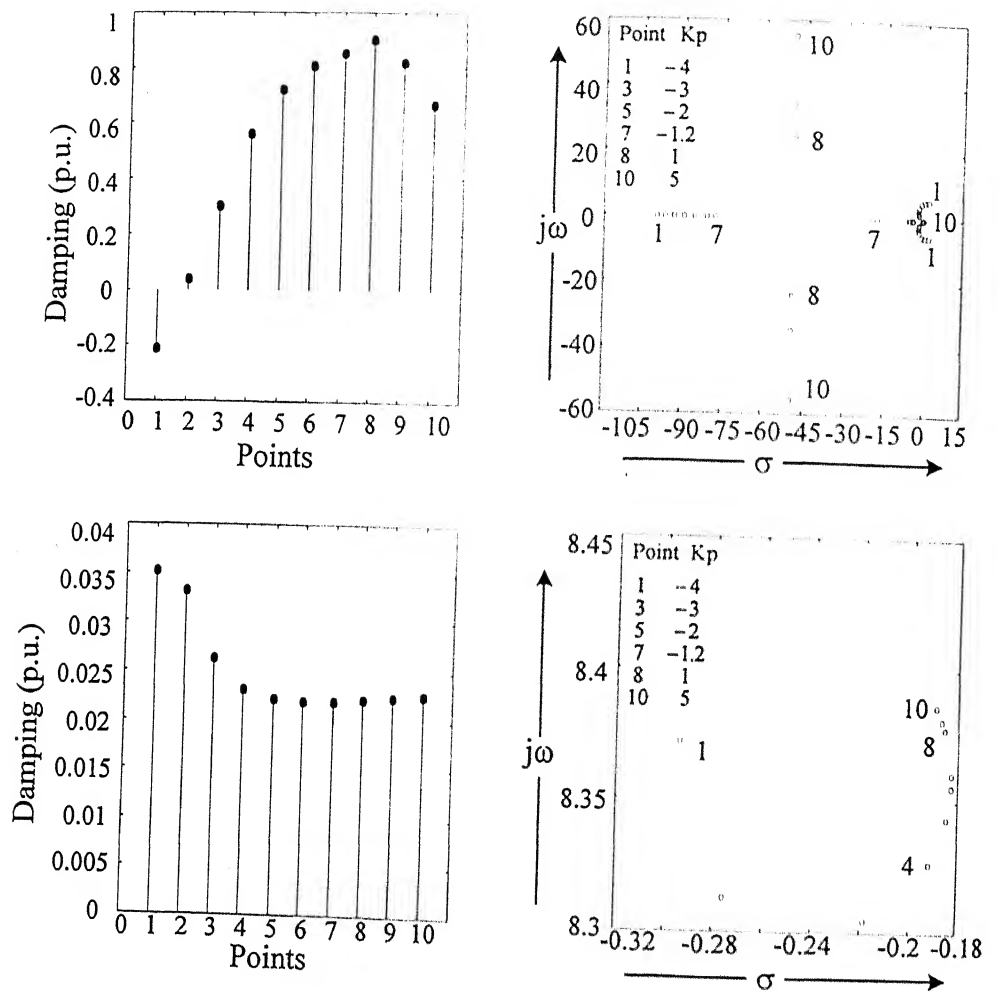


(a) Modal Damping



(b) Root loci

**Fig. 6.10** Root loci of interarea and controller modes and their corresponding modal damping for varying SVC  $K_I$  ( $K_P = 0$ ) for base case of the 9-bus system with SVC alone



(a) Modal Damping

(b) Root loci

**Fig. 6.11** Root loci of controller and interarea modes and their corresponding modal damping for varying SVC  $K_P$  ( $K_I = 5.9$ ) for base case of the 9-bus system with SVC alone

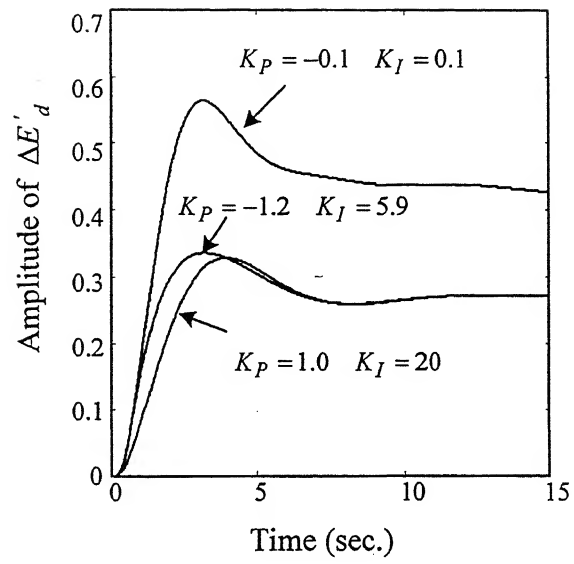
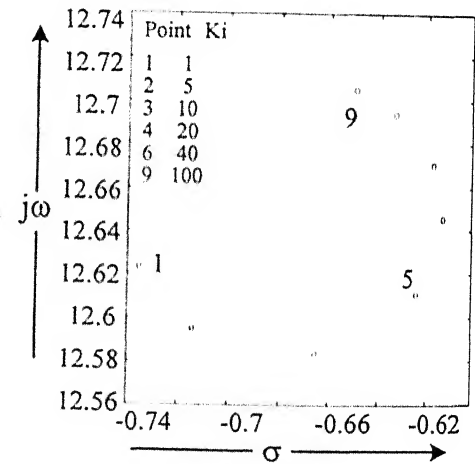
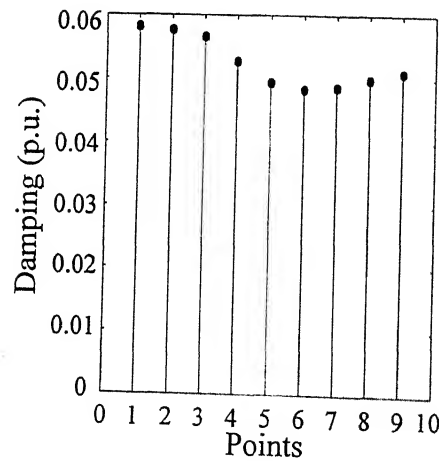
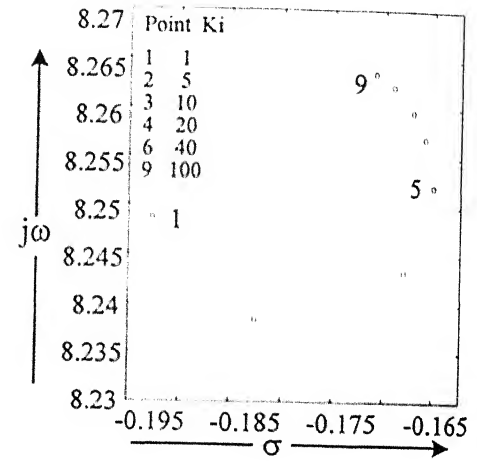
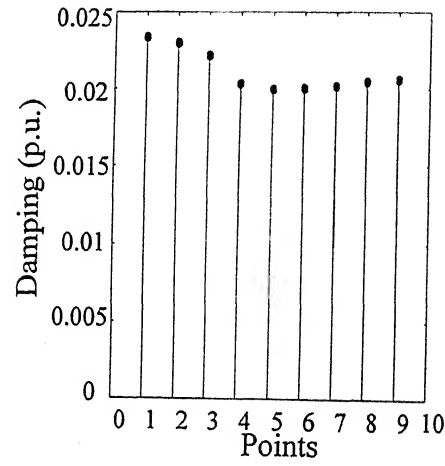
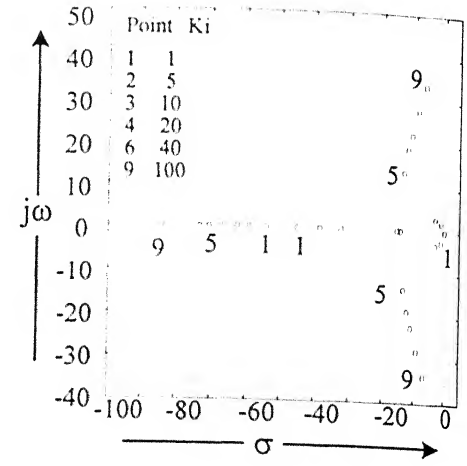
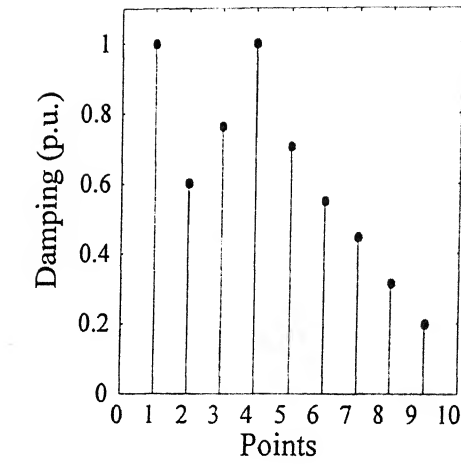


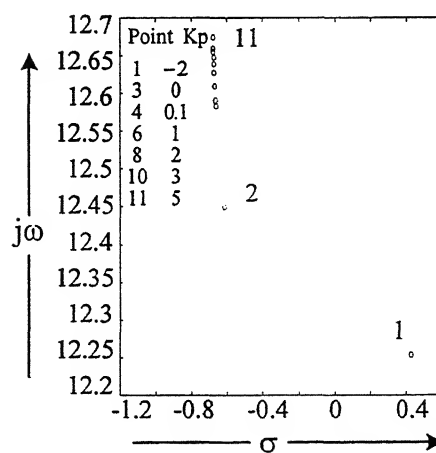
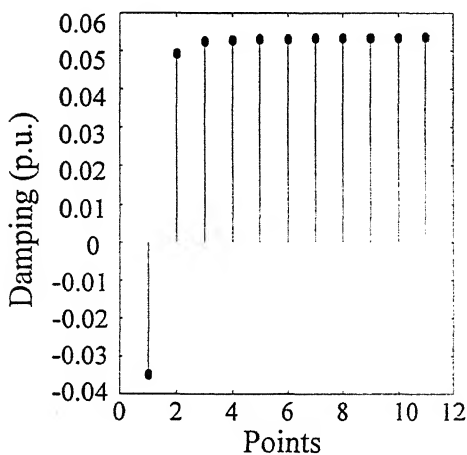
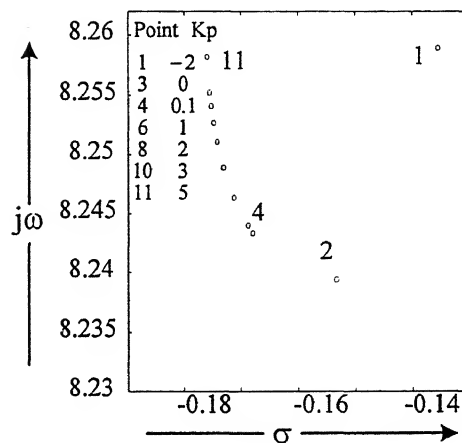
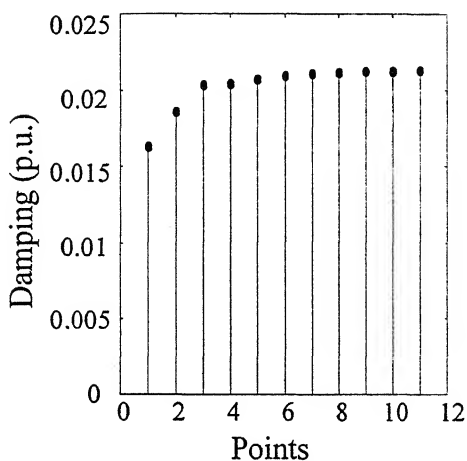
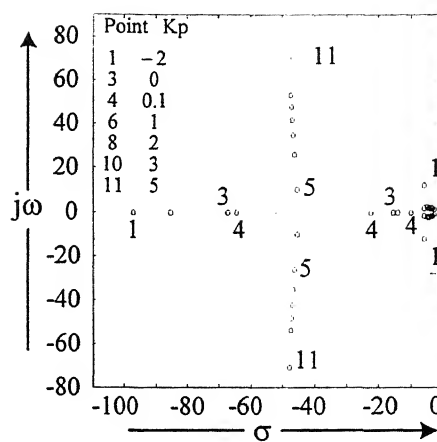
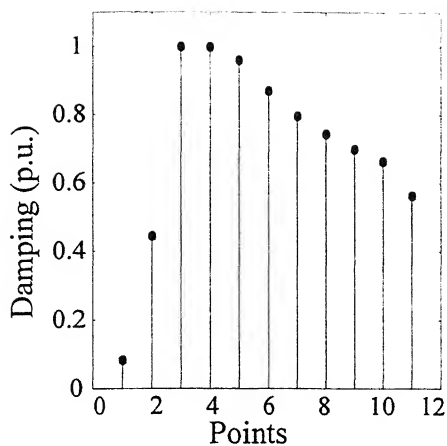
**Fig. 6.12** Step response with “best” and two other arbitrary set of controller parameters for base case of the 9-bus system (SVC alone)



(a) Modal Damping

(b) Root loci

**Fig. 6.13** Root loci of controller and interarea modes and their corresponding modal damping for varying SVC  $K_I$  ( $K_P = 0$ ) for mid-loading condition of the 9-bus system with SVC alone



(a) Modal Damping

(b) Root loci

**Fig. 6.14** Root loci of controller and interarea modes and their corresponding modal damping for varying SVC  $K_P$  ( $K_I = 20$ ) for mid-loading condition of the 9-bus system with SVC alone

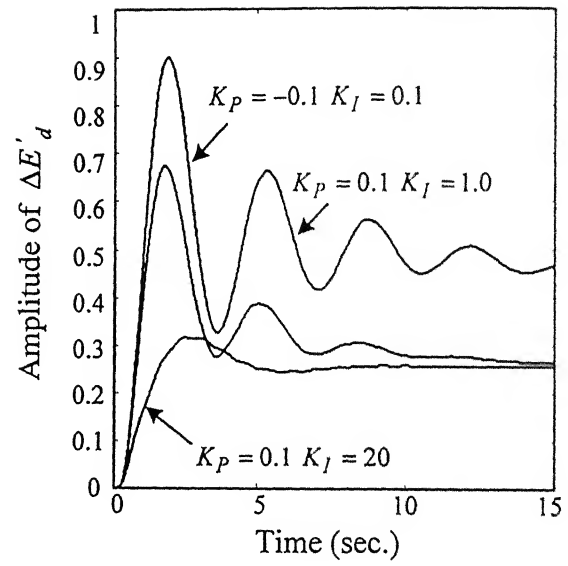


**Fig. 6.15** Step response for “best” controller parameters and two other arbitrary set of controller parameters for mid-loading condition of the 9-bus system (SVC alone)



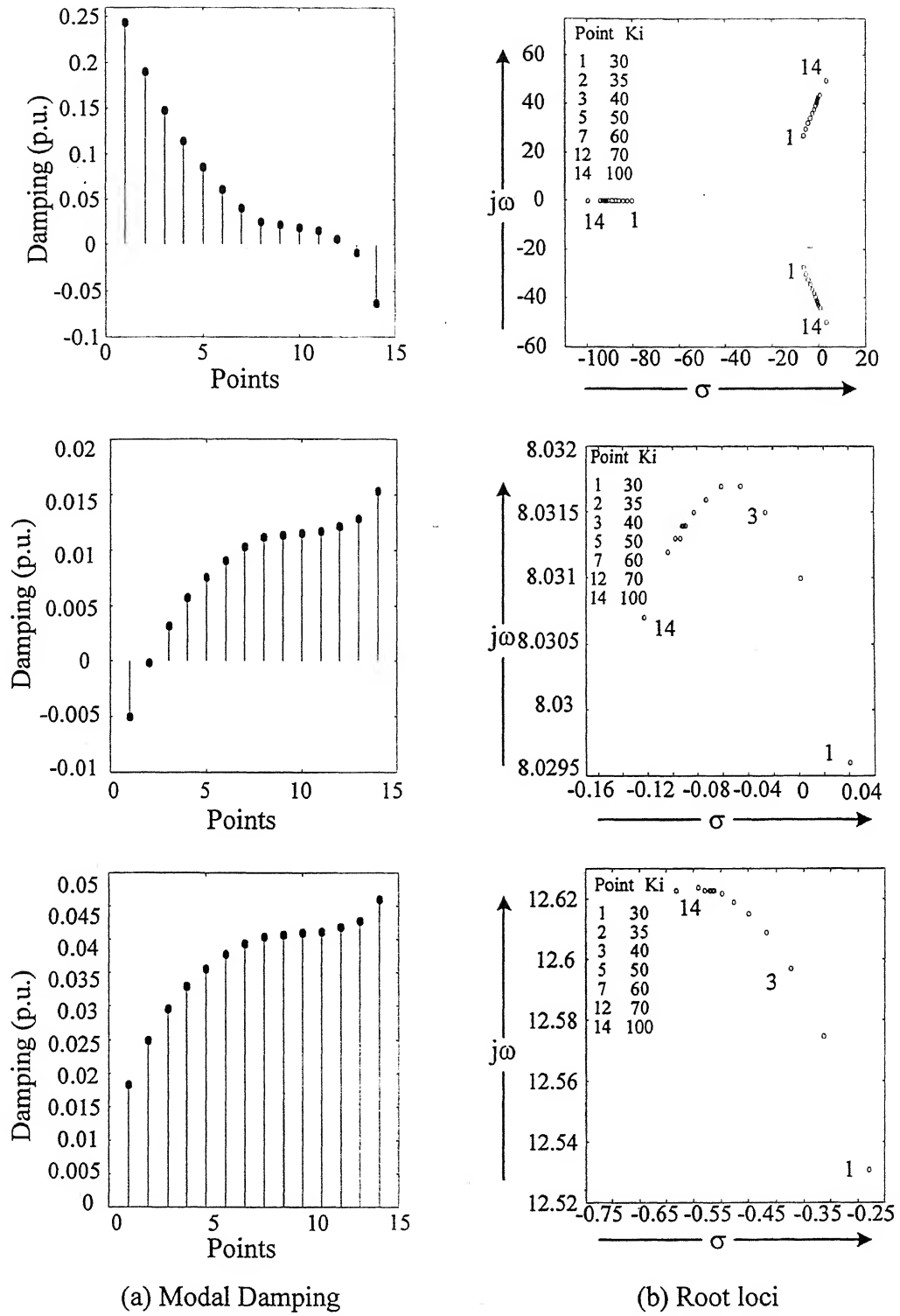


**Fig. 6.16** Root loci of controller and interarea modes and their corresponding modal damping for varying SVC  $K_I$  ( $K_P = 0$ ) for maximum loading condition of the 9-bus system with SVC alone

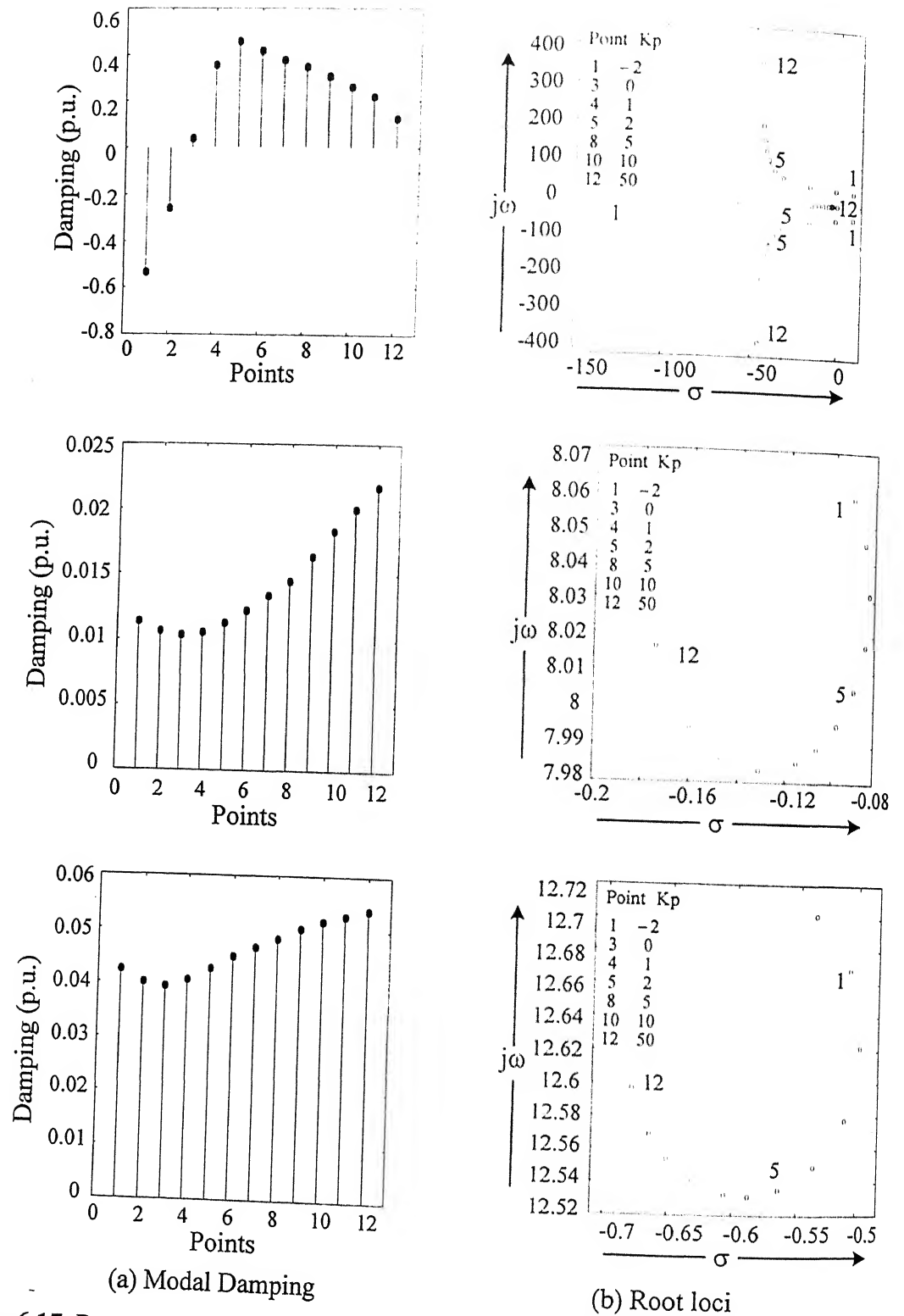


**Fig. 6.17** Root loci of controller and interarea modes and their corresponding modal damping for varying SVC  $K_P$  ( $K_I = 60$ ) for maximum loading condition of the 9-bus system with SVC alone

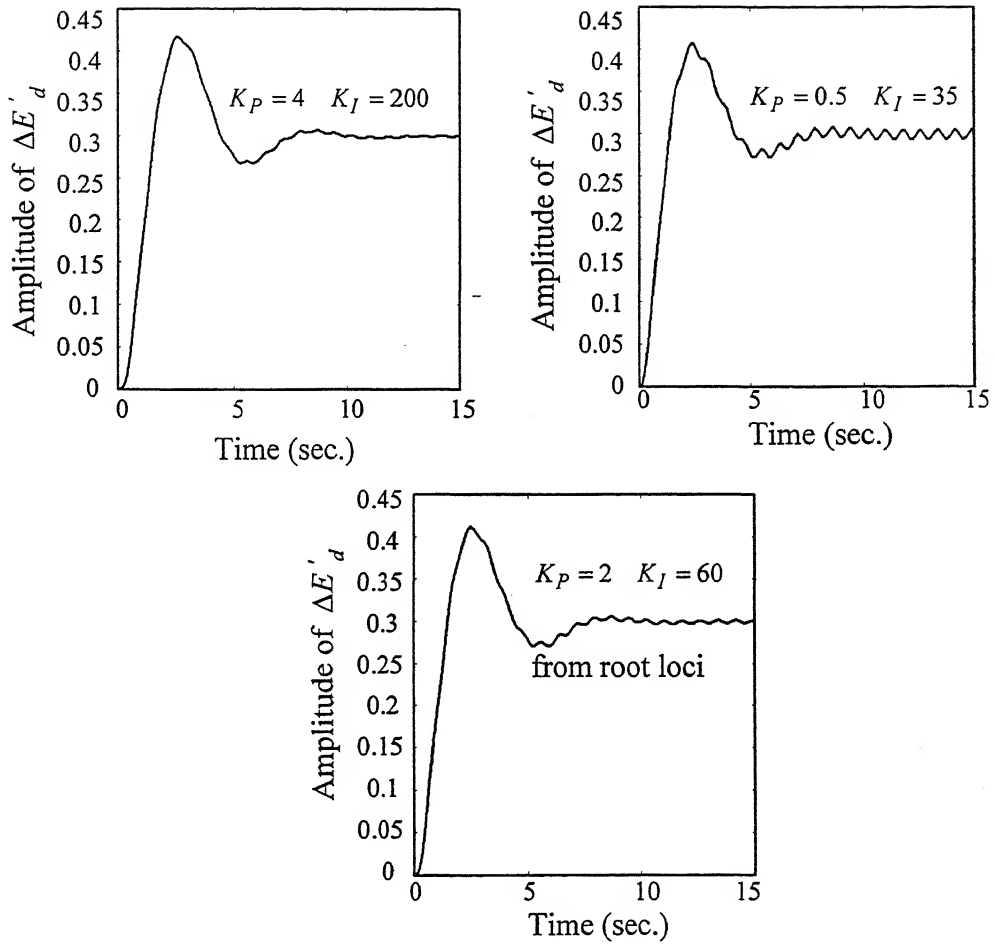


**Fig. 6.18** Step response with “best” controller parameters and two other arbitrary set of controller parameters for maximum loading condition of the 9-bus system (SVC alone)

**Table 6.3** System eigenvalues with “best” SVC controller parameters at different loading conditions

Base case loading Condition No FACTS device	Base case loading Condition With SVC	Mid loading condition With SVC	Maximum loading Condition With SVC	Remarks
	$K_P = 1.0$ $K_I = 20$	$K_P = 0.1$ $K_I = 20$	$K_P = 2$ $K_I = 60$	
	$-47.6435 \pm 20.0394i$	$-64.5326$	$-33.5211 \pm 64.9632i$	
	$-22.5505$	$-26.5848$		
$-0.7198 \pm 12.7456i$ (Damping=0.0564)	$-0.7128 \pm 12.7514i$ (Damping=0.0558)	$-0.6670 \pm 12.5907i$ (Damping=0.0529)	$-0.5370 \pm 12.5498i$ (Damping=0.0428)	Interarea mode ‘a’
$-0.1906 \pm 8.3660$ (Damping=0.0228)	$-0.1805 \pm 8.3823i$ (Damping=0.0215)	$-0.1688 \pm 8.2441i$ (Damping=0.0205)	$-0.0903 \pm 8.0053i$ (Damping=0.0113)	Interarea mode ‘b’
$-5.6867 \pm 7.9663i$	$-5.6693 \pm 7.9718i$	$-10.0551$	$-9.9438 \pm 7.0709i$	
$-5.3644 \pm 7.9311i$	$-5.3591 \pm 7.9331i$	$-7.4041 \pm 7.8915i$	$-5.2676 \pm 7.9311i$	
$-5.2287 \pm 7.8263i$	$-5.2036 \pm 7.8357i$	$-5.0459 \pm 7.8902i$	$-7.3708 \pm 7.9454i$	
$-5.1779$	$-4.0499 \pm 1.4091i$	$-6.0492 \pm 7.9755i$	$-5.3549$	
$-3.3993$	$-5.1568$	$-6.3011$	$-4.1520$	
$-0.4513 \pm 1.1997i$	$-0.5049 \pm 0.9495i$	$-4.9022$	$-0.5218 \pm 1.1066i$	
$-0.4481 \pm 0.7291i$	$-0.4526 \pm 0.7210i$	$-0.5725 \pm 1.0005i$	$-0.6193 \pm 0.6451i$	
$-0.4366 \pm 0.4868i$	$-0.4342 \pm 0.4847i$	$-0.5294 \pm 0.7222i$	$-0.7420 \pm 0.1899i$	
$-0.0000 \pm 0.0000i$	$-0.0000 \pm 0.0000i$	$-0.6021 \pm 0.4412i$	$-0.0000 \pm 0.0000i$	
$-3.2258$	$-3.2258$	$-0.0000 \pm 0.0000i$	$-3.2258$	
		$-3.2258$		

### 6.4.1 Different Loading Conditions

Four different loading conditions are considered. The base case, mid and maximum loading conditions are the same as described in Sec. 6.2.1-6.2.3. In these studies for each given loading condition, the “best” SVC controller parameters are kept as the same as obtained for that loading condition when considered alone. The “best” TCSC parameters are obtained on the same lines as explained earlier in Section 6.1 by the root loci, modal damping and step response studies. While this procedure has been done for each loading condition, the root loci, modal damping and step response results are shown only for maximum loading condition.

At the maximum loading condition, the root loci and the modal damping of sensitive modes are plotted as shown in Figs. 6.19 and 6.20. From these figures the “desirable” controller parameters are chosen as  $K_I = -0.8$  and  $K_P = 12.8$  for which the overall damping of the sensitive modes is high. Further refinement of these controller parameters is done through step response studies. It is seen that the “desirable” parameters emerge as the “best” parameters also. Step response with the “best” controller parameter and two other arbitrary sets of controller parameters are shown in Fig. 6.21.

A new “extreme” system loading condition is now defined when both SVC and TCSC are connected in the system. This loading condition is obtained when the loads and generations are increased to the point beyond which load flow does not converge. At this extreme loading condition, the TCSC controller parameters are once again obtained from modal damping and root loci studies. The SVC controller parameters are kept the same as that of maximum loading condition.

The “best” set of SVC-TCSC controller and the corresponding eigenvalues at different loading conditions of the 9-bus system are compiled in Table 6.4. Following observations are made.

- The SVC-TCSC combination dramatically improves the damping of interarea mode ‘b’ from 2.3% to 31.3%. The imparted damping increases with the loading except in case of extreme loading condition in which case the damping drops to 29.5%.

- With increased loading the frequency of interarea mode 'b' decreases implying a decline in synchronizing torque.
- The SVC-TCSC combination affects very marginally the damping of interarea mode 'a'.
- With SVC-TCSC connected together, the "best" TCSC controller parameters do not undergo any significant change with the change in loading condition. This is when the TCSC is providing 50% nominal line compensation.

## 6.5 DETERMINATION OF "BEST" TCSC PARAMETERS FOR DIFFERENT COMPENSATION LEVELS AT MAXIMUM LOADING CONDITION

In this section, a study has been performed for different compensation level at maximum loading condition to investigate the behavior of controller parameters of the TCSC. Three compensation levels i.e. 30%, 50% and 70% of the line 7-5 are considered. Again the TCSC controller parameters are obtained using root loci, modal damping and step response studies on the same lines as described Sec. 6.1. Table 6.5 summarizes the "best" controller parameters of the TCSC and the associated eigenvalues for various compensation levels at maximum loading condition. Following observations can be made.

- When no FACTS device is connected, the system is unstable at maximum loading condition.
- The SVC-TCSC dramatically improves the damping of the interarea mode 'b' from -10% (unstable) to +28.7% with the increase in compensation level.
- The damping of the interarea mode 'a' declines from 22.8% to 6.3% with the increase in compensation level.
- With SVC-TCSC connected, the "best" TCSC controller parameters vary significantly with the change in compensation level.

It may be noted that the eigenvalues corresponding to the same 50% series compensation are different in Table 6.5 and Table 6.2. This is because the same line compensation has been obtained with two different values of  $X_c$  (reactance of the fixed capacitor of TCSC). Table 6.2 was obtained with  $X_c = 0.0598$ . It was noticed that TCSC

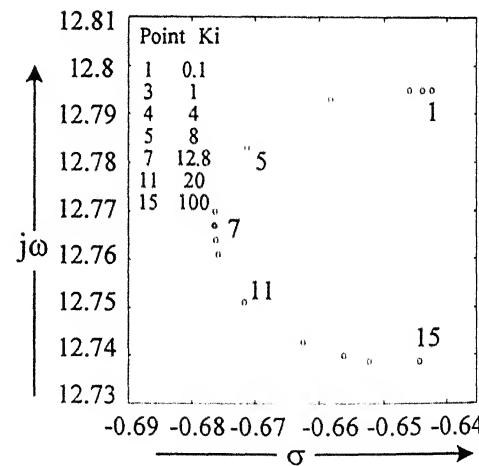
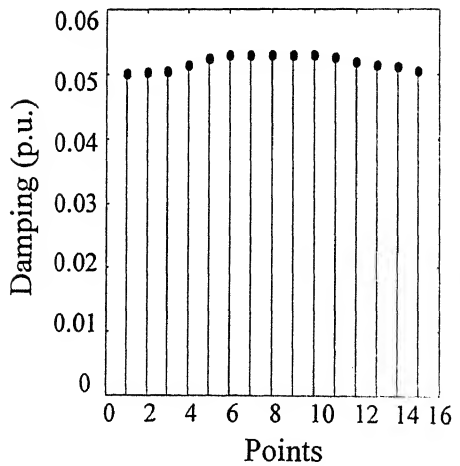
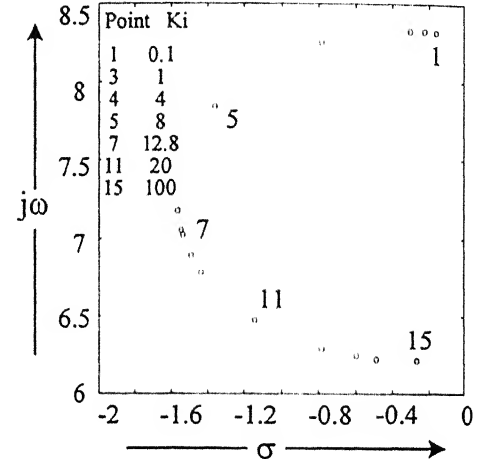
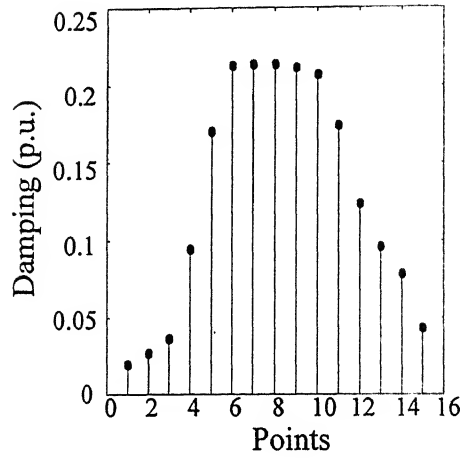
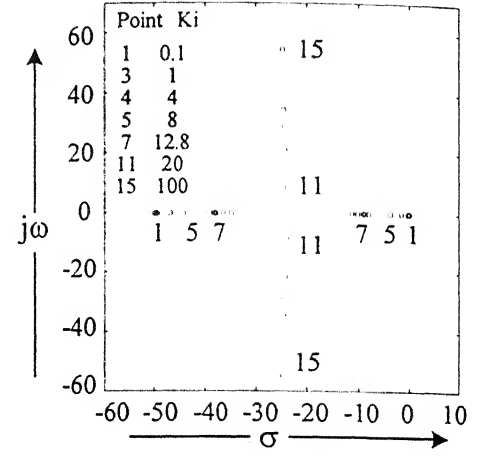
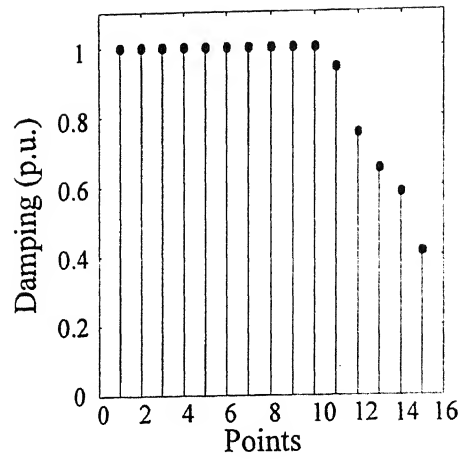
characteristic with  $X_c = 0.0598$  was not able to give the complete range of compensation from 30% to 70% (4.8% to 11.2%) of line 7-5. Hence a new value of  $X_c$  was selected as 0.0393 to provide the complete range of compensation. A graphical explanation of this is given in Appendix O.

## 6.6 DETERMINATION OF “BEST” SVC-TCSC PARAMETERS FOR DIFFERENT COMPENSATION LEVELS AT MAXIMUM LOADING CONDITION

In this section, a study has been performed for different series compensation level at maximum loading condition to investigate the behavior of controller parameters of SVC-TCSC combination. It may be recalled that the SVC is connected at bus 5 and the TCSC is connected between buses 7-5. The controller parameters of the SVC are kept fixed as obtained when the SVC was considered alone at maximum loading condition. Three compensation levels i.e. 30%, 50% and 70% of line 7-5 are considered. Again the controller parameters are obtained using root loci technique on the same lines as described earlier sections. The “best” TCSC controller parameters are obtained on the same lines as explained earlier in Sec. 6.1 by the root loci, associated modal damping and the step response studies for various compensation levels at maximum loading condition.

The “best” controller parameters of the SVC-TCSC and the associated eigenvalues for various compensation levels at maximum loading condition are compiled in Table 6.6. Following observations are made:

- When no FACTS device is connected, the system is unstable due to the interarea mode ‘b’ at maximum loading condition.
- The SVC-TCSC combination strongly stabilizes the interarea mode ‘b’ and further increases the damping of this mode from 28% to 32.9% with the increase in compensation level from 30% to 70%.
- The damping of the interarea mode ‘a’ declines from 22.8% to 5.5% with the increase in compensation level.

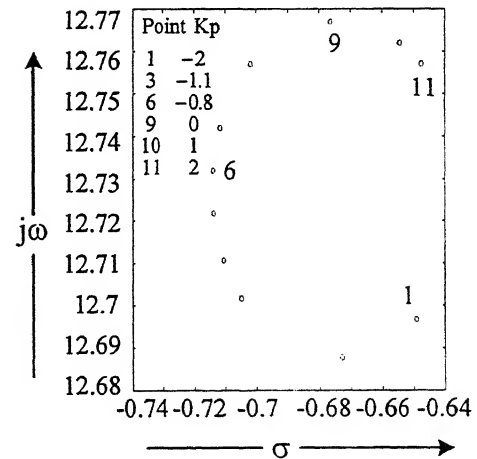
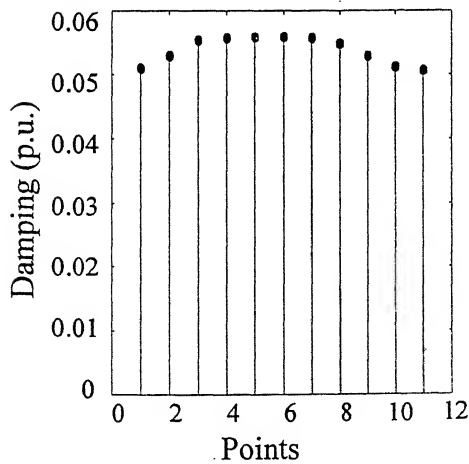
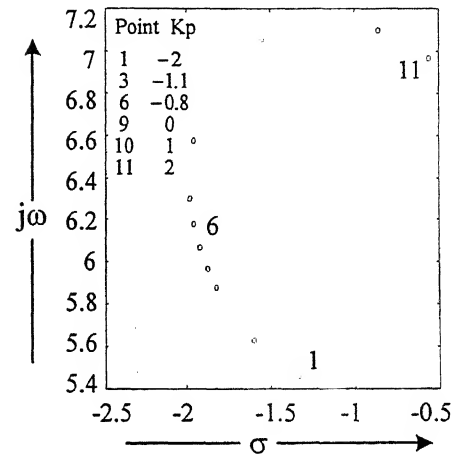
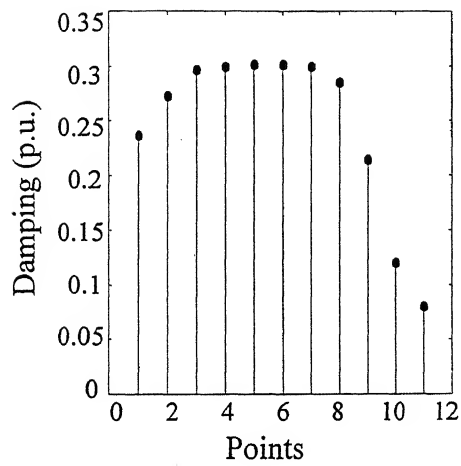
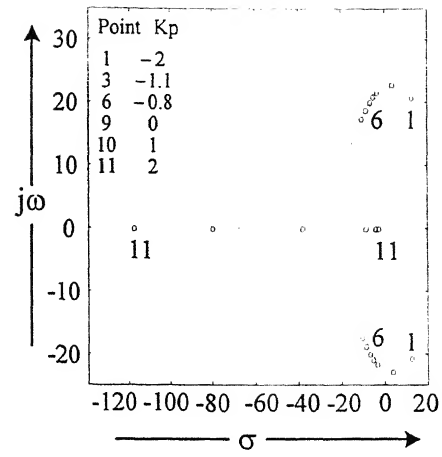
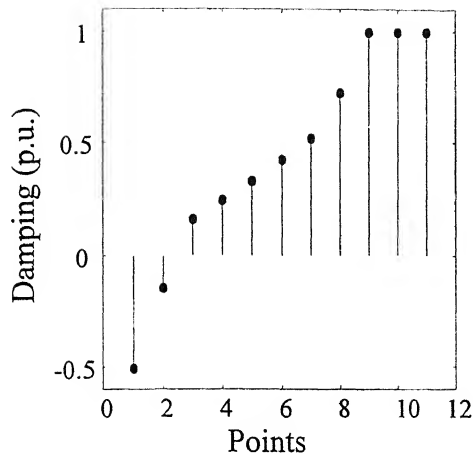


(a) Modal Damping

(b) Root loci

**Fig. 6.19** Root loci of interarea and controller modes and their corresponding modal damping for varying TCSC  $K_I$  ( $K_P = 0$ ) for maximum loading condition of the 9-bus system with SVC-TCSC combine





(a) Modal Damping

(b) Root loci

**Fig. 6.20** Root loci of interarea and controller modes and their corresponding modal damping for varying TCSC  $K_P$  ( $K_I = 12.8$ ) for maximum loading condition of the 9-bus system with SVC-TCSC combine

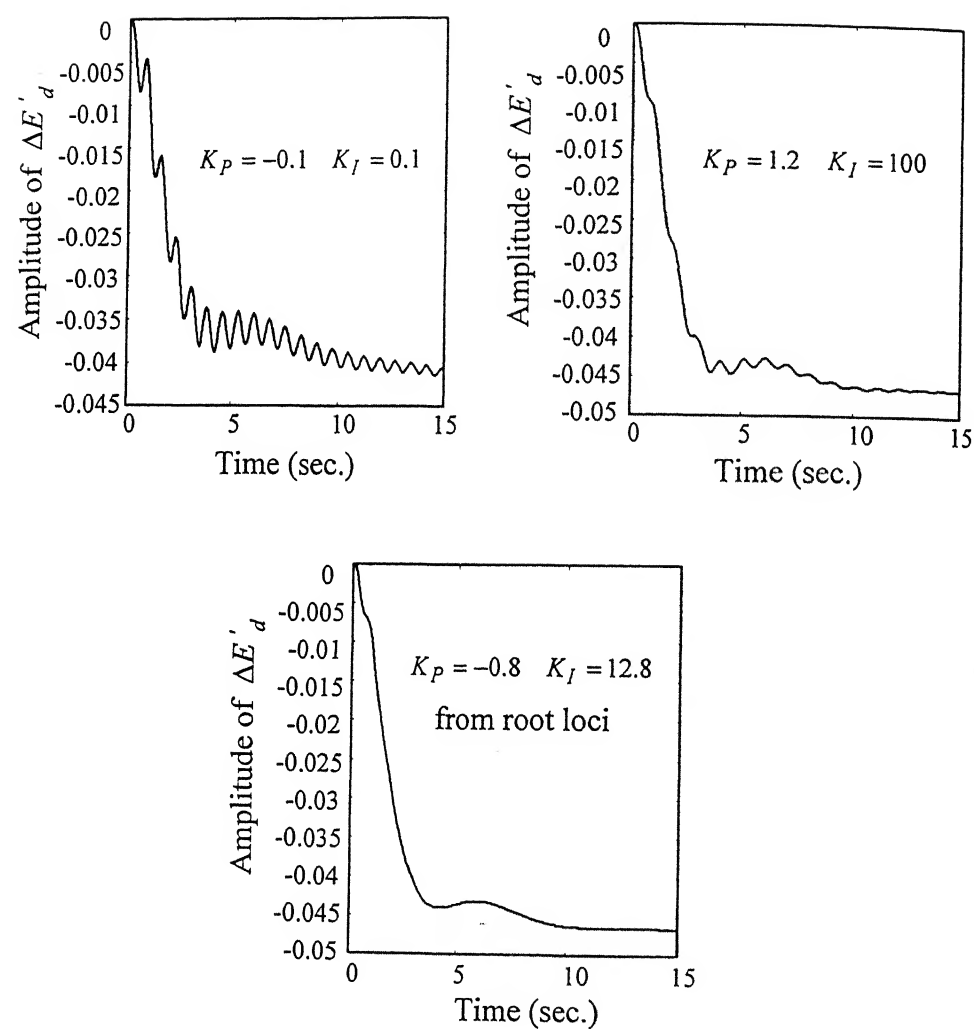


Fig. 6.21 Step response for “best” controller parameters and two other arbitrary set of controller parameters for maximum loading condition of the 9-bus system (SVC-TCSC combine)

Table 6.4 System eigenvalues with coordinated SVC-TCSC controller parameters at different loading conditions

Base case loading Condition No FACTS device	Base case loading Condition With SVC-TCSC		Mid loading condition With SVC-TCSC		Maximum loading Condition With SVC-TCSC		Extreme loading Condition With SVC-TCSC	
	SVC	TCSC	SVC	TCSC	SVC	TCSC	SVC	TCSC
	$K_P = 1$	$K_P = -0.8$	$K_P = 0.1$	$K_P = -0.8$	$K_P = 2$	$K_P = -0.8$	$K_P = 2$	$K_P = -1.0$
	$K_I = 20$	$K_I = 12.4$	$K_I = 20$	$K_I = 12.4$	$K_I = 60$	$K_I = 12.8$	$K_I = 60$	$K_I = 13$
	-48.2224 ± 17.2289i	-60.6086	-60.6086		-43.6531 ± 22.4388i		-43.5169 ± 22.8445i	
	-8.0547 ± 19.6911i	-34.7819	-34.7819		-8.7660 ± 18.4289i		-5.9168 ± 20.3241i	
-0.7198 ± 12.7456i (Damping=0.0564)	-0.7072 ± 12.7617i (Damping=0.0553)	-0.7042 ± 12.7667i (Damping=0.0551)	-0.7042 ± 12.7667i (Damping=0.0551)		-0.7176 ± 12.7331i (Damping=0.0563)		-0.7296 ± 12.6721i (Damping=0.0575)	
-0.1906 ± 8.3660i (Damping=0.0228)	-2.0397 ± 6.5747i (Damping=0.2963)	-2.0468 ± 6.3266i (Damping=0.3078)	-2.0468 ± 6.3266i (Damping=0.3078)		-2.0385 ± 6.1856i (Damping=0.3130)		-1.8012 ± 5.8370i (Damping=0.2949)	
-5.6867 ± 7.9663i	-5.6792 ± 8.0351i	-8.1496 ± 19.3949i	-8.1496 ± 19.3949i		-12.5772		-12.9887	
-5.3644 ± 7.9311i	-5.3676 ± 7.9574i	-7.1978 ± 8.0587i	-7.1978 ± 8.0587i		-9.0557 ± 7.6007i		-10.7079 ± 6.6902i	
-5.2287 ± 7.8263i	-5.2338 ± 7.8713i	-6.0745 ± 8.0261i	-6.0745 ± 8.0261i		-7.2083 ± 7.9871i		-8.4420 ± 7.7242i	
-5.1779	-6.1626	-5.2686 ± 7.8715i	-5.2686 ± 7.8715i		-5.3219 ± 7.8788i		-5.3494 ± 7.8774i	
-3.3993	-4.8293	-6.3358	-6.3358		-6.3663		-6.3800	
-0.4513 ± 1.1997i	-3.5682	-4.7548 ± 0.2212i	-4.7548 ± 0.2212i		-4.8344		-4.8345	
-0.4481 ± 0.7291i	-0.4534 ± 0.8517i	-0.4610 ± 0.8857i	-0.4610 ± 0.8857i		-0.4622 ± 0.9283i		-0.4707 ± 0.9636i	
-0.4366 ± 0.4868i	-0.4176 ± 0.4989i	-0.5439 ± 0.5412i	-0.5439 ± 0.5412i		-0.6641 ± 0.4819i		-1.2472	
-0.0000 ± 0.0000i	-0.4297 ± 0.3028i	-0.5897 ± 0.1064i	-0.5897 ± 0.1064i		-1.0420		-0.7574 ± 0.3859i	
-3.2258	-0.0000 ± 0.0000i	-0.0000 ± 0.0000i	-0.0000 ± 0.0000i		-0.3997		-0.3641	
	-3.2258	-3.2258	-3.2258		-0.0000 ± 0.0000i		-0.0000 ± 0.0000i	
					-3.2258		-3.2258	

**Table 6.5** TCSC alone at maximum loading condition with different compensation level

Maximum loading Condition No FACTS device	Maximum loading Condition With TCSC 30% compensation	Maximum loading Condition With TCSC 50% compensation	Maximum loading Condition With TCSC 70% compensation
	$K_P = -3.0$ $K_I = 32.3$	$K_P = -0.4$ $K_I = 4.3$	$K_P = -0.1$ $K_I = 1.6$
-90.9053	-44.6745	-0.4000	-42.7432
-45.3014	-5.8895 ± 18.4924i	-43.5171	-10.4343 ± 15.9664i
-2.8938 ± 12.3353i (Damping=0.2284)	-0.8003 ± 12.2126i (Damping=0.0654)	-0.7955 ± 12.2377i (Damping=0.0649)	-0.7834 ± 12.3135i (Damping=0.0635)
0.0229 ± 0.2268i (Damping=-0.1005)	-1.2844 ± 5.7226i (Damping=0.2190)	-1.4910 ± 5.6650i (Damping=0.2545)	-1.7742 ± 5.9156i (Damping=0.2873)
-10.8806 ± 5.8904i	-10.3423 ± 6.8197i		-10.2522 ± 6.8870i
-1.2151 ± 8.8486i	-5.4290 ± 7.8202i	-10.2934 ± 6.8561i	-5.4352 ± 7.8477i
-6.3982 ± 7.4235i		-5.4179 ± 7.8345i	
-7.1865	-7.3293	-5.2071 ± 19.0895i	-7.4418
-5.1023	-5.7716	-7.3950	-5.9016
-2.1747	-4.7476	-5.8324	-4.7629
-1.6763	-0.5002 ± 1.1284i	-4.7559	-1.9519
-0.7284 ± 0.3533i	-1.9692	-1.9584	-0.4885 ± 1.0700i
	-0.8765 ± 0.2428i	-0.4940 ± 1.0953i	-0.8763 ± 0.2390i
-0.0000 ± 0.0000i	-0.4983	-0.8765 ± 0.2413i	-0.5140
-3.2258	-0.0000 ± 0.0000i	-0.5059	-0.0000 ± 0.0000i
	-3.2258	0.0000 ± 0.0000i	-3.2258
		-3.2258	

**Table 6.6** SVC-TCSC at maximum loading condition with different compensation level

Maximum loading Condition No FACTS device	Maximum loading Condition With SVC-TCSC 30% compensation		Maximum loading Condition With SVC-TCSC 50% compensation		Maximum loading Condition With SVC-TCSC 70% compensation	
	SVC	TCSC	SVC	TCSC	SVC	TCSC
	$K_P = 2$ $K_I = 60$	$K_P = -2.4$ $K_I = 33.8$	$K_P = 2$ $K_I = 60$	$K_P = -0.3$ $K_I = 4.6$	$K_P = 2$ $K_I = 60$	$K_P = -0.1$ $K_I = 1.7$
-90.9053	-43.5586 ± 22.7371i	-43.5586 ± 22.7371i	-43.6568 ± 22.4311i	-43.7484 ± 22.1272i	-9.2576 ± 18.8476i	
-45.3014	-7.3837 ± 19.4627i	-7.3837 ± 19.4627i	-8.1915 ± 19.3342i	-0.7054 ± 12.7535i (Damping=0.0552)	-2.1306 ± 6.1257i (Damping=0.3285)	
-2.8938 ± 12.3353i (Damping=0.2284)	-0.7189 ± 12.7123i (Damping=0.0565)	-0.7189 ± 12.7123i (Damping=0.0565)	-0.7141 ± 12.7289i (Damping=0.0560)	-1.9463 ± 6.1356i (Damping=0.3024)	-12.2711	
0.0229 ± 0.2268i (Damping=-0.1005)	-1.8181 ± 6.1522i (Damping=0.2834)	-1.8181 ± 6.1522i (Damping=0.2834)	-1.9463 ± 6.1356i (Damping=0.3024)	-12.5822	-8.4625 ± 7.8244i	
-10.8806 ± 5.8904i	-12.8806	-12.8806	-9.0436 ± 7.6042i	-7.2054 ± 7.9874i	-7.0506 ± 8.0070i	
-1.2151 ± 8.8486i	-9.5045 ± 7.3903i	-9.5045 ± 7.3903i	-7.2054 ± 7.9874i	-5.3193 ± 7.8799i	-5.3260 ± 7.8806i	
-6.3982 ± 7.4235i	-7.3085 ± 7.9719i	-7.3085 ± 7.9719i	-5.3193 ± 7.8799i	-4.8355	-6.5753	
-7.1865	-5.3146 ± 7.8793i	-5.3146 ± 7.8793i	-4.8355	-6.3750	-4.8755	
-5.1023	-6.2255	-6.2255	-4.8044	-0.4622 ± 0.9282i	-0.4616 ± 0.9265i	
-2.1747	-4.8044	-4.8044	-0.4628 ± 0.9300i	-0.6638 ± 0.4819i	-0.6470 ± 0.4854i	
-1.6763	-0.6741 ± 0.4813i	-0.6741 ± 0.4813i	-1.0818	-1.0408	-0.9826	
-0.7284 ± 0.3533i	-1.0818	-1.0818	-0.4233	-0.3990	-0.3620	
-0.0000 ± 0.0000i	-0.4233	-0.4233	-0.0000 ± 0.0000i	-0.0000 ± 0.0000i	-0.0000 ± 0.0000i	
-3.2258	-0.0000 ± 0.0000i	-0.0000 ± 0.0000i	-3.2258	-3.2258	-3.2258	

- With SVC-TCSC connected together, the “best” TCSC controller parameters vary significantly with the change in compensation level.

## 6.7 DISCUSSION AND GENERAL OBSERVATIONS

- Various studies of this chapter at different loading conditions with TCSC alone indicate that the system response does not vary much with changes in the loading conditions. The controller parameters also do not vary significantly. This is due to the fact that the compensation of line 7-5 is fixed at 50% and firing angle is also fixed at  $160^\circ$ . Therefore the short circuit level of the system does not get changed at different loading conditions. It is known that the response of a TCSC is dependent on the interaction of TCR with a combination of fixed capacitor and equivalent line inductance. The “best” controller parameters vary significantly when the compensation level is changed at maximum loading condition.
- Since the SVC is equipped with pure voltage controller, it is not able to add damping to the interarea modes of the system [2]. If damping of the interarea mode is to be improved, the SVC must be equipped with auxiliary controller apart from PI voltage controller. However as the basic purpose of an SVC is to maintain voltage profile of a particular bus at desired level, the PI voltage controller should be optimized.
- In the case of SVC, the “best” controller parameters vary significantly (there is a large change in  $K_I$  with the change in loading condition). The reason for this is that a change in loading condition leads to change in operating condition and the average TCR conductance. This causes a change in the response time of the SVC. Hence there is a need to change  $K_P$  and  $K_I$  of the SVC to get the best response. Therefore the “best” controller parameters do vary with the change in loading condition in case of an SVC connected to the system.
- In general, SVC and TCSC stabilize the system at maximum loading condition. The effect of a TCSC is more as compared to an SVC from stability perspective. This is expected because the SVC is equipped with only voltage controller which does not contribute to system damping.

- The TCSC alone increases the damping of both the interarea modes 'a' and 'b' whereas SVC deteriorates the damping of both these interarea modes. This is evident from Tables 6.2 and 6.3. A close look at Tables 6.2 and 6.4 reveals that the SVC-TCSC combination is more effective as compared to the TCSC alone in increasing the damping of both the interarea modes.
- Tables 6.3 and 6.4 show that the SVC alone deteriorates the damping of the interarea modes whereas a combination of SVC-TCSC improves the damping of these modes significantly.
- Tables 6.5 and 6.6 show that the TCSC alone and the SVC-TCSC combination is able to stabilize the system. The SVC-TCSC improves the damping of the interarea mode 'b' significantly as compared to when the TCSC alone is considered at maximum loading condition for providing different compensation levels.
- Both these FACTS devices stabilize the system at maximum loading condition, even though the SVC does not have the same stabilizing influence as the TCSC.
- The adopted root loci technique also gives a clear insight of controller behavior for different pairs of  $K_P$  and  $K_I$ . This useful information may be used by an operator to vary the controller parameters in a range to have high degree of modal damping for the sensitive modes (interarea mode 'a', interarea mode 'b' and FACTS device controller modes) which is vital for the system stability.

## 6.8 CONCLUSIONS

In this chapter, a very simple and heuristic method of obtaining individual as well as coordinated FACTS controller parameters is presented. The results obtained from root loci and modal damping analysis are further refined using step response studies. This Chapter provides a significant insight in interaction of FACTS devices and the behavior of controller parameters with the change in system operating conditions. Based on various studies performed in this Chapter following conclusions are made:

- Increase in system loading has differing (positive and negative) influences on different interarea modes.

- FACTS devices influence one interarea mode more than other.
- TCSC has more beneficial effect on the damping of one interarea mode than SVC.
- Change in system loading does not influence the “best” setting of TCSC controller parameters but the SVC controller parameters get affected by system loading.
- TCSC controller parameters vary with the changes in percentage series compensation.

## CONCLUSIONS

A novel placement methodology termed as Extended Voltage Phasors Approach (EVPA) has been proposed in this thesis. The proposed EVPA methodology is less time intensive and a non-Jacobian based technique. To examine the efficacy of placement strategy, a general purpose versatile MATLAB program has been developed using MATLAB 5.3. The developed MATLAB program has been used for small signal analysis of four power systems (6-bus, 9-bus, 39-bus and 68-bus). Further the developed MATLAB program has features of incorporating multiple FACTS devices in modular fashion. Modeling of key FACTS devices namely SVC, TCSC, STATCOM and SSSC has been done using power balance form and these are incorporated in the developed MATLAB program in a modular fashion. Impact of coordinated control of FACTS devices has also been investigated in this thesis.

### 7.1 GENERAL CONCLUSIONS

The general conclusions of the thesis are summarized below.

#### 7.1.1 Extended Voltage Phasors Approach (EVPA) – A Novel Placement Strategy

A novel non-Jacobian based placement strategy termed as Extended Voltage Phasors Approach (EVPA) is presented for identification of critical line segment from voltage stability consideration in the power systems. It is understood that Jacobian is always utilized in load flow studies. In Jacobian based methods, the load flow Jacobian elements are utilized for calculating the indices for placement of FACTS devices. However non-Jacobian methods utilize only the load flow results and not the Jacobian elements. The results of EVPA are compared and validated by LFI approach as well as

voltage profile graphs of the system at base case loading and maximum loading conditions. EVPA is applied to four systems viz. 6-bus, 9-bus, 39-bus and 68-bus system at different loading conditions. In all these systems the EVPA approach identifies the critical path and the most critical segment correctly as identified through other methods. It also indicates the cause of the problem as either due to active power or reactive power loading of the system. In EVPA there is no need to compute four indices for each line as is done in LFI approach. Therefore EVPA is computationally more efficient. EVPA is also applied to 68-bus system at base case loading condition considering various contingencies in the system. It is found that in most cases the critical link obtained in healthy system study continues to remain critical, but in few cases some other line become more critical. One test study on 68-bus system has also been presented for multiple device placement using EVPA technique.

### **7.1.2 Development of General Purpose MATLAB Program**

A general purpose versatile MATLAB program for small signal and voltage stability analysis of multimachine power system has been developed using MATLAB 5.3. The developed MATLAB program uses two axis representation of synchronous machines and both rotating and static type of exciter can be incorporated in it [97]. The methodology of multimachine modeling is based on power balance form. The results of the developed MATLAB program are found to conform with an already published result [97].

### **7.1.3 Mathematical Modeling and Incorporation of FACTS Devices in the Developed MATLAB Program**

Mathematical modeling of various key FACTS devices viz. SVC, TCSC, STATCOM and SSSC have been done using power balance form. Different types of controller i.e. PI and state feedback controllers with integral control have been used with the FACTS devices. It is demonstrated that all the models developed are modular and can



be easily incorporated in developed MATLAB program. Multiple FACTS device incorporation in the developed MATLAB program has also been demonstrated.

#### **7.1.4 Analysis of EPVA Using Developed MATLAB Program**

Further the efficacy of EVPA has been tested utilizing developed MATLAB program and step response analysis of the system at various loading conditions. Voltage profile analysis has also been done for 6-bus, 9-bus, 39-bus and 68-bus power systems at different loading conditions. It is shown that EVPA indicates appropriate optimal location from voltage stability viewpoint. It is worth mentioning here that these places may not be the optimal places from system damping viewpoint. The controller parameters are chosen carefully so that the system performance is satisfactory. Small signal analysis of the four systems has been done utilizing both single as well as multiple FACTS device combination.

#### **7.1.5 Coordinated Control of FACTS Devices**

An attempt has also been made to study the impact of coordinated control of FACTS devices for the 9-bus system at different loading conditions using heuristic root loci technique. In this technique, the controller parameters are varied one at a time. The best controller parameters are chosen on the basis of high degree of modal damping of the concerned modes simultaneously. This technique also yields the complete range of controller parameters for satisfactory operation of the power system. The root loci technique has been applied to obtain the controller parameters when the SVC and TCSC are considered individually as well as in combination for the 9-bus system at different loading conditions. The study reveals that the TCSC has a greater impact on the system damping than the SVC since the SVC is equipped with only a pure voltage controller. It has been found that with the variation in system loading condition, individual TCSC controller parameters do not vary significantly whereas SVC parameters do. Again when the SVC-TCSC combination is considered at various loading conditions, the TCSC controller parameters do not vary significantly. This may be attributed to the fact that

compensation provided by the TCSC is same in all loading conditions. Therefore the short circuit level of the system does not get changed at different loading conditions. The SVC controller parameters vary significantly because with the change in loading condition, the reactive power requirement of the system also changes. A study has also been performed with different levels of compensation for the 9-bus system with the SVC-TCSC combination. In this case the TCSC controller parameters vary significantly. This is expected because short circuit level of the system now gets changed and so do the TCSC controller parameters.

## **7.2 SCOPE FOR FUTURE WORK**

Some suggestions for the future work are

- Validation of proposed placement strategy should be done on extremely large power systems.
- Validation of Placement strategy for transient stability study needs to be done using transient stability simulation packages.
- Models of FACTS devices should be utilized in load flow studies.
- UPFC and other FACTS device models can be developed on the same line and added in the developed MATLAB program.
- Established optimization techniques can be utilized to obtain the optimal parameters of FACTS controllers.
- Interaction between higher order controllers of both SVC (auxiliary damping controller) and TCSC (power swing damping controller) must be studied.

## REFERENCES

- [1] N. G. Hingorani and L. Gyugyi, "Understanding FACTS," *IEEE Press*, 1999.
- [2] R. K. Varma, "Control of Static Var Systems for Improvement of Dynamic Stability and Damping of Torsional Oscillations," Ph.D. Thesis, IIT Kanpur, April 1988.
- [3] W. H. Litzenberger, V. Lava, S. Grace and N. Parsons, "An Annotated Bibliography of HVDC Transmission and FACTS Devices 1991-1993," *Electric Power Research Institute*, 1994.
- [4] H. Mehta, T. W. Cease, L. Gyugyi and C. D. Schauder, "Static Condenser for Flexible AC Transmission Systems," *FACTS EPRI Workshop*, Boston, Massachusetts, May 18-22, 1992.
- [5] CIGRE Working Group, "Modeling of Static Shunt VAR Systems for System Analysis," *Electra*, Vol. 51, pp. 45-74, 1977.
- [6] L. Gyugi, N. G. Hingorani, P. R. Nannery and N. Tai, "Advanced Static VAR Compensator Using Gate Turn-Off Thyristors For Utility Applications," *CIGRE*, 23-203, 1990 session, Paris.
- [7] L. Gyugyi, C. D. Schauder and K. K. Sen, "Static Synchronous Series Compensator: A Solid State Approach to the Series Compensation of Transmission Lines," *IEEE Trans. on Power Delivery*, Vol. 12, No. 1, pp. 406-417, January 1997.
- [8] K. K. Sen, "SSSC-Static Synchronous Series Compensator: Theory, Modeling and Applications," *IEEE Trans. on Power Delivery*, Vol. 13, No. 1, pp. 241-246, January 1998.

- [9] R. L. Hauth and R. J. Moran, "The Performance of Thyristor-Controlled Static VAR Systems in HVAC Applications, Part II- Performance Modeling Concepts," *IEEE Tutorial Text* (78 EH01 35-4-PWR), pp. 65-72, IEEE PES Summer Meeting, Los Angeles, 1978.
- [10] F. Aboytes, G. Arroyo and G. Villa, "Application of Static VAR Compensators in Longitudinal Power Systems," *IEEE Trans. on PAS*, Vol. PAS-102, pp. 3460-3466, 1983.
- [11] S. C. Kapoor, "Dynamic Stability of Long Transmission Lines with Static Compensators and Synchronous Machines," *IEEE Trans. on PAS*, Vol. PAS-98, pp. 124-134, 1979.
- [12] K. R. Padiyar, *Power System Dynamics: Stability and Control*, Interline, Bangalore, 1996.
- [13] M. J Laufenberg, M. A. Pai and K. R. Padiyar, "Hopf Bifurcation Control in Power System with Static Var Compensators," *Electric Power & Energy Systems*, Vol. 19, No. 5, pp. 339-347, 1997.
- [14] IEEE Special Stability Controls Working Group, "Static VAR Compensator Models for Power Flow and Dynamic Performance Simulation," *IEEE Trans. on Power Systems*, Vol. 9, No. 1, pp. 229-240, 1994.
- [15] X. R. Chen, N. C. Pahalawaththa, U. D. Annakkage and C. S. Kumble, "Controlled Series Compensation for Improving the Stability of Multimachine Power Systems," *IEE Proceedings*, Pt. C, Vol. 142, No. 4, pp. 361-366, July 1995.

- [16] X. R. Chen, N. C. Pahalawaththa, U. D. Annakkage and C. S. Kumble, "Output Feedback TCSC Controllers to Improve Damping of Meshed Multimachine Power Systems," *IEE Proceedings*, Pt. C, Vol. 144, No. 3, pp. 243-248, May 1997.
- [17] X. R. Chen, N. C. Pahalawaththa, U. D. Annakkage and C. S. Kumble, "Enhancement of Power System Stability by Using Controlled Series Compensation," *Electric Power & Energy Systems*, Vol. 18, No. 7, pp. 475-481, 1996.
- [18] N. Martins, H. J.C.P. Pinto and J. J. Paserba, "TCSC Controls for Line Power Scheduling and System Oscillation Damping – Results for a Small Example System," *13<sup>th</sup> PSCC* in Trondheim, pp. 1244-1251, June 28-July 2<sup>nd</sup>, 1999.
- [19] C. A. Cañizares and Z. T. Faur, "Analysis of SVC and TCSC Controllers in Voltage Collapse," *IEEE Trans. on Power Systems*, Vol. 14, No. 1, pp. 158-165, February 1999.
- [20] A. Ghosh and G. Ledwich, "Modeling and Control of Thyristor-Controlled Series Compensators," *IEE Proceedings*, Pt. C, Vol. 142, No. 3, pp. 297-304, May 1995.
- [21] R. Rajaraman, I. Dobson, R. H. Lasseter and Y. Shern, "Computing the Damping of Subsynchronous Oscillations Due to a Thyristor Controlled Series Capacitor," *IEEE Trans. on Power Systems*, Vol. 11, No. 2, pp. 1120-1127, April 1996.
- [22] S. G. Jalali, R. H. Lasseter and I. Dobson, "Dynamic Response of a Thyristor Controlled Switched Capacitor," *IEEE Trans. on Power Delivery*, Vol. 9, No. 3, pp. 1609-1615, July 1994.

- [23] H. A. Othman and L. Ängquist, "Analytical Modeling of Thyristor-Controlled Series Capacitors for SSR Studies," *IEEE Trans. on Power Systems*, Vol. 11, No. 1, pp. 119-127, February 1996.
- [24] P. Mattavelli, G. C. Verghese and A. M. Stankovic, "Phasor Dynamics of Thyristor-Controlled Series Capacitor Systems," *IEEE Trans. on Power Systems*, Vol. 12, No. 3, pp. 1259-1267, August 1997.
- [25] J. S. Lai and F. Z. Peng, "Multilevel Converter - a New Breed of Power Converters," *IEEE Trans. on Industry Applications*, Vol. 32, No. 3, pp. 509-517, 1996.
- [26] F. Z. Peng, J. S. Lai, J. W. McKeever and J. Vancoeverying, "A multilevel Voltage Source Inverter with Separate DC Source for Static Var Generators," *IEEE Trans. on Industry Applications*, Vol. 32, No. 5, pp. 1130-1138, 1996.
- [27] J. B. Ekanayake and N. Jenkins, "A Three Level Advanced Static Var Compensator," *IEEE Trans. on Power Delivery*, Vol. 11, No. 1, pp. 540-545, January 1996.
- [28] K. V. Patil, R. M. Mathur, J. Jiang and S. H. Hosseini, "Distribution System Compensation Using a New Binary Multilevel Voltage Source Inverter," *IEEE Trans. on Power Delivery*, Vol. 14, No. 2, pp. 459-464, April 1999.
- [29] J. B. Ekanayake and N. Jenkins, "Mathematical Model of a Three Level Advanced Static Var Compensator," *IEE Proceedings*, Pt. C, Vol. 144, No. 2, pp. 201-206, March 1997.
- [30] C. Schauder and H. Mehta, "Vector Analysis and Control of Advanced Static VAR Compensators," *IEE Proceedings*, Pt. C, Vol. 140, No. 4, pp. 299-306, July 1993.

- [31] K. R. Padiyar and A. M. Kulkarni, "Design of Reactive Power Current and Voltage Controller of Static Condenser," *Electrical Power and Energy Systems*, Vol. 19, No. 6, pp. 397-410, 1997.
- [32] B. Das, A. Ghosh and Sachchidanand, "Suitable Configurations of ASVC for Power Transfer Applications," *Electric Power System Research*, Vol. 49, pp. 107-122, 1999.
- [33] C. Schauder, M. Gernhardt, E. Stancey, T. Lemak, L. Gyugyi, T. W. Cease and A. Edris, "Development of a  $\pm 100$  MVAR Static Condenser for Voltage Control of Transmission Systems," *IEEE Trans. on Power Delivery*, Vol. 10, No. 3, pp. 1486-1496, July 1995.
- [34] C. Schauder, M. Gernhardt, E. Stancey, T. Lemak, L. Gyugyi, T. W. Cease and A. Edris, "Operation of  $\pm 100$  MVAR TVA STATCON," *IEEE Trans. on Power Delivery*, Vol. 12, No. 4, pp. 1805-1811, October 1997.
- [35] K. R. Padiyar and A. M. Kulkarni, "Application of Static Condenser for Enhancing Power Transfer in Long Lines," *CIGRE*, 530-01, Symposium, Tokyo, 1995.
- [36] L. Sunil Kumar and A. Ghosh, "Static Synchronous Series Compensator-design, control and applications," *Electric Power System Research*, Vol. 49, pp. 139-148, 1999.
- [37] L. Sunil Kumar and A. Ghosh, "Modeling and Control design of a Static Synchronous Series Compensator," *IEEE Trans. on Power Delivery*, Vol. 14, No. 4, pp. 1448-1453, October 1999.

- [38] C. J. Hatziadoniu and A. T. Funk, "A Series Connected Solid State Synchronous Voltage Source," *IEEE Trans. on Power Delivery*, Vol. 11, No. 2, pp. 1138-1144, April 1996.
- [39] G. Ledwich and T. Jordan, "Placement of Shunt VAR Systems," *Electric Power System Research*, Vol. 5, pp. 299-306, 1982.
- [40] M. O'Brien and G. Ledwich, "Placement of Static Compensators for Stability Improvement," *IEE Proceedings*, Pt. C, Vol. 132, No. 1, pp. 30-35, January 1995.
- [41] N. Martins and L. T. G. Lima, "Determination of Suitable Locations for Power System Stabilizers and Static Var Compensators for Damping Electromechanical Oscillations in Large Scale Power Systems," *IEEE Trans. on Power Systems*, Vol. 5, No. 4, pp. 1455-1469, November 1990.
- [42] N. Yang, Q. Liu and J. D. McCalley, "TCSC Controller Design for Damping Interarea Oscillations," *IEEE Trans. on Power Systems*, Vol. 13, No. 4, pp. 1304-1310, November 1998.
- [43] E. V. Larsen, J. J. Sanchez-Gasca and J. H. Chow, "Concepts for Design of FACTS Controllers to Damp Power Swings," *IEEE Trans. on Power Systems*, Vol. 10, No. 2, pp. 948-955, 1995.
- [44] B. Gao, G. K. Morison and P. Kundur, "Voltage Stability Evaluation using Modal Analysis," *IEEE Trans. on Power Systems*, Vol. 7, No. 4, pp. 1529-1542, November 1992.
- [45] P. Kundur, *Power System Stability and Control*, New York, McGraw Hill Inc., 1994.



- [46] Y. Mansour, W. Xu, F. Alvarado and C. Rinzin, "SVC Placement using Critical Modes of Voltage Stability," *IEEE Trans. on Power Systems*, Vol. 9, No. 2, pp. 757-762, May 1994.
- [47] C. S. Chang and J. S. Huang, "Optimal SVC Placement for Voltage Stability Reinforcement," *Electric Power Systems Research*, Vol. 42, pp. 165-172, 1997.
- [48] S. Gerbex, R. Cherkaoui and A. J. Germond, "Optimal Location of FACTS Devices in a Power System using Genetic Algorithm," *13<sup>th</sup> PSCC in Trondheim*, pp. 1252-1259, June 28 – July 2<sup>nd</sup>, 1999.
- [49] C. S. Chang and J. S. Huang, "Worst-case Identification of Reactive Power Margin and Local Weakness of Power Systems," *Electric Power Systems Research*, Vol. 44, pp. 77-83, 1998.
- [50] Y. T. Hsiao, C. C. Liu, H. D. Chiang and Y. L. Chen, "A New Approach for Optimal VAR Sources Planning in Large Scale Electric Power Systems," *IEEE Trans. on Power Systems*, Vol. 8, No. 3, pp. 988-996, August 1993.
- [51] Y. T. Hsiao, C. C. Liu, H. D. Chiang and Y. L. Chen, "A Computer Package for Optimal Multi-objective VAR Planning in Large Scale Power Systems," *IEEE Trans. on Power Systems*, Vol. 9, No. 2, pp. 668-676, May 1994.
- [52] H. F. Wang, "An Eigensolution free Method of Reduced-order Modal Analysis to Select the Installing Locations and Feedback Signals of FACTS-based Stabilizers," *Electrical Power and Energy Systems*, Vol. 21, pp. 547-554, 1999.
- [53] H. F. Wang, "Selection of Robust Installing Locations and Feedback Signals of FACTS based Stabilizers in Multi-machine Power Systems," *IEEE Trans. on Power Systems*, Vol. 14, No. 2, pp. 569-574, May 1999.

- [54] P. Kessel and H. Glavitch, "Estimating the Voltage Stability of Power Systems," *IEEE Trans. on Power Delivery*, Vol. 1, No. 3, pp. 346-354, 1986.
- [55] O. O. Obadina and G. J. Berg, "Identifying Electrically Weak and Strong Segments of a Power System from a Voltage Stability Viewpoint," *IEE Proc.*, Pt. C, Vol. 137, No. 3, pp. 205-212, May 1990
- [56] H. Okamoto, A. Kurita and Y. Sekine, "A Method for Identification of Effective Locations of Variable Impedance Apparatus on Enhancement of Steady-State Stability in Large Scale Power Systems," *IEEE Trans. on Power Systems*, Vol. 10, No. 3, pp. 1401-1407, August 1995.
- [57] H. F. Wang, F. J. Swift and M. Li, "Indices for Selecting the Best Location of PSSs or FACTS-based Stabilizers in Multimachine Power Systems: A Comparative Study," *IEE Proceedings*, Pt. C, Vol. 144, No. 2, pp. 155-159, March 1997.
- [58] I. J. Perez-Arriaga, G. C. Verghese and F. C. Schweppe, "Selective Modal Analysis with Applications to Electric Power Systems, Part I and Part II," *IEEE Trans. on Power Systems*, Vol. 9, 1982.
- [59] R. A. Schlueter, I. Hu, M. W. Chang and A. Costi, "Methods for Determining Proximity to Voltage Collapse," *IEEE Trans. on Power Systems*, Vol. 6, No. 1, pp. 285-291, 1991.
- [60] B. H. Lee and K. Y. Lee, "Dynamic and Static Voltage Stability Enhancement of Power Systems," *IEEE Trans. on Power Systems*, Vol. 8, No. 1, pp. 231-238, 1993.

- [61] A. Mohamed and G. B. Jasmon, "Determining the Weak Segment of a Power System with Voltage Stability Considerations," *Electric Machines and Power Systems*, Vol. 24, pp. 555-568, 1996.
- [62] F. Gubina and B. Strmcnik, "Voltage Collapse Proximity Index Determination using Voltage Phasors Approach," *IEEE Trans. on Power Systems*, Vol. 10, No. 2, pp. 788-792, May 1995.
- [63] Y. L. Chen, "Weak Bus Oriented Optimal Multi-objective VAR Planning," *IEEE Trans. on Power Systems*, Vol. 11, No. 4, pp. 1885-1890, November 1996.
- [64] P-A Löf, T. Smed, G. Anderson and D. J. Hill, "Fast Calculation of a Voltage Stability Index," *IEEE Trans. on Power Systems*, Vol. 7, No. 1, pp. 54-64, February 1992.
- [65] P-A Löf, G. Anderson and D. J. Hill, "Voltage Stability Indices for Stressed Power Systems," *IEEE Trans. on Power Systems*, Vol. 8, No. 1, pp. 326-334, February 1993.
- [66] Z. Elrazaz and A. Al-Ohaly, "Criterion for Inductive Compensation Location to Enhance System Steady State Stability," *IEEE Trans. on Power Systems*, Vol. 8, No. 4, pp. 1545-1549, November 1993.
- [67] R. T. Byerly, D. T. Poznaniak and E. R. Taylor, "Static Reactive Compensation for Power Transmission Systems," *IEEE Trans. on Power Apparatus and Systems*, Vol. PAS-101, No. 10, pp. 3997-4005, October 1982.
- [68] I. O. Habiballah and C. A. Belhadj, "Corrective Schemes for Voltage Stability using Two Different Indicators," *Electric Machines and Power Systems*, Vol. 27, pp. 123-138, 1999.

- [69] M. Khederzadeh, "Fast Computation of SVC Location for Power System Small Signal Stability Enhancement," *13<sup>th</sup> PSCC* in Trondheim, pp. 503-509, June 28-July 2<sup>nd</sup>, 1999.
- [70] J. Griffin, D. Atanackovic and F. D. Galina, "A study of the Impact of FACTS on the Secure-Economic Operation of Power Systems," *13<sup>th</sup> PSCC* in Trondheim, pp. 1077-1082, June 28-July 2<sup>nd</sup>, 1999.
- [71] K. R. Padiyar, C. Radhakrishna, P. Rajasekharam and M. A. Pai, "Dynamic Stabilization of Power Systems through Reactive Power Modulation," *Electric Machines and Power Systems*, Vol. 11, pp. 281-293, 1986.
- [72] M. M. Begovic and A. G. Phadke, "Control of Voltage Stability using Sensitivity Analysis," *IEEE Trans. on Power Systems*, Vol. 7, No. 1, pp. 114-123, February 1992.
- [73] L. Rouco and F. L. Pagola, "An Eigenvalue Sensitivity Approach to Location and Controller Design of Controllable Series Capacitors for Damping Power System Oscillations," *IEEE Trans. on Power Systems*, Vol. 12, No. 4, pp. 1660-1666, November 1997.
- [74] E. Z. Zhou, "Application of Static Var Compensators to Increase Power System Damping," *IEEE Trans. on Power Systems*, Vol. 8, No. 2, pp. 655-661, May 1993.
- [75] A. C. Z. De Souza and N. H. M. N. Brito, "Voltage Collapse and Control Actions: Effects and Limitations," *Electric Machines and Power Systems*, Vol. 26, pp. 903-915, 1998.

- [76] A. Semlyen, B. Gao and W. Janischewskyj, "Calculation of the Extreme Loading Condition of a Power System for the Assessment of Voltage Stability," *IEEE Trans. on Power Systems*, Vol. 6, No. 1, pp. 307-312, February 1991.
- [77] R. Romero and A. Monticelli, "A Zero-One Implicit Enumeration Method for Optimizing Investments in Transmission Expansion Planning," *IEEE Trans. on Power Systems*, Vol. 9, No. 3, pp. 1385-1391, August 1994.
- [78] V. A. Levi and M. S. Calovic, "Linear Programming based Decomposition Method for Optimal Planning of Transmission network Investments," *IEE Proceedings*, Pt. C, Vol. 140, No. 6, pp. 516-522, November 1993.
- [79] M. A. Farrag and M. M. El-Metwally, "New Method for Transmission Planning using Mixed Integer Programming," *IEE Proceedings*, Pt. C, Vol. 135, No. 4, pp. 319-323, July 1988.
- [80] K. Y. lee, J. L. Ortiz, Y. M. Park and L. G. Pond, "An Optimization Technique for Reactive Power Planning of Subtransmission Network under Normal Operation," *IEEE Trans. on Power Systems*, Vol. 1, No. 2, pp. 153-159, May 1986.
- [81] A. Losi, F. Rossi, M. Russo and P. Verde, "New Tool for Reactive Power Planning," *IEE Proceedings*, Pt. C, Vol. 140, No. 4, pp. 256-262, July 1993.
- [82] Y. Y. Hong and C. C. Liu, "A Heuristic and Algorithmic Approach to VAR Planning," *IEEE Trans. on Power Systems*, Vol. 7, No. 2, pp. 505-512, May 1992.
- [83] T. T. Lie, "Method of Identifying the Strategic Placement for Compensation Devices," *IEEE Trans. on Power Systems*, Vol. 10, No. 3, pp. 1448-1453, August 1995.

- [84] E. J. de Oliveira and J. W. M. Lima, "Allocation of FACTS Devices in a Competitive Environment," *13<sup>th</sup> PSCC* in Trondheim, pp. 1184-1190, June 28-July 2<sup>nd</sup>, 1999.
- [85] D. J. Gotham and G. T. Heydt, "Power Flow Control and Power Flow Studies for Systems with FACTS Devices," *IEEE Trans. on Power Systems*, Vol. 13, No. 1, pp. 60-65, February 1998.
- [86] N. Martins, N. J. P. Macedo, L. T. G. Lima and H. J. C. P. Pinto, "Control Strategies for Multiple Static Var Compensators in Long Distance Voltage Supported Transmission Systems," *IEEE Trans. on Power Systems*, Vol. 8, No. 3, pp. 1107-1117, August 1993.
- [87] R. Yokoyama, T. Niimura and Y. Nakanishi, "A Coordinated Control of Voltage and Reactive Power by Heuristic Modeling and Approximate Reasoning," *IEEE Trans. on Power Systems*, Vol. 8, No. 2, pp. 636-642, May 1993.
- [88] K. Clark, B. Fardanesh and R. Adapa, "Thyristor Controlled Series Compensation Application Study – Control Interaction Consideration," *IEEE Trans. on Power Delivery*, Vol. 10, No. 2, pp. 1031-1036, April 1995.
- [89] F. D. Freitas, A. S. eSilva and A. J. A. S. Costa, "Coordinated Setting of Stabilizers for Synchronous Generators and FACTS Devices In Power Systems," *CIGRE*, 320-03, Symposium, Tokyo, 1995.
- [90] M. Noroozian and G. Anderson, "Damping of Inter-area and Local Modes by Use of Controllable Components," *IEEE Trans. on Power Delivery*, Vol. 10, No. 4, pp. 2007-2012, October 1995.

- [91] L. A. S. Pilotto, W. W. Ping, A. R. Carvalho, W. F. Long, F. L. Alvarado, C. L. DeMarco and A. Edris, "Coordinated Design of FACTS controllers to Enhance Power System Dynamic Performance," *International Colloquium on HVDC and FACTS*, Johannesburg, September 1997.
- [92] E. Acha and H. Ambriz-Pérez, "FACTS Device Modeling in Optimal Power Flows Using Newton's Method," *13<sup>th</sup> PSCC* in Trondheim, pp. 1277-1283, June 28-July 2<sup>nd</sup>, 1999.
- [93] J. J. Sanchez-Gasca, "Coordinated Control of Two FACTS Devices for Damping Interarea Oscillations," *IEEE Trans. on Power Systems*, Vol. 13, No. 2, pp. 428-434, May 1998.
- [94] G. Li, T. T. Lie, G. B. Shrestha and K. L. Lo, "Real-time Coordinated Optimal FACTS Controllers," *Electric Power Systems Research*, Vol. 52, pp. 273-286, 1999.
- [95] X. Z. Lei, D. Povh and K. Renz, "Improved Power Swing Damping by Coordinated FACTS Controls," *International Colloquium on HVDC and FACTS*, Johannesburg, pp. 1-6, September 1997.
- [96] W. H. Litzenberger, R. K. Varma and J. D. Flanagan, "An Annotated Bibliography of HVDC Transmission and FACTS Devices 1996-1997," *Electric Power Research Institute*, WO-3022 06, June 1998.
- [97] Peter W Sauer and M. A. Pai, *Power System Dynamics and Stability*, Prentice Hall, 1998.
- [98] Cherry Tree Scientific Software, *Matlab Power System Tool Box*, Ontario, Canada

- [99] N.G.Hingorani, "Flexible AC Transmission," *IEEE Spectrum*, Vol. 30, No.4, pp. 40-45, 1993.
- [100] P. C. Krause, *Analysis of Electric Machinery*, McGraw-Hill, NewYork, 1986.
- [101] E. V. Larsen, C. Bowler, B. Damsky and S. Nilsson, "Benefits of Thyristor Controlled Series Compensation," *CIGRE*, 14/37/38-04, Paris, 1992.
- [102] C. A. Canizares, A. C. Z. de Souza and V. H. Quintana, "Comparison of Performance Indices for Detection of Proximity to Voltage Collapse," *IEEE Trans. on Power Systems*, Vol. 11, No. 3, pp. 1441-1450, 1996.
- [103] O. O. Obadina and G. J. Berg, "Determination of Voltage Stability Limit in Multi-machine Power Systems," *IEEE Trans. on Power Systems*, Vol. 3, No. 4, pp. 1545-1554, 1988.
- [104] M. Brucoli, F. Torelli, M. Trovato, G. Carpinelli and F. Rossi, "Voltage Stability Analysis in Electric Power System by Nonlinear Programming," *Electrical Machines and Power Systems*, pp. 403-416, 1985.



# APPENDIX A

## MULTIMACHINE MODELING

### A.1 MACHINE-NETWORK TRANSFORMATION

The machine-network transformation is expressed as

$$\begin{bmatrix} F_{di} \\ F_{qi} \end{bmatrix} = \begin{bmatrix} \sin \delta_i & -\cos \delta_i \\ \cos \delta_i & \sin \delta_i \end{bmatrix} \begin{bmatrix} F_{Di} \\ F_{Qi} \end{bmatrix} \quad i = 1, 2, \dots, m$$

and

$$\begin{bmatrix} F_{Di} \\ F_{Qi} \end{bmatrix} = \begin{bmatrix} \sin \delta_i & \cos \delta_i \\ -\cos \delta_i & \sin \delta_i \end{bmatrix} \begin{bmatrix} F_{di} \\ F_{qi} \end{bmatrix} \quad i = 1, 2, \dots, m$$

where  $F$  can either be voltage  $V$  or current  $I$ . A graphical representation of the above equations is shown in Fig. A.1.

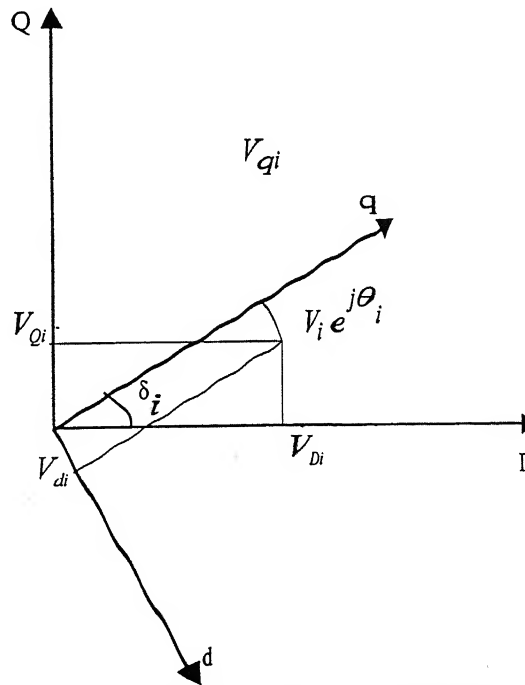


**Fig. A.1** Graphical representation of machine-network transformation

## A.2 DETAILS OF DAE MODEL

Differential equations (2.1-2.7) are linearized as

$$\frac{d\Delta\delta_i}{dt} = \Delta\omega_i \quad i = 1, 2, \dots, m \quad (\text{A.1})$$

$$\begin{aligned} \frac{d\Delta\omega_i}{dt} = & \frac{\Delta T_{Mi}}{M_i} - \frac{E'_{qio} \Delta I_{qi}}{M_i} + \frac{X'_{di} I_{dio} \Delta I_{qi}}{M_i} + \frac{X'_{qi} I_{qio} \Delta I_{di}}{M_i} \\ & - \frac{I_{qio} \Delta E'_{qi}}{M_i} - \frac{E'_{dio} \Delta I_{di}}{M_i} - \frac{I_{dio} \Delta E'_{di}}{M_i} - \frac{X'_{qi} I_{dio} \Delta_{qi}}{M_i} \\ & - \frac{X'_{qi} I_{qio} \Delta I_{di}}{M_i} - \frac{D_i \Delta\omega_i}{M_i} \quad i = 1, 2, \dots, m \end{aligned} \quad (\text{A.2})$$

$$\frac{d\Delta E'_{qi}}{dt} = \frac{-\Delta E'_{qi}}{T'_{doi}} - \frac{(X_{di} - X'_{di}) \Delta I_{di}}{T'_{doi}} + \frac{\Delta E_{fdi}}{T'_{doi}} \quad i = 1, 2, \dots, m \quad (\text{A.3})$$

$$\frac{d\Delta E'_{di}}{dt} = \frac{-\Delta E'_{di}}{T'_{qoi}} - \frac{(X_{qi} - X'_{qi}) \Delta I_{qi}}{T'_{qoi}} \quad i = 1, 2, \dots, m \quad (\text{A.4})$$

$$\frac{d\Delta E_{fdi}}{dt} = f_i(E_{fdio}) \Delta E_{fdi} + \frac{\Delta V_{Ri}}{T_{Ei}} \quad i = 1, 2, \dots, m \quad (\text{A.5})$$

$$\begin{aligned} \frac{d\Delta V_{Ri}}{dt} = & \frac{-\Delta V_{Ri}}{T_{Ai}} + \frac{K_{Ai} \Delta R_{Fi}}{T_{Ai}} - \frac{K_{Ai} K_{Fi} \Delta E_{fdi}}{T_{Ai} T_{Fi}} - \frac{K_{Ai} \Delta V_i}{T_{Ai}} \\ & + \frac{K_{Ai} \Delta V_{refi}}{T_{Ai}} \quad i = 1, 2, \dots, m \end{aligned} \quad (\text{A.6})$$

$$\frac{d\Delta R_{Fi}}{dt} = \frac{-\Delta R_{Fi}}{T_{Fi}} + \frac{K_{Fi} \Delta E_{fdi}}{(T_{Fi})^2} \quad i = 1, 2, \dots, m \quad (\text{A.7})$$

where

$$f_i(E_{fdio}) = \frac{-[K_{Ei} + E_{fdio} \partial S_E(E_{fdio}) + S_E(E_{fdio})]}{T_{Ei}}$$

and  $S_E(E_{fdi}) = A_{exi} e^{B_{exi} E_{fdi}}$

$A_{ex}$  and  $B_{ex}$  are saturation constants.

Equations (A.1-A.7) can be written in matrix notation as

$$\Delta \dot{X}_i = A_{1i} \Delta X_i + A_{2i} \Delta I_{gi} + A_{3i} \Delta V_{gi} + E_i \Delta U_i \quad i = 1, 2, \dots, m \quad (A.8)$$

where,  $\Delta I_{gi} = \begin{bmatrix} \Delta I_{di} \\ \Delta I_{qi} \end{bmatrix}$ ;  $\Delta V_{gi} = \begin{bmatrix} \Delta \theta_i \\ \Delta V_i \end{bmatrix}$ ; and  $\Delta U_i = \begin{bmatrix} \Delta T_{Mi} \\ \Delta V_{refi} \end{bmatrix}$

$$A_{1i} = \begin{bmatrix} 0 & 1 & 0 & 0 & 0 & 0 & 0 \\ 0 & \frac{-D_i}{M_i} & \frac{-I_{qio}}{M_i} & \frac{-I_{dio}}{M_i} & 0 & 0 & 0 \\ 0 & 0 & \frac{-1}{T'_{doi}} & 0 & \frac{1}{T'_{doi}} & 0 & 0 \\ 0 & 0 & 0 & \frac{-1}{T'_{qoi}} & 0 & 0 & 0 \\ 0 & 0 & 0 & 0 & f_i(E_{fdio}) & \frac{1}{T_{Ei}} & 0 \\ 0 & 0 & 0 & 0 & \frac{-K_{Ai}K_{Fi}}{T_{Ai}T_{Fi}} & \frac{-1}{T_{Ai}} & \frac{K_{Ai}}{T_{Ai}} \\ 0 & 0 & 0 & 0 & \frac{K_{Fi}}{(T_{Fi})^2} & 0 & \frac{-1}{T_{Fi}} \end{bmatrix}$$

$$A_{2i} = \begin{bmatrix} 0 & 0 \\ \frac{I_{qio}(X'_{di} - X'_{qi}) - E'_{dio}}{M_i} & \frac{I_{dio}(X'_{di} - X'_{qi}) - E'_{qio}}{M_i} \\ \frac{-(X_{di} - X'_{di})}{T'_{doi}} & 0 \\ 0 & \frac{(X_{qi} - X'_{qi})}{T'_{qoi}} \\ 0 & 0 \\ 0 & 0 \\ 0 & 0 \end{bmatrix}$$

$$A_{3i} = \begin{bmatrix} 0 & 0 \\ 0 & 0 \\ 0 & 0 \\ 0 & 0 \\ 0 & \frac{-K_{Ai}}{T_{Ai}} \\ 0 & 0 \end{bmatrix}, \quad E_i = \begin{bmatrix} 0 & 0 \\ \frac{1}{M_i} & 0 \\ 0 & 0 \\ 0 & 0 \\ 0 & \frac{K_{Ai}}{T_{Ai}} \\ 0 & 0 \end{bmatrix}$$

$$\Delta I_{gi} = \begin{bmatrix} \Delta I_{di} \\ \Delta I_{qi} \end{bmatrix}, \quad \Delta V_{gi} = \begin{bmatrix} \Delta \theta_i \\ \Delta V_i \end{bmatrix}, \quad \Delta U = \begin{bmatrix} \Delta T_{Mi} \\ \Delta V_{refi} \end{bmatrix}$$

$$\Delta X_i = [\Delta \delta_i \quad \Delta \omega_i \quad \Delta E'_{qi} \quad \Delta E'_{di} \quad \Delta E_{fdi} \quad \Delta V_{Ri} \quad \Delta R_{Fi}]^t$$

for  $i = 1, 2, \dots, m$

For m-machine system, (A.8) can be expressed as

$$\Delta \dot{X} = A_1 \Delta X + A_2 \Delta I_g + A_3 \Delta V_g + E \Delta U \quad (A.9)$$

$A_1$ ,  $A_2$ ,  $A_3$  and  $E$  are block diagonal matrices. For instance  $A_1$  is given by

$$A_1 = \begin{bmatrix} A_{11} & & & & & & \\ & A_{12} & & & & & \\ & & \ddots & & & & \\ & & & 0 & & & \\ & & & & \ddots & & \\ & 0 & & & & \ddots & \\ & & & & & & A_{1m} \end{bmatrix}$$

Linearization of (2.9) and (2.10) yields

$$\begin{aligned} \Delta E'_{di} - \sin(\delta_{io} - \theta_{io}) \Delta V_i - V_{io} \cos(\delta_{io} - \theta_{io}) \Delta \delta_i \\ + V_{io} \cos(\delta_{io} - \theta_{io}) \Delta \theta_i - R_{si} \Delta I_{di} + X'_{qi} \Delta I_{qi} = 0 \end{aligned} \quad i = 1, 2, \dots, m \quad (A.10)$$

$$\begin{aligned} \Delta E'_{qi} - \cos(\delta_{io} - \theta_{io}) \Delta V_i - V_{io} \sin(\delta_{io} - \theta_{io}) \Delta \delta_i \\ + V_{io} \sin(\delta_{io} - \theta_{io}) \Delta \theta_i - R_{si} \Delta I_{qi} - X'_{di} \Delta I_{di} = 0 \end{aligned} \quad i = 1, 2, \dots, m \quad (A.11)$$

Writing (A.10) and (A.11) in matrix form

$$0 = B_{1i} \Delta X_i + B_{2i} \Delta I_{gi} + B_{3i} \Delta V_{gi} \quad i = 1, 2, \dots, m \quad (A.12)$$

or

$$0 = B_1 \Delta X + B_2 \Delta I_g + B_3 \Delta V_g \quad (A.13)$$

where  $B_1$ ,  $B_2$  and  $B_3$  are block diagonal matrices. Various matrices of (A.12) are

$$B_{1i} = \begin{bmatrix} -V_{io} \cos(\delta_{io} - \theta_{io}) & 0 & 0 & 1 & 0 & 0 & 0 \\ V_{io} \sin(\delta_{io} - \theta_{io}) & 0 & 1 & 0 & 0 & 0 & 0 \end{bmatrix}$$

$$B_{2i} = \begin{bmatrix} -R_{si} & X'_{qi} \\ -X'_{di} & -R_{si} \end{bmatrix}$$

$$B_{3i} = \begin{bmatrix} V_{io} \cos(\delta_{io} - \theta_{io}) & -\sin(\delta_{io} - \theta_{io}) \\ -V_{io} \sin(\delta_{io} - \theta_{io}) & -\cos(\delta_{io} - \theta_{io}) \end{bmatrix}$$

Linearization of (2.13) and (2.14) gives

$$\begin{aligned} & V_{io} \sin(\delta_{io} - \theta_{io}) \Delta I_{di} + I_{dio} \sin(\delta_{io} - \theta_{io}) \Delta V_i \\ & + I_{dio} V_{io} \cos(\delta_{io} - \theta_{io}) \Delta \delta_i - I_{qio} V_{io} \sin(\delta_{io} - \theta_{io}) \Delta \delta_i \\ & + I_{qio} V_{io} \sin(\delta_{io} - \theta_{io}) \Delta \theta_i - I_{dio} V_{io} \cos(\delta_{io} - \theta_{io}) \Delta \theta_i \\ & + V_{io} \cos(\delta_{io} - \theta_{io}) \Delta I_{qi} + I_{qio} \cos(\delta_{io} - \theta_{io}) \Delta V_i \\ & - \left[ \sum_{k=1}^n V_{ko} Y_{ik} \cos(\theta_{io} - \theta_{ko} - \alpha_{ik}) \right] \Delta V_i - V_{io} \sum_{k=1}^n [Y_{ik} \cos(\theta_{io} - \theta_{ko} - \alpha_{ik})] \Delta V_k \\ & + \left[ V_{io} \sum_{\substack{k=1 \\ \neq i}}^n V_{ko} Y_{ik} \sin(\theta_{io} - \theta_{ko} - \alpha_{ik}) \right] \Delta \theta_i - V_{io} \sum_{\substack{k=1 \\ \neq i}}^n [V_{ko} Y_{ik} \sin(\theta_{io} - \theta_{ko} - \alpha_{ik})] \Delta \theta_k \\ & + \Delta P_{Li}(V_i) = 0 \quad i = 1, 2, \dots, m \end{aligned} \quad (A.14)$$

$$\begin{aligned} & V_{io} \sin(\delta_{io} - \theta_{io}) \Delta I_{di} + I_{dio} \sin(\delta_{io} - \theta_{io}) \Delta V_i + I_{dio} V_{io} \cos(\delta_{io} - \theta_{io}) \Delta \delta_i \\ & - I_{qio} V_{io} \sin(\delta_{io} - \theta_{io}) \Delta \delta_i + I_{qio} V_{io} \sin(\delta_{io} - \theta_{io}) \Delta \theta_i - I_{dio} V_{io} \cos(\delta_{io} - \theta_{io}) \Delta \theta_i \\ & + V_{io} \cos(\delta_{io} - \theta_{io}) \Delta I_{qi} + I_{qio} \cos(\delta_{io} - \theta_{io}) \Delta V_i \\ & - \left[ \sum_{k=1}^n V_{ko} Y_{ik} \cos(\theta_{io} - \theta_{ko} - \alpha_{ik}) \right] \Delta V_i - V_{io} \sum_{k=1}^n [Y_{ik} \cos(\theta_{io} - \theta_{ko} - \alpha_{ik})] \Delta V_k \\ & - \left[ V_{io} \sum_{\substack{k=1 \\ \neq i}}^n V_{ko} Y_{ik} \cos(\theta_{io} - \theta_{ko} - \alpha_{ik}) \right] \Delta \theta_i + V_{io} \sum_{\substack{k=1 \\ \neq i}}^n [V_{ko} Y_{ik} \cos(\theta_{io} - \theta_{ko} - \alpha_{ik})] \Delta \theta_k \\ & + \Delta Q_{Li}(V_i) = 0 \quad i = 1, 2, \dots, m \end{aligned} \quad (A.15)$$

Equations (A.14) and (A.15) are written in matrix form as

$$\begin{aligned}
0 = & C_{1i} \Delta X_i + C_{2i} \Delta I_{gi} + [C_{3i1} \ C_{3i2} \ \cdots \ C_{3im}] \begin{bmatrix} \Delta V_{g1} \\ \Delta V_{g2} \\ \vdots \\ \Delta V_{gm} \end{bmatrix} \\
& + [C_{4i,m} \ C_{4i,m+1} \ \cdots \ C_{4i,n}] \begin{bmatrix} \Delta V_{l,m+1} \\ \Delta V_{l,m+2} \\ \vdots \\ \Delta V_{l,n} \end{bmatrix} + \begin{bmatrix} \Delta P_{Li}(V_i) \\ \Delta Q_{Li}(V_i) \end{bmatrix} \quad i = 1, 2, \dots, m \quad (A.16)
\end{aligned}$$

For m machines (A.16) can be written as

$$\begin{aligned}
0 = & \begin{bmatrix} C_{11} & & & \\ & C_{12} & & \\ & & \ddots & \\ & & & C_{1m} \end{bmatrix} \begin{bmatrix} \Delta X_1 \\ \Delta X_2 \\ \vdots \\ \Delta X_m \end{bmatrix} + \begin{bmatrix} C_{21} & & & \\ & C_{22} & & \\ & & \ddots & \\ & & & C_{2m} \end{bmatrix} \begin{bmatrix} \Delta I_{g1} \\ \Delta I_{g2} \\ \vdots \\ \Delta I_{gm} \end{bmatrix} \\
& + \begin{bmatrix} C_{3,11} & C_{3,12} & \cdots & C_{3,1m} \\ \vdots & & & \vdots \\ \vdots & & & \vdots \\ C_{3,m1} & C_{3,m2} & & C_{3,mm} \end{bmatrix} \begin{bmatrix} \Delta V_{g1} \\ \Delta V_{g2} \\ \vdots \\ \Delta V_{gm} \end{bmatrix} \\
& + \begin{bmatrix} C_{4,1m+1} & C_{4,1m+2} & \cdots & C_{4,1n} \\ C_{4,2m+1} & & & \vdots \\ \vdots & & & \vdots \\ C_{4,mm+1} & C_{4,mm+2} & & C_{4,mn} \end{bmatrix} \begin{bmatrix} \Delta V_{lm+1} \\ \Delta V_{lm+2} \\ \vdots \\ \Delta V_{ln} \end{bmatrix} + \begin{bmatrix} \Delta P_{L1}(V_1) \\ \Delta Q_{L1}(V_1) \\ \vdots \\ \Delta P_{Lm}(V_m) \\ \Delta Q_{Lm}(V_m) \end{bmatrix} \quad (A.17)
\end{aligned}$$

Equation (A.17) can be written in a more compact form as

$$0 = C_1 \Delta X + C_2 \Delta I_g + C_3 \Delta V_g + C_4 \Delta V_l + \Delta S_{Lg}(V) \quad (A.18)$$

Linearizing (2.15) and (2.16), pertaining to load buses

$$\begin{aligned}
0 = & \Delta P_{Li}(V_i) - \left[ \sum_{k=1}^n V_{ko} Y_{ik} \cos(\theta_{io} - \theta_{ko} - \alpha_{ik}) \right] \Delta V_i \\
& + \left[ \sum_{\substack{k=1 \\ k \neq i}}^n V_{io} V_{ko} Y_{ik} \sin(\theta_{io} - \theta_{ko} - \alpha_{ik}) \right] \Delta \theta_i \\
& - V_{io} \sum_{k=1}^n [Y_{ik} \cos(\theta_{io} - \theta_{ko} - \alpha_{ik})] \Delta V_k \\
& - V_{io} \sum_{\substack{k=1 \\ k \neq i}}^n [V_{ko} Y_{ik} \sin(\theta_{io} - \theta_{ko} - \alpha_{ik})] \Delta \theta_k \quad i = m+1, \dots, n
\end{aligned} \tag{A.19}$$

$$\begin{aligned}
0 = & \Delta Q_{Li}(V_i) - \left[ \sum_{k=1}^n V_{ko} Y_{ik} \sin(\theta_{io} - \theta_{ko} - \alpha_{ik}) \right] \Delta V_i \\
& - \left[ \sum_{\substack{k=1 \\ k \neq i}}^n V_{io} V_{ko} Y_{ik} \cos(\theta_{io} - \theta_{ko} - \alpha_{ik}) \right] \Delta \theta_i \\
& - V_{io} \sum_{k=1}^n [Y_{ik} \sin(\theta_{io} - \theta_{ko} - \alpha_{ik})] \Delta V_k \\
& + V_{io} \sum_{\substack{k=1 \\ k \neq i}}^n [V_{ko} Y_{ik} \cos(\theta_{io} - \theta_{ko} - \alpha_{ik})] \Delta \theta_k \quad i = m+1, \dots, n
\end{aligned} \tag{A.20}$$

Equations (A.19) and (A.20) in matrix notation



$$\begin{aligned}
0 = & \begin{bmatrix} \Delta P_{Lm+1}(V_{m+1}) \\ \Delta Q_{Lm+1}(V_{m+1}) \\ \vdots \\ \Delta P_{Ln}(V_n) \\ \Delta Q_{Ln}(V_n) \end{bmatrix} + \begin{bmatrix} D_{1,m+1,1} & D_{1,m+1,2} & \cdots & D_{1,m+1,m} \\ D_{1,m+2,1} & D_{1,m+2,2} & \cdots & D_{1,m+2,m} \\ \vdots & \vdots & \vdots & \vdots \\ D_{1,n,1} & D_{1,n,2} & \cdots & D_{1,n,m} \end{bmatrix} \begin{bmatrix} \Delta V_{g1} \\ \Delta V_{g2} \\ \vdots \\ \Delta V_{gm} \end{bmatrix} \\
& + \begin{bmatrix} D_{2,m+1,m+1} & D_{2,m+1,m+2} & \cdots & D_{2,m+1,n} \\ D_{2,m+2,m+1} & D_{2,m+2,m+2} & \cdots & D_{2,m+2,n} \\ \vdots & \vdots & \vdots & \vdots \\ D_{2,n,m+1} & D_{2,n,m+2} & \cdots & D_{2,n,n} \end{bmatrix} \begin{bmatrix} \Delta V_{l,m+1} \\ \Delta V_{l,m+2} \\ \vdots \\ \Delta V_{l,n} \end{bmatrix} \quad (A.21)
\end{aligned}$$

or

$$0 = \Delta S_{Li}(V) + D_1 \Delta V_g + D_2 \Delta V_l \quad (A.22)$$

Rewriting (A.9), (A.13), (A.18) and (A.22) together

$$\Delta \dot{X} = A_1 \Delta X + A_2 \Delta I_g + A_3 \Delta V_g + E \Delta U \quad (A.23)$$

$$0 = B_1 \Delta X + B_2 \Delta I_g + B_3 \Delta V_g \quad (A.24)$$

$$0 = C_1 \Delta X + C_2 \Delta I_g + C_3 \Delta V_g + C_4 \Delta V_l + \Delta S_{Lg}(V) \quad (A.25)$$

$$0 = D_1 \Delta V_g + D_2 \Delta V_l + \Delta S_{Li}(V) \quad (A.26)$$

Equations (A.23-A.26) gives DAE model for the multi-machine system.

From (A.24),  $\Delta I_g$  is given as  $\Delta I_g = -B_2^{-1}(B_1 \Delta X + B_3 \Delta V_g)$ .

Substituting  $\Delta I_g$  in (A.23) and (A.25) the following equations are obtained.

$$\Delta \dot{X} = (A_1 - A_2 B_2^{-1} B_1) \Delta X + (A_3 - A_2 B_2^{-1} B_3) \Delta V_g + E \Delta U \quad (A.27)$$

$$0 = K_2 \Delta X + K_1 \Delta V_g + C_4 \Delta V_l + \Delta S_{Lg}(V) \quad (A.28)$$

where,  $K_1 \triangleq [C_3 - C_2 B_2^{-1} B_3]$ ; and  $K_2 \triangleq [C_1 - C_2 B_2^{-1} B_1]$

Equations (A.26-A.28) can be combined to form the DAE model as

$$\begin{bmatrix} \Delta \dot{X} \\ 0 \\ 0 \end{bmatrix} = \begin{bmatrix} (A_1 - A_2 B_2^{-1} B_1) & (A_3 - A_2 B_2^{-1} B_3) & 0 \\ K_2 & K_1 & C_4 \\ 0 & D_1 & D_2 \end{bmatrix} \begin{bmatrix} \Delta X \\ \Delta V_g \\ \Delta V_l \end{bmatrix} + \begin{bmatrix} 0 \\ \Delta S_{Lg}(V) \\ \Delta S_{Ll}(V) \end{bmatrix} + \begin{bmatrix} E \\ 0 \\ 0 \end{bmatrix} \Delta U \quad (A.29)$$

Equation (A.29) can be rewritten as

$$\begin{bmatrix} \Delta \dot{X} \\ 0 \\ 0 \end{bmatrix} = \begin{bmatrix} A_{1mod} & A_{2mod} & A_{3mod} \\ K_2 & K_1 & C_4 \\ G_1 & D_1 & D_2 \end{bmatrix} \begin{bmatrix} \Delta X \\ \Delta V_g \\ \Delta V_l \end{bmatrix} + \begin{bmatrix} 0 \\ \Delta S_{Lg} \\ \Delta S_{Ll} \end{bmatrix} + \begin{bmatrix} E \\ 0 \\ 0 \end{bmatrix} \Delta U \quad (A.30)$$

where

$$A_{1mod} = A_1 - A_2 B_2^{-1} B_1$$

$$A_{2mod} = A_3 - A_2 B_2^{-1} B_3$$

$A_{3mod}$  and  $G_1$  are null matrices.

A.3 DIALOG BOX OF DEVELOPED MATLAB PROGRAM

The dialog box of developed MATLAB program is shown below.

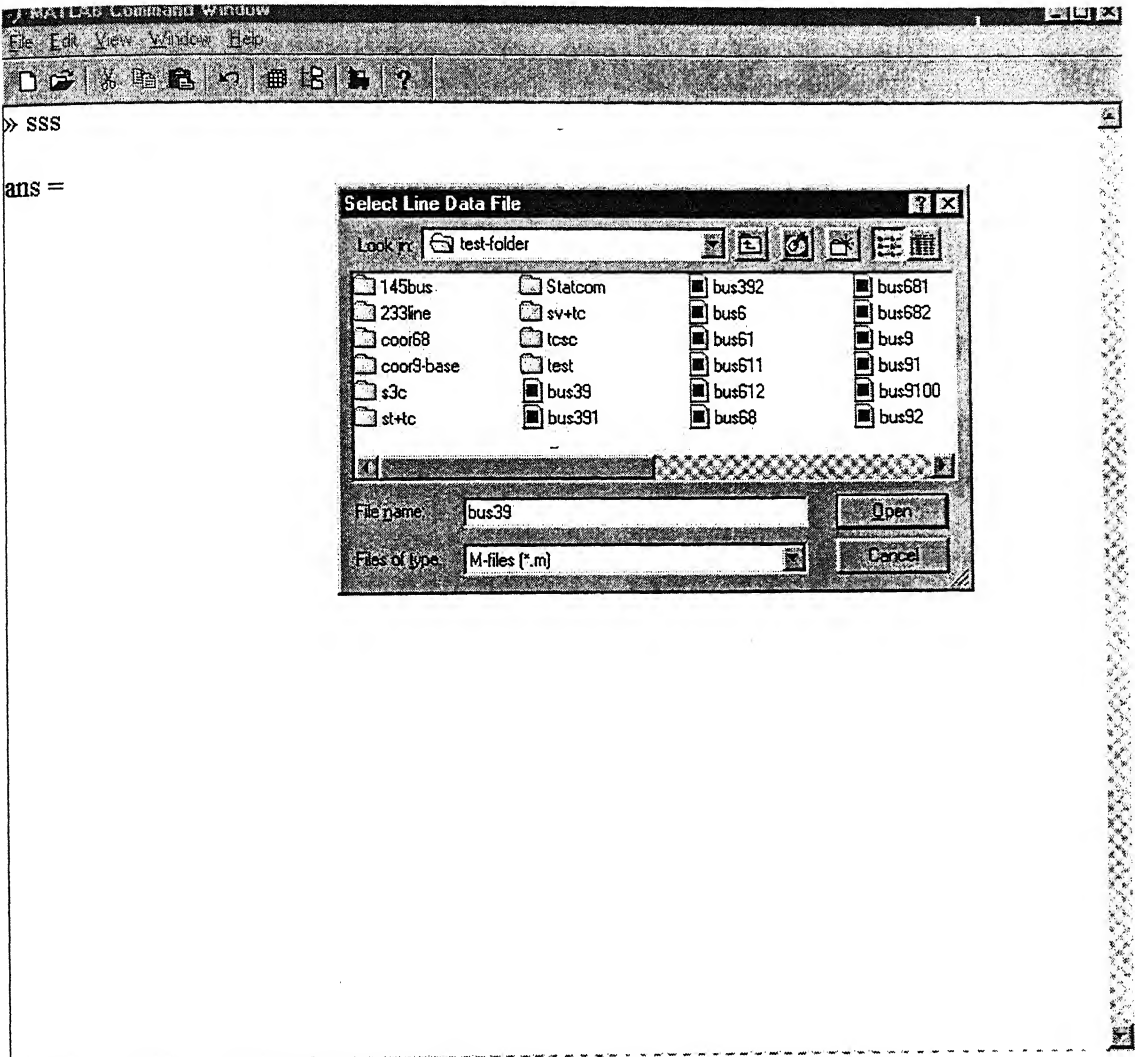
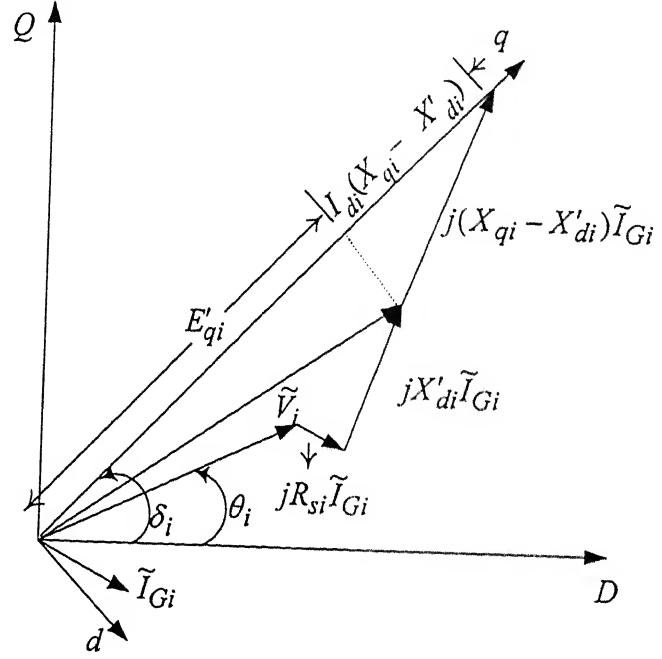


Fig. A.2 Dialog box of developed MATLAB program

## APPENDIX B

### CALCULATION OF INITIAL CONDITIONS

#### B.1 COMPUTATION OF INITIAL CONDITIONS FOR MULTIMACHINE SYSTEM



**Fig. B.1** Representation of stator algebraic equations in steady state

Phasor diagram of stator algebraic equations in steady state is shown in Fig. B.1. It is assumed that a load-flow solution of the system is available. Following steps are needed for computation of initial conditions. As an example, initial condition calculations for machine 1 of the WSCC 3-machine, 9-bus system are also presented [97].

##### Step 1 Calculation of generator currents

$$I_{Gi} e^{j\gamma_i} = \frac{(P_{Gi} - jQ_{Gi})}{\tilde{V}_i^*} \quad i = 1, 2, \dots, m$$

This current is in the network reference frame and is equal to  $(I_{di} + jI_{qi})e^{j(\delta_i - \pi/2)}$ .

**Step 2** *Calculation of rotor angle*

Rotor angle can be calculated from the “phasor diagram” as shown in Fig. B.1.

$$\delta_i = \text{angle of } (V_i e^{j\theta_i} + (R_{si} + jX_{qi}) I_{Gi} e^{j\gamma_i}) \quad i = 1, 2, \dots, m$$

**Step 3** *Calculation of  $I_{di}, I_{qi}, V_{di}, V_{qi}$* 

$$I_{di} + jI_{qi} = I_{Gi} e^{j(\gamma_i - \delta_i + \pi/2)} \quad i = 1, 2, \dots, m$$

$$V_{di} + jV_{qi} = V_i e^{j(\theta_i - \delta_i + \pi/2)} \quad i = 1, 2, \dots, m$$

**Step 4** *Calculation of  $E'_{di}$* 

$$E'_{di} = (X_{qi} - X'_{qi}) I_{qi} \quad i = 1, 2, \dots, m$$

**Step 5** *Calculation of  $E'_{qi}$* 

$$E'_{qi} = V_{qi} + R_{si} I_{qi} + X'_{di} I_{di} \quad i = 1, 2, \dots, m$$

**Step 6** *Calculation of  $E_{fdi}$* 

$$E_{fdi} = E'_{qi} + (X_{di} - X'_{di}) I_{di} \quad i = 1, 2, \dots, m$$

**Step 7** *Calculation of  $V_{Ri}, R_{Fi}, V_{refi}$  and  $T_{Mi}$* 

$$V_{Ri} = (K_{Ei} + S_{Ei}(E_{fdi})) E_{fdi} \quad i = 1, 2, \dots, m$$

## APPENDIX B

### CALCULATION OF INITIAL CONDITIONS

#### B.1 COMPUTATION OF INITIAL CONDITIONS FOR MULTIMACHINE SYSTEM

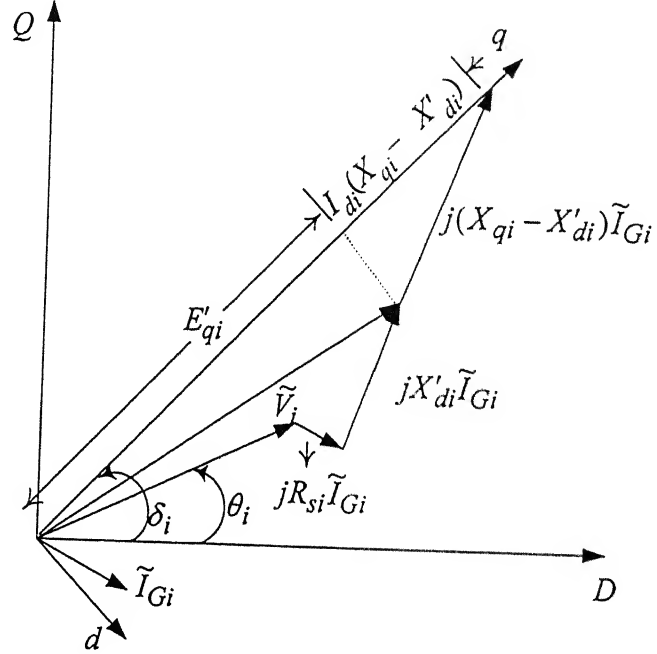


**Fig. B.1** Representation of stator algebraic equations in steady state

Phasor diagram of stator algebraic equations in steady state is shown in Fig. B.1. It is assumed that a load-flow solution of the system is available. Following steps are needed for computation of initial conditions. As an example, initial condition calculations for machine 1 of the WSCC 3-machine, 9-bus system are also presented [97].

##### Step 1 Calculation of generator currents

$$I_{Gi} e^{j\gamma_i} = \frac{(P_{Gi} - jQ_{Gi})}{\tilde{V}_i^*} \quad i = 1, 2, \dots, m$$

This current is in the network reference frame and is equal to  $(I_{di} + jI_{qi})e^{j(\delta_i - \pi/2)}$ .

**Step 2** *Calculation of rotor angle*

Rotor angle can be calculated from the “phasor diagram” as shown in Fig. B.1.

$$\delta_i = \text{angle of } (V_i e^{j\theta_i} + (R_{si} + jX_{qi}) I_{Gi} e^{j\gamma_i}) \quad i = 1, 2, \dots, m$$

**Step 3** *Calculation of  $I_{di}, I_{qi}, V_{di}, V_{qi}$* 

$$I_{di} + jI_{qi} = I_{Gi} e^{j(\gamma_i - \delta_i + \pi/2)} \quad i = 1, 2, \dots, m$$

$$V_{di} + jV_{qi} = V_i e^{j(\theta_i - \delta_i + \pi/2)} \quad i = 1, 2, \dots, m$$

**Step 4** *Calculation of  $E'_{di}$* 

$$E'_{di} = (X_{qi} - X'_{qi}) I_{qi} \quad i = 1, 2, \dots, m$$

**Step 5** *Calculation of  $E'_{qi}$* 

$$E'_{qi} = V_{qi} + R_{si} I_{qi} + X'_{di} I_{di} \quad i = 1, 2, \dots, m$$

**Step 6** *Calculation of  $E_{fdi}$* 

$$E_{fdi} = E'_{qi} + (X_{di} - X'_{di}) I_{di} \quad i = 1, 2, \dots, m$$

**Step 7** *Calculation of  $V_{Ri}, R_{Fi}, V_{refi}$  and  $T_{Mi}$* 

$$V_{Ri} = (K_{Ei} + S_{Ei}(E_{fdi})) E_{fdi} \quad i = 1, 2, \dots, m$$

$$R_{Fi} = \frac{K_{Fi} E_{fdi}}{T_{Fi}} \quad i = 1, 2, \dots, m$$

$$V_{refi} = V_i + \left( \frac{V_{Ri}}{K_{Ai}} \right) \quad i = 1, 2, \dots, m$$

$$T_{Mi} = E'_{di} I_{di} + E'_{qi} I_{qi} + (X'_{qi} - X'_{di}) I_{di} I_{qi} \quad i = 1, 2, \dots, m$$

This completes the computation of all dynamic-state initial conditions and fixed inputs.

## B.2 SAMPLE CALCULATION FOR MACHINE 1 OF WSCC SYSTEM

The load flow result at base case loading yields the following data for machine 1

$$P_{G1} = 0.716 \text{ (pu)}, \quad Q_{G1} = 0.27 \text{ (pu)}, \quad \tilde{V} = 1.04 \angle 0^\circ$$

Based on the procedure described in B.1, initial conditions for machine 1 are computed as

$$I_{G1} e^{j\gamma_1} = 0.736 \angle -20.66^\circ$$

$$\delta_1(0) = 3.58^\circ$$

$$I_{d1} = 0.302, \quad I_{q1} = 0.671$$

$$V_{d1} = 0.065, \quad V_{q1} = 1.038$$

$$E'_{d1} = 0$$

$$E'_{q1} = 1.056$$

$$E_{fd1} = 1.082$$

$$V_{R1} = 1.105, \quad R_{F1} = 0.195, \quad V_{ref1} = 1.095$$

$$T_{M1} = 0.716$$



## APPENDIX C

### SYSTEM DATA FOR WSCC 3-MACHINES, 9-BUS SYSTEM

The system data for base case loading are given below

Base MVA    100 MVA

#### Machine Data

PARAMETERS	M/C 1	M/C 2	M/C 3
$H(\text{sec})$	23.6400	6.4000	3.0100
$X_d(\text{pu})$	0.14600	0.8958	1.3125
$X'_d(\text{pu})$	0.06080	0.1198	0.1813
$X_q(\text{pu})$	0.09690	0.8645	1.2578
$X'_q(\text{pu})$	0.09690	0.1969	0.2500
$T'_{do}(\text{sec})$	8.96000	6.0000	5.8900
$T'_{qo}(\text{sec})$	0.31000	0.5350	0.6000

#### Exciter Data

PARAMETERS	EXCITER 1	EXCITER 2	EXCITER 3
$K_A$	20.0	20.0	20.0
$T_A(\text{sec})$	0.20	0.20	0.20
$K_e$	1.0	1.0	1.0
$T_e$	0.314	0.314	0.314
$K_f$	0.063	0.063	0.063
$T_f$	0.35	0.35	0.35
$R_s$	0	0	0
$A_{ex}$	0.0039	0.0039	0.0039
$B_{ex}$	1.555	1.555	1.555

$A_{ex}$  and  $B_{ex}$  are saturation constants.

### Line data

FROM	TO	R (pu)	X (pu)	Y/2 (pu)
1	4	0	0.0576	0
2	7	0	0.0625	0
3	9	0	0.0586	0
4	5	0.01	0.085	0.088
4	6	0.017	0.0920	0.079
5	7	0.032	0.161	0.153
6	9	0.039	0.17	0.179
7	8	0.0085	0.072	0.0745
8	9	0.0119	0.1008	0.1045

### Load Flow Result for Base Case of WSCC System on 100 MVA base

BUS	ANGLES (degree)	VOLTAGES (pu)	PL (pu)	QL (pu)	PG (pu)	QG (pu)
1	0	1.0400	0	0	0.7164	0.2705
2	9.3000	1.0250	0	0	1.630	0.0670
3	4.6648	1.0250	0	0	0.850	-0.1090
4	-2.2168	1.0258	0	0	0	0
5	-3.9888	0.9956	1.25	0.50	0	0
6	-3.6874	1.0127	0.90	0.30	0	0
7	3.7197	1.0258	0	0	0	0
8	0.7275	1.0159	1.00	0.35	0	0
9	1.9667	1.0324	0	0	0	0

## APPENDIX D

### SVC MODELING AND SYSTEM PARAMETERS

#### D.1 DETAILS OF SVC MODELING

Equations (3.5-3.7) can be written in matrix form as

$$\begin{aligned}
 \begin{bmatrix} \Delta \dot{X}_{1SVC} \\ \Delta \dot{X}_{2SVC} \\ \Delta \dot{X}_{3SVC} \end{bmatrix} &= \begin{bmatrix} \frac{-1}{T_m} & 0 & \frac{KV_{SVC0}}{T_m} \\ -K_I & 0 & 0 \\ \frac{-K_P}{T_c} & \frac{1}{T_c} & \frac{-1}{T_c} \end{bmatrix} \begin{bmatrix} \Delta X_{1SVC} \\ \Delta X_{2SVC} \\ \Delta X_{3SVC} \end{bmatrix} \\
 &+ \begin{bmatrix} \frac{1}{T_m}(1 + K X_{3SVC0}) \\ 0 \\ 0 \end{bmatrix} [\Delta V_{SVC}]
 \end{aligned} \tag{D.1}$$

Equation (D.1) can be written as

$$\Delta \dot{X}_{SVC} = A_{SVC} \Delta X_{SVC} + B_{SVC} \Delta V_{SVC} \tag{D.2}$$

where

$$A_{SVC} = \begin{bmatrix} \frac{-1}{T_m} & 0 & \frac{KV_{SVC0}}{T_m} \\ -K_I & 0 & 0 \\ \frac{-K_P}{T_c} & \frac{1}{T_c} & \frac{-1}{T_c} \end{bmatrix} \text{ and}$$

$$B_{SVC} = \begin{bmatrix} \frac{1}{T_m}(1 + K X_{3SVC0}) \\ 0 \\ 0 \end{bmatrix}$$

### *Network Equations of the System with SVC*

The SVC can be connected at either the existing load bus or at a new bus that is created between two buses. As DAE model is based on power-balance, rewriting of the power-balance equations at the load buses with SVC connected in the system requires modification of  $D_{2new}$  in (2.32). When SVC is connected at specified load buses, (2.15) and (2.16) get modified as given below

$$P_{SVCi} + P_{Li}(V_i) - \sum_{k=1}^n V_i V_k Y_{ik} \cos(\theta_i - \theta_k - \alpha_{ik}) = 0 \quad i = m+1, \dots, n \quad (D.3)$$

$$Q_{SVCi} + Q_{Li}(V_i) - \sum_{k=1}^n V_i V_k Y_{ik} \sin(\theta_i - \theta_k - \alpha_{ik}) = 0 \quad i = m+1, \dots, n \quad (D.4)$$

Equation (D.5) is obtained after linearization of (D.3) and (D.4) on the same lines as done in Appendix A.2.

$$C_{SVC} \Delta V_I + D_{SVC} \Delta X_{SVC} + D_1 \Delta V_g + D_2 \Delta V_I = 0 \quad (D.5)$$

or

$$D_{SVC} \Delta X_{SVC} + D_1 \Delta V_g + D_{2SVC} \Delta V_I = 0 \quad (D.6)$$

where  $D_{2SVC} = C_{SVC} + D_2$

Matrices  $D_1$  and  $D_2$  are defined in Appendix A.2. The size of these matrices will depend on the number of load buses in the power system. For example for the 9-bus system dimensions of  $D_1$  and  $D_2$  are  $14 \times 6$  and  $14 \times 14$  respectively. Dimensions of

$C_{SVC}$  and  $D_{SVC}$  will be  $14 \times 14$  and  $14 \times 3$  respectively,  $D_{SVC}$  is null matrix as  $P_{SVC}$  is zero and the entry in  $C_{SVC}$  matrix will depend at which bus the SVC is connected. If SVC is connected at bus 4,  $C_{SVC}(4,4)$  will have a non-zero entry.

Equations (D.2) and (D.6) are added to (2.30) and then reordered to get final form as

$$\begin{bmatrix} \Delta \dot{\mathbf{X}} \\ \Delta \dot{\mathbf{X}}_{SVC} \\ \mathbf{0} \\ \mathbf{0} \end{bmatrix} = \begin{bmatrix} \mathbf{A}_{1mod} & \mathbf{P}_{1svc} & \mathbf{A}_{2new} & \mathbf{A}_{3new} \\ \mathbf{P}_{2svc} & \mathbf{A}_{SVC} & \mathbf{P}_{3svc} & \mathbf{B}_{svcnew} \\ \mathbf{K}_2 & \mathbf{P}_{4svc} & \mathbf{K}_{1new} & \mathbf{C}_{4new} \\ \mathbf{G}_1 & \mathbf{D}_{SVC} & \mathbf{D}_{1new\_svc} & \mathbf{D}_{2new\_svc} \end{bmatrix} \begin{bmatrix} \Delta \mathbf{X} \\ \Delta \mathbf{X}_{SVC} \\ \Delta \mathbf{z} \\ \Delta \mathbf{v} \end{bmatrix} + \begin{bmatrix} \mathbf{E} \\ \mathbf{0} \\ \mathbf{0} \\ \mathbf{0} \end{bmatrix} \Delta \mathbf{U} \quad (\text{D.7})$$

Matrices  $\mathbf{A}_{1mod}$ ,  $\mathbf{A}_{2new}$ ,  $\mathbf{A}_{3new}$ ,  $\mathbf{K}_2$ ,  $\mathbf{K}_{1new}$ ,  $\mathbf{C}_{4new}$  and  $\mathbf{G}_1$  are defined in Appendix A.2. Matrices  $\mathbf{P}_{1svc}$ ,  $\mathbf{P}_{2svc}$  and  $\mathbf{P}_{4svc}$  are null matrices. Matrices  $\mathbf{P}_{3svc}$ ,  $\mathbf{B}_{svcnew}$ ,  $\mathbf{D}_{1new\_svc}$  and  $\mathbf{D}_{2new\_svc}$  are reordered matrices. In (D.7) dimensions of various matrices after reordering (for WSCC system with SVC connected at bus 4) are

$$\begin{bmatrix} 15 \times 15 & 15 \times 3 & 15 \times 4 & 15 \times 16 \\ 3 \times 15 & 3 \times 3 & 3 \times 4 & 3 \times 16 \\ 6 \times 15 & 6 \times 3 & 6 \times 4 & 6 \times 16 \\ 14 \times 16 & 14 \times 3 & 14 \times 4 & 14 \times 16 \end{bmatrix}$$

Let

$$A_{SV1} = \begin{bmatrix} A_{1mod} & P_{1svc} \\ P_{2svc} & A_{SVC} \end{bmatrix}, \quad A_{SV2} = \begin{bmatrix} A_{2new} & A_{3new} \\ P_{3svc} & B_{svcnew} \end{bmatrix}$$

$$A_{SV3} = \begin{bmatrix} K_2 & P_{4svc} \\ G_1 & D_{SVC} \end{bmatrix}, \quad A_{SV4} = \begin{bmatrix} K_{1new} & C_{4new} \\ D_{1new\_svc} & D_{2new\_svc} \end{bmatrix}$$

The state equation for the system with SVC is then given as follows

$$\Delta \dot{X}_{sys-svc} = A_{sys-svc} \Delta X_{sys-svc} + E_{SVC} \Delta U \quad (D.8)$$

where

$$A_{sys-svc} = A_{SV1} - (A_{SV2} * (inv(A_{SV4})) * A_{SV3}) \text{ and}$$

$$\Delta X_{sys-svc} = [\Delta X \quad \Delta X_{SVC}]^t$$

## D.2 SYSTEM DATA FOR WSCC 3-MACHINES, 9-BUS SYSTEM WITH SVC

Base MVA 100 MVA

Machine Data

PARAMETERS	M/C 1	M/C 2	M/C 3
$H(\text{sec})$	23.6400	6.4000	3.0100
$X_d(\text{pu})$	0.14600	0.8958	1.3125
$X'_d(\text{pu})$	0.06080	0.1198	0.1813
$X_q(\text{pu})$	0.09690	0.8645	1.2578
$X'_q(\text{pu})$	0.09690	0.1969	0.2500
$T'_{do}(\text{sec})$	8.96000	6.0000	5.8900
$T'_{qo}(\text{sec})$	0.31000	0.5350	0.6000
$D$	0.01254	0.0068	0.0048

**Exciter Data**

PARAMETERS	EXCITER 1	EXCITER 2	EXCITER 3
$K_A$	20.0	20.0	20.0
$T_A(\text{sec})$	0.20	0.20	0.20

**SVC Data**

$K$	$T_c$	$T_m$	$K_P$	$K_I$
0.1	0.02	0.02	0.0	100.0

**Line data**

FROM	TO	R (pu)	X (p.u.)	Y (pu)
1	5	0	0.0576	0
5	7	0.0170	0.0920	0.158
10	7	0.0390	0.1700	0.358
3	10	0	0.0586	0
10	9	0.0119	0.1008	0.209
8	9	0.0085	0.0720	0.149
8	2	0	0.0625	0
8	4	0.0160	0.0805	0.153
4	6	0.0160	0.0805	0.153
6	5	0.0100	0.0850	0.176

**Load Flow Result for Base Case of WSCC System with SVC at bus 4 on 100 MVA base**

BUS	ANGLES (degree)	VOLTAGES (pu)	PL (pu)	QL (pu)	PG (pu)	QG (pu)
1	0	1.0400	0	0	0.7163	0.2688
2	9.2499	1.0250	0	0	1.6300	0.0664
3	4.6470	1.0250	0	0	0.8500	-0.1089
4	-0.1600	1.0148	0	0	0	0
5	-2.2163	1.0259	0	0	0	0
6	-3.9822	0.9959	1.2500	0.5000	0	0
7	-3.6930	1.0127	0.9000	0.3000	0	0
8	3.6897	1.0258	0	0	0	0
9	0.7027	1.0159	1.0000	0.3500	0	0
10	1.9490	1.0324	0	0	0	0

# APPENDIX E

## DETAILS OF TCSC MODELING

### E.1 DETAILS OF (3.20)

Linearization of (3.18) and (3.19) yields

$$\Delta \dot{X}_{1TCSC} = \frac{-\Delta X_{1TCSC}}{T_{cl}} + \frac{\Delta X_{2TCSC}}{T_{cl}} - \frac{K_P \Delta P_k}{T_{cl}} \quad (E.1)$$

$$\Delta \dot{X}_{2TCSC} = -K_I \Delta P_k \quad (E.2)$$

As the TCSC controller is assumed lossless, the real power at the two ends of the bus is same. The real power feedback is taken from bus k.

Linearization of (3.12) yields

$$\begin{aligned} \Delta P_k = & \Delta V_k V_{mo} B_{TCSCo} \sin(\theta_{ko} - \theta_{mo}) \cdot \\ & + V_{ko} \Delta V_{mo} B_{TCSCo} \sin(\theta_{ko} - \theta_{mo}) \\ & + V_{ko} V_{mo} \Delta B_{TCSCo} \sin(\theta_{ko} - \theta_{mo}) \\ & + V_{ko} V_{mo} B_{TCSCo} \cos(\theta_{ko} - \theta_{mo}) \Delta \theta_k \\ & - V_{ko} V_{mo} B_{TCSCo} \cos(\theta_{ko} - \theta_{mo}) \Delta \theta_m \end{aligned}$$

Substituting value of  $\Delta P_k$  into (E.1) and (E.2) produces



$$\begin{aligned}
\Delta \dot{X}_{1TCSC} = & \frac{-\Delta X_{1TCSC}}{T_{cl}} + \frac{\Delta X_{2TCSC}}{T_{cl}} - \frac{K_P}{T_{cl}} \left[ \Delta V_k V_{mo} B_{TCSCo} \sin(\theta_{ko} - \theta_{mo}) \right. \\
& + V_{ko} \Delta V_{mo} B_{TCSCo} \sin(\theta_{ko} - \theta_{mo}) \\
& + V_{ko} V_{mo} \Delta B_{TCSCo} \sin(\theta_{ko} - \theta_{mo}) \\
& + V_{ko} V_{mo} B_{TCSCo} \cos(\theta_{ko} - \theta_{mo}) \Delta \theta_k \\
& \left. - V_{ko} V_{mo} B_{TCSCo} \cos(\theta_{ko} - \theta_{mo}) \Delta \theta_m \right]
\end{aligned} \tag{E.3}$$

$$\begin{aligned}
\Delta \dot{X}_{2TCSC} = & -K_I \left[ \Delta V_k V_{mo} B_{TCSCo} \sin(\theta_{ko} - \theta_{mo}) \right. \\
& + V_{ko} \Delta V_{mo} B_{TCSCo} \sin(\theta_{ko} - \theta_{mo}) \\
& + V_{ko} V_{mo} \Delta B_{TCSCo} \sin(\theta_{ko} - \theta_{mo}) \\
& + V_{ko} V_{mo} B_{TCSCo} \cos(\theta_{ko} - \theta_{mo}) \Delta \theta_k \\
& \left. - V_{ko} V_{mo} B_{TCSCo} \cos(\theta_{ko} - \theta_{mo}) \Delta \theta_m \right]
\end{aligned} \tag{E.4}$$

Writing (E.3) and (E.4) in matrix notation

$$\begin{bmatrix} \Delta \dot{X}_{1TCSC} \\ \Delta \dot{X}_{2TCSC} \end{bmatrix} = \mathbf{A}_{TCSC} \begin{bmatrix} \Delta X_{1TCSC} \\ \Delta X_{2TCSC} \end{bmatrix} + \mathbf{B}_{TCSC} \begin{bmatrix} \Delta \theta_k \\ \Delta V_k \\ \Delta \theta_m \\ \Delta V_m \end{bmatrix} \tag{E.5}$$

i.e.,

$$\Delta \dot{\mathbf{X}}_{TCSC} = \mathbf{A}_{TCSC} \Delta \mathbf{X}_{TCSC} + \mathbf{B}_{TCSC} \begin{bmatrix} \Delta \theta_k \\ \Delta V_k \\ \Delta \theta_m \\ \Delta V_m \end{bmatrix} \tag{E.6}$$

where  $\Delta \mathbf{X}_{TCSC} = \begin{bmatrix} \Delta X_{1TCSC} \\ \Delta X_{2TCSC} \end{bmatrix}$  and  $\mathbf{A}_{TCSC}$  and  $\mathbf{B}_{TCSC}$  are given as

$$\mathbf{A}_{TCSC} = \begin{bmatrix} \frac{-1}{T_{cl}} - \frac{K_P V_{ko} V_{mo} (FFCONS) \sin(\theta_{ko} - \theta_{mo})}{T_{cl}} & \frac{1}{T_{cl}} \\ -K_I V_{ko} V_{mo} (FFCONS) \sin(\theta_{ko} - \theta_{mo}) & 0 \end{bmatrix}$$

Details of *FFCONS* are given in Appendix E.2.

$$\mathbf{B}_{TCSC} = \begin{bmatrix} \mathcal{A} & \mathcal{B} & \mathcal{C} & \mathcal{D} \\ \mathcal{E} & \mathcal{F} & \mathcal{G} & \mathcal{H} \end{bmatrix}$$

$$\mathcal{A} = \frac{-K_P}{T_{cl}} [V_{ko} V_{mo} B_{TCSCo} \cos(\theta_{ko} - \theta_{mo})]$$

$$\mathcal{B} = \frac{-K_P}{T_{cl}} [V_{mo} B_{TCSCo} \sin(\theta_{ko} - \theta_{mo})]$$

$$\mathcal{C} = \frac{-K_P}{T_{cl}} [-V_{ko} V_{mo} B_{TCSCo} \cos(\theta_{ko} - \theta_{mo})]$$

$$\mathcal{D} = \frac{-K_P}{T_{cl}} [V_{ko} B_{TCSCo} \sin(\theta_{ko} - \theta_{mo})]$$

$$\mathcal{E} = -K_I [V_{ko} V_{mo} B_{TCSCo} \cos(\theta_{ko} - \theta_{mo})]$$

$$\mathcal{F} = -K_I [V_{mo} B_{TCSCo} \sin(\theta_{ko} - \theta_{mo})]$$

$$\mathcal{G} = -K_I [-V_{ko} V_{mo} B_{TCSCo} \cos(\theta_{ko} - \theta_{mo})]$$

$$\mathcal{H} = -K_I [V_{ko} B_{TCSCo} \sin(\theta_{ko} - \theta_{mo})]$$

## E.2 DETAILS OF CONSTANT *FFCONS*

Linearizing (3.16) gives

$$\Delta B_{TCSC} = (FFCONS) \Delta X_{1TCSC} \tag{E.7}$$

Details of *FFCONS* are obtained as shown below. It is to be noted that  $\alpha$  is also a state variable and is equal to  $\Delta X_{1TCSC}$  as shown in Fig. 3.11.

Linearization of (3.11) gives

$$\Delta B_{TCSC}(FF1) + \Delta X_{1TCSC}(FF2) = -\kappa\pi(\kappa^2 - 1)^2 \sin(\kappa\pi - \kappa X_{1TCSCo}) \Delta X_{1TCSC}$$

or

$$\Delta B_{TCSC} = \left[ \frac{-FF2 - \kappa\pi(\kappa^2 - 1)^2 \sin(\kappa\pi - \kappa X_{1TCSCo}) \Delta X_{1TCSC}}{FF1} \right] \Delta X_{1TCSC}$$

or

$$\Delta B_{TCSC} = (FFCONS) \Delta X_{1TCSC} \quad (E.8)$$

where

$$FFCONS = \left[ \frac{-FF2 - \kappa\pi(\kappa^2 - 1)^2 \sin(\kappa\pi - \kappa X_{1TCSCo}) \Delta X_{1TCSC}}{FF1} \right]$$

*FF1* and *FF2* are computed as

$$\begin{aligned} FF1 = & X_c \pi \kappa^4 \cos(\kappa\pi - \kappa X_{1TCSCo}) \\ & - X_c \pi \cos(\kappa\pi - \kappa X_{1TCSCo}) \\ & - 2\kappa^4 X_{1TCSCo} \cos(\kappa\pi - \kappa X_{1TCSCo}) X_c \\ & + 2\kappa^2 X_{1TCSCo} \cos(\kappa\pi - \kappa X_{1TCSCo}) X_c \\ & - 2\kappa^4 \sin(X_{1TCSCo}) \cos(X_{1TCSCo}) \cos(\kappa\pi - \kappa X_{1TCSCo}) X_c \\ & - 4\kappa^3 \cos^2(X_{1TCSCo}) \sin(\kappa\pi - \kappa X_{1TCSCo}) X_c \\ & - 4\kappa^2 \sin(X_{1TCSCo}) \cos(X_{1TCSCo}) \cos(\kappa\pi - \kappa X_{1TCSCo}) X_c \\ & + 2\kappa^2 \sin(X_{1TCSCo}) \cos(X_{1TCSCo}) \cos(\kappa\pi - \kappa X_{1TCSCo}) X_c \end{aligned}$$

$$\begin{aligned}
FF2 = & \kappa^5 B_{TCSCo} X_c \pi \sin(\kappa\pi - \kappa X_{1TCSCo}) \\
& - \kappa B_{TCSCo} X_c \pi \sin(\kappa\pi - \kappa X_{1TCSCo}) \\
& - 2\kappa^4 B_{TCSCo} X_c \cos(\kappa\pi - \kappa X_{1TCSCo}) \\
& - 2\kappa^5 X_{1TCSCo} B_{TCSCo} X_c \sin(\kappa\pi - \kappa X_{1TCSCo}) \\
& + 2\kappa^2 B_{TCSCo} X_c \cos(\kappa\pi - \kappa X_{1TCSCo}) \\
& + 2\kappa^3 X_{1TCSCo} B_{TCSCo} X_c \sin(\kappa\pi - \kappa X_{1TCSCo}) \\
& - 2\kappa^4 \cos^2(X_{1TCSCo}) B_{TCSCo} X_c \cos(\kappa\pi - \kappa X_{1TCSCo}) \\
& + 2\kappa^4 \sin^2(X_{1TCSCo}) B_{TCSCo} X_c \cos(\kappa\pi - \kappa X_{1TCSCo}) \\
& - 2\kappa^5 \sin(X_{1TCSCo}) \cos(X_{1TCSCo}) B_{TCSCo} X_c \sin(\kappa\pi - \kappa X_{1TCSCo}) \\
& + 8\kappa^3 \sin(X_{1TCSCo}) \cos(X_{1TCSCo}) B_{TCSCo} X_c \sin(\kappa\pi - \kappa X_{1TCSCo}) \\
& + 4\kappa^4 \cos^2(X_{1TCSCo}) B_{TCSCo} X_c \cos(\kappa\pi - \kappa X_{1TCSCo}) \\
& + 4\kappa^2 \sin^2(X_{1TCSCo}) B_{TCSCo} X_c \cos(\kappa\pi - \kappa X_{1TCSCo}) \\
& - 4\kappa^2 \cos^2(X_{1TCSCo}) B_{TCSCo} X_c \cos(\kappa\pi - \kappa X_{1TCSCo}) \\
& - 4\kappa^3 \sin(X_{1TCSCo}) \cos(X_{1TCSCo}) B_{TCSCo} X_c \sin(\kappa\pi - \kappa X_{1TCSCo}) \\
& + 2\kappa^2 \cos^2(X_{1TCSCo}) B_{TCSCo} X_c \cos(\kappa\pi - \kappa X_{1TCSCo}) \\
& - 2\kappa^2 \sin^2(X_{1TCSCo}) B_{TCSCo} X_c \cos(\kappa\pi - \kappa X_{1TCSCo}) \\
& + 2\kappa^3 \sin(X_{1TCSCo}) \cos(X_{1TCSCo}) B_{TCSCo} X_c \sin(\kappa\pi - \kappa X_{1TCSCo})
\end{aligned} \tag{E.9}$$

### E.3 DETAILS OF (3.21)

Linearizing (3.12-3.15) results in

$$\begin{aligned}
 \Delta P_k &= \Delta V_k V_{mo} B_{TCSCo} \sin(\theta_{ko} - \theta_{mo}) \\
 &+ V_{ko} \Delta V_{mo} B_{TCSCo} \sin(\theta_{ko} - \theta_{mo}) \\
 &+ V_{ko} V_{mo} \Delta B_{TCSCo} \sin(\theta_{ko} - \theta_{mo}) \\
 &+ V_{ko} V_{mo} B_{TCSCo} \cos(\theta_{ko} - \theta_{mo}) \Delta \theta_k \\
 &- V_{ko} V_{mo} B_{TCSCo} \cos(\theta_{ko} - \theta_{mo}) \Delta \theta_m
 \end{aligned} \tag{E.10}$$

$$\begin{aligned}
 \Delta Q_k &= 2V_{ko} B_{TCSCo} \Delta V_k + V_{ko}^2 \Delta B_{TCSC} \\
 &- \Delta V_k V_{mo} B_{TCSCo} \cos(\theta_{ko} - \theta_{mo}) \\
 &- V_{ko} \Delta V_m B_{TCSCo} \cos(\theta_{ko} - \theta_{mo}) \\
 &- V_{ko} V_{mo} \Delta B_{TCSC} \cos(\theta_{ko} - \theta_{mo}) \\
 &+ V_{ko} V_{mo} B_{TCSCo} \sin(\theta_{ko} - \theta_{mo}) \Delta \theta_k \\
 &- V_{ko} V_{mo} B_{TCSCo} \sin(\theta_{ko} - \theta_{mo}) \Delta \theta_m
 \end{aligned} \tag{E.11}$$

$$\begin{aligned}
 \Delta P_m &= \Delta V_k V_{mo} B_{TCSCo} \sin(\theta_{mo} - \theta_{ko}) \\
 &+ V_{ko} \Delta V_{mo} B_{TCSCo} \sin(\theta_{mo} - \theta_{ko}) \\
 &+ V_{ko} V_{mo} \Delta B_{TCSCo} \sin(\theta_{mo} - \theta_{ko}) \\
 &+ V_{ko} V_{mo} B_{TCSCo} \cos(\theta_{mo} - \theta_{ko}) \Delta \theta_m \\
 &- V_{ko} V_{mo} B_{TCSCo} \cos(\theta_{mo} - \theta_{ko}) \Delta \theta_k
 \end{aligned} \tag{E.12}$$

$$\begin{aligned}
\Delta Q_m = & 2V_{mo} B_{TCSCo} \Delta V_m + V_{mo}^2 \Delta B_{TCSC} \\
& - \Delta V_k V_{mo} B_{TCSCo} \cos(\theta_{mo} - \theta_{ko}) \\
& - V_{ko} \Delta V_m B_{TCSCo} \cos(\theta_{mo} - \theta_{ko}) \\
& - V_{ko} V_{mo} \Delta B_{TCSC} \cos(\theta_{mo} - \theta_{ko}) \\
& + V_{ko} V_{mo} B_{TCSCo} \sin(\theta_{mo} - \theta_{ko}) \Delta \theta_m \\
& - V_{ko} V_{mo} B_{TCSCo} \sin(\theta_{mo} - \theta_{ko}) \Delta \theta_k
\end{aligned} \tag{E.13}$$

Equations (E.10-E.13) can be written in matrix form.

$$\begin{bmatrix} \Delta P_k \\ \Delta Q_k \\ \Delta P_m \\ \Delta Q_m \end{bmatrix} = C_{TCSC} \Delta X_{TCSC} + D_{TCSC} \begin{bmatrix} \Delta \theta_k \\ \Delta V_k \\ \Delta \theta_m \\ \Delta V_m \end{bmatrix} \tag{E.14}$$

It is to be noted that  $C_{TCSC}$  is obtained after substituting value of  $\Delta B_{TCSC}$  from (E.7). Incorporation of (E.9), (E.14) and (2.30) gives DAE model of multimachine system with TCSC incorporated in the system. After reordering, final form of DAE model with TCSC is given as

$$\begin{bmatrix} \Delta \dot{X} \\ \Delta \dot{X}_{TCSC} \\ 0 \\ 0 \end{bmatrix} = \begin{bmatrix} A_{1mod} & P_{1tcsc} & A_{2new} & A_{3new} \\ P_{2tcsc} & A_{TCSC} & B_{tcsc1new} & B_{tcscnew} \\ K_2 & P_{4tcsc} & K_{1new} & C_{4new} \\ G_1 & C_{TCSC} & D_{1new\_tcsc} & D_{2new-tcsc} \end{bmatrix} \begin{bmatrix} \Delta X \\ \Delta X_{TCSC} \\ \Delta z \\ \Delta v \end{bmatrix} + \begin{bmatrix} E \\ 0 \\ 0 \end{bmatrix} \Delta U \tag{E.15}$$

Matrices  $A_{1mod}$ ,  $A_{2new}$ ,  $A_{3new}$ ,  $K_2$ ,  $K_{1new}$ ,  $C_{4new}$  and  $G_1$  are defined in Appendix A.2. Matrices  $P_{1tcsc}$ ,  $P_{2tcsc}$  and  $P_{4tcsc}$  are null matrices. Matrices  $B_{tcsc1new}$ ,  $B_{tcscnew}$ ,  $D_{1new\_tcsc}$  and  $D_{2new\_tcsc}$  are reordered matrices.

Let

$$A_{TC1} = \begin{bmatrix} A_{1mod} & P_{1tcsc} \\ P_{2tcsc} & A_{TCSC} \end{bmatrix}, \quad A_{TC2} = \begin{bmatrix} A_{2new} & A_{3new} \\ B_{tcsc1new} & B_{tcscnew} \end{bmatrix}$$

$$A_{TC3} = \begin{bmatrix} K_2 & P_{4tcsc} \\ G_1 & C_{TCSC} \end{bmatrix}, \quad A_{TC4} = \begin{bmatrix} K_{1new} & C_{4new} \\ D_{1new\_tcsc} & D_{2new\_tcsc} \end{bmatrix}$$

Thus from (E.12)

$$\Delta \dot{X}_{SYS-TCSC} = A_{SYS-TCSC} \Delta X_{SYS-TCSC} + E_{TCSC} \Delta U \quad (E.16)$$

where

$$E_{TCSC} = [E \quad 0 \quad 0]^t$$

$$A_{sys\_TCSC} = A_{TC1} - (A_{TC2} * (inv(A_{TC4})) * A_{TC3})$$

# APPENDIX F

## STATCOM MODELING

### F.1 DETAILS OF (3.36)

Equation (3.24) is rewritten as

$$\frac{d}{dt}i_{ast} = \frac{1}{L_{st}}[V_{at} - V_{ast} - R_{st}i_{ast}]$$

Substituting (3.27) in (F.1) gives

$$\frac{d}{dt}i_{ast} = \frac{V_{at}}{L_{st}} - \sigma \frac{16\sqrt{3}}{\pi L_{st}} V_{dc} \sin(\omega t + \alpha + \theta_t)] - \frac{R_{st}i_{ast}}{L_{st}}$$

Similarly

$$\frac{d}{dt}i_{bst} = \frac{V_{bt}}{L_{st}} - \sigma \frac{16\sqrt{3}}{\pi L_{st}} V_{dc} \sin(\omega t + \alpha + \theta_t - \frac{2\pi}{3})] - \frac{R_{st}i_{bst}}{L_{st}}$$

$$\frac{d}{dt}i_{cst} = \frac{V_{ct}}{L_{st}} - \sigma \frac{16\sqrt{3}}{\pi L_{st}} V_{dc} \sin(\omega t + \alpha + \theta_t + \frac{2\pi}{3})] - \frac{R_{st}i_{cst}}{L_{st}}$$

and from (3.34) and (3.35)

$$\begin{aligned} \frac{d}{dt}V_{dc} = & -\frac{V_{dc}}{R_{dc}C_{dc}} + \sigma \frac{16\sqrt{3}}{\pi C_{dc}} [\sin(\omega t + \alpha + \theta_t)i_{ast} + \sin(\omega t + \alpha + \theta_t - \frac{2\pi}{3})i_{bst} \\ & + \sin(\omega t + \alpha + \theta_t + \frac{2\pi}{3})i_{cst}] \end{aligned}$$

Writing (F.2-F.4) in matrix notation yields



$$\begin{aligned}
\begin{bmatrix} \dot{i}_{ast} \\ \dot{i}_{bst} \\ \dot{i}_{cst} \end{bmatrix} &= \begin{bmatrix} -\frac{R_{st}}{L_{st}} & 0 & 0 \\ 0 & -\frac{R_{st}}{L_{st}} & 0 \\ 0 & 0 & -\frac{R_{st}}{L_{st}} \end{bmatrix} \begin{bmatrix} i_{ast} \\ i_{bst} \\ i_{cst} \end{bmatrix} \\
&+ \begin{bmatrix} -KK_1 \sin \gamma & 0 & 0 \\ 0 & -KK_1 \sin(\gamma - 120^\circ) & 0 \\ 0 & 0 & -KK_1 \sin(\gamma + 120^\circ) \end{bmatrix} V_{dc} \\
&+ \begin{bmatrix} \frac{1}{L_{st}} & 0 & 0 \\ 0 & \frac{1}{L_{st}} & 0 \\ 0 & 0 & \frac{1}{L_{st}} \end{bmatrix} \begin{bmatrix} V_{at} \\ V_{bt} \\ V_{ct} \end{bmatrix}
\end{aligned} \tag{F.6}$$

where  $KK_1 = \sigma \frac{16\sqrt{3}}{\pi L_{st}}$  and  $\gamma = \omega t + \alpha + \theta_t$

Equation (F.6) can be written in state-space form as

$$\dot{\mathbf{X}}_{abc} = \mathbf{A}_{st} \mathbf{X}_{abc} + \mathbf{B}_{2st} V_{dc} + \mathbf{B}_{1st} \mathbf{U}_{abc} \tag{F.7}$$

where  $\mathbf{X}_{abc} = [i_{ast} \ i_{bst} \ i_{cst}]^t$ ,  $\mathbf{U}_{abc} = [V_{at} \ V_{bt} \ V_{ct}]^t$ ,

$$\mathbf{A}_{st} = \begin{bmatrix} -\frac{R_{st}}{L_{st}} & 0 & 0 \\ 0 & -\frac{R_{st}}{L_{st}} & 0 \\ 0 & 0 & -\frac{R_{st}}{L_{st}} \end{bmatrix},$$

$$B_{2st} = \begin{bmatrix} -KK_1 \sin \gamma & 0 & 0 \\ 0 & -KK_1 \sin(\gamma - 120^\circ) & 0 \\ 0 & 0 & -KK_1 \sin(\gamma + 120^\circ) \end{bmatrix}$$

$$B_{1st} = \begin{bmatrix} \frac{1}{L_{st}} & 0 & 0 \\ 0 & \frac{1}{L_{st}} & 0 \\ 0 & 0 & \frac{1}{L_{st}} \end{bmatrix}$$

Rewriting (F.5), the dc capacitor voltage can be written as

$$\dot{V}_{dc} = -\frac{V_{dc}}{R_{dc}C_{dc}} + KK_2 [\sin(\gamma)i_{ast} + \sin(\gamma - 120^\circ)i_{bst} + \sin(\gamma + 120^\circ)i_{cst}] \quad (F.8)$$

$$\text{where } KK_2 = \sigma \frac{16\sqrt{3}}{\pi C_{dc}}$$

Equations (F.7) and (F.8) are transformed into a synchronously rotating reference frame (DQO) using Park's transformation. The variables are scaled and then transformed [79]. The Park's transformation and scaled voltages and currents in the synchronously rotating reference frame are given below

$$T = T_{dgo} \triangleq \frac{2}{3} \begin{bmatrix} \cos \omega t & \cos(\omega t - \frac{2\pi}{3}) & \cos(\omega t + \frac{2\pi}{3}) \\ -\sin \omega t & -\sin(\omega t - \frac{2\pi}{3}) & -\sin(\omega t + \frac{2\pi}{3}) \\ \frac{1}{2} & \frac{1}{2} & \frac{1}{2} \end{bmatrix} \quad (F.9)$$

$$T^{-1} = T_{dqo}^{-1} \triangleq \frac{2}{3} \begin{bmatrix} \cos \omega t & -\sin \omega t & 1 \\ \cos(\omega t - \frac{2\pi}{3}) & -\sin(\omega t - \frac{2\pi}{3}) & 1 \\ \cos(\omega t + \frac{2\pi}{3}) & -\sin(\omega t + \frac{2\pi}{3}) & 1 \end{bmatrix} \quad (F.10)$$

Scaled voltages and currents are given as

$$\begin{bmatrix} V_D \\ V_Q \\ V_O \end{bmatrix} \triangleq \frac{1}{\sqrt{2}} T_{dqo} \begin{bmatrix} V_a \\ V_b \\ V_c \end{bmatrix} \quad (F.11)$$

$$\begin{bmatrix} I_D \\ I_Q \\ I_O \end{bmatrix} \triangleq \frac{1}{\sqrt{2}} T_{dqo} \begin{bmatrix} I_a \\ I_b \\ I_c \end{bmatrix} \quad (F.12)$$

In general, (F.11) and (F.12) can be written as

$$X_{DQO} = \frac{1}{\sqrt{2}} T X_{abc} \quad (F.13)$$

or

$$\dot{X}_{DQO} = \frac{1}{\sqrt{2}} T \dot{X}_{abc} + \frac{1}{\sqrt{2}} \dot{T} X_{abc} \quad (F.14)$$

Then

$$\frac{1}{\sqrt{2}} T \dot{X}_{abc} = \dot{X}_{DQO} - \frac{1}{\sqrt{2}} \dot{T} X_{abc} = \dot{X}_{DQO} - \frac{1}{\sqrt{2}} \dot{T} T^{-1} \sqrt{2} X_{DQO} \quad (F.15)$$

$$\frac{1}{\sqrt{2}} T \dot{X}_{abc} = \dot{X}_{DQO} - \dot{T} T^{-1} X_{DQO} \quad (F.16)$$

Pre-multiplying (F.7), following equations are obtained.

$$\frac{1}{\sqrt{2}}T\dot{X}_{abc} = \frac{1}{\sqrt{2}}TA_{st}X_{abc} + \frac{1}{\sqrt{2}}TB_{2st}V_{dc} + \frac{1}{\sqrt{2}}TB_{1st}U_{abc} \quad (F.17)$$

or

$$\frac{1}{\sqrt{2}}T\dot{X}_{abc} = \frac{1}{\sqrt{2}}TA_{st}TT^{-1}X_{abc} + \frac{1}{\sqrt{2}}TB_{2st}V_{dc} + \frac{1}{\sqrt{2}}TB_{1st}U_{abc} \quad (F.18)$$

Combining (F.16) and (F.18) we get

$$\dot{X}_{DQO} - \dot{T}T^{-1}X_{DQO} = \frac{1}{\sqrt{2}}TA_{st}TT^{-1}X_{abc} + \frac{1}{\sqrt{2}}TB_{2st}V_{dc} + \frac{1}{\sqrt{2}}TB_{1st}U_{abc}$$

i.e.

$$\dot{X}_{DQO} = \frac{1}{\sqrt{2}}TA_{st}TT^{-1}X_{abc} + \dot{T}T^{-1}X_{DQO} + \frac{1}{\sqrt{2}}TB_{2st}V_{dc} + \frac{1}{\sqrt{2}}TB_{1st}U_{abc}$$

i.e.

$$\dot{X}_{DQO} = A_{st}X_{DQO} + \dot{T}T^{-1}X_{DQO} + \frac{1}{\sqrt{2}}TB_{2st}V_{dc} + B_{1st}U_{DQO} \quad (F.19)$$

where

$$\dot{X}_{DQO} = [i_{Dst} \ i_{Qst} \ i_{Ost}]^t \text{ and } U_{DQO} = [V_{Dt} \ V_{Qt} \ V_{Ot}]^t$$

Now since

$$\dot{T}T^{-1} = \begin{bmatrix} 0 & \omega & 0 \\ -\omega & 0 & 0 \\ 0 & 0 & 0 \end{bmatrix} \text{ and } \frac{1}{\sqrt{2}}TB_{2st} = \begin{bmatrix} -\frac{KK_1 \sin(\alpha + \theta_t)}{\sqrt{2}} \\ \frac{KK_1 \cos(\alpha + \theta_t)}{\sqrt{2}} \\ 0 \end{bmatrix}$$

then (F.19) becomes

$$\dot{X}_{DQO} = A_{st} X_{DQO} + \begin{bmatrix} 0 & \omega & 0 \\ -\omega & 0 & 0 \\ 0 & 0 & 0 \end{bmatrix} X_{DQO} + \begin{bmatrix} -\frac{KK_1 \sin(\alpha + \theta_t)}{\sqrt{2}} \\ \frac{KK_1 \cos(\alpha + \theta_t)}{\sqrt{2}} \\ 0 \end{bmatrix} V_{dc} + B_{1st} U_{DQO} \quad (F.20)$$

Writing DQ components of STATCOM currents from (F.20)

$$\dot{i}_{Dst} = -\frac{R_{st}}{L_{st}} i_{Dst} + \omega i_{Qst} + \frac{1}{L_{st}} V_{Dt} - \frac{KK_1 \sin(\alpha + \theta_t)}{\sqrt{2}} V_{dc} \quad (F.21)$$

$$\dot{i}_{Qst} = -\frac{R_{st}}{L_{st}} i_{Qst} - \omega i_{Dst} + \frac{1}{L_{st}} V_{Dt} + \frac{KK_1 \cos(\alpha + \theta_t)}{\sqrt{2}} V_{dc} \quad (F.22)$$

Using (F.12), dc capacitor voltage (F.8) can be written as

$$\dot{V}_{dc} = -\frac{V_{dc}}{R_{dc} C_{dc}} + \frac{3 KK_2}{\sqrt{2}} [\sin(\alpha + \theta_t) i_{Dst} - \cos(\alpha + \theta_t) i_{Qst}] \quad (F.23)$$

Writing (F.21-F.23) in matrix notation

$$\begin{aligned}
\begin{bmatrix} i_{Dst} \\ i_{Qst} \\ \dot{V}_{dc} \end{bmatrix} &= \begin{bmatrix} -\frac{R_{st}}{L_{st}} & \omega & -\frac{KK_1 \sin(\alpha + \theta_t)}{\sqrt{2}} \\ -\omega & -\frac{R_{st}}{L_{st}} & \frac{KK_1 \cos(\alpha + \theta_t)}{\sqrt{2}} \\ \frac{3KK_2}{\sqrt{2}} \sin(\alpha + \theta_t) & -\frac{3KK_2}{\sqrt{2}} \cos(\alpha + \theta_t) & -\frac{1}{R_{dc}C_{dc}} \end{bmatrix} \begin{bmatrix} i_{Dst} \\ i_{Qst} \\ V_{dc} \end{bmatrix} \\
&+ \begin{bmatrix} \frac{1}{L_{st}} & 0 & 0 \\ 0 & \frac{1}{L_{st}} & 0 \\ 0 & 0 & 0 \end{bmatrix} \begin{bmatrix} V_{Dt} \\ V_{Qt} \\ 0 \end{bmatrix}
\end{aligned} \tag{F.24}$$

The quantities in (F.24) are actual values and must be converted in a common per unit base. Equation (F.24) involves an ac system and a dc system. The ac side quantities are defined on ac system MVA base and ac transmission line kV base. The dc side quantities are defined as [85,11].

$$V_{dc} (base) = \left( \frac{\pi \sqrt{2}}{\sigma 16 \sqrt{3}} \right) V_{ac} (base)$$

Thus on normalization, (F.24) becomes

$$\begin{bmatrix} i_{Dst} \\ i_{Qst} \\ \dot{V}_{dc} \end{bmatrix} = \begin{bmatrix} -\frac{\omega R_{st}}{X_{st}} & \omega & -\frac{\omega \sin(\alpha + \theta_t)}{X_{st}} \\ -\omega & -\frac{\omega R_{st}}{X_{st}} & \frac{\omega \cos(\alpha + \theta_t)}{X_{st}} \\ 3\omega X_{dc} \sin(\alpha + \theta_t) & -3\omega X_{dc} \cos(\alpha + \theta_t) & -\frac{\omega X_{dc}}{R_{dc}} \end{bmatrix} \begin{bmatrix} i_{Dst} \\ i_{Qst} \\ V_{dc} \end{bmatrix} \\
+ \begin{bmatrix} \frac{\omega}{X_{st}} & 0 & 0 \\ 0 & \frac{\omega}{X_{st}} & 0 \\ 0 & 0 & 0 \end{bmatrix} \begin{bmatrix} V_{Dt} \\ V_{Qt} \\ 0 \end{bmatrix} \quad (F.25)$$

where  $X_{st} = \omega L_{st}$  and  $X_{dc} = \frac{1}{\omega C_{dc}}$

In DAE multimachine model, the bus voltages are defined as

$$V_{Di} + jV_{Qi} = V_i e^{j\theta_i} = V_i (\cos \theta_i + j \sin \theta_i) \quad (F.26)$$

In multimachine model without any FACTS device, the states are machine states and variables are voltages and associated angles at various buses. In order to incorporate STATCOM model in multimachine system, the STATCOM model must be defined on the same lines, i.e., D and Q components of the bus voltage where the STATCOM is connected should be expressed in terms of voltage magnitude and associated angle.

Using (F.26), (F.25) can be written as

$$\begin{bmatrix} \dot{i}_{Dst} \\ \dot{i}_{Qst} \\ \dot{V}_{dc} \end{bmatrix} = \begin{bmatrix} -\frac{\omega R_{st}}{X_{st}} & \omega & -\frac{\omega \sin(\alpha + \theta_t)}{X_{st}} \\ -\omega & -\frac{\omega R_{st}}{X_{st}} & \frac{\omega \cos(\alpha + \theta_t)}{X_{st}} \\ 3\omega X_{dc} \sin(\alpha + \theta_t) & -3\omega X_{dc} \cos(\alpha + \theta_t) & -\frac{\omega X_{dc}}{R_{dc}} \end{bmatrix} \begin{bmatrix} i_{Dst} \\ i_{Qst} \\ V_{dc} \end{bmatrix} \\
+ \begin{bmatrix} \frac{\omega}{X_{st}} & 0 & 0 \\ 0 & \frac{\omega}{X_{st}} & 0 \\ 0 & 0 & 0 \end{bmatrix} \begin{bmatrix} V_t \cos \theta_t \\ V_t \sin \theta_t \\ 0 \end{bmatrix} \quad (F.27)$$

Here  $V_t$  and  $\theta_t$  denotes voltage and associated angle of the bus where STATCOM is connected.

Equation (F.27) can be rewritten as

$$\dot{i}_{Dst} = -\frac{\omega R_{st}}{X_{st}} i_{Dst} + \omega i_{Qst} - \frac{\omega \sin(\alpha + \theta_t)}{X_{st}} V_{dc} + \frac{\omega}{X_{st}} V_t \cos \theta_t \quad (F.28)$$

$$\dot{i}_{Qst} = -\omega i_{Dst} - \frac{\omega R_{st}}{X_{st}} i_{Qst} + \frac{\omega \cos(\alpha + \theta_t)}{X_{st}} V_{dc} + \frac{\omega}{X_{st}} V_t \sin \theta_t \quad (F.29)$$

$$\dot{V}_{dc} = 3\omega X_{dc} \sin(\alpha + \theta_t) i_{Dst} - 3\omega X_{dc} \cos(\alpha + \theta_t) i_{Qst} - \frac{\omega X_{dc}}{R_{dc}} V_{dc} \quad (F.30)$$

Now in order to get state-space model of the STATCOM, (F.28-F.30) must be linearized. The linearization results in

$$\begin{aligned} \Delta \dot{i}_{Dst} = & -\frac{\omega R_{st}}{X_{st}} \Delta i_{Dst} + \omega \Delta i_{Qst} - \frac{\omega \sin(\alpha_o + \theta_{to})}{X_{st}} \Delta V_{dc} - \frac{\omega}{X_{st}} V_{dco} \cos(\alpha_o + \theta_{to}) \Delta \alpha \\ & - \frac{\omega}{X_{st}} V_{dco} \cos(\alpha_o + \theta_{to}) \Delta \theta_t + \frac{\omega}{X_{st}} \cos \theta_{to} \Delta V_t - \frac{\omega}{X_{st}} V_{to} \sin \theta_{to} \Delta \theta_t \end{aligned} \quad (F.31)$$



$$\begin{aligned}\Delta i_{Qst} = & -\omega \Delta i_{Dst} - \frac{\omega R_{st}}{X_{st}} \Delta i_{Qst} + \frac{\omega \cos(\alpha_o + \theta_{to})}{X_{st}} \Delta V_{dc} - \frac{\omega}{X_{st}} V_{dco} \sin(\alpha_o + \theta_{to}) \Delta \alpha \\ & - \frac{\omega}{X_{st}} V_{dco} \sin(\alpha_o + \theta_{to}) \Delta \theta_t + \frac{\omega}{X_{st}} \sin \theta_{to} \Delta V_t + \frac{\omega}{X_{st}} V_{to} \cos \theta_{to} \Delta \theta_t\end{aligned}\quad (F.32)$$

$$\begin{aligned}\Delta \dot{V}_{dc} = & 3\omega X_{dc} \sin(\alpha_o + \theta_{to}) \Delta i_{Dst} + 3\omega X_{dc} i_{Dsto} \cos(\alpha_o + \theta_{to}) \Delta \alpha \\ & + 3\omega X_{dc} i_{Dsto} \cos(\alpha_o + \theta_{to}) \Delta \theta_t - 3\omega X_{dc} \cos(\alpha_o + \theta_{to}) \Delta i_{Qst} \\ & + 3\omega X_{dc} i_{Qsto} \sin(\alpha_o + \theta_{to}) \Delta \alpha + 3\omega X_{dc} i_{Qsto} \sin(\alpha_o + \theta_{to}) \Delta \theta_t \\ & - \frac{\omega X_{dc}}{R_{dc}} \Delta V_{dc}\end{aligned}\quad (F.33)$$

Writing (F.31-F.33) in matrix notation

$$\begin{aligned}\begin{bmatrix} \Delta i_{Dst} \\ \Delta i_{Qst} \\ \Delta \dot{V}_{dc} \end{bmatrix} = & \begin{bmatrix} -\frac{\omega R_{st}}{X_{st}} & \omega & -\frac{\omega \sin(\alpha_o + \theta_{to})}{X_{st}} \\ -\omega & -\frac{\omega R_{st}}{X_{st}} & \frac{\omega \cos(\alpha_o + \theta_{to})}{X_{st}} \\ 3\omega X_{dc} \sin(\alpha_o + \theta_{to}) & -3\omega X_{dc} \cos(\alpha_o + \theta_{to}) & -\frac{\omega X_{dc}}{R_{dc}} \end{bmatrix} \begin{bmatrix} \Delta i_{Dst} \\ \Delta i_{Qst} \\ \Delta V_{dc} \end{bmatrix} \\ & + \begin{bmatrix} -\frac{\omega}{X_{st}} V_{dco} \cos(\alpha_o + \theta_{to}) \\ -\frac{\omega}{X_{st}} V_{dco} \sin(\alpha_o + \theta_{to}) \\ 3\omega X_{dc} [i_{Dsto} \cos(\alpha_o + \theta_{to}) + i_{Qsto} \sin(\alpha_o + \theta_{to})] \end{bmatrix} [\Delta \alpha] \\ & + \begin{bmatrix} -\frac{\omega}{X_{st}} V_{dco} \cos(\alpha_o + \theta_{to}) - \frac{\omega}{X_{st}} V_{to} \sin \theta_{to} & \frac{\omega}{X_{st}} \cos \theta_{to} \\ -\frac{\omega}{X_{st}} V_{dco} \sin(\alpha_o + \theta_{to}) + \frac{\omega}{X_{st}} V_{to} \cos \theta_{to} & \frac{\omega}{X_{st}} \sin \theta_{to} \\ 3\omega X_{dc} [i_{Dsto} \cos(\alpha_o + \theta_{to}) + i_{Qsto} \sin(\alpha_o + \theta_{to})] & 0 \end{bmatrix} \begin{bmatrix} \Delta \theta_t \\ \Delta V_t \end{bmatrix}\end{aligned}\quad (F.34)$$

In compact form (F.34) can be written as

$$\Delta \dot{X}_{stcom} = L_{1stcom} \Delta X_{stcom} + L_{2stcom} \Delta \alpha + L_{3stcom} \Delta V_{st} \quad (F.35)$$

where

$$\Delta X_{stcom} = [\Delta i_{Dst} \quad \Delta i_{Qst} \quad \Delta V_{dc}]^t, \quad \Delta V_{st} = [\Delta \theta_t \quad \Delta V_t]^t$$

$$L_{1stcom} = \begin{bmatrix} -\frac{\omega R_{st}}{X_{st}} & \omega & -\frac{\omega \sin(\alpha_o + \theta_{to})}{X_{st}} \\ -\omega & -\frac{\omega R_{st}}{X_{st}} & \frac{\omega \cos(\alpha_o + \theta_{to})}{X_{st}} \\ 3\omega X_{dc} \sin(\alpha_o + \theta_{to}) & -3\omega X_{dc} \cos(\alpha_o + \theta_{to}) & -\frac{\omega X_{dc}}{R_{dc}} \end{bmatrix}$$

$$L_{2stcom} = \begin{bmatrix} -\frac{\omega}{X_{st}} V_{dco} \cos(\alpha_o + \theta_{to}) \\ -\frac{\omega}{X_{st}} V_{dco} \sin(\alpha_o + \theta_{to}) \\ 3\omega X_{dc} [i_{Dsto} \cos(\alpha_o + \theta_{to}) + i_{Qsto} \sin(\alpha_o + \theta_{to})] \end{bmatrix}$$

$$L_{3stcom} = \begin{bmatrix} -\frac{\omega}{X_{st}} V_{dco} \cos(\alpha_o + \theta_{to}) - \frac{\omega}{X_{st}} V_{to} \sin \theta_{to} & \frac{\omega}{X_{st}} \cos \theta_{to} \\ -\frac{\omega}{X_{st}} V_{dco} \sin(\alpha_o + \theta_{to}) + \frac{\omega}{X_{st}} V_{to} \cos \theta_{to} & \frac{\omega}{X_{st}} \sin \theta_{to} \\ 3\omega X_{dc} [i_{Dsto} \cos(\alpha_o + \theta_{to}) + i_{Qsto} \sin(\alpha_o + \theta_{to})] & 0 \end{bmatrix}$$

## F.2 DETAILS OF (3.46)

Simplifying (3.45)

$$P_{stcom} + jQ_{stcom} = V_t e^{j\theta_t} \left( \frac{V_{st} e^{j(\alpha+\theta_t)} - V_t e^{j\theta_t}}{R_{st} + jX_{st}} \right)^*$$

or

$$P_{stcom} + jQ_{stcom} = V_t e^{j\theta_t} \left( \frac{V_{st} e^{-j(\alpha+\theta_t)} - V_t e^{-j\theta_t}}{R_{st} - jX_{st}} \right)$$

The above equation can be simplified as

$$P_{stcom} + jQ_{stcom} = \frac{V_t V_{st} e^{-j\alpha} - V_t^2}{R_{st} - jX_{st}} \quad (F.36)$$

Now the ac side voltage  $V_{st}$  of STATCOM is related to dc link capacitor voltage  $V_{dc}$  by the relationship  $V_{st} = K_{st} V_{dc}$

where  $K_{st} = \frac{16}{\pi\sqrt{2}}$  and turns ratio  $\sigma = \frac{1}{\sqrt{3}}$

Equation (F.36) can be written as

$$P_{stcom} + jQ_{stcom} = \frac{V_t K_{st} V_{dc} e^{-j\alpha} - V_t^2}{R_{st} - jX_{st}}$$

i.e.,

$$P_{stcom} + jQ_{stcom} = \frac{V_t K_{st} V_{dc} (\cos \alpha - j \sin \alpha) - V_t^2}{R_{st} - jX_{st}}$$

The above equation can be written as

$$P_{stcom} + jQ_{stcom} = \frac{(V_t K_{st} V_{dc} \cos \alpha - jV_t K_{st} V_{dc} \sin \alpha - V_t^2)(R_{st} + jX_{st})}{R_{st}^2 + jX_{st}^2}$$

i.e.,

$$P_{stcom} + jQ_{stcom} = \frac{1}{R_{st}^2 + jX_{st}^2} \begin{pmatrix} V_t K_{st} V_{dc} R_{st} \cos \alpha - jV_t K_{st} V_{dc} R_{st} \sin \alpha \\ -V_t^2 R_{st} + jV_t K_{st} V_{dc} X_{st} \cos \alpha \\ + X_{st} V_t K_{st} V_{dc} \sin \alpha - jX_{st} V_t^2 \end{pmatrix} \quad (F.37)$$

Separating real and imaginary parts

$$P_{stcom} = \frac{1}{R_{st}^2 + jX_{st}^2} (V_t K_{st} V_{dc} R_{st} \cos \alpha - V_t^2 R_{st} + X_{st} V_t K_{st} V_{dc} \sin \alpha) \quad (F.38)$$

$$Q_{stcom} = \frac{1}{R_{st}^2 + jX_{st}^2} (-V_t K_{st} V_{dc} R_{st} \sin \alpha + V_t K_{st} V_{dc} X_{st} \cos \alpha - X_{st} V_t^2) \quad (F.39)$$

Linearization of the above two equations results in

$$\Delta P_{stcom} = \frac{1}{R_{st}^2 + jX_{st}^2} \begin{pmatrix} K_{st} R_{st} V_{dco} \cos \alpha_o \Delta V_t + K_{st} R_{st} V_{to} \cos \alpha_o \Delta V_{dc} \\ -K_{st} R_{st} V_{to} V_{dco} \sin \alpha_o \Delta \alpha - 2V_{to} R_{st} \Delta V_t \\ + K_{st} X_{st} V_{dco} \sin \alpha_o \Delta V_t + K_{st} X_{st} V_{to} \sin \alpha_o \Delta V_{dc} \\ + K_{st} X_{st} V_{to} V_{dco} \cos \alpha_o \Delta \alpha \end{pmatrix} \quad (F.40)$$

$$\Delta Q_{stcom} = \frac{1}{R_{st}^2 + jX_{st}^2} \begin{pmatrix} -K_{st} R_{st} V_{dco} \sin \alpha_o \Delta V_t - K_{st} R_{st} V_{to} \sin \alpha_o \Delta V_{dc} \\ -K_{st} R_{st} V_{to} V_{dco} \cos \alpha_o \Delta \alpha + K_{st} X_{st} V_{dco} \cos \alpha_o \Delta V_t \\ + K_{st} X_{st} V_{to} \cos \alpha_o \Delta V_{dc} - K_{st} X_{st} V_{to} V_{dco} \sin \alpha_o \Delta \alpha \\ - 2X_{st} V_{to} \Delta V_t \end{pmatrix} \quad (F.41)$$

In matrix notation (F.40) and (F.41) can be written as

$$\begin{aligned}
\begin{bmatrix} \Delta P_{stcom} \\ \Delta Q_{stcom} \end{bmatrix} &= \frac{1}{R_{st}^2 + jX_{st}^2} \begin{bmatrix} 0 & 0 & K_{st}R_{st}V_{to} \cos \alpha_o + K_{st}X_{st}V_{to} \sin \alpha_o \\ 0 & 0 & -K_{st}R_{st}V_{to} \sin \alpha_o + K_{st}X_{st}V_{to} \cos \alpha_o \end{bmatrix} \begin{bmatrix} \Delta I_{Dst} \\ \Delta I_{Qst} \\ \Delta V_{dc} \end{bmatrix} \\
&+ \frac{1}{R_{st}^2 + jX_{st}^2} \begin{bmatrix} -K_{st}R_{st}V_{to}V_{dco} \sin \alpha_o + K_{st}X_{st}V_{to}V_{dco} \cos \alpha_o \\ -K_{st}R_{st}V_{to}V_{dco} \cos \alpha_o - K_{st}X_{st}V_{to}V_{dco} \sin \alpha_o \end{bmatrix} [\Delta \alpha] \\
&+ \frac{1}{R_{st}^2 + jX_{st}^2} \begin{bmatrix} K_{st}R_{st}V_{dco} \cos \alpha_o - 2V_{to}R_{st} \\ 0 \\ 0 \\ -K_{st}R_{st}V_{dco} \sin \alpha_o \\ 0 \\ +K_{st}X_{st}V_{dco} \cos \alpha_o - 2X_{st}V_{to} \end{bmatrix} \begin{bmatrix} \Delta \theta_t \\ \Delta V_t \end{bmatrix} \quad (F.42)
\end{aligned}$$

In compact form this is written as

$$\begin{bmatrix} \Delta P_{stcom} \\ \Delta Q_{stcom} \end{bmatrix} = N_{1new} \Delta X_{stat} + N_3 \Delta \alpha + N_2 \Delta V_{st} \quad (F.43)$$

where

$$\Delta X_{stat} = [\Delta I_{Dst} \quad \Delta I_{Qst} \quad \Delta V_{dc}]^t$$

$$\Delta V_{st} = [\Delta \theta_t \quad \Delta V_t]^t$$

$$N_{1new} = \frac{1}{R_{st}^2 + jX_{st}^2} \begin{bmatrix} 0 & 0 & K_{st}R_{st}V_{to} \cos \alpha_o + K_{st}X_{st}V_{to} \sin \alpha_o \\ 0 & 0 & -K_{st}R_{st}V_{to} \sin \alpha_o + K_{st}X_{st}V_{to} \cos \alpha_o \end{bmatrix}$$

$$N_3 = \frac{1}{R_{st}^2 + jX_{st}^2} \begin{bmatrix} -K_{st}R_{st}V_{to}V_{dco} \sin \alpha_o + K_{st}X_{st}V_{to}V_{dco} \cos \alpha_o \\ -K_{st}R_{st}V_{to}V_{dco} \cos \alpha_o - K_{st}X_{st}V_{to}V_{dco} \sin \alpha_o \end{bmatrix}$$

$$N_2 = \frac{1}{R_{st}^2 + jX_{st}^2} \begin{bmatrix} K_{st}R_{st}V_{dco} \cos \alpha_o - 2V_{to}R_{st} \\ 0 \\ 0 \\ -K_{st}R_{st}V_{dco} \sin \alpha_o \\ 0 \\ +K_{st}X_{st}V_{dco} \cos \alpha_o - 2X_{st}V_{to} \end{bmatrix}$$

Again from (3.41)

$$\Delta\alpha = -K_{onst} \Delta X_{stat}$$

Therefore (F.43) can be written as

$$\begin{bmatrix} \Delta P_{stcom} \\ \Delta Q_{stcom} \end{bmatrix} = N_{1new} \Delta X_{stat} - N_3 K_{onst} \Delta X_{stat} + N_2 \Delta V_{st}$$

i.e.,

$$\begin{bmatrix} \Delta P_{stcom} \\ \Delta Q_{stcom} \end{bmatrix} = N_{1mod} \Delta X_{stat} + N_2 \Delta V_{st} \quad (F.44)$$

where

$$N_{1mod} = N_{1new} - N_3 K_{onst}$$

### F.3 Details of (3.51)

Equation (3.51) is rewritten as

$$\begin{bmatrix} \Delta \dot{X} \\ \Delta \dot{X}_{stat} \\ 0 \\ 0 \end{bmatrix} = \begin{bmatrix} A_{1mod} & P_{1stat} & A_{2new} & A_{3new} \\ P_{2stat} & A_{stnew} & B_{stat1new} & B_{statnew} \\ K_2 & P_{3stat} & K_{1new} & C_{4new} \\ G_1 & N_{1mod} & D_{1new\_stat} & D_{2new\_stat} \end{bmatrix} \begin{bmatrix} \Delta X \\ \Delta X_{stat} \\ \Delta z \\ \Delta v \end{bmatrix} + \begin{bmatrix} E \\ 0 \\ 0 \\ 0 \end{bmatrix} \Delta U \quad (F.45)$$

In (F.45), the dimensions of various matrices are not fixed and will depend on the type of system chosen. Matrices  $A_{1mod}$ ,  $A_{2new}$ ,  $A_{3new}$ ,  $K_2$ ,  $K_{1new}$ ,  $C_{4new}$  and  $G_1$  are

defined in Appendix A.2. Matrices  $P_{1stat}$ ,  $P_{2stat}$  and  $P_{3stat}$  are null matrices. Matrices

$B_{stat1new}$ ,  $B_{statnew}$ ,  $D_{1new\_stat}$  and  $D_{2new\_stat}$  are reordered matrices.

Let

$$T1 = \begin{bmatrix} A_{1mod} & P_{1stat} \\ P_{2stat} & A_{stnew} \end{bmatrix}, \quad T2 = \begin{bmatrix} A_{2new} & A_{3new} \\ B_{stat1new} & B_{statnew} \end{bmatrix}$$

$$T3 = \begin{bmatrix} K_2 & P_{3stat} \\ G_1 & N_{1mod} \end{bmatrix}, \quad T4 = \begin{bmatrix} K_{1new} & C_{4new} \\ D_{1new\_stat} & D_{2new\_stat} \end{bmatrix}$$

The state equation of the system with STATCOM can be written as

$$\Delta \dot{X}_{sys\_statcom} = A_{sys\_statcom} \Delta X_{sys\_statcom} + E_{stat} \Delta U \quad (F.46)$$

where

$$A_{sys\_statcom} = T1 - (T2 * (inv(T4)) * T3) \text{ and}$$

$$\Delta X_{sys\_stat} = [\Delta X \quad \Delta X_{stat}]^t$$

# APPENDIX G

## SSSC MODELING

### G.1 DETAILS OF (3.68)

Equation (G.1) is obtained on the same lines as (F.24)

$$\begin{bmatrix} i_{Dsc} \\ i_{Qsc} \\ \dot{V}_{dcsc} \end{bmatrix} = \begin{bmatrix} -\frac{\omega R_{sc}}{X_{sc}} & \omega & -\frac{\omega \sin \theta_f}{X_{sc}} \\ -\omega & -\frac{\omega R_{sc}}{X_{sc}} & \frac{\omega \cos \theta_f}{X_{sc}} \\ 3\omega X_{dcsc} \sin \theta_f & -3\omega X_{dcsc} \cos \theta_f & -\frac{\omega X_{dcsc}}{R_{dcsc}} \end{bmatrix} \begin{bmatrix} i_{Dsc} \\ i_{Qsc} \\ V_{dcsc} \end{bmatrix} + \begin{bmatrix} \frac{\omega}{X_{sc}} & 0 & 0 \\ 0 & \frac{\omega}{X_{sc}} & 0 \\ 0 & 0 & 0 \end{bmatrix} \begin{bmatrix} V_{Dtsc} \\ V_{Qtsc} \\ 0 \end{bmatrix} \quad (G.1)$$

where  $X_{sc} = \omega L_{sc}$  and  $X_{dcsc} = \frac{1}{\omega C_{dcsc}}$

In DAE multimachine model, the bus voltages are defined as

$$V_{Di} + jV_{Qi} = V_i e^{j\theta_i} = V_i (\cos \theta_i + j \sin \theta_i) \quad (G.2)$$

In order to incorporate SSSC model in multimachine system, SSSC model must be defined on the same lines, i.e., D and Q components of the sending and receiving end voltages should be expressed in terms of magnitude and associated angle. Sending and receiving end are two ends between which SSSC is connected.

Using (G.2), (G.1) can be written as



$$\begin{aligned}
\begin{bmatrix} i_{Dsc} \\ i_{Qsc} \\ \dot{V}_{dcsc} \end{bmatrix} &= \begin{bmatrix} -\frac{\omega R_{sc}}{X_{sc}} & \omega & -\frac{\omega \sin \theta_f}{X_{sc}} \\ -\omega & -\frac{\omega R_{sc}}{X_{sc}} & \frac{\omega \cos \theta_f}{X_{sc}} \\ 3\omega X_{dcsc} \sin \theta_f & -3\omega X_{dcsc} \cos \theta_f & -\frac{\omega X_{dcsc}}{R_{dcsc}} \end{bmatrix} \begin{bmatrix} i_{Dsc} \\ i_{Qsc} \\ V_{dcsc} \end{bmatrix} \\
&+ \begin{bmatrix} \frac{\omega}{X_{sc}} & 0 & 0 \\ 0 & \frac{\omega}{X_{sc}} & 0 \\ 0 & 0 & 0 \end{bmatrix} \begin{bmatrix} V_{ssc} \cos \theta_s \\ V_{ssc} \sin \theta_s \\ 0 \end{bmatrix} - \begin{bmatrix} \frac{\omega}{X_{sc}} & 0 & 0 \\ 0 & \frac{\omega}{X_{sc}} & 0 \\ 0 & 0 & 0 \end{bmatrix} \begin{bmatrix} V_{rsc} \cos \theta_r \\ V_{rsc} \sin \theta_r \\ 0 \end{bmatrix} \quad (G.3)
\end{aligned}$$

where  $V_{ssc}$  and  $V_{rsc}$  are magnitudes of sending end and receiving end voltages respectively,  $\theta_s$  and  $\theta_r$  are angles associated with sending and receiving end respectively.

Equation (G.3) can be rewritten as

$$\begin{aligned}
i_{Dsc} &= -\frac{\omega R_{sc}}{X_{sc}} i_{Dsc} + \omega i_{Qsc} - \frac{\omega \sin \theta_f}{X_{sc}} V_{dcsc} + \frac{\omega}{X_{sc}} V_{ssc} \cos \theta_s \\
&\quad - \frac{\omega}{X_{sc}} V_{rsc} \cos \theta_r \quad (G.4)
\end{aligned}$$

$$\begin{aligned}
i_{Qsc} &= -\omega i_{Dsc} - \frac{\omega R_{sc}}{X_{sc}} i_{Qsc} + \frac{\omega \cos \theta_f}{X_{sc}} V_{dcsc} + \frac{\omega}{X_{sc}} V_{ssc} \sin \theta_s \\
&\quad - \frac{\omega}{X_{sc}} V_{rsc} \sin \theta_r \quad (G.5)
\end{aligned}$$

$$\dot{V}_{dcsc} = 3\omega X_{dcsc} \sin \theta_f i_{Dsc} - 3\omega X_{dcsc} \cos \theta_f i_{Qsc} - \frac{\omega X_{dcsc}}{R_{dcsc}} V_{dcsc} \quad (G.6)$$

Linearizing (G.4-G.6)

$$\begin{aligned}
\Delta \dot{i}_{Dsc} = & -\frac{\omega R_{sc}}{X_{sc}} \Delta i_{Dsc} + \omega \Delta i_{Qsc} - \frac{\omega \sin \theta_{fo}}{X_{sc}} \Delta V_{dcsc} - \frac{\omega}{X_{sc}} V_{dcsc} \cos \theta_{fo} \Delta \theta_f \\
& + \frac{\omega}{X_{sc}} \cos \theta_{so} \Delta V_{ssc} - \frac{\omega}{X_{sc}} V_{ssc} \sin \theta_{so} \Delta \theta_s - \frac{\omega}{X_{sc}} \cos \theta_{ro} \Delta V_{rsc} \\
& + \frac{\omega}{X_{sc}} V_{rsc} \sin \theta_{ro} \Delta \theta_r
\end{aligned} \tag{G.7}$$

$$\begin{aligned}
\Delta \dot{i}_{Qsc} = & -\omega \Delta i_{Dsc} - \frac{\omega R_{sc}}{X_{sc}} \Delta i_{Qsc} + \frac{\omega \cos \theta_{fo}}{X_{sc}} \Delta V_{dcsc} - \frac{\omega}{X_{sc}} V_{dcsc} \sin \theta_{fo} \Delta \theta_f \\
& + \frac{\omega}{X_{sc}} \sin \theta_{so} \Delta V_{ssc} + \frac{\omega}{X_{sc}} V_{ssc} \cos \theta_{so} \Delta \theta_s - \frac{\omega}{X_{sc}} \sin \theta_{ro} \Delta V_{rsc} \\
& - \frac{\omega}{X_{sc}} V_{rsc} \cos \theta_{ro} \Delta \theta_r
\end{aligned} \tag{G.8}$$

$$\begin{aligned}
\Delta \dot{V}_{dcsc} = & 3\omega X_{dcsc} \sin \theta_{fo} \Delta i_{Dsc} + 3\omega X_{dcsc} i_{Dsc} \cos \theta_{fo} \Delta \theta_f - 3\omega X_{dcsc} \cos \theta_{fo} \Delta i_{Qsc} \\
& + 3\omega X_{dcsc} i_{Qsc} \sin \theta_{fo} \Delta \theta_f - \frac{\omega X_{dcsc}}{R_{dcsc}} \Delta V_{dcsc}
\end{aligned} \tag{G.9}$$

Equations (G.7-G.9) can be written in matrix notation as

$$\Delta \dot{\mathbf{X}}_{sc} = \mathbf{M}_{1ssc} \Delta \mathbf{X}_{sc} + \mathbf{M}_{2ssc} \Delta \theta_f + \mathbf{M}_{3ssc} \Delta V_{ssc} \tag{G.10}$$

where

$$\Delta \mathbf{X}_{sc} = [\Delta i_{Dsc} \quad \Delta i_{Qsc} \quad \Delta V_{dcsc}]^t$$

$$\Delta V_{ssc} = [\Delta \theta_s \quad \Delta V_{ssc} \quad \Delta \theta_r \quad \Delta V_{rsc}]^t$$

$$\mathbf{M}_{1ssc} = \begin{bmatrix} -\frac{\omega R_{sc}}{X_{sc}} & \omega & -\frac{\omega}{X_{sc}} \sin \theta_{fo} \\ -\omega & -\frac{\omega R_{sc}}{X_{sc}} & \frac{\omega}{X_{sc}} \cos \theta_{fo} \\ 3\omega X_{dc} \sin \theta_{fo} & -3\omega X_{dc} \cos \theta_{fo} & -\frac{\omega X_{dcsc}}{R_{dcsc}} \end{bmatrix}$$

$$M_{2ssc} = \begin{bmatrix} -\frac{\omega}{X_{sc}} V_{dcsc} \cos \theta_{fo} \\ -\frac{\omega}{X_{sc}} V_{dcsc} \sin \theta_{fo} \\ 3 \omega X_{dc} (i_{Dsc} \cos \theta_{fo} + i_{Qsc} \sin \theta_{fo}) \end{bmatrix}$$

$$M_{3ssc} = \begin{bmatrix} -\frac{\omega}{X_{sc}} V_{ssco} \sin \theta_{so} & \frac{\omega}{X_{sc}} \cos \theta_{so} & \frac{\omega}{X_{sc}} V_{rsc} \sin \theta_{ro} & -\frac{\omega}{X_{sc}} \cos \theta_{ro} \\ \frac{\omega}{X_{sc}} V_{ssco} \cos \theta_{so} & \frac{\omega}{X_{sc}} \sin \theta_{so} & -\frac{\omega}{X_{sc}} V_{rsc} \cos \theta_{ro} & -\frac{\omega}{X_{sc}} \sin \theta_{ro} \\ 0 & 0 & 0 & 0 \end{bmatrix}$$

Equation (G.10) represents state-space model of SSSC without controller.

## G.2 DETAILS OF (3.78)

The SSSC is a series device. The complex power given by the SSSC to the system at any end can be written as

$$S = \tilde{V} \tilde{i}^* \quad (G.11)$$

where  $S$  is complex power.  $\tilde{V}$  is complex voltage of the bus (sending or receiving) and  $\tilde{i}^*$  is current flowing through the transmission line (direction of current is reverse when computing complex power for receiving end).

The power given by SSSC at the sending is given as

$$P_{ssc} + jQ_{ssc} = \tilde{V}_{ssc} \tilde{i}_{sc}^* \quad (G.12)$$

where  $P_{ssc}$  and  $Q_{ssc}$  are the real and reactive power at the sending end bus.  $\tilde{V}_{ssc}$  is the sending end complex voltage and  $\tilde{i}_{sc}^*$  is the current flowing through SSSC.  $\tilde{i}_{sc}^*$  is the line current.

Equation (G.12) is equivalent to

$$P_{ssc} + jQ_{ssc} = V_{ssc} e^{j\theta_s} \left[ \frac{V_{ssc} e^{j\theta_s} - V_{rsc} e^{j\theta_r} - V_{sc} e^{j\theta_f}}{R_{scl} + jX_{scl}} \right]^* \quad (G.13)$$

where  $V_{ssc}$ ,  $V_{rsc}$  and  $V_{sc}$  are the sending end, receiving end and injected voltage magnitudes respectively and  $\theta_s$ ,  $\theta_r$  and  $\theta_f$  are the angles associated with the sending end, receiving end and injected voltage respectively,  $R_{scl}$  and  $X_{scl}$  are the composite resistance and reactance of the line and SSSC together.

The above equation is simplified as

$$P_{ssc} + jQ_{ssc} = V_{ssc} e^{j\theta_s} \left[ \frac{V_{ssc} e^{-j\theta_s} - V_{rsc} e^{-j\theta_r} - V_{sc} e^{-j\theta_f}}{R_{scl} - jX_{scl}} \right]$$

or

$$P_{ssc} + jQ_{ssc} = \frac{V_{ssc}^2 - V_{ssc} V_{rsc} e^{j(\theta_s - \theta_r)} - V_{ssc} V_{sc} e^{j(\theta_s - \theta_f)}}{R_{scl} - jX_{scl}}$$

or

$$P_{ssc} + jQ_{ssc} = \frac{\left[ V_{ssc}^2 - V_{ssc} V_{rsc} e^{j(\theta_s - \theta_r)} - V_{ssc} V_{sc} e^{j(\theta_s - \theta_f)} \right] (R_{scl} + jX_{scl})}{R_{scl}^2 + X_{scl}^2} \quad (G.14)$$

Since  $R_{scl}$  is very small, it is neglected. Equation (G.14) then can be expanded as

$$P_{ssc} + jQ_{ssc} = \frac{\begin{bmatrix} V_{ssc}^2 - V_{ssc}V_{rsc}[\cos(\theta_s - \theta_r) + j\sin(\theta_s - \theta_r)] \\ -V_{ssc}V_{sc}[\cos(\theta_s - \theta_f) + j\sin(\theta_s - \theta_f)] \end{bmatrix} (jX_{scl})}{X_{scl}^2}$$

or

$$P_{ssc} + jQ_{ssc} = \frac{\begin{bmatrix} V_{ssc}^2 - V_{ssc}V_{rsc} \cos(\theta_s - \theta_r) - jV_{ssc}V_{rsc} \sin(\theta_s - \theta_r) \\ -V_{ssc}V_{sc} \cos(\theta_s - \theta_f) - jV_{ssc}V_{sc} \sin(\theta_s - \theta_f) \end{bmatrix} (jX_{scl})}{X_{scl}^2}$$

or

$$P_{ssc} + jQ_{ssc} = \frac{\begin{bmatrix} jV_{ssc}^2 - jV_{ssc}V_{rsc} \cos(\theta_s - \theta_r) + V_{ssc}V_{rsc} \sin(\theta_s - \theta_r) \\ -jV_{ssc}V_{sc} \cos(\theta_s - \theta_f) + V_{ssc}V_{sc} \sin(\theta_s - \theta_f) \end{bmatrix}}{X_{scl}} \quad (G.15)$$

Equating real and imaginary parts of (G.15)

$$P_{ssc} = \frac{[V_{ssc}V_{rsc} \sin(\theta_s - \theta_r) + V_{ssc}V_{sc} \sin(\theta_s - \theta_f)]}{X_{scl}} \quad (G.16)$$

$$Q_{ssc} = \frac{V_{ssc}^2 - V_{ssc}V_{rsc} \cos(\theta_s - \theta_r) - V_{ssc}V_{sc} \cos(\theta_s - \theta_f)}{X_{scl}} \quad (G.17)$$

The relationship between injected ac voltage magnitude  $V_{sc}$  and the dc link voltage of the capacitor of SSSC is given as  $V_{sc} = K_{sc} V_{dcsc}$

where  $K_{sc} = \frac{16}{\pi\sqrt{2}}$  and turns ratio  $\mu = \frac{1}{\sqrt{3}}$

Equations (G.18) and (G.19) are rewritten as

$$P_{ssc} = \frac{[V_{ssc}V_{rsc} \sin(\theta_s - \theta_r) + V_{ssc}K_{sc}V_{dcsc} \sin(\theta_s - \theta_f)]}{X_{scl}} \quad (G.18)$$

$$Q_{ssc} = \frac{V_{ssc}^2 - V_{ssc}V_{rsc} \cos(\theta_s - \theta_r) - V_{ssc}K_{sc}V_{dcsc} \cos(\theta_s - \theta_f)}{X_{scl}} \quad (G.19)$$

Linearization of (G.18) and (G.19) yields

$$\Delta P_{ssc} = \frac{1}{X_{scl}} \left[ \begin{aligned} &V_{rsc0} \sin(\theta_{so} - \theta_{ro}) \Delta V_{ssc} + V_{ssco} \sin(\theta_{so} - \theta_{ro}) \Delta V_{rsc} \\ &+ V_{ssco}V_{rsc0} \cos((\theta_{so} - \theta_{ro})\Delta\theta_s - V_{ssco}V_{rsc0} \cos((\theta_{so} - \theta_{ro})\Delta\theta_r \\ &+ K_{sc}V_{dcsc0} \sin(\theta_{so} - \theta_{fo}) \Delta V_{ssc} \\ &+ K_{sc}V_{ssco} \sin(\theta_{so} - \theta_{fo}) \Delta V_{dcsc} \\ &+ K_{sc}V_{ssco}V_{dcsc0} \cos(\theta_{so} - \theta_{fo}) \Delta\theta_s \\ &- K_{sc}V_{ssco}V_{dcsc0} \cos(\theta_{so} - \theta_{fo}) \Delta\theta_f \end{aligned} \right] \quad (G.20)$$

$$\Delta Q_{ssc} = \frac{1}{X_{scl}} \left[ \begin{aligned} &2V_{ssco} \Delta V_{ssc} \\ &-V_{rsc0} \cos(\theta_{so} - \theta_{ro}) \Delta V_{ssc} - V_{ssco} \cos(\theta_{so} - \theta_{ro}) \Delta V_{rsc} \\ &+ V_{ssco}V_{rsc0} \sin(\theta_{so} - \theta_{ro}) \Delta\theta_s \\ &- V_{ssco}V_{rsc0} \sin(\theta_{so} - \theta_{ro}) \Delta\theta_r \\ &- K_{sc}V_{dcsc0} \cos(\theta_{so} - \theta_{fo}) \Delta V_{ssc} \\ &- K_{sc}V_{ssco} \cos(\theta_{so} - \theta_{fo}) \Delta V_{dcsc} \\ &+ K_{sc}V_{ssco}V_{dcsc0} \sin(\theta_{so} - \theta_{fo}) \Delta\theta_s \\ &- K_{sc}V_{ssco}V_{dcsc0} \sin(\theta_{so} - \theta_{fo}) \Delta\theta_f \end{aligned} \right] \quad (G.21)$$

Equations (G.20) and (G.21) are written in matrix notation as

$$\begin{bmatrix} \Delta P_{ssc} \\ \Delta Q_{ssc} \end{bmatrix} = \mathbf{AMAT1} \Delta \mathbf{X}_{sc} + \mathbf{B}_{scl} \Delta \theta_f + \mathbf{C}_{sc} \Delta \mathbf{V}_{ssc} \quad (G.22)$$

where

$$\mathbf{AMAT1} = \frac{1}{X_{scl}} \begin{bmatrix} 0 & 0 & K_{sc}V_{ssco} \sin(\theta_{so} - \theta_{fo}) \\ 0 & 0 & -K_{sc}V_{ssco} \cos(\theta_{so} - \theta_{fo}) \end{bmatrix}$$

$$\Delta X_{sc} = [\Delta i_{Dsc} \quad \Delta i_{Qsc} \quad \Delta V_{dcsc}]^t$$

$$B_{scl} = \frac{1}{X_{scl}} \begin{bmatrix} -K_{sc} V_{ssco} V_{dcsc} \cos(\theta_{so} - \theta_{fo}) \\ -K_{sc} V_{ssco} V_{dcsc} \sin(\theta_{so} - \theta_{fo}) \end{bmatrix}$$

$$C_{sc} = \frac{1}{X_{scl}} \begin{bmatrix} C_{sc}(1,1) & C_{sc}(1,2) & C_{sc}(1,3) & C_{sc}(1,4) \\ C_{sc}(2,1) & C_{sc}(2,2) & C_{sc}(2,3) & C_{sc}(2,4) \end{bmatrix}$$

$$C_{sc}(1,1) = V_{ssco} V_{rsc} \cos((\theta_{so} - \theta_{ro}) + K_{sc} V_{ssco} V_{dcsc} \cos(\theta_{so} - \theta_{fo})$$

$$C_{sc}(1,2) = V_{rsc} \sin(\theta_{so} - \theta_{ro}) + K_{sc} V_{dcsc} \sin(\theta_{so} - \theta_{fo})$$

$$C_{sc}(1,3) = -V_{ssco} V_{rsc} \cos((\theta_{so} - \theta_{ro})$$

$$C_{sc}(1,4) = V_{ssco} \sin(\theta_{so} - \theta_{ro})$$

$$C_{sc}(2,1) = V_{ssco} V_{rsc} \sin(\theta_{so} - \theta_{ro}) + K_{sc} V_{ssco} V_{dcsc} \sin(\theta_{so} - \theta_{fo})$$

$$C_{sc}(2,2) = 2V_{ssco} - V_{rsc} \cos(\theta_{so} - \theta_{ro}) - K_{sc} V_{dcsc} \cos(\theta_{so} - \theta_{fo})$$

$$C_{sc}(2,3) = -V_{ssco} V_{rsc} \sin(\theta_{so} - \theta_{ro})$$

$$C_{sc}(2,4) = -V_{ssco} \cos(\theta_{so} - \theta_{ro})$$

$$\Delta V_{ssc} = [\Delta \theta_s \quad \Delta V_{ssc} \quad \Delta \theta_r \quad \Delta V_{rsc}]^t$$

The power delivered by the SSSC at the receiving end is given as

$$P_{rsc} + jQ_{rsc} = -\tilde{V}_{rsc} \tilde{i}_{sc}^* \quad (G.23)$$

where  $P_{rsc}$  and  $Q_{rsc}$  are the real and reactive power at the receiving end bus,  $\tilde{V}_{rsc}$  is receiving end complex voltage and  $\tilde{i}_{sc}^*$  is the current flowing through SSSC, which is also the line current. The above equation can be rewritten as

$$P_{rsc} + jQ_{rsc} = V_{rsc} e^{j\theta_r} \left[ \frac{V_{rsc} e^{j\theta_r} + V_{sc} e^{j\theta_f} - V_{ssc} e^{j\theta_s}}{R_{scl} + jX_{scl}} \right]^* \quad (G.24)$$

where  $V_{ssc}$ ,  $V_{rsc}$  and  $V_{sc}$  are the sending end, receiving end and injected voltage magnitudes respectively and  $\theta_s$ ,  $\theta_r$  and  $\theta_f$  are the angles associated with the sending end, receiving end and injected voltage respectively.

Simplifying (G.26) results in

$$P_{rsc} + jQ_{rsc} = V_{rsc} e^{j\theta_r} \left[ \frac{V_{rsc} e^{-j\theta_r} + V_{sc} e^{-j\theta_f} - V_{ssc} e^{-j\theta_s}}{R_{scl} - jX_{scl}} \right]$$

or

$$P_{rsc} + jQ_{rsc} = \frac{V_{rsc}^2 + V_{rsc} V_{sc} e^{j(\theta_r - \theta_f)} - V_{rsc} V_{ssc} e^{j(\theta_r - \theta_s)}}{R_{scl} - jX_{scl}}$$

or

$$P_{rsc} + jQ_{rsc} = \frac{\left[ V_{rsc}^2 + V_{rsc} V_{sc} e^{j(\theta_r - \theta_f)} - V_{rsc} V_{ssc} e^{j(\theta_r - \theta_s)} \right] (R_{scl} + jX_{scl})}{R_{scl}^2 + X_{scl}^2} \quad (G.25)$$

Neglecting  $R_{scl}$ , (G.25) can be modified and expanded as

$$P_{rsc} + jQ_{rsc} = \frac{\left[ V_{rsc}^2 + V_{rsc} V_{sc} [\cos(\theta_r - \theta_f) + j \sin(\theta_r - \theta_f)] \right. \\ \left. - V_{rsc} V_{ssc} [\cos(\theta_r - \theta_s) + j \sin(\theta_r - \theta_s)] \right] (jX_{scl})}{X_{scl}^2}$$

or

$$P_{rsc} + jQ_{rsc} = \frac{\left[ V_{rsc}^2 + V_{rsc} V_{sc} \cos(\theta_r - \theta_f) + j V_{rsc} V_{sc} \sin(\theta_r - \theta_f) \right. \\ \left. - V_{rsc} V_{ssc} \cos(\theta_r - \theta_s) - j V_{rsc} V_{ssc} \sin(\theta_r - \theta_s) \right] (jX_{scl})}{X_{scl}^2}$$

or



$$P_{rsc} + jQ_{rsc} = \frac{\begin{bmatrix} jV_{rsc}^2 + jV_{rsc}V_{sc} \cos(\theta_r - \theta_f) - V_{rsc}V_{sc} \sin(\theta_r - \theta_f) \\ -jV_{rsc}V_{ssc} \cos(\theta_r - \theta_s) + V_{rsc}V_{ssc} \sin(\theta_r - \theta_s) \end{bmatrix} (jX_{scl})}{X_{scl}^2} \quad (G.26)$$

Equating real and imaginary parts of (G.26) the following equations are obtained

$$P_{rsc} = \frac{[-V_{rsc}V_{sc} \sin(\theta_r - \theta_f) + V_{rsc}V_{ssc} \sin(\theta_r - \theta_s)]}{X_{scl}} \quad (G.27)$$

$$Q_{rsc} = \frac{V_{rsc}^2 + V_{rsc}V_{sc} \cos(\theta_r - \theta_f) - V_{rsc}V_{ssc} \cos(\theta_r - \theta_s)}{X_{scl}} \quad (G.28)$$

Using  $V_{sc} = K_{sc} V_{dcsc}$

where  $K_{sc} = \frac{16}{\pi\sqrt{2}}$  and  $\mu = \frac{1}{\sqrt{3}}$

$$P_{rsc} = \frac{[-V_{rsc}K_{sc}V_{dcsc} \sin(\theta_r - \theta_f) + V_{rsc}V_{ssc} \sin(\theta_r - \theta_s)]}{X_{scl}} \quad (G.29)$$

$$Q_{rsc} = \frac{V_{rsc}^2 + V_{rsc}K_{sc}V_{dcsc} \cos(\theta_r - \theta_f) - V_{rsc}V_{ssc} \cos(\theta_r - \theta_s)}{X_{scl}} \quad (G.30)$$

Linearizing (G.29) and (G.30) the following equations are obtained

$$\Delta P_{rsc} = \frac{1}{X_{scl}} \begin{bmatrix} -K_{sc}V_{dcsc} \sin(\theta_{ro} - \theta_{fo})\Delta V_{rsc} \\ -K_{sc}V_{rsc} \sin(\theta_{ro} - \theta_{fo})\Delta V_{dcsc} \\ -K_{sc}V_{rsc}V_{dcsc} \cos(\theta_{ro} - \theta_{fo})\Delta\theta_r \\ +K_{sc}V_{rsc}V_{dcsc} \cos(\theta_{ro} - \theta_{fo})\Delta\theta_f \\ +V_{ssc} \sin(\theta_{ro} - \theta_{so})\Delta V_{rsc} + V_{rsc} \sin(\theta_{ro} - \theta_{so})\Delta V_{ssc} \\ +V_{rsc}V_{ssc} \cos(\theta_{ro} - \theta_{so})\Delta\theta_r - V_{rsc}V_{ssc} \cos(\theta_{ro} - \theta_{so})\Delta\theta_s \end{bmatrix} \quad (G.31)$$

$$\Delta Q_{rsc} = \frac{1}{X_{scl}} \begin{bmatrix} 2V_{rsc0}\Delta V_{rsc} \\ + K_{sc}V_{dcsc0} \cos(\theta_{ro} - \theta_{fo})\Delta V_{rsc} \\ + K_{sc}V_{rsc0} \cos(\theta_{ro} - \theta_{fo})\Delta V_{dcsc} \\ - K_{sc}V_{rsc0}V_{dcsc0} \sin(\theta_{ro} - \theta_{fo})\Delta\theta_r \\ + K_{sc}V_{rsc0}V_{dcsc0} \sin(\theta_{ro} - \theta_{fo})\Delta\theta_f \\ - V_{ssco} \cos(\theta_{ro} - \theta_{so})\Delta V_{rsc} - V_{rsc0} \cos(\theta_{ro} - \theta_{so})\Delta V_{ssco} \\ + V_{rsc0}V_{ssco} \sin(\theta_{ro} - \theta_{so})\Delta\theta_r - V_{rsc0}V_{ssco} \sin(\theta_{ro} - \theta_{so})\Delta\theta_s \end{bmatrix} \quad (G.32)$$

Equations (G.31) and (G.32) are written in matrix notation as

$$\begin{bmatrix} \Delta P_{rsc} \\ \Delta Q_{rsc} \end{bmatrix} = \mathbf{AMAT2} \Delta \mathbf{X}_{sc} + \mathbf{B}_{sc2} \Delta\theta_f + \mathbf{C}_{rc} \Delta V_{ssco} \quad (G.33)$$

where

$$\mathbf{AMAT2} = \frac{1}{X_{scl}} \begin{bmatrix} 0 & 0 & -K_{sc}V_{rsc0} \sin(\theta_{ro} - \theta_{fo}) \\ 0 & 0 & K_{sc}V_{rsc0} \cos(\theta_{ro} - \theta_{fo}) \end{bmatrix}$$

$$\Delta \mathbf{X}_{sc} = [\Delta i_{Dsc} \quad \Delta i_{Qsc} \quad \Delta V_{dcsc}]^t$$

$$\mathbf{B}_{sc2} = \frac{1}{X_{scl}} \begin{bmatrix} K_{sc}V_{rsc0}V_{dcsc0} \cos(\theta_{ro} - \theta_{fo}) \\ K_{sc}V_{rsc0}V_{dcsc0} \sin(\theta_{ro} - \theta_{fo}) \end{bmatrix}$$

$$\mathbf{C}_{rc} = \frac{1}{X_{scl}} \begin{bmatrix} C_{rc}(1,1) & C_{rc}(1,2) & C_{rc}(1,3) & C_{rc}(1,4) \\ C_{rc}(2,1) & C_{rc}(2,2) & C_{rc}(2,3) & C_{rc}(2,4) \end{bmatrix}$$

$$C_{rc}(1,1) = -V_{rsc0}V_{ssco} \cos(\theta_{ro} - \theta_{so})$$

$$C_{rc}(1,2) = V_{rsc0} \sin(\theta_{ro} - \theta_{so})$$

$$C_{rc}(1,3) = -K_{sc}V_{rsc0}V_{dcsc0} \cos(\theta_{ro} - \theta_{fo}) + V_{rsc0}V_{ssco} \cos(\theta_{ro} - \theta_{so})$$

$$C_{rc}(1,4) = -K_{sc}V_{dcsc0} \sin(\theta_{ro} - \theta_{fo}) + V_{ssco} \sin(\theta_{ro} - \theta_{so})$$

$$C_{rc}(2,1) = -V_{rsc0}V_{ssco} \sin(\theta_{ro} - \theta_{so})$$

$$C_{rc}(2,2) = -V_{rsc0} \cos(\theta_{ro} - \theta_{so})$$

$$C_{rc}(2,3) = -K_{sc}V_{rsc0}V_{dcsc0} \sin(\theta_{ro} - \theta_{fo}) + V_{rsc0}V_{ssco} \sin(\theta_{ro} - \theta_{so})$$

$$C_{rc}(2,4) = 2V_{rsc0} + K_{sc}V_{dcsc0} \cos(\theta_{ro} - \theta_{fo}) - V_{ssc0} \cos(\theta_{ro} - \theta_{so})$$

$$\Delta V_{ssc} = [\Delta \theta_s \quad \Delta V_{ssc} \quad \Delta \theta_r \quad \Delta V_{rsc}]^t$$

Equations (G.22) and (G.33) are the required power equations of SSSC. In order to incorporate these equations in mutlimachine model, these equations are modified as

$$\begin{bmatrix} \Delta P_{ssc} \\ \Delta Q_{ssc} \end{bmatrix} = SSC\_1 \Delta X_{sssc} + B_{sc1} \Delta \theta_f + C_{sc} \Delta V_{ssc} \quad (G.34)$$

$$\begin{bmatrix} \Delta P_{rsc} \\ \Delta Q_{rsc} \end{bmatrix} = SSC\_2 \Delta X_{sssc} + B_{sc2} \Delta \theta_f + C_{rc} \Delta V_{ssc} \quad (G.35)$$

where  $SSC\_1 = [AMAT1 \quad 0]$  and  $SSC\_2 = [AMAT2 \quad 0]$

Eliminating  $\theta_f$  using (3.79) ,i.e.,  $\Delta \theta_f = -K_{onssc} \Delta X_{sssc}$  , (G.34) can be rewritten as

$$\begin{bmatrix} \Delta P_{ssc} \\ \Delta Q_{ssc} \end{bmatrix} = SSC\_1 \Delta X_{sssc} - B_{sc1} K_{onssc} \Delta X_{sssc} + C_{sc} \Delta V_{ssc}$$

or

$$\begin{bmatrix} \Delta P_{ssc} \\ \Delta Q_{ssc} \end{bmatrix} = A_{sssc1} \Delta X_{sssc} + C_{sc} \Delta V_{ssc} \quad (G.36)$$

where  $A_{sssc1} = SSC\_1 - B_{sc1} K_{onssc}$

In a similar way the (G.35) is written as

$$\begin{bmatrix} \Delta P_{rsc} \\ \Delta Q_{rsc} \end{bmatrix} = SSC\_2 \Delta X_{sssc} - B_{sc2} K_{onssc} \Delta X_{sssc} + C_{rc} \Delta V_{ssc}$$

$$\begin{bmatrix} \Delta P_{rsc} \\ \Delta Q_{rsc} \end{bmatrix} = A_{sssc2} \Delta X_{sssc} + C_{rc} \Delta V_{ssc} \quad (G.37)$$

where  $A_{sssc2} = SSC\_2 - B_{sc2} K_{onssc}$ . Combining (G.36) and (G.37) the following is obtained

$$\begin{bmatrix} \Delta P_{ssc} \\ \Delta Q_{ssc} \\ \Delta P_{rsc} \\ \Delta Q_{rsc} \end{bmatrix} = A_{SSSC1} \Delta X_{sssc} + A_{SSSC2} \Delta V_{ssc} \quad (G.38)$$

When SSSC is connected in the system between specified load buses, (2.15) and (2.16) get modified as shown below

$$P_{sssc i} + P_{Li}(V_i) - \sum_{k=1}^n V_i V_k Y_{ik} \cos(\theta_i - \theta_k - \alpha_{ik}) = 0 \quad i = m+1, \dots, n \quad (G.39)$$

$$Q_{sssc i} + Q_{Li}(V_i) - \sum_{k=1}^n V_i V_k Y_{ik} \sin(\theta_i - \theta_k - \alpha_{ik}) = 0 \quad i = m+1, \dots, n \quad (G.40)$$

Equation (G.41) is obtained after linearization of (G.39) and (G.40) on the same lines as done before

$$A_{sssc2\_new} \Delta V_{ssc} + A_{SSSC1} \Delta X_{sssc} + D_1 \Delta V_g + D_2 \Delta V_l = 0$$

where  $A_{sssc2\_new}$  incorporates  $A_{SSSC2}$  and has same dimension as  $D_2$ .  $V_{ssc}$  is a part of  $V_l$ . Above equation is rewritten as

$$A_{sssc1} \Delta X_{sssc} + D_1 \Delta V_g + D_{2sssc} \Delta V_l = 0 \quad (G.41)$$

where  $D_{2sssc} = A_{sssc2\_new} + D_2$

### G.3 DETAILS OF (3.80)

Equations (G.10) and (G.41) are added to (2.30) and then reordered to get final form as

$$\begin{bmatrix} \Delta \dot{X} \\ \Delta \dot{X}_{SSSC} \\ 0 \\ 0 \end{bmatrix} = \begin{bmatrix} A_{1mod} & P_{1SSSC} & A_{2new} & A_{3new} \\ P_{2SSSC} & A_{SSSCnew} & B_{SSSC1new} & B_{SSSCnew} \\ K_2 & P_{3SSSC} & K_{1new} & C_{4new} \\ G_1 & A_{SSSC1} & D_{1new\_SSSC} & D_{2new\_SSSC} \end{bmatrix} \begin{bmatrix} \Delta X \\ \Delta X_{SSSC} \\ \Delta z \\ \Delta v \end{bmatrix} + \begin{bmatrix} E \\ 0 \\ 0 \\ 0 \end{bmatrix} \Delta U \quad (G.42)$$

In (G.42) dimensions of various matrices are not fixed and will depend on the type of system chosen. Matrices  $A_{1mod}$ ,  $A_{2new}$ ,  $A_{3new}$ ,  $K_2$ ,  $K_{1new}$ ,  $C_{4new}$  and  $G_1$  are defined in Appendix A Sec. A.2. Matrices  $P_{1SSSC}$ ,  $P_{2SSSC}$  and  $P_{3SSSC}$  are null matrices. Matrices  $B_{SSSC1new}$ ,  $B_{SSSCnew}$ ,  $D_{1new\_SSSC}$  and  $D_{2new\_SSSC}$  are reordered matrices. Let

$$\begin{aligned} T_{SSC1} &= \begin{bmatrix} A_{1mod} & P_{1SSSC} \\ P_{2SSSC} & A_{SSSCnew} \end{bmatrix}, & T_{SSC2} &= \begin{bmatrix} A_{2new} & A_{3new} \\ B_{SSSC1new} & B_{SSSCnew} \end{bmatrix} \\ T_{SSC3} &= \begin{bmatrix} K_2 & P_{3SSSC} \\ G_1 & A_{SSSC1} \end{bmatrix}, & T_{SSC4} &= \begin{bmatrix} K_{1new} & C_{4new} \\ D_{1new\_SSSC} & D_{2new\_SSSC} \end{bmatrix} \end{aligned}$$

The state equation of the system with SSSC can be written as

$$\Delta \dot{X}_{sys\_SSSC} = A_{sys\_SSSC} \Delta X_{sys\_SSSC} + E_{SSC} \Delta U \quad (G.43)$$

where

$$A_{sys\_sssc} = T_{SSC1} - (T_{SSC2} * (inv(T_{SSC4})) * T_{SSC3}) \text{ and}$$

$$\Delta X_{sys\_sssc} = [\Delta X \quad \Delta X_{sssc}]^t$$

# APPENDIX H

## INCORPORATION OF MULTIPLE FACTS DEVICES

### H.1 DETAILS OF (3.81)

Equation (3.81) is given as

$$\begin{bmatrix} \Delta \dot{X} \\ \Delta \dot{X}_{SVC} \\ \Delta \dot{X}_{TCSC} \\ 0 \\ 0 \end{bmatrix} = \begin{bmatrix} A_{1mod} & P_{1svc} & P_{1tcsc} & A_{2new} & A_{3new} \\ P_{2svc} & A_{SVC} & P_{1svtc} & B_{svclnew} & B_{svcnew} \\ P_{2tcsc} & P_{2svtc} & A_{TCSC} & B_{tcsc1new} & B_{tcscnew} \\ K_2 & P_{4svc} & P_{4tcsc} & K_{1new} & C_{4new} \\ G_1 & D_{SVC} & C_{TCSC} & D_{1newsvtc} & D_{2newsvtc} \end{bmatrix} \begin{bmatrix} \Delta X \\ \Delta X_{SVC} \\ \Delta X_{TCSC} \\ 0 \\ 0 \end{bmatrix} + \begin{bmatrix} E \\ 0 \\ 0 \\ 0 \\ 0 \end{bmatrix} \Delta U \quad (H.1)$$

Matrices  $A_{1mod}$ ,  $A_{2new}$ ,  $A_{3new}$ ,  $K_2$ ,  $K_{1new}$ ,  $C_{4new}$  and  $G_1$  are defined in Appendix A Sec. A.2. Matrices  $P_{1svc}$ ,  $P_{2svc}$ ,  $P_{4svc}$ ,  $P_{1tcsc}$ ,  $P_{2tcsc}$ ,  $P_{4tcsc}$ ,  $P_{1svtc}$ ,  $P_{2svtc}$  are null matrices. Matrices  $B_{svclnew}$ ,  $B_{svcnew}$ ,  $B_{tcsc1new}$ ,  $B_{tcscnew}$ ,  $D_{1newsvtc}$  and  $D_{2newsvtc}$  are reordered matrices.

Let the following matrices be defined as

$$A_{SVTC1} = \begin{bmatrix} A_{1mod} & P_{1svc} & P_{1tcsc} \\ P_{2svc} & A_{SVC} & P_{1svtc} \\ P_{2tcsc} & P_{2svtc} & A_{TCSC} \end{bmatrix}$$

$$A_{SVTC2} = \begin{bmatrix} A_{2new} & A_{3new} \\ B_{svclnew} & B_{svcnew} \\ B_{tcsc1new} & B_{tcscnew} \end{bmatrix}$$

$$A_{SVTC3} = \begin{bmatrix} K_2 & P_{4svc} & P_{4tcsc} \\ G_1 & D_{SVC} & C_{TCSC} \end{bmatrix}$$

$$A_{SVTC4} = \begin{bmatrix} K_{1new} & C_{4new} \\ D_{1newsvtc} & D_{2newsvtc} \end{bmatrix}$$

Equation (H.1) can then be written as

$$\Delta \dot{X}_{SVTC} = A_{SVTC} \Delta X_{SVTC} + E_{SVTC} \Delta U \quad (H.2)$$

where

$$E_{SVTC} = [E \quad 0 \quad 0 \quad 0 \quad 0]^t$$

$$A_{SVTC} = A_{SVTC1} - (A_{SVTC2} * (inv(A_{SVTC4})) * A_{SVTC3})$$



# APPENDIX I

## SYSTEM DATA FOR 6-BUS SYSTEM

Base MVA    100 MVA

### Machine Data

Parameters	M/C 1	M/C 2
$H(\text{sec})$	54.0	23.640
$X_d(\text{pu})$	0.20	0.1460
$X'_d(\text{pu})$	0.033	0.0608
$X_q(\text{pu})$	0.190	0.0969
$X'_q(\text{pu})$	0.061	0.0969
$T'_{do}(\text{sec})$	8.0	8.96
$T'_{qo}(\text{sec})$	0.050	0.3100

### Exciter Data

Parameters	Exciter 1	Exciter 2
$K_A$	20.0	20.0
$T_A(\text{sec})$	0.20	0.20
$K_e$	1.0	1.0
$T_e$	0.314	0.314
$K_f$	0.063	0.063
$T_f$	0.35	0.35
$R_s$	0	0
$A_{ex}$	0.0039	0.0039
$B_{ex}$	1.555	1.555

$A_{ex}$  and  $B_{ex}$  are saturation constants.

Line data

Line number	Bus		Impedance	
	From	To	R (pu)	X (pu)
1	1	6	0.1020	0.4130
2	1	4	0.1100	0.4800
3	4	6	0.1200	0.5160
4	6	5	0.1900	0.8200
5	2	5	0.3680	1.4900
6	2	3	0.1150	0.5160
7	3	4	0.0800	0.3600

Load flow result at base case

Bus	Type	Angles (degree)	Voltages (pu)	PL (pu)	QL (pu)	PG (pu)	QG (pu)
1	SL	0	1.0000	0	0	0.6222	0.1820
2	PV	-1.9496	1.0000	0	0	0.4000	0.1464
3	PQ	-9.9409	0.9306	0.3800	0.0500	0	0
4	PQ	-7.2330	0.9419	0.1000	0.0200	0	0
5	PQ	-12.7897	0.8883	0.2000	0.0500	0	0
6	PQ	-8.4689	0.9298	0.3000	0.0300	0	0

LFIs at base case loading condition (6-bus system)

Line number	From bus	To bus	LFISP	LFISQ	LFIRP	LFIRQ
1	1	6	0.1406	0.1677	-0.1687	-0.0951
2	1	4	0.1130	0.1407	-0.1310	-0.0878
3	4	6	0.0214	0.0306	-0.0221	-0.0294
4	6	5	0.0716	0.1131	-0.0798	-0.0990
5	2	5	0.1763	<b>0.2989</b>	-0.2337	-0.2113
6	2	3	0.1223	0.1787	-0.1456	-0.1192
7	3	4	-0.0431	-0.0014	0.0416	0.0103

## APPENDIX J

### SYSTEM DATA FOR WSCC 3-MACHINES, 9-BUS SYSTEM

Base MVA    100 MVA

#### Machine Data

Parameters	M/C 1	M/C 2	M/C 3
$H(\text{sec})$	23.6400	6.4000	3.0100
$X_d(\text{pu})$	0.14600	0.8958	1.3125
$X'_d(\text{pu})$	0.06080	0.1198	0.1813
$X_q(\text{pu})$	0.09690	0.8645	1.2578
$X'_q(\text{pu})$	0.09690	0.1969	0.2500
$T'_{do}(\text{sec})$	8.96000	6.0000	5.8900
$T'_{qo}(\text{sec})$	0.31000	0.5350	0.6000

#### Exciter Data

Parameters	Exciter 1	Exciter 2	Exciter 3
$K_A$	20.0	20.0	20.0
$T_A(\text{sec})$	0.20	0.20	0.20
$K_e$	1.0	1.0	1.0
$T_e$	0.314	0.314	0.314
$K_f$	0.063	0.063	0.063
$T_f$	0.35	0.35	0.35
$R_s$	0	0	0
$A_{ex}$	0.0039	0.0039	0.0039
$B_{ex}$	1.555	1.555	1.555

### Line data

Line number	Bus		Impedance		
	From	To	R (p.u.)	X (p.u.)	Y/2 (p.u.)
1	2	7	0	0.0625	0
2	1	4	0	0.0576	0
3	3	9	0	0.0586	0
4	4	6	0.0170	0.0920	0.0790
5	4	5	0.0100	0.0850	0.0880
6	5	7	0.0320	0.1610	0.1530
7	6	9	0.0390	0.1700	0.1790
8	9	8	0.0119	0.1008	0.1045
9	8	7	0.0085	0.0720	0.0745

### Load Flow Result for Base Case of WSCC Nine Bus System

Bus	Type	Angles	Voltages	PL	QL	PG	QG
1	SL	0	1.0400	0	0	0.7164	0.2705
2	PV	9.2800	1.0250	0	0	1.6300	0.0665
3	PV	4.6648	1.0250	0	0	0.8500	-0.1086
4	PQ	-2.2168	1.0258	0	0	0	0
5	PQ	-3.9888	0.9956	1.2500	0.5000	0	0
6	PQ	-3.6874	1.0127	0.9000	0.3000	0	0
7	PQ	3.7197	1.0258	0	0	0	0
8	PQ	0.7275	1.0159	1.0000	0.3500	0	0
9	PQ	1.9667	1.0324	0	0	0	0

### LFIs at base case loading condition (9-bus system)

Line number	From bus	To bus	LFISP	LFISQ	LFIRP	LFIRQ
4	4	6	0.0198	0.0323	-0.0204	-0.0304
5	4	5	0.0155	0.1014	-0.0165	-0.1056
6	5	7	-0.1118	0.0246	<b>0.1026</b>	0.0469
7	6	9	-0.0925	0.0322	0.0871	0.0064
8	9	8	0.0108	0.0533	-0.0111	-0.0536
9	8	7	-0.0252	-0.0085	0.0245	0.0192

# APPENDIX K

## SYSTEM DATA FOR 10-MACHINES, 39-BUS SYSTEM

Base MVA 100 MVA

### Machine Data

Parameter	$H(\text{sec})$	$X_d(\text{pu})$	$X'_d(\text{pu})$	$X_q(\text{pu})$	$X'_q(\text{pu})$	$T'_{do}(\text{sec})$	$T'_{qo}(\text{sec})$
M/C 1	30.3	0.2950	0.0647	0.282	0.0647	6.56	1.5
M/C 2	500	0.02	0.006	0.019	0.006	6.00	0.7
M/C 3	35.8	0.2495	0.0531	0.2370	0.0531	5.70	1.5
M/C 4	26.0	0.33	0.066	0.31	0.066	5.40	0.44
M/C 5	28.6	0.262	0.0436	0.258	0.0436	5.69	1.0
M/C 6	34.8	0.254	0.05	0.241	0.05	7.30	0.4
M/C 7	26.4	0.295	0.049	0.292	0.049	5.66	1.5
M/C 8	24.3	0.29	0.057	0.28	0.057	6.7	0.41
M/C 9	34.5	0.2106	0.057	0.205	0.057	4.79	1.96
M/C 10	42	0.2	0.004	0.196	0.004	5.7	0.5

### Exciter Data

	$K_A$	$T_A(\text{sec})$	$K_e$	$T_e$	$K_f$	$T_f$	$R_s$	$A_{ex}$	$B_{ex}$
Ex1	6	0.05	-0.63	0.41	0.25	0.5	0	0.705	0.288
Ex2	20	0.2	1.0	0.314	0.063	0.35	0	0	0
Ex3	5	0.06	-0.02	0.5	0.08	1.0	0	0.0184	0.625
Ex4	40	0.02	1.0	0.73	0.03	1.0	0	0	0
Ex5	5	0.06	-0.05	0.5	0.08	1.0	0	0.0035	0.82
Ex6	5	0.02	-0.04	0.47	0.075	1.25	0	0.0021	0.857
Ex7	40	0.02	1.0	0.73	0.03	1.0	0	0.493	0.311
Ex8	5	0.02	-0.05	0.53	0.085	1.26	0	0.0028	0.837
Ex9	40	0.02	1.0	1.4	0.03	1.0	0	0.61	0.3
Ex10	25	0.06	-0.02	0.50	0.08	1.0	0	0	0

# Line data

Line number	Bus		Impedance		
	From	To	R (p.u.)	X (p.u.)	Y/2 (p.u)
1	22	6	0	0.0143	0
2	16	1	0	0.0250	0
3	20	3	0	0.0200	0
4	39	30	0.0007	0.0138	0
5	39	5	0.0007	0.0142	0
6	32	33	0.0016	0.0435	0
7	32	31	0.0016	0.0435	0
8	30	4	0.0009	0.0180	0
9	29	9	0.0008	0.0156	0
10	25	8	0.0008	0.0232	0
11	23	7	0.0005	0.0272	0
12	12	10	0	0.0181	0
13	37	27	0.0013	0.0173	0.1608
14	37	30	0.0007	0.0082	0.06595
15	36	24	0.0003	0.0059	0.0340
16	36	21	0.0008	0.0135	0.1274
17	36	39	0.0016	0.0195	0.1520
18	36	37	0.0007	0.0089	0.0671
19	35	36	0.0009	0.0094	0.0855
20	34	35	0.0018	0.0217	0.1830
21	33	34	0.0009	0.0101	0.08615
22	28	29	0.0014	0.0151	0.1245
23	26	29	0.0057	0.0625	0.5145
24	26	29	0.0043	0.0474	0.3901
25	26	27	0.0014	0.0147	0.1198
26	25	26	0.0032	0.0323	0.2565
27	23	24	0.0022	0.0350	0.1805
28	22	23	0.0008	0.0096	0.0923
29	21	22	0.0008	0.0135	0.1274
30	20	33	0.0004	0.0043	0.03645
31	20	31	0.0004	0.0043	0.03645
32	19	2	0.0010	0.0250	0.6000
33	18	19	0.0023	0.0363	0.1902
34	17	18	0.0004	0.0046	0.0390
35	16	31	0.0007	0.0082	0.06945
36	16	17	0.0006	0.0092	0.0565
37	15	18	0.0008	0.0112	0.0738
38	15	18	0.0002	0.0026	0.0217
39	14	34	0.0008	0.0129	0.0691
40	14	15	0.0008	0.0128	0.0671
41	13	38	0.0011	0.0133	0.1069
42	13	14	0.0013	0.0213	0.1107
43	12	25	0.0070	0.0086	0.0730
44	12	13	0.0013	0.0151	0.1286
45	11	12	0.0035	0.0411	0.34935
46	11	2	0.0010	0.0250	0.3750

### Load Flow Result of 10-Machines, 39-Bus System at Base Case Loading

Bus	Type	Angles	Voltages	PL	OL	PG	OG
1	SL	0	0.9820	0.0920	0.0460	5.4282	1.5724
2	PV	-10.969	1.0300	11.0400	2.5000	10.0000	2.2624
3	PV	2.3411	0.9831	0	0	6.5000	1.6606
4	PV	3.1662	1.0123	0	0	5.0800	1.5510
5	PV	4.1895	0.9972	0	0	6.3200	0.8381
6	PV	5.1982	1.0493	0	0	6.5000	2.8105
7	PV	7.9916	1.0635	0	0	5.6000	2.2967
8	PV	1.8417	1.0278	0	0	5.4000	0.2757
9	PV	7.5440	1.0265	0	0	8.3000	0.5970
10	PV	-4.0075	1.0475	0	0	2.5000	1.8388
11	PQ	-9.3204	1.0350	0	0	0	0
12	PQ	-6.4428	1.0166	0	0	0	0
13	PQ	-9.4407	0.9855	3.2200	0.0240	0	0
14	PQ	-10.372	0.9498	5.0000	1.8400	0	0
15	PQ	-9.1191	0.9506	0	0	0	0
16	PQ	-8.3461	0.9521	0	0	0	0
17	PQ	-10.802	0.9441	2.3380	0.8400	0	0
18	PQ	-11.365	0.9448	5.2200	1.7600	0	0
19	PQ	-11.183	1.0071	0	0	0	0
20	PQ	-5.5889	0.9585	0	0	0	0
21	PQ	-4.3401	0.9849	2.7400	1.1500	0	0
22	PQ	0.1908	1.0149	0	0	0	0
23	PQ	-0.0816	1.0122	2.7450	0.8466	0	0
24	PQ	-6.8016	0.9735	3.0860	0.9220	0	0
25	PQ	-4.9744	1.0257	2.2400	0.4720	0	0
26	PQ	-6.2086	1.0124	1.3900	0.1700	0	0
27	PQ	-8.3297	0.9918	2.8100	0.7550	0	0
28	PQ	-2.4678	1.0164	2.0600	0.2760	0	0
29	PQ	0.4580	1.0187	2.8350	0.2690	0	0
30	PQ	-2.0190	0.9842	6.2800	1.0300	0	0
31	PQ	-6.5292	0.9549	0	0	0	0
32	PQ	-6.5128	0.9349	0.0750	0.8800	0	0
33	PQ	-6.3776	0.9560	0	0	0	0
34	PQ	-8.2165	0.9546	0	0	0	0
35	PQ	-8.5349	0.9568	3.2000	1.5300	0	0
36	PQ	-6.8917	0.9737	3.2940	0.3230	0	0
37	PQ	-8.1014	0.9814	0	0	0	0
38	PQ	-9.0864	0.9815	1.5800	0.3000	0	0
39	PQ	-1.0189	0.9849	0	0	0	0

**LFIs for 10-machines, 39-bus system at base case loading condition**

Line number	From bus	To bus	LFISP	LFISQ	LFIRP	LFIRQ
13	37	27	0.0010	-0.0438	-0.0009	0.0425
14	37	38	0.0058	-0.0057	-0.0058	0.0068
15	36	24	-0.0003	0.0011	0.0003	-0.0011
16	36	21	-0.0108	-0.0315	0.0105	0.0385
17	36	39	-0.0342	0.0091	0.0331	0.0325
18	36	37	0.0064	-0.0375	-0.0064	0.0382
19	35	36	-0.0117	-0.0581	0.0113	0.0588
20	34	35	0.0018	-0.0110	-0.0018	0.0110
21	33	34	0.0114	-0.0035	-0.0114	0.0076
22	28	29	-0.0190	0.0150	0.0188	-0.0046
23	26	29	-0.0427	0.0441	0.0417	0.0094
24	26	28	-0.0238	0.0163	0.0235	0.0006
25	26	27	0.0144	0.0684	-0.0150	-0.0664
26	25	26	0.0088	0.0435	-0.0091	-0.0430
27	23	24	0.0287	0.1448	-0.0312	-0.1019
28	22	23	0.0012	0.0094	-0.0012	-0.0094
29	21	22	-0.0197	-0.0914	0.0185	0.1087
30	20	33	0.0052	0.0056	-0.0052	-0.0049
31	20	31	0.0061	0.0094	-0.0062	-0.0084
32	19	2	-0.0007	-0.0922	0.0007	0.0863
33	18	19	-0.0019	-0.2790	0.0017	<b>0.2306</b>
34	17	18	0.0034	-0.0061	-0.0034	0.0065
35	16	31	-0.0109	0.0011	0.0108	0.0029
36	16	17	0.0112	0.0259	-0.0114	-0.0189
37	15	18	0.0112	0.0162	-0.0113	-0.0132
38	15	16	-0.0042	-0.0018	0.0042	0.0025
39	14	34	-0.0094	-0.0080	0.0093	0.0136
40	14	15	-0.0055	0.0031	0.0055	-0.0011
41	13	38	-0.0019	0.0181	0.0019	-0.0182
42	13	14	0.0044	0.1361	-0.0047	-0.1504
43	12	25	-0.0653	0.0296	0.0633	-0.0277
44	12	13	0.0182	0.1064	-0.0194	-0.1038
45	11	12	-0.0162	0.0901	0.0167	-0.0858
46	11	2	0.0046	0.0163	-0.0047	-0.0131



# **APTP and RPTP for 39-bus system at base case loading**

Active Power Transmission Paths	
Path number	Line connection from bus to bus
A1	(1-16)(16-17)(17-18)
A2	(1-16)(16-15)(15-14)
A3	(1-16)(16-15)(15-18)
A4	(2-19)(19-18)
A5	(3-20)(20-31)(31-16)(16-17)(17-18)
A6	(3-20)(20-31)(31-16)(16-15)(15-14)
A7	(3-20)(20-31)(31-16)(16-15)(15-18)
A8	(3-20)(20-33)(33-32)(32-31)(31-16)(16-17)(17-18)
A9	(3-20)(20-33)(33-32)(32-31)(31-16)(16-15)(15-14)
A10	(3-20)(20-33)(33-32)(32-31)(31-16)(16-15)(15-18)
A11	(3-20)(20-33)(33-34)(34-14)
A12	(3-20)(20-33)(33-34)(34-35)
A13	(4-30)
A14	(5-39)(39-30)
A15	(5-39)(39-36)(36-35)
A16	(5-39)(39-36)(36-37)(37-27)
A17	(5-39)(39-36)(36-37)(37-38)(38-13)(13-14)
A18	(6-22)(22-21)(21-36)(36-35)
A19	(6-22)(22-21)(21-36)(36-37)(37-27)
A20	(6-22)(22-21)(21-36)(36-37)(37-38)(38-13)(13-14)
A21	(7-23)(23-24)(24-36)(36-35)
A22	(7-23)(23-24)(24-36)(36-37)(37-27)
A23	(7-23)(23-24)(24-36)(36-37)(37-38)(38-13)(13-14)
A24	(8-25)(25-26)(26-27)
A25	(8-25)(25-12)(12-11)(11-2)
A26	(8-25)(25-12)(12-13)(13-14)
A27	(9-29)(29-28)
A28	(9-29)(29-26)
A29	(9-29)(29-26)(26-27)
A30	(10-12)(12-11)(11-2)
A31	(10-12)(12-13)(13-14)

Reactive Power Transmission Paths	
Path number	Line connection from bus to bus
R1	(1-16)(16-17)
R2	(1-16)(16-15)(15-18)(18-17)
R3	(1-16)(16-15)(15-14)
R4	(2-19)(19-18)(18-17)
R5	(3-20)(20-31)(31-16)(16-15)(15-18)(18-17)
R6	(3-20)(20-31)(31-16)(16-15)(15-14)
R7	(3-20)(20-31)(31-16)(16-17)
R8	(3-20)(20-31)(31-32)
R9	(3-20)(20-33)(33-32)
R10	(3-20)(20-33)(33-34)(34-14)
R11	(4-30)
R12	(5-39)(39-36)(36-24)
R13	(5-39)(39-36)(36-35)(35-34)(34-14)
R14	(6-22)(22-23)(23-24)
R15	(6-22)(22-21)(21-36)(36-24)
R16	(6-22)(22-21)(21-36)(36-35)(35-34)(34-14)
R17	(7-23)(23-24)
R18	(8-25)(25-26)(26-27)(27-37)(37-36)(36-24)
R19	(8-25)(25-26)(26-27)(27-37)(37-36)(36-35)(35-34)(34-14)
R20	(8-25)(25-12)(12-13)(13-14)
R21	(8-25)(25-12)(12-13)(13-38)(38-37)(37-36)(36-24)
R22	(8-25)(25-12)(12-13)(13-38)(38-37)(37-36)(36-35)(35-34)(34-14)
R23	(9-29)(29-28)(28-26)(26-27)(27-37)(37-36)(36-24)
R24	(9-29)(29-28)(28-26)(26-27)(27-37)(37-36)(36-35)(35-34)(34-14)
R25	(9-29)(29-26)(26-27)(27-37)(37-36)(36-24)
R26	(9-29)(29-26)(26-27)(27-37)(37-36)(36-35)(35-34)(34-14)
R27	(10-12)(12-13)(13-14)
R28	(10-12)(12-13)(13-38)(38-37)(37-36)(36-24)
R29	(10-12)(12-13)(13-38)(38-37)(37-36)(36-35)(35-34)(34-14)

**APTP and RPTP for 39-bus system at maximum loading condition**

Active Power Transmission Paths	
Path number	Line connection from bus to bus
A1	(1-16)(16-17)
A2	(1-16)(16-15)(15-18)(18-17)
A3	(1-16)(16-15)(15-14)
A4	(2-11)(11-12)(12-25)(25-26)(26-27)
A5	(2-11)(11-12)(12-13)(13-38)(38-37)(37-27)
A6	(2-11)(11-12)(12-13)(13-38)(38-37)(37-36)(36-24)
A7	(2-11)(11-12)(12-13)(13-38)(38-37)(37-36)(36-35)
A8	(2-11)(11-12)(12-13)(13-14)
A9	(2-19)(19-18)(18-17)
A10	(3-20)(20-31)(31-16)(16-17)
A11	(3-20)(20-31)(31-16)(16-15)(15-18)(18-17)
A12	(3-20)(20-31)(31-16)(16-15)(15-14)
A13	(3-20)(20-31)(31-32)(32-33)(33-34)(34-35)
A14	(3-20)(20-31)(31-32)(32-33)(33-34)(34-14)
A15	(3-20)(20-33)(33-34)(34-35)
A16	(3-20)(20-33)(33-34)(34-14)
A17	(4-30)
A18	(5-39)(39-36)(36-35)
A19	(5-39)(39-36)(36-24)
A20	(6-22)(22-23)(23-24)
A21	(6-22)(22-21)(21-36)(36-24)
A22	(6-22)(22-21)(21-36)(36-35)
A23	(7-23)(23-24)
A24	(8-25)(25-26)(26-27)
A25	(9-29)(29-28)(28-26)(26-27)
A26	(9-29)(29-26)(26-27)
A27	(10-12)(12-25)(25-26)(26-27)
A28	(10-12)(12-13)(13-38)(38-37)(37-36)(36-35)
A29	(10-12)(12-13)(13-14)

Reactive Power Transmission Paths	
Path number	Line connection from bus to bus
R1	(1-16)(16-15)(15-14)
R2	(1-16)(16-17)(17-18)
R3	(1-16)(16-15)(15-14)
R4	(2-11)(11-12)(12-13)(13-14)
R5	(2-19)(19-18)
R6	(3-20)(20-31)(31-32)
R7	(3-20)(20-33)(33-32)
R8	(3-20)(20-33)(33-34)(34-14)
R9	(3-20)(20-31)(31-16)(16-15)(15-14)
R10	(3-20)(20-31)(31-16)(16-17)(17-18)
R11	(3-20)(20-31)(31-16)(16-15)(15-18)
R12	(4-30)(30-39)(39-36)(36-24)
R13	(4-30)(30-39)(39-36)(36-35)(35-34)(34-14)
R14	(5-39)(39-36)(36-24)
R15	(5-39)(39-36)(36-35)(35-34)(34-14)
R16	(6-22)(22-23)(23-24)
R17	(6-22)(22-21)(21-36)(36-24)
R18	(6-22)(22-21)(21-36)(36-37)(37-38)(38-13)(13-14)
R19	(6-22)(22-21)(21-36)(36-35)(35-34)(34-14)
R20	(7-23)(23-24)
R21	(8-25)(25-12)(12-13)(13-14)
R22	(8-25)(25-26)(26-27)(27-37)(37-38)(38-13)(13-14)
R23	(9-29)(29-28)(28-26)(26-27)(27-37)(37-38)(38-13)(13-14)
R24	(9-29)(29-26)(26-27)(27-37)(37-38)(38-13)(13-14)
R25	(10-12)(12-13)(13-14)

# APPENDIX L

## SYSTEM DATA FOR 16-MACHINES, 68-BUS SYSTEM

Base MVA 100 MVA

### Machine Data

Parameter	$H(\text{sec})$	$X_d(\text{pu})$	$X'_d(\text{pu})$	$X_q(\text{pu})$	$X'_q(\text{pu})$	$T'_{do}(\text{sec})$	$T'_{qo}(\text{sec})$
M/C 1	496	0.0148	0.0028	0.0143	0.0025	5.9	1.5
M/C 2	42	0.031	0.025	0.069	0.028	10.2	1.5
M/C 3	30.2	0.0697	0.05	0.282	0.06	6.56	1.5
M/C 4	35.8	0.0531	0.045	0.237	0.05	5.7	1.5
M/C 5	28.6	0.0436	0.035	0.258	0.04	5.69	1.5
M/C 6	26.0	0.066	0.05	0.31	0.06	5.4	0.44
M/C 7	34.8	0.05	0.04	0.241	0.045	7.3	0.4
M/C 8	26.4	0.049	0.04	0.292	0.045	5.66	1.5
M/C 9	24.3	0.057	0.045	0.28	0.05	6.7	0.41
M/C 10	34.5	0.057	0.045	0.205	0.05	4.79	1.96
M/C 11	31.0	0.0457	0.04	0.115	0.045	9.37	1.5
M/C 12	28.2	0.018	0.012	0.123	0.015	4.1	1.5
M/C 13	92.3	0.031	0.025	0.095	0.028	7.4	1.5
M/C 14	300	0.00285	0.0023	0.0173	0.0025	4.1	1.5
M/C 15	300	0.00285	0.0023	0.0173	0.0025	4.1	1.5
M/C 16	450	0.0036	0.0028	0.0167	0.003	7.8	1.5

# Exciter Data

	$K_A$	$T_A$ (sec)	$K_e$	$T_e$	$K_f$	$T_f$	$R_s$	$A_{ex}$	$B_{ex}$	$D$
Ex1	40.0	0.02	1.0	0.785	0.03	1.0	0	0.07	0.91	1.0
Ex2	5.0	0.06	-0.0485	0.25	0.04	1.0	0	0.08	0.26	0.04
Ex3	6.2	0.05	-0.0633	0.405	0.057	0.5	0	0.66	0.88	0.0975
Ex4	5.0	0.06	-0.0198	0.5	0.08	1.0	0	0.13	0.34	0.10
Ex5	5.0	0.06	-0.0525	0.5	0.08	1.0	0	0.08	0.314	0.10
Ex6	40.0	0.02	1.0	0.785	0.03	1.0	0	0.07	0.91	0.03
Ex7	5.0	0.02	-0.0419	0.471	0.0754	1.246	0	0.064	0.251	0.10
Ex8	40.0	0.02	1.0	0.730	0.03	1.0	0	0.53	0.74	0.08
Ex9	5.0	0.02	-0.047	0.528	0.0854	1.26	0	0.072	0.282	0.09
Ex10	40.0	0.02	1.0	1.4	0.03	1.0	0	0.062	0.85	0.14
Ex11	6.2	0.05	-0.0633	0.405	0.057	0.5	0	0.66	0.88	0.0556
Ex12	5.0	0.06	-0.0525	0.5	0.08	1.0	0	0.08	0.314	0.136
Ex13	40.0	0.02	1.0	0.785	0.03	1.0	0	0.07	0.91	0.33
Ex14	40.0	0.02	1.0	0.785	0.03	1.0	0	0.07	0.91	1.0
Ex15	40.0	0.02	1.0	0.785	0.03	1.0	0	0.07	0.91	1.0
Ex16	40.0	0.02	1.0	0.785	0.03	1.0	0	0.07	0.91	0.50

Line data

Line number	Bus		Impedance		
	From	To	R (p.u.)	X (p.u.)	Y/2 (p.u.)
1	65	53	0.00350	0.04110	0.34935
2	65	30	0.00080	0.00740	0.24000
3	53	54	0.00130	0.01510	0.12860
4	53	25	0.00700	0.00860	0.07300
5	2	53	0	0.01810	0
6	54	55	0.00130	0.02130	0.11070
7	54	18	0.00110	0.01330	0.10690
8	55	56	0.00080	0.01280	0.06710
9	55	66	0.00080	0.01290	0.06910
10	56	57	0.00020	0.00260	0.02170
11	56	59	0.00080	0.01120	0.07380
12	57	58	0.00060	0.00920	0.05650
13	57	62	0.00070	0.00820	0.06945
14	57	3	0	0.02500	0
15	58	59	0.00040	0.00460	0.03900
16	59	60	0.00230	0.03630	0.19020
17	61	62	0.00040	0.00430	0.03645
18	61	64	0.00040	0.00430	0.03645
19	61	4	0	0.02000	0
20	63	62	0.00160	0.04350	0
21	63	64	0.00160	0.04350	0
22	64	66	0.00090	0.01010	0.08615
23	66	67	0.00180	0.02170	0.18300
24	67	68	0.00090	0.00940	0.08550
25	68	17	0.00070	0.00890	0.06710
26	68	19	0.00160	0.01950	0.15200
27	68	21	0.00080	0.01350	0.12740
28	68	24	0.00030	0.00590	0.03400
29	17	18	0.00070	0.00820	0.06595
30	17	27	0.00130	0.01730	0.16080
31	19	20	0.00070	0.01380	0
32	19	5	0.00070	0.01420	0
33	20	6	0.00090	0.01800	0
34	21	22	0.00080	0.01400	0.12825
35	22	23	0.00060	0.00960	0.09230
36	22	7	0	0.01430	0
37	23	24	0.00220	0.03500	0.18050
38	23	8	0.00050	0.02720	0

Line number	Bus		Impedance		
	From	To	R (p.u.)	X (p.u.)	Y/2 (p.u.)
39	25	26	0.00320	0.03230	0.26550
40	25	9	0.00060	0.02320	0
41	26	27	0.00140	0.01470	0.11980
42	26	28	0.00430	0.04740	0.39010
43	26	29	0.00570	0.06250	0.51450
44	28	29	0.00140	0.01510	0.12450
45	29	10	0.00080	0.01560	0
46	60	33	0.00950	0.00915	0.29000
47	60	36	0.00110	0.00980	0.34000
48	36	37	0.00050	0.00450	0.16000
49	34	36	0.00330	0.01110	0.72500
50	35	34	0.00010	0.00740	0
51	33	34	0.00110	0.01570	0.10100
52	32	33	0.00080	0.00990	0.08400
53	30	31	0.00130	0.01870	0.16650
54	30	32	0.00240	0.02880	0.24400
55	65	31	0.00160	0.01630	0.12500
56	31	38	0.00110	0.01470	0.12350
57	33	38	0.00360	0.04440	0.34650
58	38	46	0.00220	0.02840	0.21500
59	46	49	0.00180	0.02740	0.13500
60	65	47	0.00130	0.01880	0.65500
61	47	40	0.00125	0.01340	0.40000
62	48	40	0.00200	0.02200	0.64000
63	35	45	0.00070	0.01750	0.69500
64	37	43	0.00050	0.02760	0
65	43	44	0.00010	0.00110	0
66	44	45	0.00250	0.07300	0
67	39	44	0	0.04110	0
68	39	45	0	0.08390	0
69	45	51	0.00040	0.01050	0.36000
70	50	52	0.00120	0.02880	1.03000
71	50	51	0.00090	0.02210	0.81000
72	49	52	0.00760	0.11410	0.58000
73	52	42	0.00400	0.06000	1.12500
74	42	41	0.00400	0.06000	1.12500
75	41	40	0.00600	0.08400	1.57500
76	31	11	0	0.02600	0



Line number	Bus		Impedance		
	From	To	R (p.u.)	X (p.u.)	Y/2 (p.u.)
77	32	12	0	0.01300	0
78	36	13	0	0.00750	0
79	37	1	0	0.00330	0
80	41	14	0	0.00150	0
81	42	15	0	0.00150	0
82	52	16	0	0.00300	0
83	65	27	0.03200	0.32000	0.20500

### Load Flow Result of 16-Machines, 68-Bus System at Base Case Loading

Bus	Type	Angles	Voltages	PL	QL	PG	QG
1	SL	0	1.0110	0	0	36.4054	9.6478
2	PV	11.9726	1.0450	0	0	2.5000	1.5655
3	PV	15.3520	0.9800	0	0	5.4500	1.6794
4	PV	17.7062	0.9830	0	0	6.5000	1.7157
5	PV	19.1495	0.9970	0	0	6.3200	0.5192
6	PV	17.6812	1.0110	0	0	5.0520	1.3839
7	PV	21.9200	1.0500	0	0	7.0000	2.4622
8	PV	24.2667	1.0630	0	0	5.6000	1.9901
9	PV	17.6297	1.0300	0	0	5.4000	0.2622
10	PV	22.2206	1.0250	0	0	8.0000	0.3337
11	PV	16.9735	1.0100	0	0	5.0000	-0.4477
12	PV	19.6951	1.0000	0	0	10.000	-0.3944
13	PV	5.2146	1.0156	0	0	13.500	3.4578
14	PV	47.5579	1.0000	0	0	17.850	0.8397
15	PV	41.1735	1.0000	0	0	10.000	0.6973
16	PV	46.7884	1.0000	0	0	40.000	4.9374
17	PQ	7.5703	0.9927	0	0	0	0
18	PQ	6.6282	0.9900	1.5800	0.3000	0	0
19	PQ	13.9500	0.9892	0	0	0	0
20	PQ	12.5184	0.9859	6.8000	1.0300	0	0
21	PQ	11.5959	0.9942	2.7400	1.1500	0	0
22	PQ	16.5620	1.0209	0	0	0	0
23	PQ	16.2395	1.0194	2.4800	0.8500	0	0
24	PQ	8.9526	0.9957	3.0900	-0.9200	0	0
25	PQ	10.8443	1.0281	2.2400	0.4700	0	0

Bus	Type	Angles	Voltages	PL	QL	PG	QG
26	PQ	9.2714	1.0200	1.3900	0.1700	0	0
27	PQ	7.2640	1.0037	2.8100	0.7600	0	0
28	PQ	12.5961	1.0201	2.0600	0.2800	0	0
29	PQ	15.3860	1.0209	2.8400	0.2700	0	0
30	PQ	7.1189	1.0337	0	0	0	0
31	PQ	9.7920	1.0296	0	0	0	0
32	PQ	12.3255	1.0135	0	0	0	0
33	PQ	8.5692	1.0155	1.1200	0	0	0
34	PQ	3.2035	1.0169	0	0	0	0
35	PQ	3.1879	1.0194	0	0	0	0
36	PQ	-0.5354	0.9951	1.0200	-0.1946	0	0
37	PQ	-6.9171	0.9867	60.0000	3.0000	0	0
38	PQ	9.8060	1.0261	0	0	0	0
39	PQ	-8.3429	0.9841	2.6700	0.1260	0	0
40	PQ	16.4732	1.0494	0.6563	0.2353	0	0
41	PQ	46.0222	0.9991	10.0000	2.5000	0	0
42	PQ	40.3132	0.9991	11.5000	2.5000	0	0
43	PQ	-7.5901	0.9854	0	0	0	0
44	PQ	-7.6168	0.9853	2.6755	0.0484	0	0
45	PQ	3.1701	1.0128	2.0800	0.2100	0	0
46	PQ	10.7221	1.0065	1.5070	0.2850	0	0
47	PQ	8.4072	1.0512	2.0312	0.3259	0	0
48	PQ	10.3701	1.0551	2.4120	0.0220	0	0
49	PQ	14.0083	0.9899	1.6400	0.2900	0	0
50	PQ	20.3129	1.0074	1.0000	-1.4700	0	0
51	PQ	7.2621	1.0169	3.3700	-1.2200	0	0
52	PQ	39.8438	0.9925	24.7000	1.2300	0	0
53	PQ	9.5367	1.0188	0	0	0	0
54	PQ	6.3158	0.9896	3.2200	0.0200	0	0
55	PQ	5.0812	0.9497	5.0000	1.8400	0	0
56	PQ	6.1395	0.9458	0	0	0	0
57	PQ	6.9136	0.9474	0	0	0	0
58	PQ	4.3300	0.9364	2.3400	0.8400	0	0
59	PQ	3.7113	0.9357	5.2200	1.7700	0	0
60	PQ	3.0657	0.9745	1.0400	1.2500	0	0
61	PQ	9.7654	0.9573	0	0	0	0
62	PQ	8.7956	0.9526	0	0	0	0

From	To	Angles	Voltages	PL	QL	PG	QG
63	PQ	8.8187	0.9335	0.0900	0.8800	0	0
64	PQ	9.0026	0.9557	0	0	0	0
65	PQ	7.6688	1.0353	2.5270	1.1856	0	0
66	PQ	7.2416	0.9566	0	0	0	0
67	PQ	7.0975	0.9672	3.2000	1.5300	0	0
68	PQ	8.7692	0.9876	3.2900	0.3200	0	0

**LFIs for 16-machines, 68-bus system at base case loading condition**

Line number	From bus	To bus	LFISP	LFISQ	LFIRP	LFIRQ
1	65	53	-0.0104	0.0748	0.0107	-0.0747
2	65	30	0.0042	0.0022	-0.0042	-0.0018
3	53	54	0.0194	0.0986	-0.0207	-0.0930
4	53	25	-0.0601	0.0236	0.0582	-0.0220
6	54	55	0.0056	0.1504	-0.0061	-0.1675
7	54	18	-0.0018	0.0003	0.0018	-0.0001
8	55	56	-0.0045	0.0215	0.0046	-0.0205
9	55	66	-0.0095	-0.0168	0.0093	0.0222
10	56	57	-0.0042	-0.0022	0.0042	0.0029
11	56	59	0.0121	0.0338	-0.0124	-0.0273
12	57	58	0.0118	0.0383	-0.0121	-0.0311
13	57	62	-0.0114	-0.0085	0.0112	0.0127
15	58	59	0.0037	-0.0005	-0.0038	0.0010
16	59	60	0.0023	-0.1750	-0.0021	0.1551
17	61	62	0.0064	0.0138	-0.0064	-0.0128
18	61	64	0.0050	0.0021	-0.0050	-0.0014
22	64	66	0.0108	-0.0128	-0.0108	0.0164
23	66	67	0.0005	-0.0454	-0.0005	0.0439
24	67	68	-0.0121	-0.0718	0.0116	0.0714
25	68	17	0.0064	-0.0264	-0.0064	0.0276
26	68	19	-0.0296	0.0389	0.0293	-0.0068
27	68	21	-0.0118	-0.0101	0.0116	0.0196
28	68	24	-0.0007	-0.0323	0.0007	0.0316
29	17	18	0.0056	0.0058	-0.0057	-0.0047
30	17	27	0.0014	-0.0461	-0.0013	0.0447
31	19	20	0.0051	0.0095	-0.0051	-0.0070
34	21	22	-0.0207	-0.0727	0.0195	0.0972

Line number	From bus	To bus	LFISP	LFISQ	LFIRP	LFIRQ
35	22	23	0.0014	0.0045	-0.0014	-0.0044
37	23	24	0.0313	0.0909	-0.0330	-0.0296
39	25	26	0.0110	0.0219	-0.0112	-0.0192
41	26	27	0.0135	0.0520	-0.0140	-0.0491
42	26	28	-0.0209	0.0270	0.0208	-0.0138
43	26	29	-0.0388	0.0568	0.0383	-0.0125
44	28	29	-0.0180	0.0194	0.0179	-0.0101
46	60	30	-0.2886	0.0376	0.2403	-0.0184
47	60	36	0.0273	-0.1067	-0.0263	0.1133
48	36	37	0.0485	0.0092	-0.0499	0.0398
49	34	36	0.0759	0.0166	-0.0808	0.0004
51	33	34	0.0260	-0.0142	-0.0261	0.0483
52	32	33	0.0210	-0.0205	-0.0210	0.0370
53	30	31	-0.0128	0.0327	0.0129	-0.0246
54	30	32	-0.0290	0.1194	0.0300	-0.0953
55	65	31	-0.0142	0.0385	0.0143	-0.0340
56	31	38	0	0.0135	0	-0.0137
57	33	38	-0.0073	-0.0338	0.0071	0.0348
58	38	46	-0.0044	0.0796	0.0046	-0.0836
59	48	49	-0.0145	0.0850	0.0149	-0.0768
60	65	47	-0.0039	-0.0580	0.0038	0.0562
61	47	48	-0.0129	0.0004	0.0127	0.0043
62	48	40	-0.0381	0.0002	0.0382	-0.0378
63	35	45	0.0001	0.0256	-0.0001	-0.0262
64	37	43	0.0008	0.0047	-0.0009	-0.0042
65	43	44	0.0002	0.0002	-0.0002	-0.0002
66	44	45	-0.0265	-0.0126	0.0250	0.1465
67	39	44	0	-0.0046	0	0.0052
68	39	45	0	-0.0341	0	0.1824
69	45	51	-0.0109	0.0049	0.0108	0.0154
70	50	52	-0.0551	0.3114	0.0560	0.1135
71	50	51	0.0368	0.0292	-0.0365	0.1681
72	49	52	-0.1174	0.4409	0.1137	0.2708
73	52	42	-0.0023	-0.0243	0.0023	0.0241
74	42	41	-0.0265	0.0456	0.0263	-0.0067
75	41	40	0.1434	0.1865	-0.1342	0.6502

# APTP and RPTP for 68-bus system at base case loading

Active Power Transmission Paths	
Path number	Line connection from bus to bus
A1	((1-37)(37-43)(43-44)(44-39)
A2	(2-53)(53-54)(54-55)
A3	(2-53)(53-65)(65-30)(30-60)(60-36)(36-37)(37-43)(43-44)(44-39)
A4	(3-57)(57-58)(58-59)(59-60)(60-36)(36-37)(37-43)(43-44)(44-39)
A5	(3-57)(57-56)(56-55)
A6	(3-57)(57-56)(56-59)(59-60)(60-36)(36-37)(37-43)(43-44)(44-39)
A7	(4-61)(61-62)(62-57)(57-56)(56-55)
A8	(4-61)(61-62)(62-57)(57-58)(58-59)(59-60)(60-36)(36-37)(37-43)(43-44)(44-39)
A9	(4-61)(61-64)(64-63)(63-62)(62-57)(57-58)(58-59)(59-60)(60-36)(36-37)(37-43)(43-44)(44-39)
A10	(4-61)(61-64)(64-63)(63-62)(62-57)(57-56)(56-55)
A11	(4-61)(61-64)(64-66)(66-55)
A12	(4-61)(61-64)(64-66)(66-67)
A13	(5-19)(19-20)
A14	(5-19)(19-68)(68-67)
A15	(5-19)(19-68)(68-17)(17-18)(18-54)(54-55)
A16	(5-19)(19-68)(68-17)(17-27)
A17	(6-20)
A18	(7-22)(22-23)(23-24)(24-68)(68-67)
A19	(7-22)(22-23)(23-24)(24-68)(68-17)(17-18)(18-54)(54-55)
A20	(7-22)(22-23)(23-24)(24-68)(68-17)(17-27)
A21	(7-22)(22-21)(21-68)(68-67)
A22	(7-22)(22-21)(21-68)(68-17)(17-18)(18-54)(54-55)
A23	(7-22)(22-21)(21-68)(68-17)(17-27)
A24	(8-23)(23-24)(24-68)(68-67)
A25	(8-23)(23-24)(24-68)(68-17)(17-18)(18-54)(54-55)
A26	(8-23)(23-24)(24-68)(68-17)(17-27)
A27	(9-25)(25-53)(53-54)(54-55)
A28	(9-25)(25-53)(53-65)(65-30)(60-36)(36-37)(37-43)(43-44)(44-39)
A29	(9-25)(25-26)(26-27)
A30	(10-29)(29-26)(26-27)
A31	(10-29)(29-28)(28-26)(26-27)
A32	(11-31)(31-30)(30-60)(60-36)(36-37)(37-43)(43-44)(44-39)

Active Power Transmission Paths	
Path Number	Line connection from bus to bus
A33	(11-31)(31-65)(65-27)
A34	(12-32)(32-30)(30-60)(60-36)(36-37)(37-43)(43-44)(44-39)
A35	(12-32)(32-33)(33-34)(34-36)(36-37)(37-43)(43-44)(44-39)
A36	(12-32)(32-33)(33-34)(34-35)((35-45)(45-44)(44-39)
A37	(12-32)(32-33)(33-34)(34-35)((35-45)(45-39)
A38	(13-36)(36-37)(37-43)(43-44)(44-39)
A39	(14-41)(41-42)(42-52)(52-50)(50-51)(51-45)(45-44)(44-39)
A40	(14-41)(41-42)(42-52)(52-50)(50-51)(51-45)(45-39)
A41	(14-41)(41-42)(42-52)(52-49)(49-46)(46-38)(38-33)(33-34) (34-36)(36-37)(37-43)(43-44)(44-39)
A42	(14-41)(41-42)(42-52)(52-49)(49-46)(46-38)(38-33)(33-34) (34-35)(35-45)(45-44)(44-39)
A43	(14-41)(41-42)(42-52)(52-49)(49-46)(46-38)(38-33)(33-34) (34-35)(35-45)(45-39)
A44	(14-41)(41-42)(42-52)(52-49)(49-46)(46-38)(38-31)(31-30) (30-60)(60-36)(36-37)(37-43)(43-44)(44-39)
A45	(14-41)(41-42)(42-52)(52-49)(49-46)(46-38)(38-31)(31-65) (65-27)
A46	(14-41)(41-42)(42-52)(52-49)(49-46)(46-38)(38-31)(31-65) (65-30)(30-60)(60-36)(36-37)(37-43)(43-44)(44-39)
A47	(14-41)(41-40)(40-48)(48-47)(47-65)(65-27)
A48	(14-41)(41-40)(40-48)(48-47)(47-65)(65-30)((30-60)(60-36) (36-37)(37-43)(43-44)(44-39)
A49	(15-42)(42-52)(52-50)(50-51)(51-45)(45-44)(44-39)
A50	(15-42)(42-52)(52-50)(50-51)(51-45)(45-39)
A51	(15-42)(42-52)(52-49)(49-46)(46-38)(38-33)(33-34) (34-36)(36-37)(37-43)(43-44)(44-39)
A52	(15-42)(42-52)(52-49)(49-46)(46-38)(38-33)(33-34) (34-35)(35-45)(45-44)(44-39)
A53	(15-42)(42-52)(52-49)(49-46)(46-38)(38-33)(33-34) (34-35)(35-45)(45-39)
A54	(15-42)(42-52)(52-49)(49-46)(46-38)(38-31)(31-30) (30-60)(60-36)(36-37)(37-43)(43-44)(44-39)
A55	(15-42)(42-52)(52-49)(49-46)(46-38)(38-31)(31-65) (65-27)
A56	(15-42)(42-52)(52-49)(49-46)(46-38)(38-31)(31-65) (65-30)(30-60)(60-36)(36-37)(37-43)(43-44)(44-39)
A57	(16-52)(52-50)(50-51)(51-45)(45-44)(44-39)
A58	(16-52)(52-50)(50-51)(51-45)(45-39)

Active Power Transmission Paths	
Path Number	Line connection from bus to bus
A59	(16-52)(52-49)(49-46)(46-38)(38-33)(33-34)(34-36)(36-37)(37-43)(43-44)(44-39)
A60	(16-52)(52-49)(49-46)(46-38)(38-33)(33-34)(34-35)(35-45)(45-44)(44-39)
A61	(16-52)(52-49)(49-46)(46-38)(38-33)(33-34)(34-35)(35-45)(45-39)
A62	(16-52)(52-49)(49-46)(46-38)(38-31)(31-30)(30-60)(60-36)(36-37)(37-43)(43-44)(44-39)
A63	(16-52)(52-49)(49-46)(46-38)(38-31)(31-65)(65-27)
A64	(16-52)(52-49)(49-46)(46-38)(38-31)(31-65)(65-30)(30-60)(60-36)(36-37)(37-43)(43-44)(44-39)

Reactive Power Transmission Paths	
Path number	Line connection from bus to bus
R1	(1-37)(37-43)(43-44)(44-39)
R2	(2-53)(53-54)(54-55)(55-56)(56-59)
R3	(3-57)(57-58)(58-59)
R4	(3-57)(57-56)(56-59)
R5	(4-61)(61-62)(62-57)(57-58)(58-59)
R6	(4-61)(61-62)(62-57)(57-56)(56-59)
R7	(4-61)(61-62)(62-63)
R8	(4-61)(61-64)
R9	(5-19)(19-20)
R10	(5-19)(19-68)(68-67)(67-66)(66-64)(64-63)
R11	(5-19)(19-68)(68-67)(67-66)(66-55)(55-56)(56-59)
R12	(6-20)
R13	(7-22)(22-23)(23-24)(24-68)(68-67)(67-66)(66-64)(64-63)
R14	(7-22)(22-23)(23-24)(24-68)(68-67)(67-66)(66-55)(55-56)(56-59)
R15	(7-22)(22-21)(21-68)(68-67)(67-66)(66-64)(64-63)
R16	(7-22)(22-21)(21-68)(68-67)(67-66)(66-55)(55-56)(56-59)
R17	(8-23)(23-24)(24-68)(68-67)(67-66)(66-55)(55-56)(56-59)
R18	(8-23)(23-24)(24-68)(68-67)(67-66)(66-64)(64-63)
R19	(9-25)(25-53)(53-54)(54-55)(55-56)(56-59)
R20	(9-25)(25-26)(26-27)(27-17)(17-18)(18-54)(54-55)(55-56)(56-59)
R21	(9-25)(25-26)(26-27)(27-17)(17-68)(68-67)(67-66)(66-64)(64-63)
R22	(9-25)(25-26)(26-27)(27-17)(17-68)(68-67)(67-66)(66-55)(55-56)(56-59)
R24	(10-29)(29-26)(26-27)(27-17)(17-18)(18-54)(54-55)(55-56)(56-59)
R24	(10-29)(29-26)(26-27)(27-17)(17-68)(68-67)(67-66)(66-64)(64-63)
R25	(10-29)(29-26)(26-27)(27-17)(17-68)(68-67)(67-66)(66-55)(55-56)(56-59)
R26	(10-29)(29-28)(28-26)(26-27)(27-17)(17-18)(18-54)(54-55)(55-56)(56-59)
R27	(10-29)(29-28)(28-26)(26-27)(27-17)(17-68)(68-67)(67-66)(66-64)(64-63)
R28	(13-36)(36-60)(60-59)
R29	(13-36)(36-37)(37-43)(43-44)(44-39)
R30	(14-41)(41-42)(42-52)(52-49)
R31	(15-42)(42-52)(52-49)
R32	(16-52)(52-49)



**APTP and RPTP for 68-bus system at maximum loading condition**

Active Power Transmission Paths	
Path number	Line connection from bus to bus
A1	(1-37)(37-43)(43-44)(44-39)
A2	(2-53)(53-54)(54-18)-
A3	(2-53)(53-54)(54-55)
A4	(3-57)(57-58)(58-59)
A5	(3-57)(57-56)(56-59)
A6	(3-57)(57-56)(56-55)
A7	(4-61)(61-62)(62-63)
A8	(4-61)(61-62)(62-57)(57-58)(58-59)
A9	(4-61)(61-62)(62-57)(57-56)(56-59)
A10	(4-61)(61-62)(62-57)(57-56)(56-55)
A11	(4-61)(61-64)(64-63)
A12	(4-61)(61-64)(64-66)(66-67)
A13	(4-61)(61-64)(64-66)(66-55)
A14	(5-19)(19-20)
A15	(5-19)(19-68)(68-67)
A16	(5-19)(19-68)(68-17)(17-27)
A17	(5-19)(19-68)(68-17)(17-18)
A18	(6-20)
A19	(7-22)(22-23)(23-24)(24-68)(68-67)
A20	(7-22)(22-23)(23-24)(24-68)(68-17)(17-18)
A21	(7-22)(22-23)(23-24)(24-68)(68-17)(17-27)
A22	(7-22)(22-21)(21-68)(68-67)
A23	(7-22)(22-21)(21-68)(68-17) (17-18)
A24	(7-22)(22-21)(21-68)(68-17) (17-27)
A25	(8-23)(23-24)(24-68)(68-67)
A26	(8-23)(23-24)(24-68) (68-17)(17-18)
A27	(8-23)(23-24)(24-68) (68-17) (17-27)
A28	(9-25)(25-53)(53-54)(54-55)
A29	(9-25)(25-53)(53-54)(54-18)
A30	(9-25)(25-26)(26-27)
A31	(10-29)(29-26)(26-27)
A32	(10-29)(29-28)(28-26)(26-27)
A33	(11-31)(31-65)(65-27)
A34	(11-31)(31-65)(65-30)(30-60)(60-59)
A35	(11-31)(31-65)(65-30)(30-60)(60-36)(36-37)(37-43)(43-44)(44-39)

Active Power Transmission Paths	
Path number	Line connection from bus to bus
A36	(11-31)(31-30)(30-60)(60-59)
A37	(11-31)(31-30)(30-60)(60-36)(36-37)(37-43)(43-44)(44-39)
A38	(11-31)(31-65)(65-53)(53-54)(54-18)
A39	(11-31)(31-65)(65-53)(53-54)(54-55)
A40	(12-32)(32-30)(30-60)(60-59)
A41	(12-32)(32-30)(30-60)(60-36)(36-37)(37-43)(43-44)(44-39)
A42	(12-32)(32-33)(33-34)(34-36)(36-37)(37-43)(43-44)(44-39)
A43	(13-36)(36-37)(37-43)(43-44)(44-39)
A44	(14-41)(41-42)(42-52)(52-50)(50-51)(51-45)(45-44)(44-39)
A45	(14-41)(41-42)(42-52)(52-50)(50-51)(51-45)(45-35)(35-34)(34-36)(36-37)(37-43)(43-44)(44-39)
A46	(14-41)(41-42)(42-52)(52-49)(49-46)(46-38)(38-33)(33-34)(34-36)(36-37)(37-43)(43-44)(44-39)
A47	(14-41)(41-42)(42-52)(52-49)(49-46)(46-38)(38-31)(31-65)(65-27)
A48	(14-41)(41-42)(42-52)(52-49)(49-46)(46-38)(38-31)(31-30)(30-60)(60-36)(36-37)(37-43)(43-44)(44-39)
A49	(14-41)(41-40)(40-48)(48-47)(47-65)(65-27)
A50	(14-41)(41-40)(40-48)(48-47)(47-65)(65-30)(30-60)(60-36)(36-37)(37-43)(43-44)(44-39)
A51	(14-41)(41-40)(40-48)(48-47)(47-65)(65-53)(53-54)(54-18)
A52	(14-41)(41-40)(40-48)(48-47)(47-65)(65-53)(53-54)(54-55)
A53	(14-41)(41-42)(42-52)(52-50)(50-51)(51-45)(45-39)
A54	(15-42)(42-52)(52-50)(50-51)(51-45)(45-39)
A55	(15-42)(42-52)(52-50)(50-51)(51-45)(45-44)(44-39)
A56	(15-42)(42-52)(52-50)(50-51)(51-45)(45-35)(35-34)(34-36)(36-37)(37-43)(43-44)(44-39)
A57	(15-42)(42-52)(52-49)(49-46)(46-38)(38-33)(33-34)(34-36)(36-37)(37-43)(43-44)(44-39)
A58	(15-42)(42-52)(52-49)(49-46)(46-38)(38-31)(31-65)(65-27)
A59	(15-42)(42-52)(52-49)(49-46)(46-38)(38-31)(31-30)(30-60)(60-36)(36-37)(37-43)(43-44)(44-39)
A60	(16-52)(52-50)(50-51)(51-45)(45-39)
A61	(16-52)(52-50)(50-51)(51-45)(45-44)(44-39)
A62	(16-52)(52-50)(50-51)(51-45)(45-35)(35-34)(34-36)(36-37)(37-43)(43-44)(44-39)
A63	(16-52)(52-49)(49-46)(46-38)(38-33)(33-34)(34-36)(36-37)(37-43)(43-44)(44-39)
A64	(16-52)(52-49)(49-46)(46-38)(38-31)(31-65)(65-27)
A65	(16-52)(52-49)(49-46)(46-38)(38-31)(31-30)(30-60)(60-36)(36-37)(37-43)(43-44)(44-39)

Reactive Power Transmission Paths	
Path Number	Line connection from bus to bus
R1	(1-37)(37-43)(43-44)(44-39)
R2	(1-37)(37-43)(43-44)(44-45)(45-39)
R3	(1-37)(37-43)(43-44)(44-45)(45-51)(51-50)
R4	(2-53)(53-54)(54-55)(55-56)(56-59)
R5	(2-53)(53-65)(65-47)(47-48)(48-40)
R6	(3-57)(57-58)(58-59)
R7	(3-57)(57-56)(56-59)
R8	(4-61)(61-62)(62-57)(57-58)(58-59)
R9	(4-61)(61-62)(62-57)(57-56)(56-59)
R10	(4-61)(61-62)(62-63)
R11	(4-61)(61-64)(64-63)
R12	(4-61)(61-64)(64-66)(66-55)(55-56)(56-59)
R13	(5-19)(19-20)
R14	(5-19)(19-68)(68-67)(67-66)(66-55)(55-56)(56-59)
R15	(6-20)
R16	(7-22)(22-23)(23-24)(24-68)(68-67)(67-66)(66-55)(55-56)(56-59)
R17	(7-22)(22-21)(21-68)(68-67)(67-66)(66-55)(55-56)(56-59)
R18	(8-23)(23-24)(24-68)(68-67)(67-66)(66-55)(55-56)(56-59)
R19	(9-25)(25-53)(53-54)(54-55)(55-56)(56-59)
R20	(9-25)(25-26)(26-27)((27-17)(17-18)(18-54)(54-55)(55-56)(56-59)
R21	(9-25)(25-26)(26-27)(27-65)(65-47)(47-48)(48-40)
R22	(9-25)(25-53)(53-65)(65-47)(47-48)(48-40)
R23	(10-29)(29-26)(26-27)(27-17)(17-18)(18-54)(54-55)(55-56)(56-59)
R24	(10-29)(29-26)(26-27)(27-65)(65-47)(47-48)(48-40)
R25	(10-29)(29-28)(28-26)(26-27)(17-18)(18-54)(54-55)(55-56)(56-59)
R26	(10-29)(29-28)(28-26)(26-27)(27-65)(65-47)(47-48)(48-40)
R27	(11-31)((31-65)(65-47)(47-48)(48-40)
R28	(11-31)(31-38)(38-46)(46-49)
R29	(12-32)(32-30)(30-65)(65-47)(47-48)(48-40)
R30	(12-32)(32-30)(30-31)(31-65)(65-47)(47-48)(48-40)
R31	(12-32)(32-30)(30-60)(60-59)
R32	(12-32)(32-33)(33-38)(38-46)(46-49)
R33	(12-32)(32-33)(33-34)(34-35)(35-45)(45-39)

Reactive Power Transmission Paths	
Path number	Line connection from bus to bus
R34	(12-32)(32-33)(33-34)(34-35)(35-45)(45-51)(51-50)
R35	(13-36)(36-34)(34-35)(34-35)(35-45)(45-51)(51-50)
R36	(13-36)(36-34)(34-35)(34-35)(35-45)(45-39)
R37	(13-36)(36-37)(37-43)(43-44)(44-39)
R38	(13-36)(36-37)(37-43)(43-44)(44-45)(45-39)
R39	(13-36)(36-37)(37-43)(43-44)(44-45)(45-51)(51-50)
R40	(13-36)(36-60)(60-59)
R41	(14-41)(41-40)
R42	(15-42)(42-52)(52-50)
R43	(15-42)(42-52)(52-49)
R44	(16-52)(52-50)
R45	(16-52)(52-49)

## APPENDIX M

### APTP AND RPTP FOR 68-BUS SYSTEM AT MAXIMUM LOADING

#### CONDITION WITH SVC AT BUS 40

Active Power Transmission Paths	
Path number	Line connection from bus to bus
A1	(1-37)(37-43)(43-44)(44-39)
A2	(2-53)(53-54)(54-18)
A3	(2-53)(53-54)(54-55)
A4	(3-57)(57-58)(58-59)
A5	(3-57)(57-56)(56-59)
A6	(3-57)(57-56)(56-55)
A7	(4-61)(61-62)(62-57)(57-58)(58-59)
A8	(4-61)(61-62)(62-57)(57-56)(56-59)
A9	(4-61)(61-62)(62-57)(57-56)(56-55)
A10	(4-61)(61-62)(62-63)
A11	(4-61)(61-64)(64-63)
A12	(4-61)(61-64)(64-66)(66-55)
A13	(4-61)(61-64)(64-66)(66-67)
A14	(5-19)(19-20)
A15	(5-19)(19-68)(68-67)
A16	(5-19)(19-68)(68-17)(17-18)
A17	(5-19)(19-68)(68-17)(17-27)
A18	(6-20)
A19	(7-22)(22-23)(23-24)(24-68)(68-67)
A20	(7-22)(22-23)(23-24)(24-68)(68-17)(17-18)
A21	(7-22)(22-23)(23-24)(24-68)(68-17)(17-27)
A22	(7-22)(22-21)(21-68)(68-67)
A23	(7-22)(22-21)(21-68)(68-17) (17-18)
A24	(7-22)(22-21)(21-68)(68-17) (17-27)
A25	(8-23)(23-24)(24-68)(68-67)
A26	(8-23)(23-24)(24-68) (68-17)(17-18)
A27	(8-23)(23-24)(24-68) (68-17) (17-27)
A28	(9-25)(25-53)(53-54)(54-18)
A29	(9-25)(25-53)(53-54)(54-55)
A30	(9-25)(25-26)(26-27)
A31	(10-29)(29-26)(26-27)
A32	(10-29)(29-28)(28-26)(26-27)
A33	(11-31)(31-65)(65-27)
A34	(11-31)(31-30)(30-60)(60-59)

A35	(11-31)(31-30)(30-60)(60-36)(36-37)(37-43)(43-44)(44-39)
-----	--

Active Power Transmission Paths	
Path Number	Line connection from bus to bus
A36	(11-31)(31-65)(65-53)(53-54)(54-18)
A37	(11-31)(31-65)(65-53)(53-54)(54-55)
A38	(11-31)(31-65)(65-30)(30-60)(60-59)
A39	(11-31)(31-65)(65-30)(30-60)(60-36)(36-37)(37-43)(43-44)(44-39)
A40	(12-32)(32-30)(30-60)(60-59)
A41	(12-32)(32-30)(30-60)(60-36)(36-37)(37-43)(43-44)(44-39)
A42	(12-32)(32-33)(33-34)(34-36)(36-37)(37-43)(43-44)(44-39)
A43	(13-36)(36-37)(37-43)(43-44)(44-39)
A44	(14-41)(41-42)(42-52)(52-49)(49-46)(46-38)(38-31)(31-65)(65-27)
A45	(14-41)(41-42)(42-52)(52-49)(49-46)(46-38)(38-31)(31-30)(30-60)(60-59)
A46	(14-41)(41-42)(42-52)(52-49)(49-46)(46-38)(38-31)(31-30)(30-60)(60-36)(36-37)(37-43)(43-44)(44-39)
A47	(14-41)(41-42)(42-52)(52-49)(49-46)(46-38)(38-33)(33-34)(34-36)(36-37)(37-43)(43-44)(44-39)
A48	(14-41)(41-42)(42-52)(52-50)(50-51)(51-45)(45-35)(35-34)(34-36)(36-37)(37-43)(43-44)(44-39)
A49	(14-41)(41-42)(42-52)(52-50)(50-51)(51-45)(45-39)
A50	(14-41)(41-42)(42-52)(52-50)(50-51)(51-45)(45-44)(44-39)
A51	(14-41)(41-40)(40-48)(48-47)(47-65)(65-27)
A52	(14-41)(41-40)(40-48)(48-47)(47-65)(65-30)(30-60)(60-59)
A53	(14-41)(41-40)(40-48)(48-47)(47-65)(65-30)(30-60)(60-36)(36-37)(37-43)(43-44)(44-39)
A54	(14-41)(41-42)(42-52)(52-49)(49-46)(46-38)(38-31)(31-65)(65-53)(53-54)(54-18)
A55	(14-41)(41-42)(42-52)(52-49)(49-46)(46-38)(38-31)(31-65)(65-53)(53-54)(54-55)
A56	(14-41)(41-42)(42-52)(52-49)(49-46)(46-38)(38-31)(31-65)(65-30)(30-60)(60-59)
A57	(14-41)(41-42)(42-52)(52-49)(49-46)(46-38)(38-31)(31-65)(65-30)(30-60)(60-36)(36-37)(37-43)(43-44)(44-39)
A58	(15-42)(42-52)(52-49)(49-46)(46-38)(38-31)(31-65)(65-27)
A59	(15-42)(42-52)(52-49)(49-46)(46-38)(38-31)(31-30)(30-60)(60-59)
A60	(15-42)(42-52)(52-49)(49-46)(46-38)(38-31)(31-30)(30-60)(60-36)(36-37)(37-43)(43-44)(44-39)
A61	(15-42)(42-52)(52-49)(49-46)(46-38)(38-33)(33-34)(34-36)

(36-37) (37-43)(43-44)(44-39)
-------------------------------

Active Power Transmission Paths	
Path Number	Line connection from bus to bus
A62	(15-42)(42-52)(52-50)(50-51)(51-45)(45-35)(35-34) (34-36)(36-37) (37-43)(43-44)(44-39)-
A63	(15-42)(42-52)(52-50)(50-51)(51-45)(45-39)
A64	(15-42)(42-52)(52-50)(50-51)(51-45)(45-44)(44-39)
A65	(15-42)(42-52)(52-49)(49-46)(46-38)(38-31)(31-65)(65-53) (53-54)(54-18)
A66	(15-42)(42-52)(52-49)(49-46)(46-38)(38-31)(31-65)(65-53) (53-54)(54-55)
A67	(15-42)(42-52)(52-49)(49-46)(46-38)(38-31)(31-65)(65-30) (30-60)(60-59)
A68	(15-42)(42-52)(52-49)(49-46)(46-38)(38-31)(31-65)(65-30) (30-60)(30-60)(60-36)(36-37)(37-43)(43-44)(44-39)
A69	(16-52)(52-49)(49-46)(46-38)(38-31)(31-65)(65-27)
A70	(16-52)(52-49)(49-46)(46-38)(38-31)(31-30)(30-60) (60-59)
A71	(16-52)(52-49)(49-46)(46-38)(38-31)(31-30)(30-60) (60-36)(36-37)(37-43)(43-44)(44-39)
A72	(16-52)(52-49)(49-46)(46-38)(38-33)(33-34)(34-36) (36-37) (37-43)(43-44)(44-39)
A73	(16-52)(52-50)(50-51)(51-45)(45-35)(35-34) (34-36)(36-37) (37-43)(43-44)(44-39)
A74	(16-52)(52-50)(50-51)(51-45)(45-39)
A75	(16-52)(52-50)(50-51)(51-45)(45-44)(44-39)
A76	(16-52)(52-49)(49-46)(46-38)(38-31)(31-65)(65-53)(53-54) (54-18)
A77	(16-52)(52-49)(49-46)(46-38)(38-31)(31-65)(65-53)(53-54) (54-55)
A78	(16-52)(52-49)(49-46)(46-38)(38-31)(31-65)(65-30)(30-60) (60-59)
A79	(16-52)(52-49)(49-46)(46-38)(38-31)(31-65)(65-30)(30-60) (30-60)(60-36)(36-37)(37-43)(43-44)(44-39)

Reactive Power Transmission Paths	
Path number	Line connection from bus to bus
R1	(1-37)(37-43)(43-44)(44-39)
R2	(1-37)(37-43)(43-44)(44-45)(45-39)
R3	(1-37)(37-43)(43-44)(44-45)(45-51)(51-50)
R4	(2-53)(53-54)(54-55)(55-56)(56-59)
R5	(2-53)(53-65)(65-47)(47-48)(48-40)(40-41)
R6	(2-53)(53-65)(65-27)(27-17)(17-18)(18-54)(54-55)(55-56)(56-59)
R7	(2-53)(53-65)(65-27)(27-17)(17-68)(68-67)(67-66)(66-55)(55-56)(56-59)
R8	(2-53)(53-65)(65-31)(31-38)(38-46)(46-49)
R9	(3-57)(57-58)(58-59)
R10	(3-57)(57-56)(56-59)
R11	(4-61)(61-62)(62-57)(57-58)(58-59)
R12	(4-61)(61-62)(62-57)(57-56)(56-59)
R13	(4-61)(61-62)(62-63)
R14	(4-61)(61-64)(64-63)
R15	(4-61)(61-64)(64-66)(66-55)(55-56)(56-59)
R16	(5-19)(19-20)
R17	(5-19)(19-68)(68-67)(67-66)(66-55)(55-56)(56-59)
R18	(6-20)
R19	(7-22)(22-23)(23-24)(24-68)(68-67)(67-66)(66-55)(55-56)(56-59)
R20	(7-22)(22-21)(21-68)(68-67)(67-66)(66-55)(55-56)(56-59)
R21	(8-23)(23-24)(24-68)(68-67)(67-66)(66-55)(55-56)(56-59)
R22	(9-25)(25-53)(53-54)(54-55)(55-56)(56-59)
R23	(9-25)(25-26)(26-27)(27-17)(17-18)(18-54)(54-55)(55-56)(56-59)
R24	(9-25)(25-26)(26-27)(27-17)(17-68)(68-67)(67-66)(66-55)(55-56)(56-59)
R25	(10-29)(29-26)(26-27)(27-17)(17-18)(18-54)(54-55)(55-56)(56-59)
R26	(10-29)(29-26)(26-27)(27-17)(17-68)(68-67)(67-66)(66-55)(55-56)(56-59)
R27	(10-29)(29-28)(28-26)(26-27)(27-17)(17-18)(18-54)(54-55)(55-56)(56-59)
R28	(10-29)(29-28)(28-26)(26-27)(27-17)(17-68)(68-67)(67-66)(66-55)(55-56)(56-59)
R29	(11-31)(31-38)(38-46)(46-49)
R30	(12-32)(32-33)(33-34)(34-35)(35-45)(45-51)(51-50)
R31	(12-32)(32-33)(33-34)(34-35)(35-45)(45-39)



Reactive Power Transmission Paths	
Path number	Line connection from bus to bus
R32	(12-32)(32-33)(33-34)(34-36)(36-60)(60-59)
R33	(12-32)(32-33)(33-34)(34-36)(36-37)(37-43)(43-44)(44-39)
R34	(12-32)(32-33)(33-34)(34-36)(36-37)(37-43)(43-44)(44-45) (45-39)
R35	(12-32)(32-33)(33-34)(34-36)(36-37)(37-43)(43-44)(44-45) (45-51)(51-50)
R36	(13-36)(36-60)(60-59)
R37	(13-36)(36-37)(37-43)(43-44)(44-39)
R38	(13-36)(36-37)(37-43)(43-44)(44-45)(45-39)
R39	(13-36)(36-37)(37-43)(43-44)(44-45)(45-51)(51-50)
R40	(14-41)
R41	(15-42)(42-41)
R42	(15-42)(42-52)(52-50)
R43	(15-42)(42-52)(52-49)
R44	(16-52)(52-50)
R45	(16-52)(52-49)

## APPENDIX N

### EIGENVALUES FOR 68-BUS SYSTEM AT BASE CASE LOADING SHOWN IN THREE COLUMNS

-49.3498	-0.3886 ± 6.5793i	-1.8691 ± 0.2858i
-49.3467	-7.9241	-0.2187
-49.1517	-7.5545	-1.8431 ± 0.1274i
-48.1999	-6.5619	-0.2567
-48.3647	-0.4544 ± 4.9673i	-0.7274 ± 0.4755i
-48.5059	-0.2848 ± 4.1451i	-1.7670
-48.4179	-5.0200	-0.4555
-48.6019	-0.1931 ± 3.3344i	-1.5530
-48.4543	-1.6243 ± 2.9567i	-1.5427 ± 0.0348i
-48.5838	-1.6409 ± 2.8168i	-1.4644
-0.5851 ± 12.0779i	-0.2417 ± 2.2552i	-1.4131
-15.5292	-3.2993	-1.3626
-15.8474	-3.2793	-1.2632 ± 0.1617i
-15.8275	-1.6178 ± 1.9721i	-1.2284
-15.7843	-0.8151 ± 1.7428i	-0.8866
-15.8023	-1.5117 ± 1.3838i	-0.6926
-14.0344 ± 1.2413i	-2.4098	-0.9242
-11.7038	-0.8817 ± 1.0808i	-0.9860
-0.6511 ± 10.1218i	-0.3683 ± 0.8178i	-0.7188
-0.6223 ± 9.9461i	0.0000	-0.7339
-0.8185 ± 9.8868i	-0.3754 ± 0.7116i	-1.0510
-0.3904 ± 8.5142i	-0.3374 ± 0.5764i	-1.1334
-0.5008 ± 8.3996i	-0.2483 ± 0.4971i	-1.1166
-0.3803 ± 8.0569i	-0.1781 ± 0.4291i	
-0.4687 ± 7.7676i	-0.2090 ± 0.4450i	
-0.5217 ± 7.4364i	-0.5792 ± 0.5378i	
-0.3820 ± 7.0022i	-1.7248 ± 0.4461i	

#### STATCOM and SSSC Data for the 9-Bus System

MVA Base	KV Base	$R_{st}$	$X_{st}$	$C_{dc}$ ( $\mu F$ )	$R_{off}$	$R_{on}$	$\alpha$ (degree)
100	230	0.00025	.0144	4000	1.0e06	0.01	-0.55

## APPENDIX O

### TCSC CHARACTERISTIC WITH DIFFERENT VALUES OF $X_c$

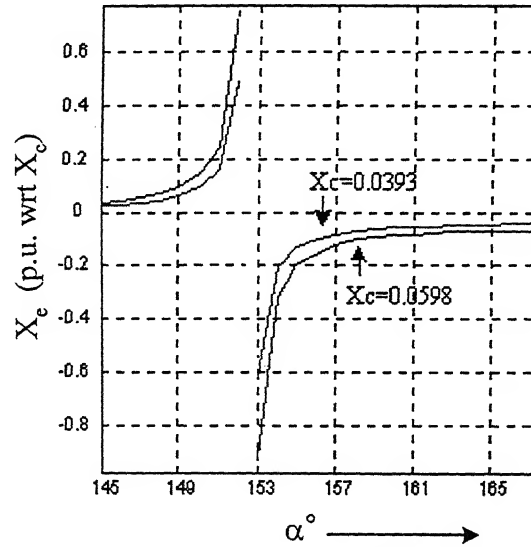


Fig. O.1 TCSC characteristic with different values of  $X_c$

A TCSC characteristic is obtained using (3.16). It is also important to note that when compensation studies at maximum loading condition are performed, the value of  $X_c$  of TCSC is taken to be 0.0393 per unit and firing angle  $\alpha$  is varied to get different compensation levels, whereas in all other studies value of  $X_c$  is used as 0.0598 per unit and firing angle as  $160^\circ$ . Because of this fact the controller parameters are different at 50% compensation of line 7-5 in Tables 6.2 and 6.5 and Tables 6.4 and 6.6 respectively for TCSC alone and SVC-TCSC combine. The TCSC characteristic for both values of  $X_c$  is shown in Fig. O.1. The TCSC characteristic with  $X_c = 0.0598$  per unit was not able to give the complete range of compensation from 30% to 70% (4.8% to 11.2%) of line 7-5. It shows that TCSC characteristic should be chosen carefully to give maximum compensation range.

